MSc in Civil Engineering, 4th. Semester
Sohngaardsholmsvej 57, 9000 Aalborg
Phone: +45 9940 8530
http://www.bsn.aau.dk

Title:
Wave Height Reduction by Means of Wave Energy Converters

Project Period:
B10, spring 2010

Students:
Jørgen Harck Nørgaard
Mark Poulsen

Supervisors:
Thomas Lykke Andersen
Jens Peter Kofoed

Circulation: 5 copies

Number of Pages: 133

Number of Appendices: 31

Completed: June 14., 2010

Synopsis:

This thesis deals with the implementation of wave energy converters for use in wave height reduction. A casestudy of Santander Bay on the Cantabrian coast of Spain is performed, to study whether wave energy converters can be used as a green alternative to other types of structures used in coastal protection. The thesis mainly focus on the wave height reduction in the wake of a farm of wave energy converters - Wave Dragons (WD's), which are based on the overtopping principle.
The wave height reduction from a single WD is evaluated from physical tests on a scaled model in the laboratory, scale 1:51.8 of a 260×150, $24kW/m$ WD. Different stiffness of the mooring system and reflectors are considered, along with different wave steepness and relative floating ratios of the WD. Conclusions are given on the influence from heaving motions of the floating structure on the transmission characteristics.
Results from the physical tests are further used to perform a calibration of the depth integrated MIKE21 BW -model by DHI for analyzing the effect of different WD-farm layouts on the wave height reduction in Santander. A single storm is considered, and to evaluate the effects of reduced wave heights from an offshore WD-farm, a brief study of the expected changes in cross shore sediment transport at Santander spit is performed using the SBEACH-model by Veri-Tech.
Front page photo: Own production, Surfers Paradise, Australia 2009

The content of this report is freely available, but may not be published without the authors consent.

Resumé (In Danish)

Nærværende afgangsprojekt omhandler undersøgelser omkring implementering af bølgeenergimaskiner, i dette tilfælde Wave Dragons (WD's) - baseret på overskylningsprincippet, til beskyttelse af kyststrækninger med udgangspunkt i et casestudie ved Santander Bay på den spanske nordkyst. Dette er gjort, da det forventes, at de besparelser der må forekomme ved at benytte bølgeenergimaskiner som multifunktionelle bølgebrydere, kan hjælpe til at introducere WD's som et "grønt" alternativ til andre kystbeskyttende konstruktioner. Der er ikke foretaget et egentlig studie af forventede besparelser, men det er evalueret hvilken bølgehøjdereduktion der kan forventes bag en farm af WD's.

Bølgereduktionen fra en enkelt WD er evalueret via af fysiske tests på en skaleret model, skala 1:51.8 af 260×150, 24 kW/m -modellen, i et laboratoriebassin. Forskellige stivheder af forankringssystemet er evalueret, og indflydelsen på bølgeenergitransmissionen gennem en WD fra forskellige bølgestejlheder og relative flydeforhold er analyseret. Konklusioner er bl.a. givet mht. indflydelsen fra horisontale- og vertikale flytninger på transmissionen gennem den flydende konstruktion.

Resultater fra målinger på den skalerede model er yderligere benyttet til kalibrering af den dybdeintegrerede MIKE21 BW -model fra DHI, som er brugt til bestemmelse af bølgehøjdereduktionen i Santander fra forskellige layouts af WD-farms. En enkelt storm er betragtet, hvor bølgehøjdereduktioner og sedimenttransport ved Santander spit er undersøgt. Til analyse af sedimenttransport er SBEACH fra Veri-Tech benyttet.

Det er konkluderet, at en bølgehøjdereduktion på op til 23% kan opnås ved brug af 5 WD's placeret i et forskudt mønster ved indsejlingen til bugten i Santander. Bølgehøjdereduktionen er yderligere forøget hvis de enkelte WD's er fastholdt mod vertikale- og horisontale flytninger. Det er desuden konkluderet at stranderosionen, som følge af reducerede bølgehøjder, er betydelig nedsat.

Preface

The following master thesis is produced on the 4th. semester of the Master of Science in Civil Engineering at Aalborg University in the period 01.02.10-14.06.10. In the project period, associate professors Thomas Lykke Andersen and Jens Peter Kofoed have served as supervisors.

Reading Guide

Throughout the thesis, citation will be given on the author, year form. Example (Author, year). All uncited figures are created by the authors. Referenced appendices are found in an appendix report on an enclosed appendix CD, in the file *Appendix.pdf*. The appendix report also contains a list of numerical models created throughout the project, as well as their location on the appendix CD.

Jørgen Harck Nørgaard

Mark Poulsen

Aalborg, June 2010

List of Symbols

Symbols

H_s	Significant wave height$\approx H_{m0}$ for Rayleigh distributed waves $[m]$
H_{m0}	Estimate of significant wave height from spectral analysis $[m]$
H	Wave height $[m]$
T	Wave period $[s]$
T_p	Peak period, the inverse of the peak frequency $[s]$
L_0	Deep water wave length $[m]$
h	Water depth $[m]$
a	Wave amplitude $[m]$
k	Wave number $[rad/m]$
$K_d = \frac{H}{H_i}$	Wave disturbance coefficient $[-]$
dx	Spatial resolution along the x-axis $[m]$
dy	Spatial resolution along the y-axis $[m]$
dt	Time step $[s]$
$S(f)$	Spectral density $[m^2 s]$
γ	Peak enhancement parameter in JONSWAP spectrum $[-]$
f	Frequency $[Hz]$
P	Wave power $[kW/m]$
ρ	Density $[kg/m^3]$
g	Gravitational acceleration $[m/s^2]$
d	Draft $[m]$
Q	Overtopping rate $[m^3/s]$
y	Crest freeboard $[m]$
μ	Reduction factor in sponge layers $[-]$
η	Surface elevation $[m]$
K_r	Reflection coefficient $[-]$
K_t	Transmission coefficient $[-]$
S	Porosity values $[-]$
Θ	Wave angle $[°]$
D_{50}	Mean stone size $[m]$
R_c	Crest freeboard $[m]$
λ	Scale factor $[-]$
$D(\theta)$	Angular spreading function $[-]$
σ_θ	Guassian standard deviation $[-]$
s	Spreading parameter for short crested waves $[-]$
R^2	Regression coefficient $[-]$

Subscripts

i	Incident
p	Peak (values corresponding to peak period)
$mean$	Mean value
$meas$	Measured
$spec$	Specified
min	Minimum
max	Maximum
e	Energy
t	Transmission
r	Reflection
a	Absorbtion
N	Non-dimensional
F	Force
ρ	Density
L	Length
S	Stiffness
$normal$	Normal conditions, no WD present
R	Reflector
B	Main body

Abbreviations

WEC	Wave Energy Converter
WD	Wave Dragon
"Fixed"	Refers to test setup with the WD body fixed to the bottom using struts.
"Free"	Refers to test setup with the WD body floating, only restricted by the mooring system.
"Free/Free"	Refers to test setup with the WD in *"Free"* condition for the WD body, and limited restriction of the reflectors.
"Fixed/Free"	Refers to test setup with the WD in *"Fixed"* condition for the WD body, and limited restriction of the reflectors.
"Free/Fixed"	Refers to test setup with the WD in *"Free"* condition for the WD body, and limited movement in the reflectors.
"Fixed/Fixed"	Refers to test setup with the WD in *"Fixed"* condition for the WD body, and limited movement in the reflectors.

Contents

1 Introduction to Project and Project objectives **1**
1.1 Description of Case Study Site . . . 1
1.2 Climate Changes and Expected Effect on Study Site . . . 5
1.3 Wave Energy Converters in General and for use in Coastal Protection . . . 7
1.4 Project Description . . . 11
I Preliminary Study **13**

2 State of the Art and Choice of Appropriate Wave Propagation Model **15**
2.1 Present State of Knowledge . . . 15
2.2 Choice and Description of Appropriate Model for Simulation of WEC-Farms . . . 18
2.3 Summary of Findings in present Chapter . . . 20

3 Detailed Description of WD **21**
3.1 Description of Wave Energy in General and Analytical Study of the WD . . . 21
3.2 Summary of Findings in present Chapter . . . 28

4 Preliminary Study- and Verification of MIKE21 BW **29**
4.1 Verification and Preliminary Study of Absorption/Reflection/Transmission in MIKE21 BW 30
4.2 Wave Scattering in MIKE21 BW . . . 40
4.3 Refraction in MIKE21 BW . . . 48
4.4 Possibilities and Considerations when Implementing and Tuning a WD in MIKE21 BW . 48
4.5 Summary of Findings in present Chapter . . . 53
II Analysis of Experimental Data and Calibration of Numerical Model **55**
4.6 Basis for Tests . . . 57
4.7 Tests on Scaled WD-Model . . . 61
4.8 Sea States and Test Schedule . . . 64
4.9 Evaluation- and Analysis of Measured Data Concerning Wave Disturbance from WD . . 68
4.10 Summary of Findings in present Chapter . . . 77

5 Implementation of Test Results in Numerical Wave Propagation Model **79**
5.1 Calibration of WD . . . 79
5.2 Summary of Findings in present Chapter . . . 85
III Case Study **87**

6 Modeling and Investigation of Wake Behind WD's in Santander Bay **89**
6.1 Setup of Numerical Model of Santander Bay . . . 89
6.2 Positioning and Layout of Considered WD-farms in Santander Bay . . . 92
6.3 Investigation of Wave Height Reduction Behind Different WD-farm Layouts in Santander Bay . . . 94
6.4 Investigation of Wave Period and -Direction in Wake of WD-farm in Santander Bay . . . 105
6.5 Investigation of Reduced Wave Heights in Harbour Entrance . . . 108
6.6 Investigation of Influence on Reduced Wave Heights in Surf Zone from an Offshore WD-farm . . . 110
6.7 Summary of Findings in present Chapter . . . 111

7 Sediment Transport at Santander **113**
7.1 Expected Influence on Cross Shore Sediment Transport from WD-farm in Santander . . 113
7.2 Setup of Cross Shore Sediment Transport Model . . . 115

7.3 Modeling- and Investigation of Effects on Cross Shore Profile at Santander Spit from Offshore WD-farm . . . 116
7.4 Summary of Findings in present Chapter . . . 121

IV Conclusions and Discussion 123

8 Conclusions in Project and Discussion of Results 125
8.1 Summary and Conclusions from the Different Parts in the Project . . . 125
8.2 Discussion of Assumptions and Shortcomings . . . 128
8.3 Discussion of Findings . . . 129
8.4 Recommendation- and Proposal for Further Study . . . 129

Bibliography 0

V Appendix (on enclosed CD) 1

A Overview of Numerical Model Types and Description of MIKE21 BW 3
A.1 Available Numerical Wave Propagation Models . . . 3
A.2 General Discretization- and Model Setup Recommendations from Model Developer . . . 5
A.3 Description of Governing Equations in MIKE21 BW . . . 6

B Calibration of Wave Bassin 9
B.1 Tests for use in Calibration of Laboratory Basin . . . 9
B.2 Evaluation of Results Concerning Wave Disturbance and Reflection in Empty Wave Basin 11
B.3 Calibration of Numerical Model . . . 14

C Setup of Numerical Model of Santander Bay 19
C.1 Wave Generation and Investigation of Influence from Absorbing Boundaries . . . 19
C.2 Convergence Analysis on Wave Disturbance . . . 20
C.3 Sensitivity Analysis on Influence from Bottom Friction . . . 21
C.4 Preliminary Study of Wake Behind WD . . . 23

D SBEACH Theory 27
D.1 General Description . . . 27
D.2 Applied Theory . . . 27

E List of Files 33
E.1 MIKE21 BW Models . . . 33
E.2 Test Data . . . 33
E.3 Photographs . . . 33

Chapter 1

Introduction to Project and Project objectives

The following chapter introduces key topics and problems related to numerical and experimental modeling of the effectiveness of a wave energy converter (WEC), in means of coastal protection. Moreover, the study site will be described. A large number of different wave energy concepts are currently being investigated by companies and academic research groups around the world, and a short description of specific patents will be presented in this chapter, followed by a choice of appropriate WEC for use at the case study site in this project. Further, a brief introduction to the problems of future climate changes, and how climate changes are expected to affect the study site, will be given. Finally, the objectives of the present project will be described, together with the general delimitations.

This master thesis is inspired by the THESEUS project; *"Innovative technologies for safer European coasts in a changing climate"*. One of the general objectives in the THESEUS project is to examine the application of innovative combined coastal mitigation and adaptation technologies, generally aiming at delivering a safe (or low-risk) coast for human use/development and healthy coastal habitats despite sea levels rise and climate changes. Within coastal engineering THESEUS is proposing to adopt wave energy converters for beach defence purposes for mitigation of flooding and coastal erosion hazard in the context of increasing storminess and sea level rise. A proposal from the THESEUS project is to place wave energy converters close to the shoreline for contemporary attenuating wave attacks and thereby produce a secondary benefit.
(THESEUS, 2009)

1.1 Description of Case Study Site

In this project, a study site is included to analyse the specific influence from offshore located WEC's. However, it is expected that a part of the conclusions and observations from the specific site can be used in the general at an arbitrary location with similar wave climate and topology.

The study site is located in the north of Santander Bay, on the Cantabrian coast of Spain - Gulf of Biscay, see Figure 1.1. The beach of interest is a 2.5 km long sand spit, named El Puntal, see Figure 1.2. The coast of the Magdelena peninsula mainly consists of cliffs, while the spit is made up of beaches and dunes of sand with a mean grain size along the spit of 0.3 mm. Due to this, the spit is more vulnerable to the effects of incoming waves than the peninsula and hence more vulnerable to the effects of climate change, such as sea level rise and altered wave climate.

Even at present, the El Puntal spit, together with the Magdalena beach, is affected by periodic flooding events, and for this reason the following study will focus on adoption of WEC's for mitigation of flooding and coastal erosion in this area. This project, only deals with El Puntal spit, and the Magdalena beach will not be described or evaluated any further.
(THESEUS, 2009), (Medellín, 2007)

Figure 1.1 *Study site on the Cantabrian coast of Spain. Image is orientated to the north. (Google maps, 2010)*

Figure 1.2 *Beach of interest. Image is orientated to the north. (Google maps, 2010)*

1.1.1 Wave Climate at Santander Spit

The yearly variation of waves, obtained from the so-called "Oluca-SP model" (GIOC, 2001) which solves a parabolic approximation of the mild-slope equation for spectral waves, is illustrated in Figure 1.3.

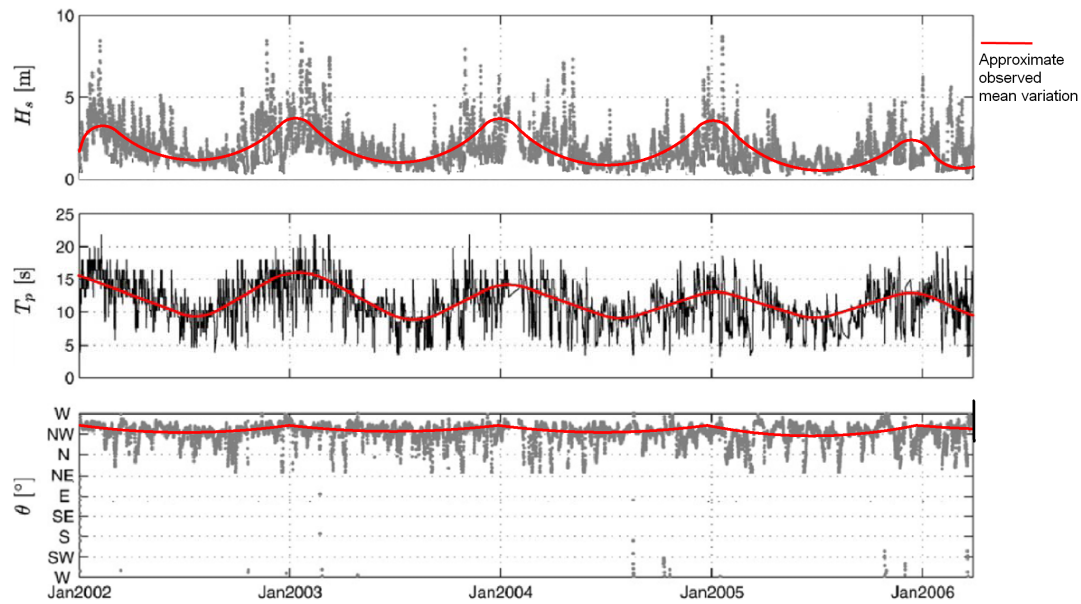

Figure 1.3 *Significant wave height, H_s, peak period, T_p, and wave angle, θ, at a location offshore of the El Puntal spit, from January 2002 to March 2006. (Medellín, 2007)*

Seasonal variation of significant wave height, H_s, and peak period, T_p, is evident cf. Figure 1.3. A mean significant wave height of approximately $H_s = 1\ m$ is present, while the typical winter storm produces 5 m waves (Medellín, 2007). The wave direction, however, does not show a clear seasonal variation. Peak periods are relatively large, ranging from around 5 to 20 s leading to relatively large Iribarren numbers (surf similarity parameter), which are waves of low steepness on a steep beach, with a predominant collapsing or surging breaking type. Mean tidal range is given as 3 m while the spring tidal range is 5 m. These values are subject to change as a result of climate changes.
(THESEUS, 2009), (Medellín, 2007)

Waves affecting the bay, mostly approaches from north west, where they have free access from the North Atlantic Ocean. In Figure 1.4 it is observed, that especially the middle and eastern parts of the spit are fully exposed to the NW Cantabrian swell waves, which however, seems to refract along the coast and turn into a more northerly direction.

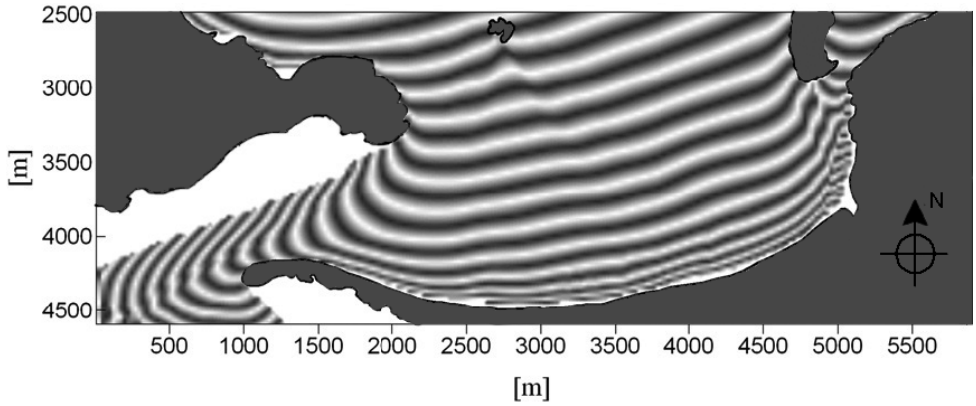

Figure 1.4 *Wave propagation associated with typical storm wave conditions ($H_s = 5\ m$, $T_p = 16\ s$) from the NW-direction during high tide, performed by (GIOC, 2001). Figure is orientated to the north.*

1.1.2 Topology and Coastline Evolution of Santander Spit

The morphology of the El Puntal spit has been substantially modified in the past two centuries. In Figure 1.5 the historical evolution of the entrance to Santander bay is illustrated in the period from year 1730 to 1985. According to (Losada, 1991) a loss of sand of approximately $2 \cdot 10^6\ m^3$ along the spit between its end and the Las Quebrantas dune has appeared in the period. Further, the Loredo region has retreated about 200 m (Losada, 1991). Since the historical evolution of the beach shows that it is retreating, the same can be expected in the future if no measures are taken. Especially with increased storminess and water levels due to climate changes.

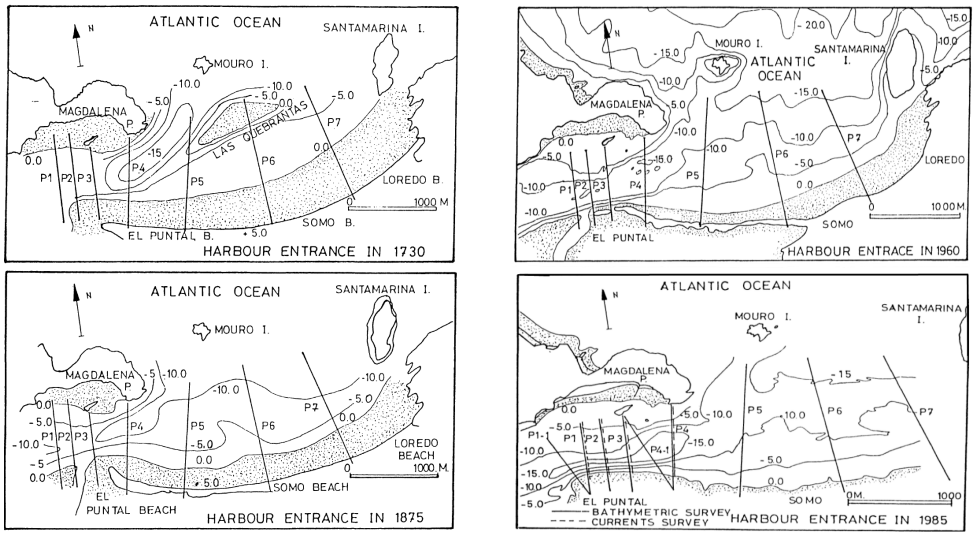

Figure 1.5 *The historical evolution of the entrance to Santander bay in the period from year 1730 to 1985. (Losada, 1991)*

The present bathymetry of El Puntal spit is illustrated in Figure 1.6 (a) together with a bathymetric profile in Figure 1.6 (b) from the spit, which shows a relatively mild-slope. Coastline undulations are usually observed on the west end of the spit during winter (which is also illustrated in Figure 1.6 (b)), for periods that last approximately two months.
(Medellín, 2007)

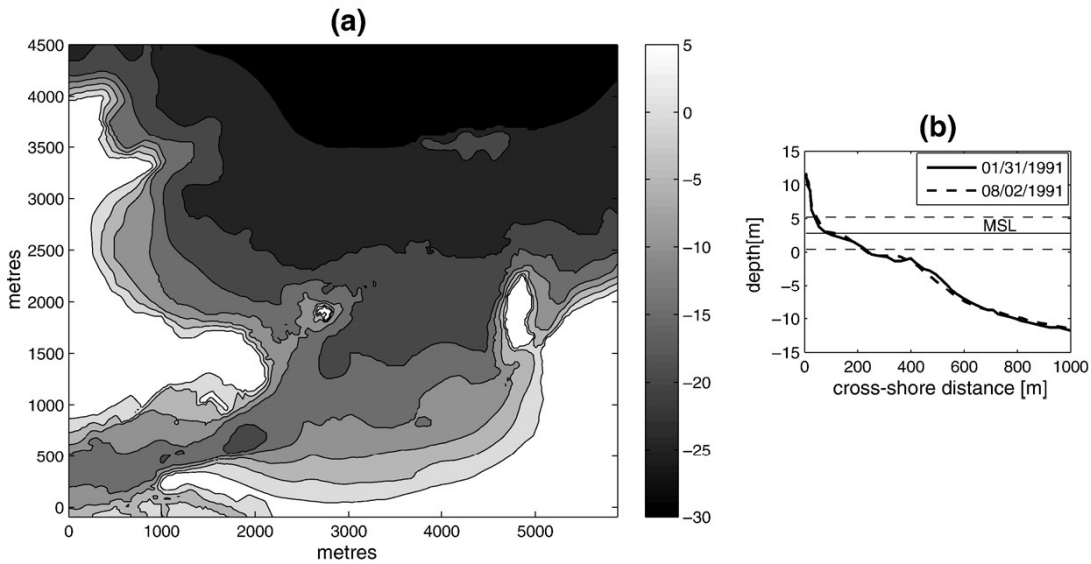

Figure 1.6 *(a) present bathymetry of El Puntal spit (orientated to the north), (b) bathymetric profile cross shore from the spit. (Medellín, 2007)*

1.2 Climate Changes and Expected Effect on Study Site

The mean air temperature has risen approximately 1 ^oC during the last 150 years, and forecasts predicts that this tendency will proceed. It is discussed wether the global warming is natural or whether it is due to the use of fossil fuels. In any case the tendency shows that a gradually warming climate can be expected in the future, and thus a higher sea level due to the melting ice on the poles. The Intergovernmental Panel on Climate Change (IPCC) is working with 40 different scenarios for the progress of greenhouse gas emissions and aerosols. The scenarios, which covers a broad range of demographic, economic and technological developments, can be grouped into different main categories of which the two most commonly used are listed in the following:

- **A2:** The A2 scenario is characterized by a large population (15 billion), high total energy use, and moderate levels of fossil fuel dependency (mostly coal) in year 2100. A2 is the most well-studied of the SRES-scenarios (Special Report on Emissions Scenarios) which assume no attempt to address global warming. (IPPC, 2000)
- **B2:** The B2 scenario is characterized by a continuously increasing population, but at a slower rate than in A2, emphasis on local rather than global solutions to economic, social and environmental stability. (IPPC, 2000)

Even with a stabilization of the temperature increase in 2100, which implies that global greenhouse gas emissions peak within a few decades (B1-scenario) and then reduced to a small fraction of the current emission, the sea rise problem will continue for many centuries. This means, that the current sea rise is a long term challenge, and not only temporary solutions are sufficient. In Figure 1.7 the lowest curve represents the CO_2-emission from scenario B1, which states that the CO_2-emission will peak before 2100 and then reduce to a minimum. The CO_2 in the atmosphere along with the temperature will proceed increasing until it stabilizes, and hence the sea level will also proceed rising, both due to melting ice and expansion of the water.
(ATV, 2003)

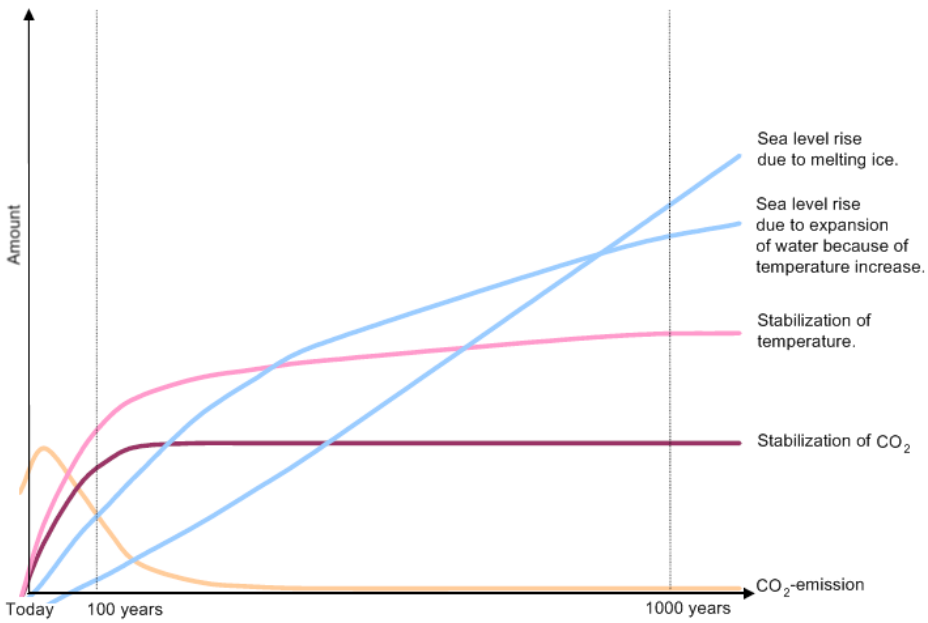

Figure 1.7 *Stabilization curves for the B1 scenario. (ATV, 2003)*

1.2.1 Effect on Coast of Spain

The North Atlantic Ocean is the source of winter storms in western and central Europe. If CO^2-emissions continue to rise unabated (A2-scenario), the frequency and intensity of storms over the North Atlantic are likely to increase, and storms, floods and droughts are likely to become increasingly frequent with a significant rise in temperature. In Figure 1.8, results from an analysis using the IPCC A2 Emissions Scenario which predicts that atmospheric CO^2-concentration will reach 771 ppm by year 2090, are illustrated.

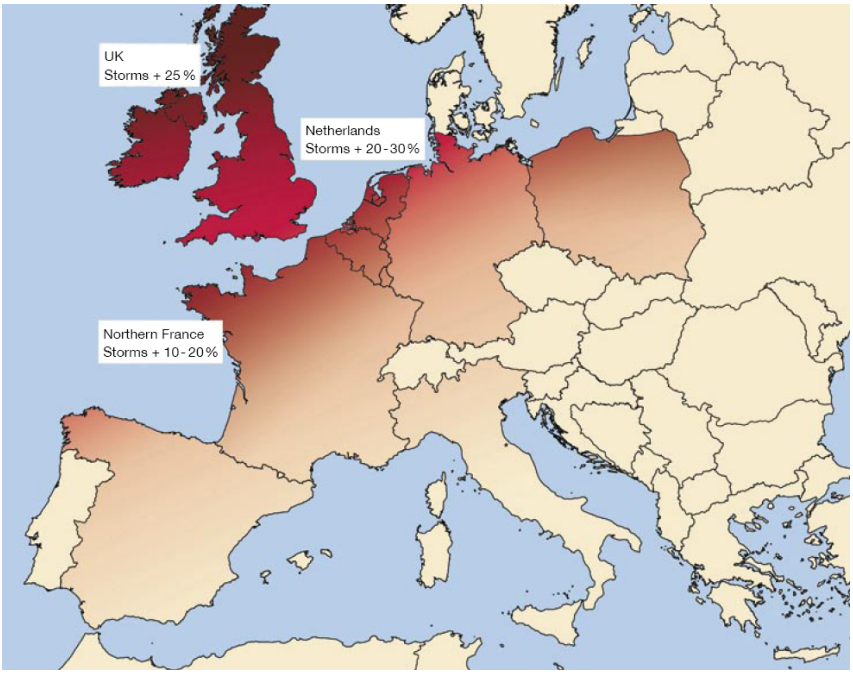

Figure 1.8 *Results from an analysis using the IPCC A2 Emissions Scenario. (WWF, 2006)*

Spain has nearly 8 000 km of coastline (including Canary Islands and Balearic Islands). Half of it lies along the Atlantic, and the rest borders the Mediterranean. Higher storm activity under climate change over the adjacent Atlantic is likely to lead to an increase in the intensity of winds over some parts of the country by the end of the century. According to (WWF, 2006) maximum wind speeds are expected to increase with 2-4% in north western Spain by the end of the century, while in Galicia, the number of days with high winds are expected to increase by up to 10%.
(WWF, 2006)

No actual adds to the wave height and water depth in Santander bay is considered in the present study. However, the expected increasing amount of windy days with increasing wind speeds, results in a growing need for wave barriers to protect the coastline and surrounding areas.

1.3 Wave Energy Converters in General and for use in Coastal Protection

Estimates concludes that approximately 8000- 80000 TWh/yr or $1-10\,TW$ of wave energy is present in the entire ocean (Boud, 2003). Moreover, wave energy provides 15-20 times more available energy per square meter than either wind or solar (Wavemill Energy Corp., 2005).

A large number of different wave energy concepts are currently being investigated by companies and academic research groups around the world. Although many working designs have been developed, and numerical and laboratory tests (particularly wave tank-tests) have been performed, only a few concepts so far have progressed to sea testing. Many concepts for wave power conversion, with an installed capacity of a few kilowatts up to more than one megawatt, have been invented during the last three decades. This has resulted in more than 1000 patents over recent years, but at the present time only fifteen have reached a stage of large scale sea trials, summarized in Figure 1.9.
(WAVEPLAM, 2009), (Muetze, 2005), (Boud, 2003)

COUNTRY	COMPANY	DEVICE	TYPE	PROTOTYPE RATING	PHASE (TRL)	SCALE	TEST RATING
UK	Aquamarine Power	Oyster	Inertia	500 kW	3-4	1:1	500 kW
Finland	AW Energy Oy	WaveRoller	Inertia	5*15 kW	3	1:1	15 kW
UK	AWS Ocean Energy	Wave Swing	Inertia	2 MW	3	1:1.75	250kW
Canada	Finavera	AquaBuOY	Inertia	250 kW	3	1:2	25 kW
Norway	Fred Olsen	FOBOX3	Inertia	2.5 MW	3	1.3	50 kW
Ireland	Ocean Energy	OE Buoy	Floating OWC	2 MW	3	1:4	15 kW
Australia	Oceanlinx	Oceanlinx	Floating OWC	2 MW	3	1:3	45 kW
USA	OPT	PowerBuoy	Inertia	150 kW	3	1:1.5	40 kW
UK	Pelamis Wave Power	Pelamis	Inertia	750 kW	4-5	1:1	750 kW
Australia	Seapower Pacific	CETO	Inertia	180 kW	3	1:6 (1:3)	10 kW
Denmark	Wave Dragon	Wave Dragon	Floating Overtopping	7 MW	3	1:5.2	20 kW
Ireland	Wavebob	Wavebob	Inertia	2 MW	3	1:4	15 kW
UK	Wavegen	Limpet	Fixed OWC	500 kW	4	1:1	500 kW
Norway	WAVEnergy	SSG	Fixed Overtopping	150 kW	2	1:1	150 kW
Denmark	WavePlane	WavePlane	Floating Overtopping	500 kW	3-4	1:1-2	250 kW
Denmark	Wavestar	Wavestar	Inertia	5 MW	3	1:10	5.5 kW

Figure 1.9 *Leading technologies in wave energy converters. (WAVEPLAM, 2009)*

Generally, two fundamental concepts of WEC's are distinguished, The *turbine concept*, which was the first to receive attention from the research community, and the *buoy-concept* which has received increased interest more recently. The turbine-concept, and the buoy-concept are usually subdivided based on their orientation and functionality. The most prominent turbine-concepts of WEC's are the oscillating water column (OWC), and the overtopping WEC, while the most prominent buoy-concept WEC is the point absorber, illustrated in Figure 1.10.
(Vining and Muetze, 2007)

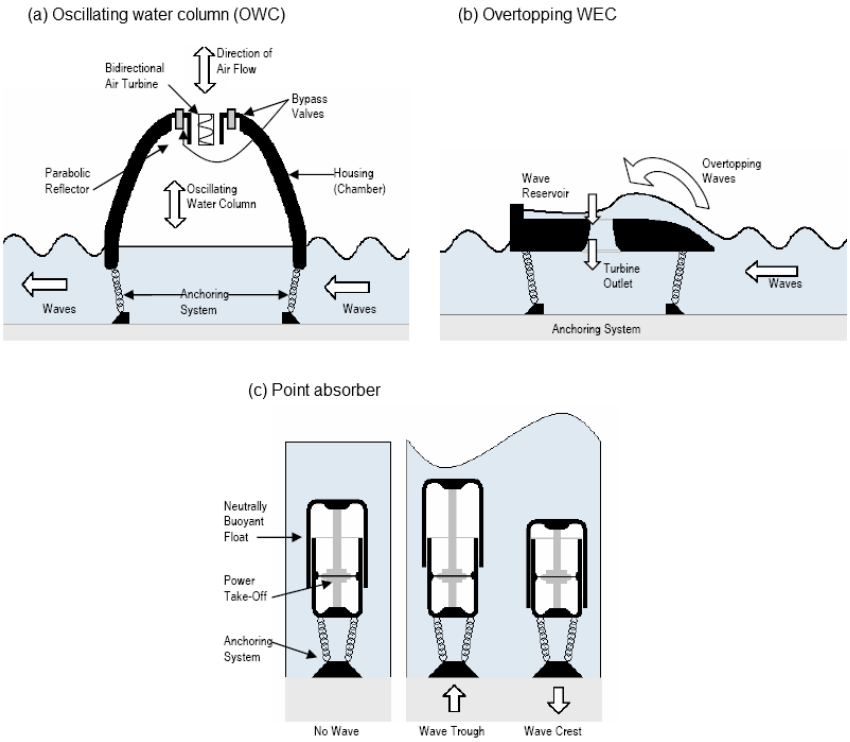

Figure 1.10 *Illustration of the concepts; Oscillating water column (OWC)(a), overtopping WEC (b), and the point absorber (c). (Vining and Muetze, 2007)*

In the following, a description of a specific patent from the different categories of concepts will be given. It should be noted, that other patents in the same categories exists.

Oscillating Water Column (OWC)

The function of the OWC, Figure 1.10 (a), is very similar to the function of a wind turbine due to the principle of waveinduced air pressurization. The concept is build on a closed containment housing (air chamber) which is placed above the water. From the passage of waves, which changes the water level within the housing, the rising and falling water level increase and decrease the air pressure within the housing - introducing a bidirectional air flow. By placing a turbine on top of the chamber, air will pass in and out of it with the changing air pressure levels. The OWC-devices can be placed on the shoreline where the waves break, or offshore where the devices are moored to the ocean bottom.
(Muetze, 2005)

An example of a OWC is the "SPERBOY" which is developed and patented by Embley Energy, (Embley-Energy, 2010), illustrated in Figure 1.11. The dimensions of the SPERBOY vary, depending on sea conditions at the deployment site. Max envisaged measure of the SPERBOY is; diameter 30 m, overall

height 50 m, and draft 35 m. The SPERBOY is circular in plane and is invariant to wave direction. A study carried out during the Carbon Trust's Marine Energy Challenge has concluded, conservatively, that 450 kW mean annual output per device would be obtained at Benbecula, in the Outer Hebrides (or Western Isles) off the coast of Scotland. According to (Muetze, 2005) technological risks of the SPERBOY are; storm survivability, potential mooring, and air turbine failure.
(Muetze, 2005)

Figure 1.11 *SPERBOY (OWC), developed and patented by Embley Energy. (Muetze, 2005)*

Overtopping WEC

Another type of WEC is the overtopping WEC, Figure 1.10 (b), which works much like a hydroelectric dam where waves roll into a collector that funnels the water into a hydro turbine. The overtopping WEC can be placed on the shoreline or further offshore.
(Muetze, 2005)

An example of the overtopping WEC is the Wave Dragon which is developed and patented by Wave Dragon ApS, (Wave-Dragon, 2010), illustrated in Figure 1.12. The physical dimensions, width, weight and length, of a Wave Dragon can be optimized to the wave climate at the deployment site. The wave dragon is a moored floating structure, and has flexible arms to focus the waves into a slope on which the wave overtops into a reservoir. A size-proposal from (Wave-Dragon, 2010) is the 4 MW-model designed for 24 kW/m wave power available, with a total width and length of 260×150 m and a weight of 22000 t. In March 2003 a 260 t, 20 kW a 1:4.5 scale prototype was launched, which has shown that technological risks are storm survivability in means of mooring and deflectors.

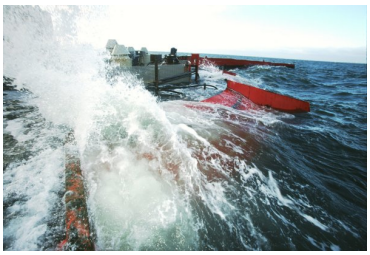

Figure 1.12 *Wave Dragon (overtopping WEC), developed and patented by Wave Dragon ApS. (Wave-Dragon, 2010)*

Point Absorber

The point absorber, Figure 1.10 (c), which is a "buoy-type WEC" because it harvests energy from all directions at one point in the ocean, is placed at or near the ocean surface away from the shoreline. The wave energy is converted from a vertically submerged float that drives a power take-off device such as a piston or a linear generator.
(Muetze, 2005)

An example of the point absorber WEC is the FO3 which is developed by the Norwegian ship owner and entrepreneur, Fred Olsen, (www.ABB.com, 2006), illustrated in Figure 1.13. The dimensions of the FO3 are (36 m × 36 m) and consists of several (12 or 21) heaving point absorbers placed in a floating platform. A laboratory platform at scale 1:3 was constructed at the Brevik ship yard in Norway and was launched in the sea in February 2005 off the southern coast of Norway. As for the SPERBOY and Wave Dragon it is expected, that technological risks is mainly the storm survivability.
(www.ABB.com, 2006)

Figure 1.13 *FO3 (point absorber), developed by the Norwegian ship owner and entrepreneur, Fred Olsen. (SEEWEC, 2010)*

1.3.1 Choice of Appropriate Type of Wave Energy Converter in Means of Coastal Protection for use in Present Study

When installing WEC's offshore, it is obvious that the highest possible extraction of wave energy is wanted to achieve a profitable investment. The specific type of WEC is designed for converting energy in specific wave conditions, and hence this will normally form the primary basis of the WEC-choice. In this project, however, the choice of WEC is primarily based on the appliance in wave height reduction, but still with a realistic idea of the use for wave energy conversion, at the specific location. It is not necessary that the device itself is a competitive energy producer as it serves also a purpose of coastal protection.

Most considered WEC's are floating structures, meaning that some of the wave energy will be transmitted under the devices. The advantage of a floating structure is the flexibility in relation to changing water levels from tides and possible climate changes, which are both present at the study site. When considering point absorbers, e.g. the FO3 with a size of (36 m × 36 m), a large number of units are expected to be required in order to affect the wave climate in a larger area, due to the relative small size of each device. This is also the case for the floating oscillating water column, e.g. the SPERBOY with a diameter of 30 m. Further, the point absorbers and OWC's are not expected to cause any notable wave energy absorption.

In contrast, the overtopping WEC is expected to have better properties for wave height reduction. If the Wave Dragon is considered, the wave energy is partially channeled from the reflectors to a slope on which the waves breaks and- or reflects/overtops. Further, the size of the Wave Dragon makes it very useable for protecting a larger area, and hence the use of a Wave Dragon (named WD in the following) as a wave barrier will be studied throughout the rest of this Thesis. A more detailed description of the WD will be given in a later chapter.

1.4 Project Description

At the moment, wave energy cannot compete with the cheapest forms of renewal energy sources, such as offshore wind farms on shallow waters. However, as continuous developments are going on, they might with time be more competitive and wind turbines may become more expensive due to limited shallow water areas. It should thus be investigated, whether or not it is possible to use the wave energy converters as a green alternative to other types of coastal protection. To perform such a study accurately, detailed information on the absorption- and reflection characteristics from a single device in different sea conditions are needed. These can be determined from physical tests where the wave height reduction in the wake behind a single WD is measured. From this, the wave climate behind e.g. an array of energy converters can then be estimated numerically, where additionally a further optimization of the array layout can be performed. This requires calibration of a numerical model to the transmission characteristics obtained in the physical model. Based on this, it can be evaluated whether the concept can function as coastal protection at a specific site by applying the calibrated WD's at a specific bathymetry.

1.4.1 Project Objectives

The objective is to determine the effectiveness of WD's in means of wave height reduction and shore protection. In addition, the effect from heaving motions of the floating structure, on the reflection and transmission characteristics will be analysed, and it will be investigated whether the effects can be included in a depth integrated numerical wave propagation model. A case study of Santander Spit will be performed and conclusions will be based on results obtained from scaled physical tests in a laboratory basin, and from simulations on the bathymetry of Santander in a numerical wave propagation model. A single winter storm will be evaluated, with a significant wave height of $H_s = 5\ m$, but with different wave periods; $T_p = 10\ s$, $T_p = 12\ s$, and $T_p = 16\ s$. It is general belief, that a reduced wave height in the wake of offshore WD's leads to reduced sediment transport. Hence the influence on the cross shore sediment transport during a winter storm will be briefly evaluated in a numerical model.

1.4.2 Project Contents

The project is subdivided into 5 different parts. After the present introduction (*Part 1.*), a preliminary study will be performed (*Part 2.*) where a concise overview and summary of the present state of knowledge is given. This is followed by a detailed description of the reflection and transmission characteristics of a WD. Hereafter, different available types of numerical wave propagation models will be evaluated, and the most appropriate model will be chosen where different model-parameters will be studied and verified.

In *Part 3.* measurements from a scale-model in the laboratory will be analysed to determine the sensitivity of e.g. heaving motions on the transmission of a WD, and to study the influence from waves with different lengths and heights. The WD will then be implemented in the chosen appropriate wave propagation model, where it will be tuned to obtain correct wave disturbance by use of the measurements.

When a calibrated model is obtained, the bathymetry of Santander will be implemented in the numerical model in *Part 4.*, and WD's will be installed offshore to study how they affect the wave climate in Santander bay. In the second half of *Part 4.* the obtained wave climate from the WD's will be used in a brief study of how they are expected to affect the cross shore sediment transport at the El Puntal spit.

A summary of the conclusions from the different parts of the project will be presented in *Part 5.*

1.4.3 Delimitations and Assumptions

General delimitations are presented in the following, while more specific delimitations and assumptions related to specific problems will be presented in the respective sections and chapters.

- In the case study only Santander Spit is considered, and influences on Magdalena beach will not be analysed. No data study from Santander is performed, hence long period effects of the WD's will not be evaluated. Only individual storms, with $H_s = 5\ m$ are considered, to which the return period is estimated to be one year. Expected climate changes are not accounted for in the project, but it is studied how e.g. a rising water level may affect the cross shore sediment transport in Santander.
- Since no measurements from the study site are available, the numerical simulations of wave conditions in Santander will be performed on an un-calibrated model. However, different calibration factors will be evaluated
- It is evident, that wave loads on the WD during a storm are very large compared to average conditions. Some types of WEC's account for this with a survival mode which they can enter during storms to prevent failure. In this project, however, it is assumed that the considered WD's can withstand the extreme loads and hence function normally during a storm.
- No actual study of the electricity production will be investigated in the present thesis, and hence no cost benefit analysis on the placement of WD's in Santander will be performed. It should be mentioned that, as written before, it is expected that there is a growing need for wave height reduction Santander and exposed coasts in general, due to climate changes, which is a deciding factor if a cost benefit analysis is performed.

Part I

Preliminary Study

Chapter 2

State of the Art and Choice of Appropriate Wave Propagation Model

Several methods to model a farm of WEC's have been developed, and in this chapter a concise overview and summary of the present state of knowledge concerning WEC-farm modeling will be given. Especially the applicability of wave propagation models for wave farm modeling is discussed. This is followed by a choice of specific numerical model for use in this master thesis. The chosen numerical model will then be further studied in a later chapter.

2.1 Present State of Knowledge

To be cost effective, WEC's can be deployed in arrays as a "wave farm", see Figure 2.1 where a farm of Pelamis WEC's (Pelamis, 2010) is illustrated. When a number of devices are installed in arrays, the power production of each individual device will depend on the geometric configuration of the WEC-farm and thereby include parameters such as device spacing and orientation to the predominant wave direction.

Figure 2.1 *Pelamis WEC illustrated in a farm. (Pelamis, 2010)*

A great amount of research has been carried out on the hydrodynamic behavior of oscillating WEC's during the past years. The study has especially been concentrating on the performance of oscillating devices as an array to optimize electricity production. Recent study, however, has concentrated on the wake of a single- or multible WEC's. Especially numerical propagation models are found to be a powerful tool in this study, since these can be used to analyse the effect of a WEC-farm at a specific bathymetry and under the specific wave conditions present at a site. The reduced wave height in the lee of a wave farm, can then be used in an evaluation on the possibilities for protection of the coast. Further, it is possible to study the effect on the downstream sediment transport patterns from a WEC-farm, and to give an indication of how, and to what extend, the sediment flow patterns and shoreline topography may be changed.

2.1.1 Modeling of WEC-Farms in Numerical Wave Propagation Models

The hydrodynamics of wave power absorption by oscillating bodies (WEC's) involves the combination of wave diffraction and wave radiation. Radiation effects on neighboring wave climate from floating bodies in a farm are neglected in most studies. However, it is demonstrated in (Kountandos et al., 2005), where the heaving motion of an oscillating and floating breakwater is analysed, that the body-length-to-wavelength ratio, B/L, has a strong effect on the response from a floating obstacle. Especially the reflection and transmission properties of the floating obstacle are very dependent on the wave length and affected by the heaving motion. In (Kountandos et al., 2005) it is seen, by comparing the transmission of a fixed- and a heaving floating- breakwater, that the transmission is slightly increased in case of heaving motions, but proportional to the width/wavelength and draught/water depth ratios of the structure. The reflection from different B/L-ratios, however, is greatly affected by the heaving motions, and is much smaller for the non-fixed floating breakwater.

Modeling of Wake Behind Hypothetical Obstacles with Hypothetical Transmission Properties

(Smith and Venugopal, 2007) presents the results of a study carried out to determine the change in wave climate from an array of hypothetical WEC's at a specific site with a specific bathymetry - off shore of the Orkney Islands. The main objective of this work has been to investigate the change in wave height upstream and downstream of the devices for different levels of applied wave absorption. This is achieved by using the MIKE 21 Boussinesq-model where partial reflecting and partial transmitting WEC's are implemented as porous structures, which has changing transmission/reflection-properties depending on the wave conditions and porosity levels. The domain used in the paper has an extension of $5 \times 4.5\ km$ with a spatial resolution of 10 m. Maximum water depth in the domain is 65 m, and the minimum water depth for closing the shore is 2.5 m to avoid wave breaking. The study shows, that porous structures are well suited for modeling partial transmitting WEC's, where an increasing porosity (increasing transmission) causes a decreasing downstream wave height reduction. The results also show the presence of regions of augmented wave energy behind the array, due to diffraction and interference, which position depends on the wave properties and the dimensions of the array.

Modeling of Wake Behind Specific Devices with Specific Transmission Properties

In the study of (Mendes, 2010), the depth integrated mild-slope REFDIF model is adapted in order to model the energy extraction from WEC-farms in the maritime zone at the West coast off Portugal. More precisely, the impact of energy absorption from a farm of Pelamis-WEC's on the nearshore wave climate, together with the influence from the incident wave conditions and the number and position of devices in the wave farm, is studied and discussed. The area of the domain is 320 km^2 and three different sinusoidal incident wave conditions are considered in the study. In general, the relative differences, between the significant wave heights with- and without the wave farms (whatever the configuration) are found to

be less then 23%. The maximum length of the coast affected by the farms is 26 km, while a wave height change higher than approximately 15 cm is observed along only 0.6 km of coast. The method followed for the study in (Mendes, 2010) differs from the study in (Smith et al., 2007) and (Smith and Venugopal, 2007) by the fact, that instead of modeling the energy extraction from hypothetical obstacles, the transmission is specified from the specific amount of energy absorption estimated by the developer.

(Beels, 2009a) have used a mild-slope wave model (MildWAVE) where a developed WEC implementation, based on varying sponge layer coefficients for tuning the power absorption, is used and applied to a single- and multiple WD's in a farm. The implemented WD in MildWAVE is tuned to exhibit the same reflection- and absorption characteristics as obtained for a prototype WD, where the implementation of the reflectors is based on an analytically determined amount of energy flux integrated from the draft of the reflector up to the surface. The implemented floating WD is assumed to be restrained and consequently movements, which may disturb the wave pattern and affect the transmission characteristics, are neglected. The wave height reduction behind a single WD is studied in detail for long- and short crested waves where it is found, that the wake reduction is decreasing with increasing directional spreading. The wake in the lee of a farm of five WD's, installed in a staggered grid, is determined for three in-between distances of respectively D, $2D$ and $3D$, (where D is the distance between the tips of the wave reflectors of a single WD). Here it is concluded, that when installing multiple WD's in a farm, the placing of a WD in a second row right behind a WD in the first row, should be avoided - a staggered grid lay-out is preferred. Five WD's installed in a staggered grid with an individual distance of $2D$ will produce 5 times more than a single WD in a North Sea wave climate, as the incident wave power for the second row is not affected by the first row. Directional spreading of the incident waves is, however, not taken into account when considering the WD's in a grid. The wake zone behind the WD is gradually filled up due to diffraction effects, and a faster wave redistribution is observed for short-crested waves than for long crested. The study of (Beels, 2009a) mostly differs from the study in (Mendes, 2010) by the fact, that a more extensive work is performed on the tuning of energy absorption from energy production. Further, the WD is implemented in the numerical propagation model with correct dimensions and design, unlike the work in (Mendes, 2010) where the WD's are implemented as boxes.

Modeling of Impact from Wake Behind WEC's on the Littoral Processes

(Vidal, 2007) analyses the impact of a WEC farm in the nearshore dynamics. The WEC farm is located 4 km northeast of Berria beach in Santoña, northern Spain. The farm is installed in a water depth of approximately 50 m and occupy a rectangular area of 800 by 600 m, consisting of a field of 10 150 kW Ocean Power Technologies buoys, with the long side oriented towards the dominant wave direction. After an approximate evaluation of the wave transmission of the WEC farm, waves are propagated to the coast with- and without the presence of the farm, and the differences on wave height and direction, wave-driven currents, and nearshore transport are evaluated and analysed. The propagation of sea states is carried out using the numerical spectral model OLUCA-SP which solves the parabolic version of the mild slope equation. The wave climate with- and without the presence of a WEC-farm is then used in the numerical model of coastal currents COPLA-SP, which solves the Navier Stokes equations, and the transport model MOPLA-SP to obtain the time averaged currents and sediment transport in the study area. It is found, that the wave height reduction on the surrounding areas is maximum 4 % which produces very small changes in the bottom transport, and hence variations in the morphology of the beaches due to the presence of the plant are not expected.

2.1.2 Shortcomings

The approach of (Smith and Venugopal, 2007) has the major limitation, that when considering a hypothetical WEC, diffraction, transmission is not simulated accurately. Shortcomings in (Mendes, 2010), (Beels, 2009a), and (Vidal, 2007), are present, since the considered WECs are assumed to be bottom fixed and hence the effect of heaving motions on the transmission characteristics are not accounted for. This may provide rather conservative conclusions concerning the wave height reduction in these studies.

2.2 Choice and Description of Appropriate Model for Simulation of WEC-Farms

Several types of numerical models are considered for modeling the WD farm. A description, and evaluation, of each model can be found in Appendix A. As a sum up from Appendix A, the mild-slope equations describe the transformation of linear water waves when propagating from deep to shallow water while the Boussinesq equations predicts the propagation of nonlinear waves with high accuracy, especially in shallow water, but are more computationally demanding. The phase averaged SWAN-model has the limitation, that time series can not be extracted from the model and compared with e.g measured series. A major constraint in the Boussinesq model is the introduced error in case of deep-water waves, $h/L_0 \leq 0.5$, due to a gradually increasing celerity error for for increasing h/L_0. In Table 2.1 the capabilities of the different available models described in Appendix A are summarized.

	SWAN	**MildSim**	**MIKE21 EMS**	**MIKE21 PMS**	**MIKE 21 BW**
Solution method	Phase ave.	Phase res.	Phase res.	Phase res.	Phase res.
Refraction	Yes	Yes	Yes	Yes	Yes
Shoaling	Yes	Yes	Yes	Yes	Yes
Diffraction	Yes (Approx.)	Yes	Yes	Yes (Approx.)	Yes
Wave-wave int.	Yes	No	No	No	Yes
Wave breaking	Yes	Yes	Yes	Yes	Yes
Reflection	Yes	Yes	Yes	No	Yes
Transmission	Yes	Yes	Yes	No	Yes
Bottom friction	Yes	Yes	Yes	Yes	Yes
Irregular waves	Yes	Yes	No	Yes	Yes

Table 2.1 *Summary of capabilities of the five considered wave propagation models.*

SWAN will not be considered further due to the phase averaging, and MIKE21 EMS and MIKE21 PMS will not be considered further due to the inability for including irregular waves and to describe diffraction, respectively. From Table 2.1 it can be seen, that MildSim accounts for all listed wave propagation- generation, -dissipation, and -redistribution processes except wave-wave interaction. It is not know, whether nonlinear effects will have any influence on the wave climate around a WD, but since comparisons with measured data from the laboratory will be performed, a very exact description of wave disturbance etc. is needed. Further, MIKE21 BW introduces the possibility for including porous structures, which has varying transmission/reflection-characteristics through a spectrum of waves with different wave heights and periods. The transmission through a WD is expected to show the same behavior, and due to this, the MIKE21 BW model is expected, to be most applicable for use throughout the rest of this thesis. A description of governing equations and numerical scheme in MIKE21 BW is given in Appendix A.

The use of MIKE21 BW, however, requires some cautions due to the introduced error in case of deep-water waves, which are further described in the following.

2.2.1 Phase Celerity Error and Rescaling of Truncated JONSWAP Spectrum

As written, the minimum wave period which can be resolved is governed by the maximum water depth in the model area. When using the enhanced Boussinesq equations with improved frequency dispersion characteristics, a maximum depth to deep-water wave length ratio of $h/L_0 \leq 0.5$ is recommended. According to (Madsen and Sørensen, 1991) this leads to an of phase celerity relative to Stokes first-order theory $(100 \cdot (c - c_{stokes})/c_{stokes})$ of ≈ 0.5 %, see Figure 2.2.

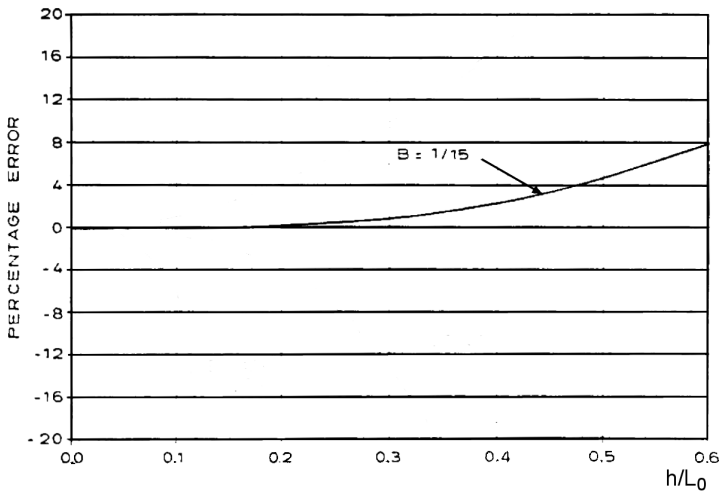

Figure 2.2 *Percentage error of the phase celerity in the Boussinesq equations relative to Stokes first-order theory (Madsen and Sørensen, 1991).*

Rescaled Truncated JONSWAP Spectrum

The irregular waves in MIKE21 BW are generated using the parameterized JONSWAP spectrum (Hasselmann et al., 1973), given in (2.1).

$$S(f) = \frac{1.4}{\gamma}\frac{5}{16}H_s^2 f_p^4 f^{-5}\gamma^{\delta}\left(-\frac{5}{4}\left(\frac{f_p}{f}\right)^4\right) \tag{2.1}$$

where
$S(f)$ is the spectral density $[m^2 s]$
$\delta = e^{\left(-\frac{(f-f_p)^2}{2\sigma_f^2 f_p^2}\right)}$
$\sigma_f = 0.1$ for $f \leq f_p$
$\sigma_f = 0.15$ for $f > f_p$
γ is the peak enhancement parameter, for controlling the sharpness of the spectral peak, $\gamma = 3.3$ $[-]$
f is the frequency $[Hz]$
f_p is the peak frequency corresponding to the peak period $[Hz]$

In order to fulfill the requirements of a maximum depth to deep-water wave length ratio of $h/L_0 \leq 0.5$ it can be necessary to perform a frequency cut-off in the JONSWAP spectrum to avoid small wave lengths. As an example; if a spectrum with $H_s = 0.1$ m and $T_p = 1.39$ s at a depth of $h = 0.39$ m is wanted, the minimum period in a standard parameterized JONSWAP spectrum will be $T_{min} \approx T_p/2 = 0.695$ s, see the plotted standard spectrum in Figure 2.3 (top).

A period of $T_{min} = 0.695\ s$ at $h = 0.39\ m$ is corresponding to a wave length of $L \approx 0.76$, which again corresponds to a ratio of $h/L = 0.39/0.76 = 0.513 > 0.5$. Therefore, in order to fulfill the ratio requirements, a frequency cut-off needs to be performed to avoid small wave periods and high frequencies. However, to maintain the wanted H_s, a rescaling needs to be performed, which can be done using the MIKE21 BW toolbox. In Figure 2.3 a standard parameterized JONSWAP spectrum is plotted together with a truncated, and a rescaled truncated spectrum, where it can be seen, how the rescaling affects the spectral density distribution and thereby H_s. The rescaling of the truncated JONSWAP spectra is be used in a later chapter in cases with small peak periods. When truncating the spectrum one should be aware that small periods are left out of the spectrum.

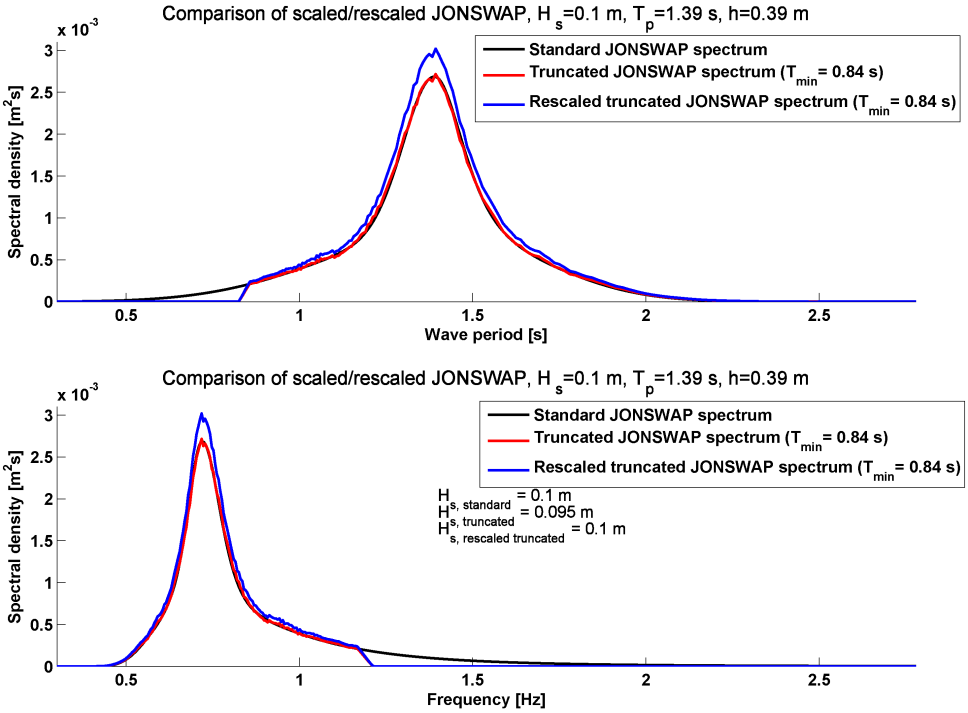

Figure 2.3 *Standard parameterized JONSWAP spectrum together with a truncated, and a rescaled truncated spectrum, where it can be seen, how the rescaling affects the spectral density distribution and thereby H_s.*

2.3 Summary of Findings in present Chapter

General key findings from the present chapter are listed in the following.

- No actual measurements of the wave disturbance behind e.g. a WD are performed in previous studies, where heaving effects are neglected and hence bottom fixed structures are assumed. This may provide rather conservative conclusions concerning the wave height reduction behind the considered WECs in these studies. Further, since numerical models are calibrated against power production, no distinction between reflection and transmission is included.
- MIKE21 BW is concluded to be most applicable for use in the present study, since it introduces the possibility for including a porous structure, which has varying transmission/reflection-characteristics through a spectrum of waves. This is expected to be highly usable when modeling a WD. Caution needs to be taken where truncated spectrums are needed.

Chapter 3

Detailed Description of WD

A brief description of wave energy in general is given, to obtain a realistic idea of a profitable position for the WD's off the coast of Santander. This is followed by an analytical study of the WD, in means of reflection and transmission characteristics, to get an idea of the influence from the structure-geometry and the wave climate on the transmissive and reflective properties.

3.1 Description of Wave Energy in General and Analytical Study of the WD

Ocean waves arise from the transfer of energy from the sun to wind and then to the water, where solar energy creates wind over the ocean, converting wind energy to wave energy. When installing WD's in an area, the wave climate must be defined. The wave climate describes the wave height and length distribution, and the water depth. To these comes parameters such as directional spreading and wave propagation directions. When all parameters are known, one can compute wave power levels. A sea state or wave climate is defined by a combination of the significant wave height H_s and mean wave period, T_m, or peak period, T_p. The significant wave height is the average of the wave heights of the one-third highest waves, and the peak period T_p is the inverse of the peak frequency that corresponds to the highest spectral density in a wave spectrum.

As written in Chapter 1, the objective of this thesis is not to study the possibilities for electricity production when placing a WD-farm in a given location, but instead, to determine the wake effects in means of wave disturbance behind the farm. However, to get a realistic idea of a profitable position for the WD's off the coast of Santander, from which coastal protection is still provided, a brief study of the available wave power in a give location will be performed. This is done in the following.

3.1.1 Wave Climate and Energy Flux

The mean transport rate of the wave energy through a vertical plane of unit width, parallel to a wave crest, is called the wave energy flux. In deep water, where the water depth is larger than half the wavelength, the wave energy flux is given by (3.1).

$$P = \frac{\rho_{water} g^2}{64\pi} T_e H_{m0}^2 \tag{3.1}$$

ρ_{water} is the density of seawater, $\rho_{water} = 1025\ [kg/m^3]$
g is the acceleration due to gravity, $g = 9.82\ [m/s^2]$
H_{m0} is the significant wave height $[m]$
T_e is the energy period $[s]$

H_{m0} and T_e are used if the wave energy is analysed in the spectral domain ($H_s = H_{m0}$, $T_e = 0.9 \cdot T_p$ in a JONSWAP spectrum where where the wave height follows the Rayleigh distribution). In Figure 3.1 it is illustrated how the wave power per meter wave front, P, is affected from the wave period, T_e, and wave height, H_{m0}, respectively. It can be seen, that an increase in both H_{m0} and T_e causes an increase in P.

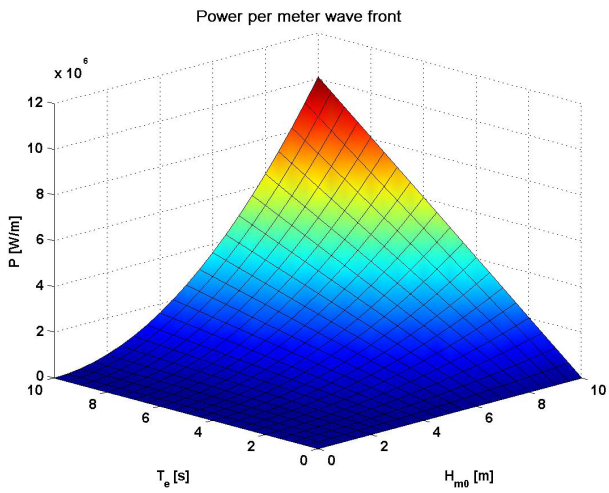

Figure 3.1 *Illustration of wave power per meter crest as a function of wave height and wave period.*

Generally, the wave energy offshore is greater than that at the shoreline, due dissipation by wave breaking and bed friction, and hence it is more favorable to place the devices at deep water when considering the electricity production.

A specific wave energy converter is designed to function in a predefined wave climate and to produce power in a specific range of wave heights and wave periods. Hence the efficiency of the WD, in means of wave energy conversion, depends on H_s and T_p. Consequently a part of the available wave power will not be converted to electricity and the wave absorption/transmission of the WD is depending on the wave climate. Reflection- and transmission characteristics of the WD will be described in the following.

3.1.2 Description of the Transmission, Reflection- and Absorbtion-Properties of the Considered WD

The considered WD in this project is the $260 \times 150\ m$, $24\ kW/m$ WD-model illustrated in Figure 3.2. The WD consists of two wave reflectors which focuses the incoming waves towards a main body where the focussed waves runs up a doubly curved ramp and overtops into a water reservoir above mean sea level, illustrated in Figure 3.3. Potential energy, compared to the surrounding sea, is then stored in the reservoir which is converted to electricity from a set of low head hydro turbines when the water in the reservoir drains back to the sea through the turbines. The WD is moored and is able to turn and face the mean incident wave direction.
(Tedd, 2005)

Concerning the crest freeboard, an advanced pneumatic system is used to adjust the floating level of the WD. This is done to adjust the rate of overtopping, and hence maximize the energy captured for a given significant wave height. The time scale for the WD to adjust the floating level is approximately 250 wave periods. (Tedd, 2007)

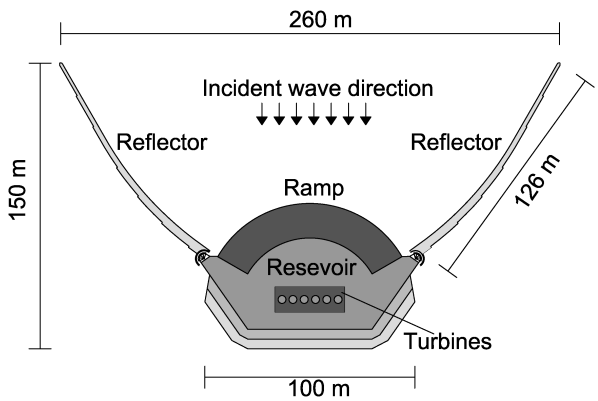

Figure 3.2 *Illustration of the WD with two wave reflectors which focuses the incoming waves towards a main body and turbines.*

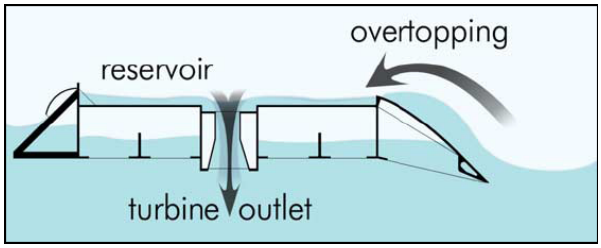

Figure 3.3 *Illustration of the focused waves which runs up a doubly curved ramp and overtops into a water reservoir above mean sea level, from where the water drains back to the sea through the turbines. (Tedd, 2005)*

In Figure 3.4 a definition sketch of the reflection/transmission/absorption from the WD-reflectors and -body is illustrated. Subscripts in Figure 3.4, and in the following, are; reflector R, main body B, transmission t, reflection r, and absorbtion a.

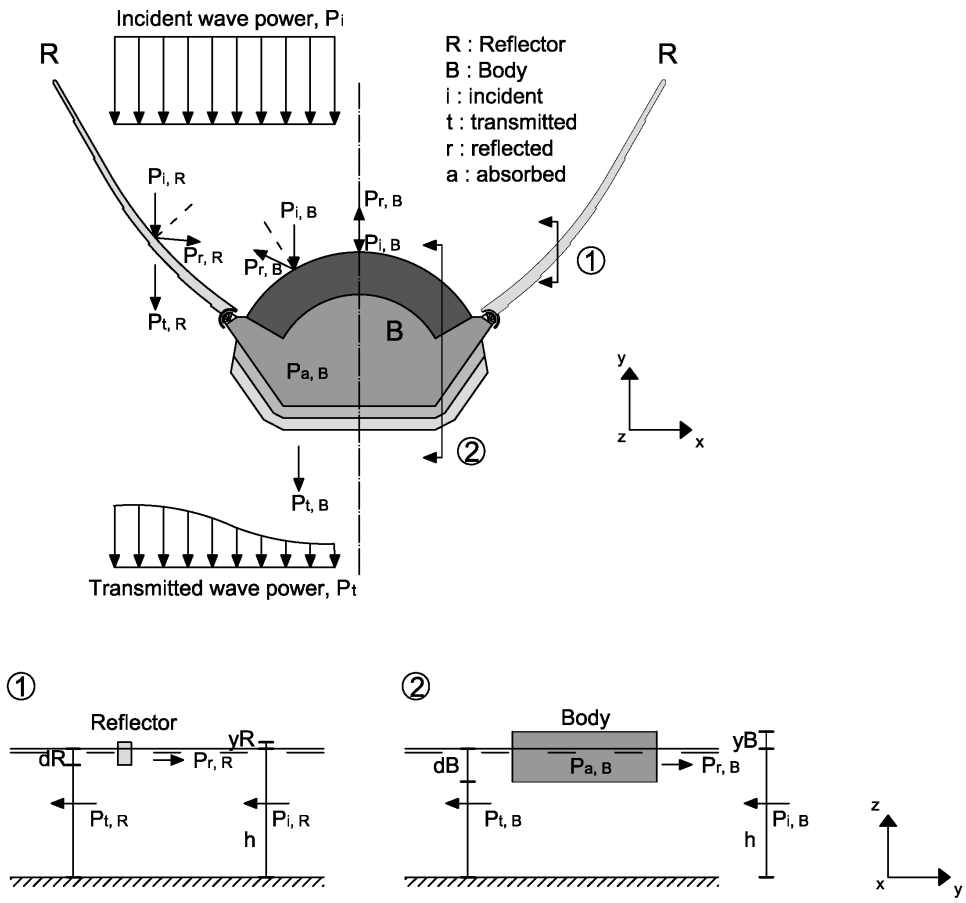

Figure 3.4 *Definition sketch of the reflection on- and transmission under- the wave reflector, together with the reflection on-, transmission under- and absorption by- the main body.*

Analytical Determination of Effect from Wave Reflectors

The purpose of the wave reflectors is to increase incident wave heights approaching the WD-body and thereby increase overtopping. The two wave reflectors have an analytical and numerical verified effect of increasing the energy capture by up to 70% in typical wave conditions. This increase is, however, not observed from laboratory tests on a scaled prototype.

Each reflector have a varying draft - decreasing from the WD-shoulder (8 m) towards the tip (6 m), and hence varying reflection and transmission are present. No wave energy is absorbed by the reflectors. The ratio between the time averaged reflected wave power (over one period) from the reflector $P_{r,R}$, and the incident wave power on the reflector $P_{i,R}$ at a given position with a specific draft d_R, is given in (3.2).

$$\lambda_R = \frac{P_{r,R}}{P_{i,R}} = 1 - \frac{\sinh\left(2k_p h\left(1 - \frac{d_R}{h}\right)\right) + 2k_p h\left(1 - \frac{d_R}{h}\right)}{\sinh\left(2k_p h\right) + 2k_p h} \tag{3.2}$$

where
$P_{r,R}$ is the reflected wave power on the reflector $[W/m]$
$P_{i,R}$ is the incident wave power on the reflector $[W/m]$
k_p is the wave number at peak period, $k_p = \frac{2\pi}{L_p}$ $[m^{-1}]$

h is the water depth $[m]$
d_R is the draft of the reflectors $[m]$
(Kofoed, 2002)

From (3.2), and the fact that no absorption from the reflectors is present, the ratio between transmitted wave power and the incident power can be determined, cf. (3.3). Here it is assumed, that no overtopping is present, and hence energy is only transmitted under the reflectors.
(Beels, 2009b)

$$\begin{aligned} P_{t,R} &= P_{i,R} - P_{r,R} \Downarrow \\ P_{t,R} &= P_{i,R}(1 - P_{r,R}/P_{i,R}) \Downarrow \\ P_{t,R} &= P_{i,R}(1 - \lambda_R) \Downarrow \\ \frac{P_{t,R}}{P_{i,R}} &= 1 - \lambda_R \end{aligned} \tag{3.3}$$

where
$\lambda_R = P_{r,R}/P_{i,R}\ [-]$
(Beels, 2009b)

With $h = 25\ m$ the variation of $P_{r,R}/P_{i,R}$ and $P_{t,R}/P_{i,R}$ is plotted in Figure 3.5. Here it can be seen, that $P_{t,R}/P_{i,R}$ increases with increasing T and L (decreasing wave steepness, H/L) and decreasing d_R, meaning that more wave energy is transmitted under the reflectors with high wave periods/length and small drafts.

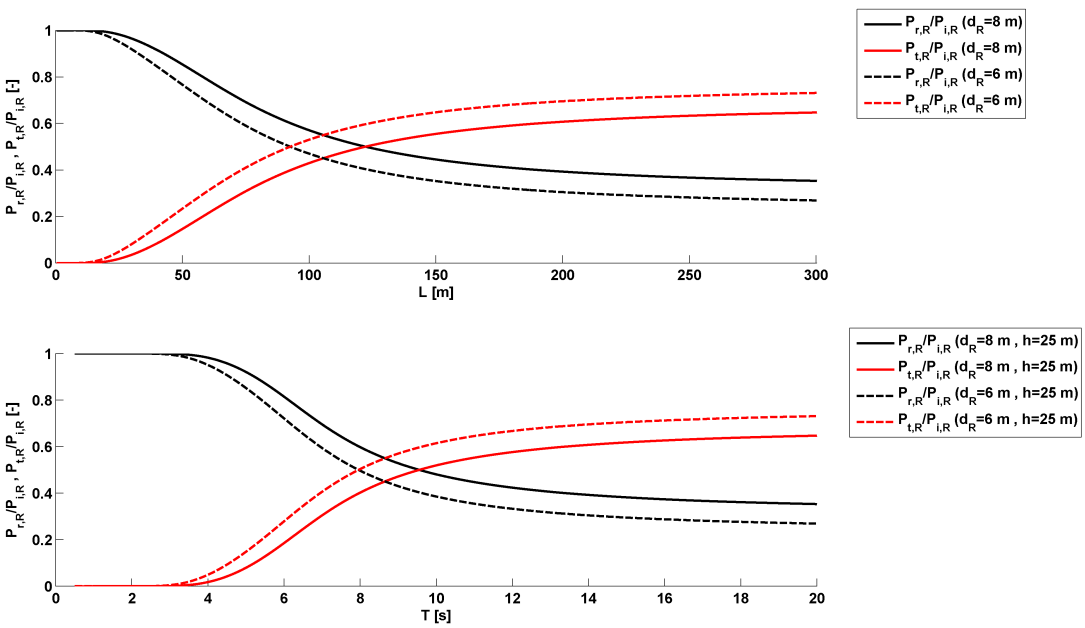

Figure 3.5 *$P_{r,R}/P_{i,R}$ and $P_{t,R}/P_{i,R}$ as a function of T and L in case of a draft of $d_R = 8$ and $d_R = 6$. Note that the axes are not identical in the two plots.*

It should be noted that the presented variation of transmitted and reflected wave power in Figure 3.5 is only approximate. Recent study has shown, that the reflectors are less effective than expected.

Analytical Determination of Influence on Absorption from Overtopping of WD-Body

As written, the body of the WD converts wave energy into electricity from overtopped waves and hence a part of the incident wave energy is absorbed by the WD due to overtopping. Several factors influence the overtopping of the WD, such as the geometrical design and the wave climate. The factors listed in Table 3.1 affects the overtopping of a marine structure:

Structure geometry/behavior:	**Wave climate:**
Floating/non-floating	Wave height, wave period
Crest level and crest width	Wave obliqueness
Slope, angle, and shape	

Table 3.1 *Factors affecting the overtopping of a marine structure from structure geometry/behavior and wave climate.*

Concerning the geometry of the WD, the most important parameter is the crest freeboard R_c, where an increasing crest width results in a decreasing overtopping discharge. Concerning wave climate, the overtopping discharge depends on the significant wave height, and the wave length. However, various studies have shown additional parameters related to the wave climate. Among these is the incident wave angle, from which the overtopping discharge decreases with increasing angle of wave attack (0° head on waves).

The amount of absorbed wave power from an incident wave approaching the WD body is calculated as given in (3.4), presented by (Kofoed, 2002).

$$P_{a,B} = \overline{Q} \cdot y_B \cdot g \cdot \rho \tag{3.4}$$

where
$P_{a,B}$ is the absorbed power on the body of the WD due to overtopping $[W/m]$
$\overline{Q}$ is the overtopping rate, $\overline{Q} = Q_N \lambda_B \sqrt{gH_s^3}$, $[m^3/s]$
Q_N is a non-dimensional overtopping rate, $Q_N = 0.4\exp^{-3.2y_b/H_s}$, $[-]$
y_B is the crest freeboard $[m]$
y_B/H_s is the relative floating level $[-]$
(Kofoed, 2002)

The influence of the relative floating level y_B/H_s, or so-called crest freeboard ratio R_c/H_s, on the overtopping rate Q_N is illustrated in Figure 3.6, where the overtopping flow is measured on the WD-body without reflectors. It can be seen, that a lower freeboard or deeper draft compared to H_s, results in an increasing overtopping rate.

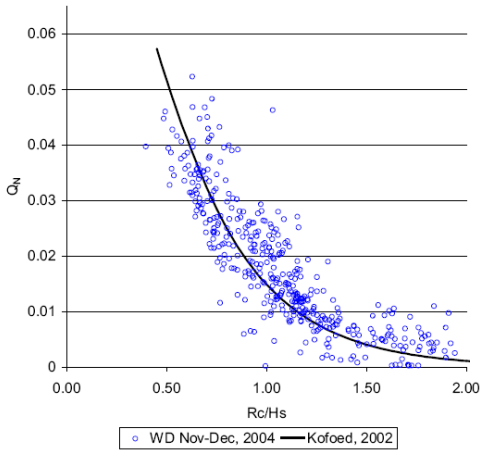

Figure 3.6 *Comparison of measured overtopping flow on the WD prototype without reflectors, to two dimensional theory. (Kofoed, 2002)*

In Figure 3.7 the variation of $P_{a,B}$ as a function of T_p and H_s, in case of different relative floating levels y_B/H_s, is illustrated. Again it can be seen, that a lower relative floating level results in an increasing power absorption due to increasing overtopping. Further it can be seen, that an increasing period results in a decreasing absorption. An increasing wave height results in an increasing absorption of wave power.

It is slightly more complicated to determine the amount of transmitted energy under the body than for the reflectors, since both reflection, absorption, and transmission is present. However, due to the decreasing absorption with increasing values of T_p, it is expected that, as for the reflectors, an increasing transmission under the body is present with increasing wave period or wave length (decreasing wave steepness, H_s/L_p).

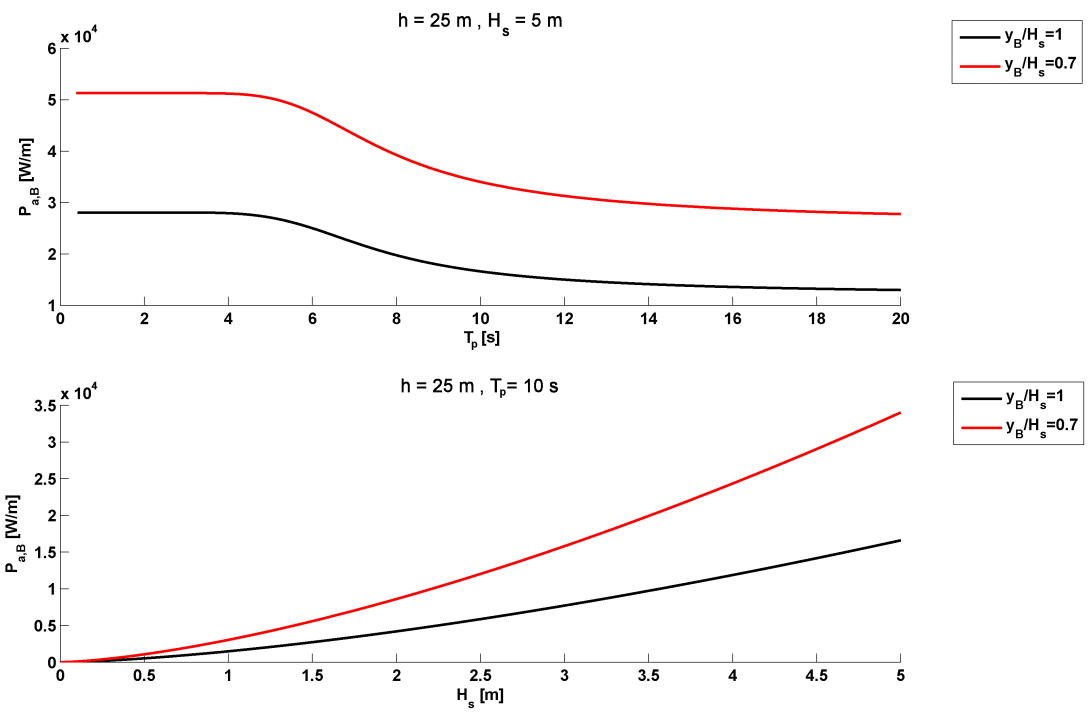

Figure 3.7 *Variation of $P_{a,B}$ as a function of T_p and H_s, in case of different relative floating levels y_B/H_s.*

From Figure 3.5 and Figure 3.7 it is seen, that the WD is most effective in case of relatively steep waves, with small wave period and big wave heights, where less energy is transmitted under the reflectors and more energy is absorbed by the WD body. Hence the wave climate in Santander, cf. Section 1.3, may not provide the optimal wave energy capture and wave height reduction of the WD.

3.2 Summary of Findings in present Chapter

General key findings from the present chapter are listed in the following.

- The wave energy offshore is greater than that at the shoreline, due dissipation by wave breaking and bed friction, and hence it is more favorable to place the devices at deep water when considering the electricity production.
- More wave energy is expected to be transmitted under the reflectors and WD-body with high wave periods/length (small wave steepness) and small drafts. Hence the WD is most effective in case of relatively steep waves, with small wave period and big wave heights.

Chapter 4

Preliminary Study- and Verification of MIKE21 BW

The present chapter deals with a preliminary study of MIKE21 BW, where possibilities of modeling boundaries and porous structures will be studied. In addition, the sufficient time- and spatial-discretization for obtaining convergence in the extreme cases of full absorbtion and full reflection, together with wave scattering, will be studied. Moreover, a verification of the diffraction around fully- and partial reflecting structures is performed, and finally the different possibilities and cautions when implementing the WD in the depth integrated MIKE21 BW-model are evaluated and described.

Before utilizing MIKE21 BW for a specific hydrodynamic problem, it needs to be checked, whether the program converges at the expected rate, and whether possible errors decrease with the number of discrete elements in the expected way. Further it needs to be ensured that the solution agrees with accepted solutions produced either analytically, by another code, or experiments. Generally, numerical solutions often include three kinds of systematic errors, listed below:

- **Modeling error**, which is the *difference between the real flow and the exact solution of the mathematical model*. The principle behind Boussinesq formulations is to incorporate the effects of non-hydrostatic pressure, while eliminating the vertical coordinate, thus significantly reducing the computational effort relative to a fully three-dimensional solution. An example of introduced errors in the Boussinesq equations is their inability to describe deep water waves where the original form of the equations introduce large celerity errors. Even when the governing equations in the model are exact, approximations made at the boundaries may affect the solution.
- **Discretization error**, which is the *difference between the exact solution of the equations and the exact solution of the algebraic system of equations obtained by discretization*. In this case, where the domain is covered by a structured grid and solved by the Finite Difference method, one has to employ appropriate approximations for derivatives of a partial differential equation in each node defined by the spatial discretization step $dx = dy$. Further, a time averaging is introduced by the time discretization, dt. It is difficult to avoid a somewhat small dependency on the domain/time-resolution and calibration constants, since some averaging in time and space is necessary. When the resolution of the model is increased, the model becomes more time consuming, and hence the optimum time step- and mesh resolution is a compromise between the calculation time and the incorporated inaccuracies due to time averaging.
- **Iteration error**, which is the *difference between the iterative and exact solutions of the algebraic equations systems*. Normally, the discretization process produces a coupled set of non-linear algebraic equations which are then solved by an iterative method, since a direct solution is usually too

time consuming. The iteration process has to be stopped at some stage, which introduces iteration errors. In this case, however, a so called Alternating Direction Implicit algorithm is applied in MIKE21 BW, which is non-iterative, and hence iteration errors are not produced here.

(Ferziger and Perie, 2002)[p. 34, 329 - 332], (DHI, 2008c)

In the proceeding sections, a preliminary study of MIKE21 BW will be performed. This is done in order to ascertain the effects of different methods of modeling boundaries, and to verify that MIKE21 BW produce results in accordance with theory - hence possible modeling errors will be determined. Further it will be studied, how spatial discretization dx and time discretization dt affects model results, and how model-requirements, such as mass conservation, are fulfilled. Here possible discretization errors will be determined.

In Appendix A a description of general recommendations from the model developer, DHI, concerning model setup and model discretization is given. These will, in combination with the findings in following section, give an idea of the difference between ”optimal” and ”compromised” model-discretization for obtaining usable results.

4.1 Verification and Preliminary Study of Absorption/Reflection/Transmission in MIKE21 BW

The knowledge from the study of absorption/reflection/transmission properties in MIKE21 BW will mainly be used in proceeding simulations, to get an idea of the possibilities for tuning the model to specific problems. The following listed phenomenons will be analysed:

1. Full absorption of waves (sponge layers)
2. Full reflection of waves (land boundary)
3. Partial Reflection, -Transmission, and -Absorption (Porosity Layers)

As mentioned, the choice of the grid spacing and time step is often a compromise between accuracy and accepted computer costs. Optimum spatial- and time-discretizations, and their influence on model-output, will be studied in following sections.

4.1.1 Full Absorption of Waves (Sponge Layers)

In numerical modeling of waves, one of the biggest constraints is the computational domain which in most cases is very limited compared to nature, due to available computer power and CPU-time. To comply with the available computer capacity, open boundaries are introduced to bound the computational mesh from the surrounding infinite field which is left out of the computation. Hence the open boundaries must account for the coupling between the wave field on the computational mesh and the field in the infinite domain. It is important to make sure, that open boundaries do not affect the waves in the model domain, and that waves reflected from e.g. structures pass through the wave generation boundary without being re-reflected. In Figure 4.1 the different types of boundaries are illustrated.

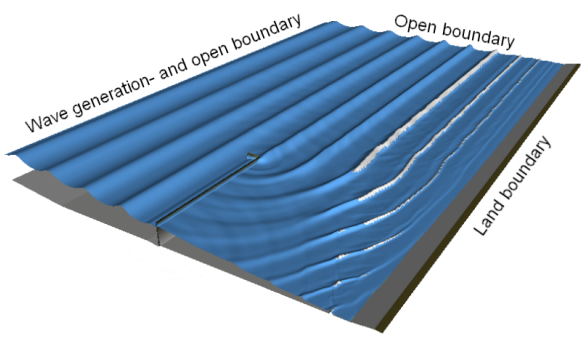

Figure 4.1 *Illustration of different types of boundaries. Figure is from (DHI, 2008d) but adjusted for use in the given case.*

Sponge Layers in MIKE21 BW

In MIKE21 BW open boundaries can be included by use of absorption obtained from so-called "sponge-layers" where the approach is to introduce artificial damping of the waves through the layers. In the code this is done by dividing the surface elevation and the flux on a number of grid lines placed next to the boundary at each time step, by a set of numbers which increase towards the open boundary. Basically, a reduction factor, μ, is specified for each grid-point in the sponge layer. In each time step the surface elevation, η, is calculated, and the η-values in the sponge layers are multiplied by the corresponding μ-factors. Thus energy is extracted from the system. In MIKE 21 BW the value in each sponge layer, μ, increases from 1, before the first layer, towards a given value at the last sponge layer following the function in (4.1). (Larsen and Dancy, 1983)

$$C_{sponge} = a^{r^{i-1}} \tag{4.1}$$

where
a and b are parameters which are depending on the number of sponge layers. $i = 1..N_{sponge}$ [-]
N_{sponge} is the total amount of sponge layers [-]
(Larsen and Dancy, 1983)

To illustrate the absorption effect of the sponge layers in a simple 1D example, two layers with a width of $5\Delta x$ are arranged symmetrical about $x = 250$, as shown in Figure 4.2. The grid spacing in the domain is $\Delta x = 10\ m$, and at the left boundary a regular wave is generated with a wave height of $H = 1\ m$. From Figure 4.2 it can be seen, that the surface elevation is hardly visible after the double passage through the sponge layers.

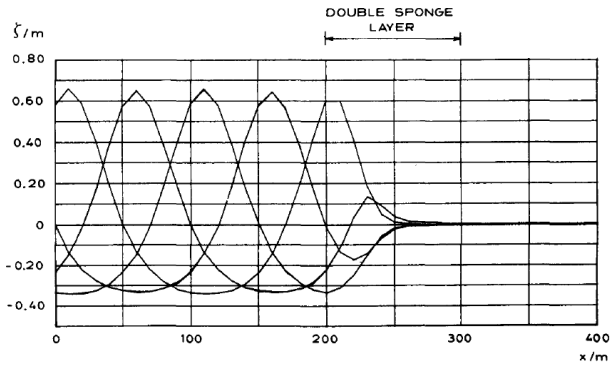

Figure 4.2 *1D example of the absorption effect from two sponge layers with a width of* $5\Delta x$*, arranged symmetrical about* $x = 250$ *(Larsen and Dancy, 1983).*

Absorbtion Efficiency as Function of Sponge Layer Thickness

(DHI, 2008d) recommends to apply a sponge layer thickness corresponding to at least one wave length of the most energetic waves (corresponding to the spectral peak wave period) in order to achieve the best efficiency.

A small study is performed to analyse how the absorption efficiency is connected to the number of layers. This is done using a simple setup consisting of a 15 m deep wave flume with a length of $x = 500\ m$ and a width of $y = 100\ m$, as illustrated in Figure 4.3. The flume is implemented in MIKE21 BW with a spatial spacing of $dx = dy = 2\ m$. Two sections with an equal amount of sponge layers, corresponding to the length x, are included in the model. One section behind the wave generation line at the left boundary and one section at the right boundary. Three gauges are placed in the flume to determine reflection, placed with appropriate distances proposed by (Mansard and Funke, 1980). The study is carried out by determining the reflection coefficient, K_r, from different amounts of layers at the sponge sections in case of both regular and irregular waves.

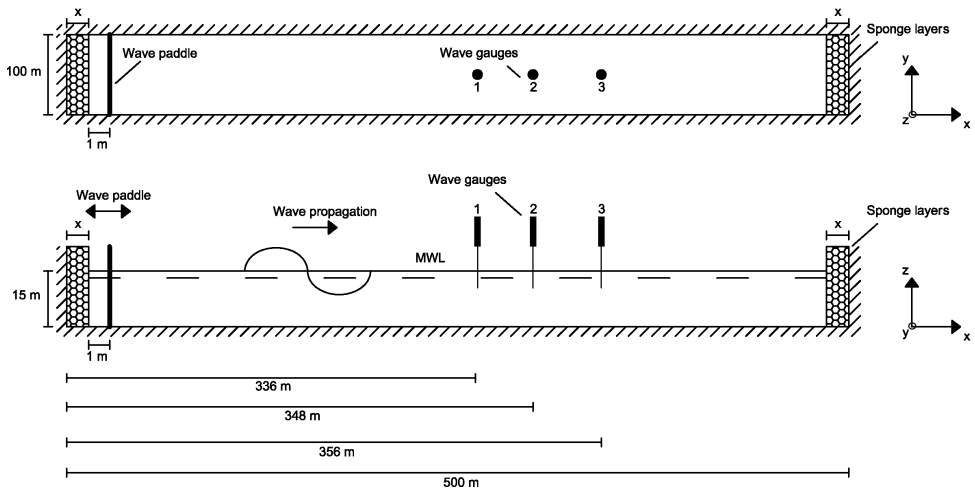

Figure 4.3 *Set-up, implemented in MIKE21 BW, for the study of absorption efficiency in MIKE21 BW.*

Regular Waves In the regular test case, a wave with height $H = 2\ m$ and period $T = 8\ s$, resulting in a wave length of $\approx 80\ m$, is generated at the left boundary with a time discretization of $dt = 0.1\ s$. In the regular case the reflection coefficient, K_r, is determined from time series obtained from gauge 1 and 2 illustrated in Figure 4.3 by use of the method proposed by (Goda and Suzuki, 1976). K_r as a function of the number of layers in the two sections is illustrated in Figure 4.4. As expected, the reflection from the absorbing sponge sections is decreasing with an increasing amount of sponge layers. It should, however, be noted, that the wave energy is not completely absorbed from the sponge section. Even in case of a sponge section width of 100 m (50 layers), which is bigger than the wave length, a reflection coefficient of $K_r \approx 0.015$ is obtained from the open boundary. The model discretization may, however, slightly affect the results.

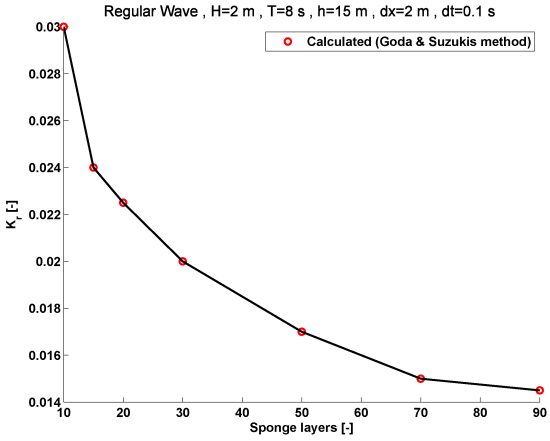

Figure 4.4 *K_r as a function of the number of sponge layers in Figure 4.3.*

Irregular Waves In the irregular test case, a JONSWAP spectrum is generated with $\gamma = 3.3$, $H_s = 2\ m$, $T_p = 8\ s$, and $T_{min} = 4\ s$. In Figure 4.5 the variation of K_r through the wave spectrum, with different amounts of sponge layers, is illustrated. In the irregular case K_r is determined from (4.2) to which the reflected spectrum is determined in WaveLab (AAU, 2010) by use of the method proposed by (Mansard and Funke, 1980) with output from gauge 1, 2, and 3. Again, a small reflection is present, which is, as for the case of regular waves, slightly decreasing with an increasing amount of layers. The mean values of K_r in case of 10 sponge layers and 90 sponge layers is 0.0470 and 0.0296, respectively.

$$K_r = \sqrt{\frac{S_r(f)}{S_i(f)}} \tag{4.2}$$

where
K_r is the reflection coefficient $[-]$
$S_r(f)$ is the reflected spectrum $[m^2 s]$
$S_i(f)$ is the incident spectrum $[m^2 s]$

The almost coinciding measured spectrum (measured from a single gauge) and standard spectrum in Figure 4.5, indicates, that despite the presence of minor reflection, the reflected spectrum only has a small influence on the waves in the flume.

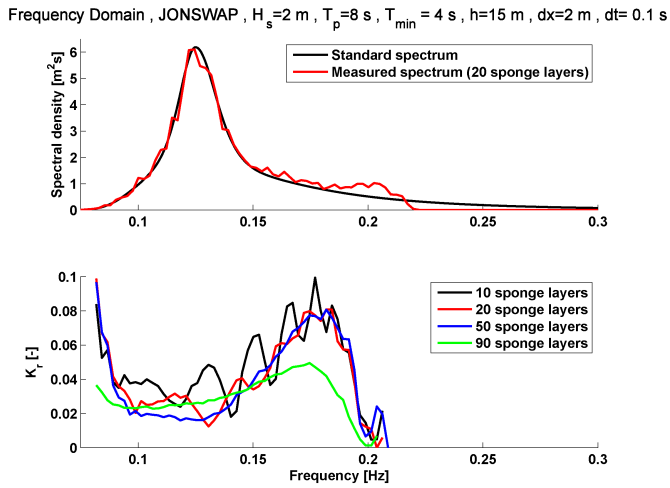

Figure 4.5 *Variation of K_r through the wave spectrum, in case of different amounts of sponge layers.*

Influence on Absorption from Time- and Spatial Discretization

In order to study how the reflection depends on dt and dx, a regular wave with $H = 0.5\ m$ and $T = 6\ s$ is used to compare the value of K_r at different increment sizes. To fulfill the requirements of the Courant number criterion, presented in Appendix A, a relatively small variation of dt is given ($dt = 0.1\ s$ - $dt = 0.01\ s$), while a bigger variation of dx is performed ($dx = 0.2\ m$ - $dx = 20\ m$). The increments are normalized with respect to T and L. In addition to the study of correlation between time-/spatial discretization and K_r, the correlation with the wave height H is studied in order to determine whether numerical damping may occur in coarse grids. Numerical damping introduces an incident H which is smaller than the specified. The variation of K_r and the relative deviation of the modelled wave amplitude $a = H/2$ from the true amplitude $a = 0.25\ m$, can be seen in Figure 4.6 and Figure 4.7. It should be noted, that the axes in the two figures are not identical.

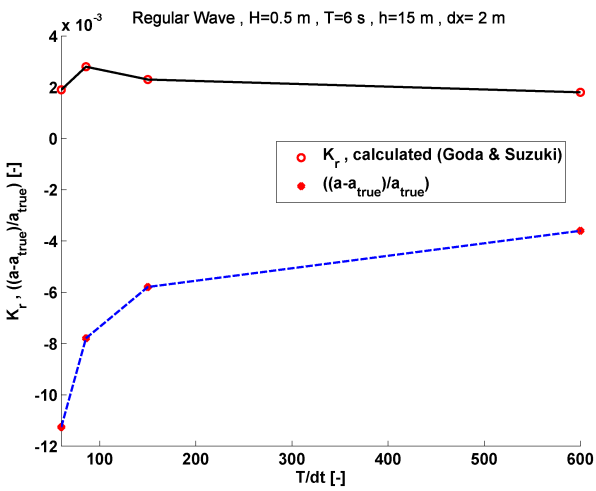

Figure 4.6 *K_r and the relative deviation of the modelled wave amplitude $a = H/2$ from the true amplitude $a = 0.25\ m$ as a function of the size of dt.*

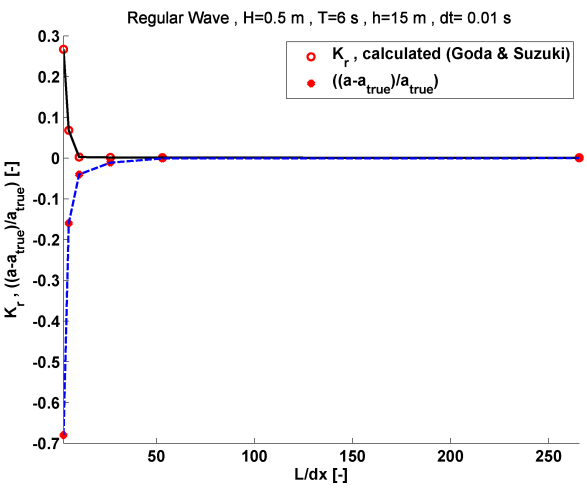

Figure 4.7 *K_r and the relative deviation of the modelled wave amplitude $a = H/2$ from the true amplitude $a = 0.25\ m$ as a function of the size of dx.*

From Figure 4.6 it can be seen, that in the relative small tested interval of dt, no variation of either K_r appears nor H. A bigger variation of K_r and H appears when varying dx, which can be seen from Figure 4.7. When changing the increment of $dx = 2\ m$, which was used in Figure 4.5, to $dx = 0.2$, the reflection coefficient changes from $K_r = 0.0015$ to $K_r = 0.0008$, and the wave height changes from $H = 0.247\ m$ to $H = 0.2495\ m$, which is a relative improvement of 87.5 %, and 1 %, respectively. A spatial resolution of $L/dx = 20$ to $L/dx = 40$, stated by (DHI, 2008d) seems to be sufficient, concerning absorption.

4.1.2 Full Reflection of Waves

Full reflection appears from non-absorbing/transmitting structures. In the test case a fully reflecting 10 m high wall is inserted at the right boundary, and a fully absorbing sponge section (90 sponge layers) is inserted at the left boundary, behind the wave generation line. Alongside an analysis of the reflection, the flux through a vertical section in the flume is determined, to study whether mass conservation is fulfilled. Since the vertical wall at the right boundary is supposed to reflect all wave energy, the incident flux should equal the reflected flux. The test set-up is illustrated in Figure 4.8.

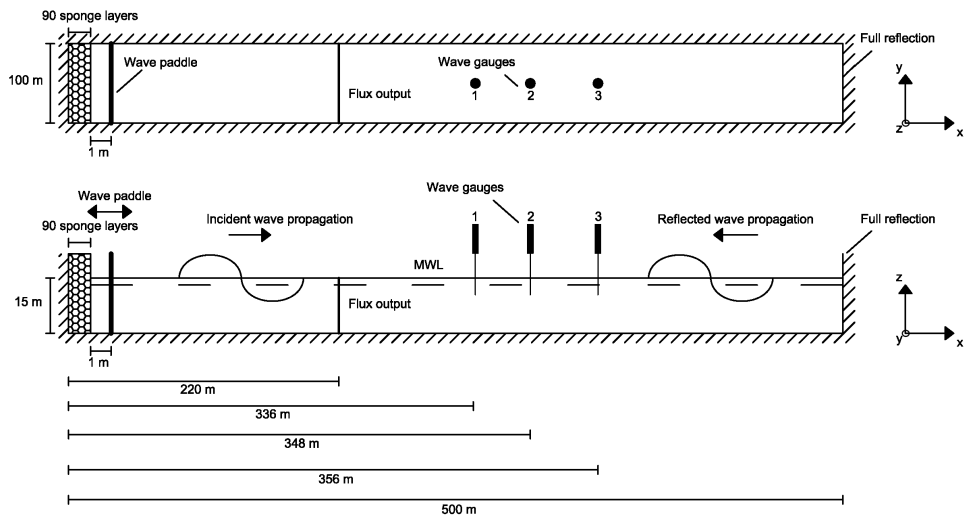

Figure 4.8 *Set-up for testing the ability of MIKE21 BW to model full reflection, and to test whether conservation of mass is fulfilled.*

Only an irregular wave spectrum is tested for this case, a JONSWAP spectrum with $\gamma = 3.3$, $H_s = 2\ m$, $T_p = 8\ s$, and $T_{min} = 4\ s$. In Figure 4.9 the variation of K_r through the spectrum is illustrated, and in Figure 4.10 the flux at x=220 m is plotted. Positive values in Figure 4.10 indicates a right propagating flux.

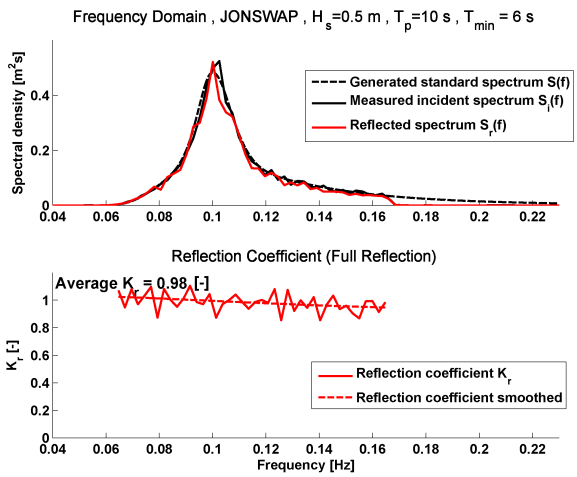

Figure 4.9 *Variation of K_r through a JONSWAP spectrum.*

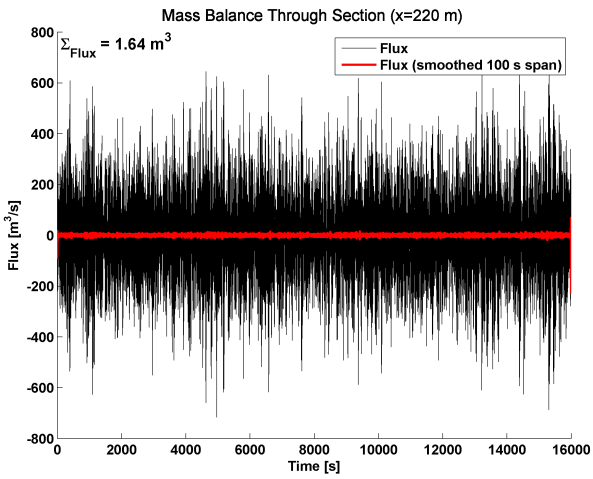

Figure 4.10 *Flux at $x = 220\ m$ in Figure 4.8.*

From Figure 4.9 it can be seen, that K_r slightly decreases with increasing frequency, f, (decreasing wave period, T). The mass budget in Figure 4.10 is very close to zero and it should be noted, that in order to obtain a more exact total flux through the vertical section, the surface must be stagnant at the last time step of measurement. This is not the case here, since waves were generated up until the last output step. Hence it is concluded that conservation of mass is fulfilled.

Influence on Reflection from Time- and Spatial Discretization

In order to study how the reflection depends on dt and dx, a regular wave with $H = 0.5\ m$ and $T = 6\ s$ is used to compare the value of K_r at different increment sizes. In Figure 4.11 and 4.12, K_r is calculated from simulations with different increments of dt and dx, respectively. Again, the increments are normalized to T and L, and a relatively small variation of dt is given ($dt = 0.1\ s$ - $dt = 0.01\ s$), while a bigger variation of dx is performed ($dx = 0.2\ m$ - $dx = 20\ m$).

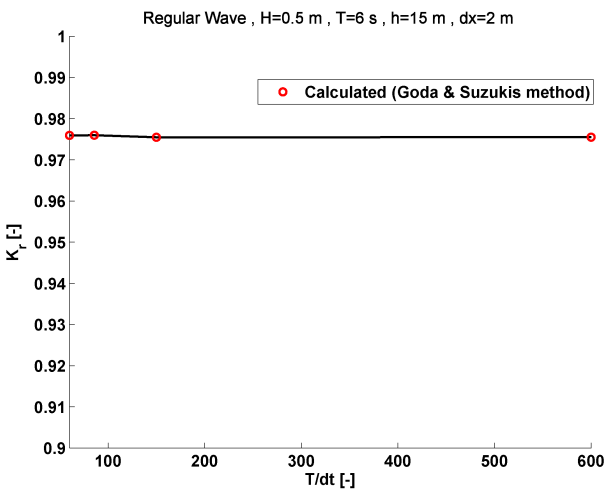

Figure 4.11 *K_r from simulations with different increments of dt.*

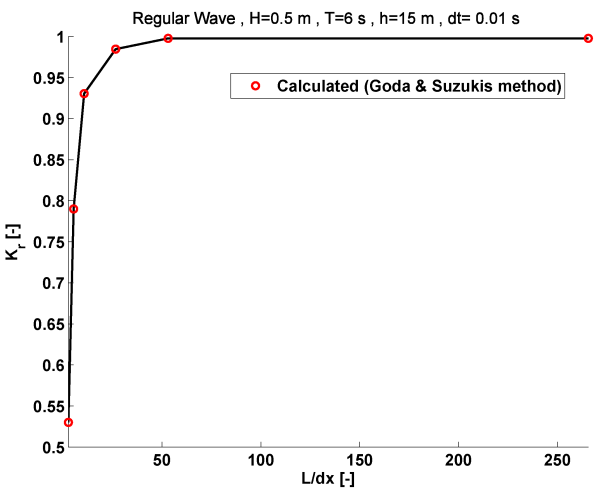

Figure 4.12 *K_r from simulations with different increments of dx.*

From Figure 4.11 it can be seen, that a variation of dt does not have any influence on K_r. In contrast it can be seen from Figure 4.12, that the spatial discretization dx has a greater influence on the reflection, as the case from reflection from absorbing layers in Section 4.1.1. Again, a spatial resolution of $L/dx = 20$ to $L/dx = 40$ seems to be sufficient.

4.1.3 Partial Reflection, -Transmission, and -Absorption (Porosity Layers)

Porous structures, which are partly reflecting-, partly transmitting-, and partly absorbing wave energy, can be modelled by use of so called porosity layers in MIKE 21. These are layers with a specified porosity factor varying from 0 to 1, where 0 specifies a fully impermeable structure, and 1 specifies open water grid. The effect of the porosity layers is introduced by additional turbulent friction terms for describing losses due to flow through the porous structure. Porosity layers introduces partial reflection and absorption if they are backed up by land, and partial reflection and transmission if open water grid points are to be found behind the porosity layers.

Porosity Layers in MIKE21 BW

The transmission- and reflection properties from porosity layers in MIKE21 BW depends on the water depth h, wave height H, wave period T, and width of porous structure $x_{\text{porosity layer}}$. (DHI, 2008d)

In this case, when implementing a WD in MIKE, the porosity coefficients and -layers will be tuned and calibrated to fit the wanted amount of reflection and transmitted energy. When inputting the above listed parameters, K_r and the transmission coefficient, K_t, can be determined from the MIKE 21 BW toolbox based on the theory from (Madsen, 1983). K_t describes the amount of transmitted wave energy through e.g a structure, and can be determined by use of (4.3).

$$K_t = \sqrt{\frac{S_i(f)}{S_t(f)}} \tag{4.3}$$

where
$S_t(f)$ is the transmitted spectrum $[m^2 s]$
$S_i(f)$ is the incident spectrum $[m^2 s]$

Analytically Determined Variation of K_r and K_t

MIKE21 toolbox can be used to estimate reflection and transmission of linear shallow water waves from a vertical porous wave absorber on a horizontal bottom. The theoretical solution is further described in (Madsen, 1983), where it is emphasized, that when considering reflection of irregular wave trains, the analytical solution is not very accurate, due to non-linear wave height and wave length.

To get an idea of the dependence on reflection and transmission in the model, K_r and K_t are determined from the MIKE21 toolbox as a function of the porosity factor S, width of porous structure $x_{\text{porosity layer}}$, T, H, and h, respectively. It is seen, that K_r and K_t are coupled, where the dependence of increasing parameters, affecting K_r and K_t, are listed in Table 4.1.

Increasing values of:	K_r	K_t
T	Increasing	Increasing
H	Increasing	Decreasing
$x_{\text{porosity layer}}$	Varying	Decreasing
h	Decreasing	Increasing
S	Decreasing	Increasing

Table 4.1 *Dependence of increasing parameters, and coupling between K_r and K_t.*

Comparison of Modelled- and Analytically Determined K_r and K_t

In order to study whether K_r, determined from the numerical model, corresponds to the analytical value from MIKE21 toolbox, a simple set-up, is implemented in MIKE21 BW. The set-up consists of a wave flume with transmitting obstacle in the middle (porosity layers), as illustrated in Figure 4.13. A sufficient spatial- and time-discretization is applied, determined from the requirement for convergence in case of full reflection in Section 4.1.2.

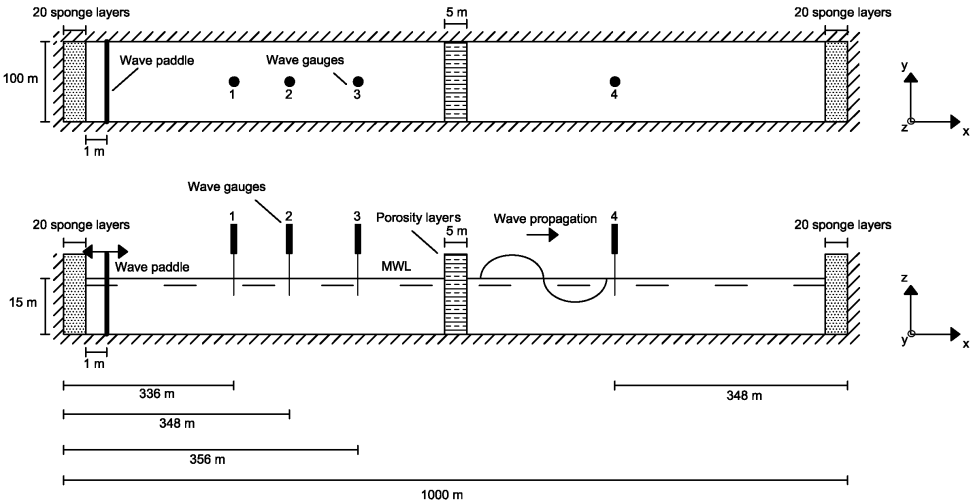

Figure 4.13 *Set-up implemented in MIKE21 BW, consisting wave flume with a transmitting obstacle consisting of porosity layers.*

A regular wave with $H = 0.5\ m$, and $T = 8\ s$ is generated, and the reflection and transmission is determined from gauge 1, 2, 3, and 4 in Figure 4.13. The comparison of the modelled- and analytical -determined K_r and K_t, can be seen in Figure 4.14. Here it is concluded, that a good agreement is obtained.

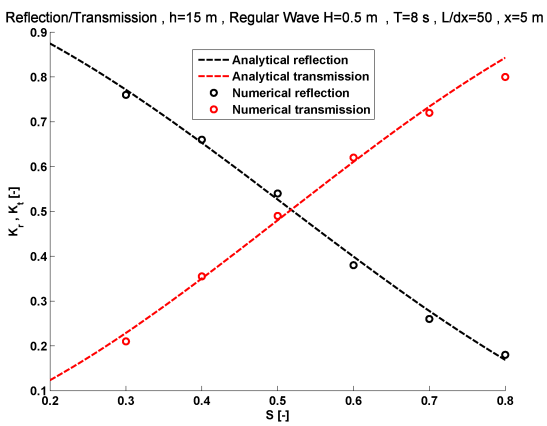

Figure 4.14 *Comparison of modelled- and analytical -determined K_r and K_t*

Spectral Dependent Modelled K_r and K_t

In case of irregular wave trains (DHI, 2008d) recommends to specify H_s and T_p when using the MIKE21 toolbox, which will then give and idea of the reflection from a given porous structure. In the following, the variation of K_r and K_t across a wave spectra will be analysed. In order to study the frequency

dependent porosity properties, the wave flume with a transmitting obstacle consisting of porosity layers, illustrated in Figure 4.13, is used. A JONSWAP spectrum is generated with $\gamma = 3.3$, $H_s = 0.5\ m$, $T_p = 10\ s$, and $T_{min} = 6\ s$. The reflection and transmission is determined from gauge 1, 2, 3, and 4 in Figure 4.13. In Figure 4.15 K_r and K_t can be seen in case of a porosity coefficient of $S = 0.7$, and in Figure 4.16 in case of a porosity coefficient of $S = 0.9$. Further, the degree of absorbed power P_a/P_i in deep water is calculated, and shown in the figures, by use of conservation of energy at deep water (no bottom dissipation), with the expression in (4.4).

$$
\begin{aligned}
1 &= K_a^2 + K_r^2 + K_t^2 \Downarrow \\
K_a^2 &= 1 - K_r^2 - K_t^2 \\
\frac{P_a}{P_i} &= 1 - K_r^2 - K_t^2
\end{aligned}
\tag{4.4}
$$

where
$\frac{P_a}{P_i}$ is the degree of absorbed power $[-]$
K_r^2 is the amount of absorbed energy $[W]$
K_r^2 is the amount of reflected energy $[W]$
K_t^2 is the amount of transmitted energy $[W]$

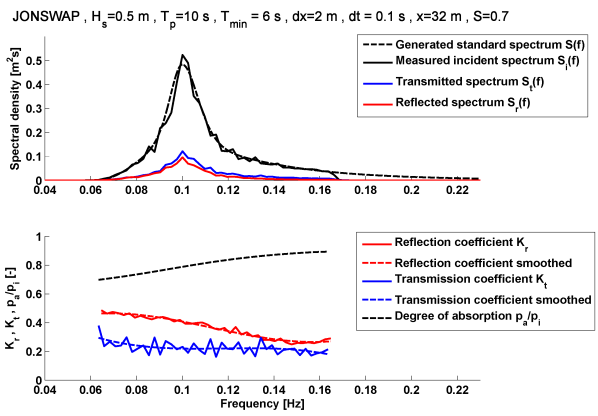

Figure 4.15 *Variation of K_r, K_t, and P_a/P_i through a spectrum in case of a porosity coefficient of $S = 0.7$.*

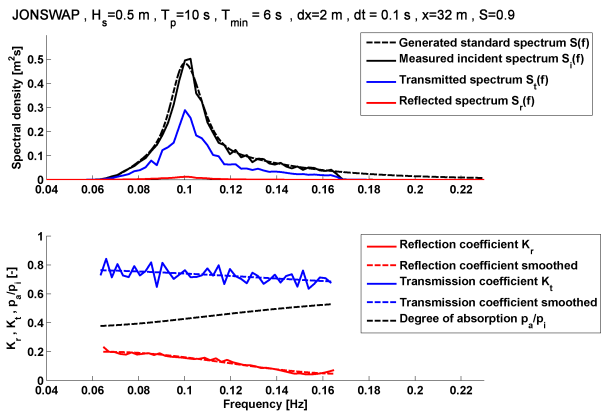

Figure 4.16 *Variation of K_r, K_t, and P_a/P_i through a spectrum in case of a porosity coefficient of $S = 0.9$.*

As expected from Table 4.1, it can be seen in Figure 4.15 and 4.16, that when increasing the porosity from $S = 0.7$ to $S = 0.9$, an increase of transmission and decrease of reflection is obtained. Further it is observed, that a decreasing T (high frequencies in the JONSWAP spectrum) results in both a decreasing K_t and K_r, which was also expected from Table 4.1.

From the MIKE21 toolbox it is found, that $K_r \approx 0.4$ and $K_t \approx 0.3$ for $S = 0.7$ when $T = 10\ s$, $H_s = 0.5\ m$, $h = 15\ m$, and $x = 32\ m$, which is approximately found for the spectral peak period, T_p, and significant wave height, H_s, in Figure 4.15. The same approximate match is found in case of $S = 0.9$, and hence the MIKE21 toolbox can be used as a good guideline of expected reflection and transmission for both regular and irregular waves despite the inaccuracies when considering non-linear waves. This will be kept in mind for use in a later chapter when implementing a WD in the model.

4.2 Wave Scattering in MIKE21 BW

Incident waves approaching a farm of WD's are redistributed through several different physical processes. Among these is the wave scattering, in the form of diffraction. Diffraction is described by the diffraction/disturbance coefficient K_d, which is defined as the diffracted/disturbed wave height divided by the incident wave height, H/H_i.

In this section, the ability of the MIKE21 BW module to describe wave diffraction around fully- and partial reflecting obstacles will be analysed. Further it will be studied, how a finite width of the domain in e.g a laboratory basin may affect the wave-field, which is important in later laboratory experiments. However, first it will be studied how the spatial discretization influences wave disturbance around an arbitrary obstacle.

4.2.1 Influence on Wave Scattering from Spatial Discretization

From Section 4.1.1 and Section 4.1.2 it was seen, that especially the spatial resolution dx has a great influence on the accuracy of the model-results, and hence only the influence from dx will be tested in the following, and dt will be chosen sufficient to comply with requirements of the Courant number criteria.

In Figure 4.17 the implemented test set-up in MIKE21 BW is illustrated, where a fully reflecting obstacle is placed in the domain. The wave disturbance, K_d, measured in an arbitrarily point located behind a fully reflecting obstacle, is compared for different dx. In case of an incident irregular JONSWAP spectrum with $H_s = 0.5\ m$, $T_p = 6\ s$, and $T_{min} = 3\ s$, it is observed, that K_d stabilizes after some time, see Figure 4.18. Hence converged K_d-values can be used for comparison in the following.

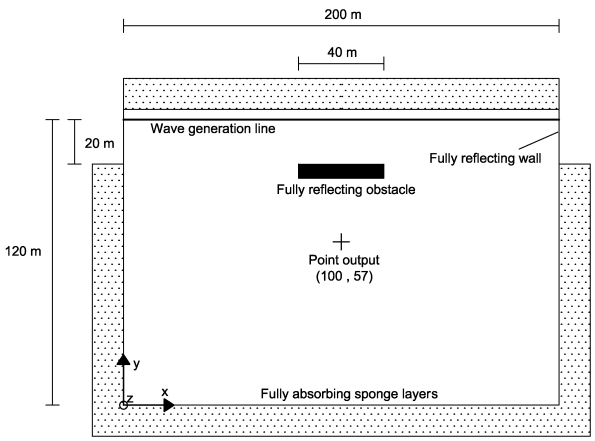

Figure 4.17 *Set-up implemented in MIKE21 BW, consisting of a wave basin with a fully reflecting obstacle.*

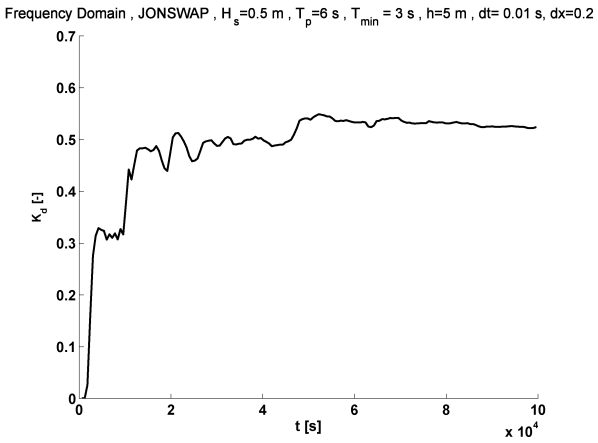

Figure 4.18 *Time series of K_d extracted at point $(x, y) = (100m, 57m)$, where it can be seen that convergence appears after some time.*

In Figure 4.19 the converged value of K_d is plotted as a function of the amount of grid-points per wavelength, L_p/dx. It is seen, that approximately $L_p/dx = 50$ is sufficient for accurately describing the wave disturbance.

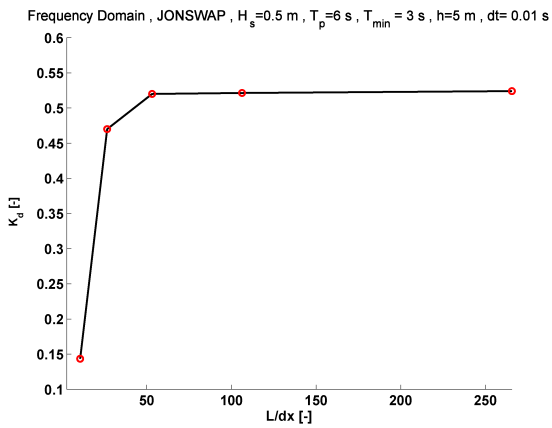

Figure 4.19 *K_d as a function of the amount of grid-points per wavelength, L_p/dx. K_d is extracted at point $(x, y) = (100m, 57m)$.*

4.2.2 Wave Disturbance from Absorbing/partial Reflecting Boundaries

As mentioned in Section 4.2.1, it is necessary to include fully- or partially absorbing layers at boundaries where the wave propagation is perpendicular. These boundaries, however, introduces wave disturbance due to diffraction. Partially absorbed contours with respect to the incident waves are, according to (Mattioli and Turrini, 1988), obtained when the boundaries parallel to the wave propagation have a reflection coefficient generally less than one, $K_r < 1$.

In the following, it will be studied how the wave field along the partially absorbing boundaries is affected from different values of K_r. In Figure 4.20 the test set-up, implemented in MIKE21 BW, is illustrated, where porosity layers are included at the boundaries parallel to the wave propagation. Then, by applying a JONSWAP spectrum with $H_s = 0.5\ m$, $T_p = 6\ s$, and, $T_{min} = 3\ s$, the wave disturbance can be obtained. In Figure 4.21 the contours of $K_d = 0.5$ for $K_r = 0.2$ and $K_r = 0.8$ are illustrated. As expected, the wave field around the absorbing boundaries is subjected to a greater disturbance for lower values of K_r - corresponding to greater absorption.

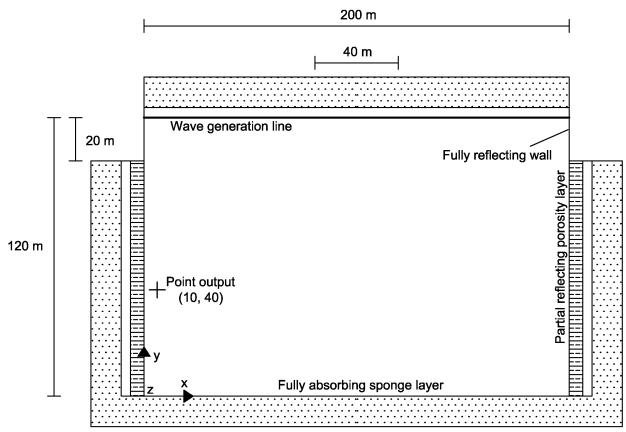

Figure 4.20 *Set-up implemented in MIKE21 BW, consisting of a wave basin with partial reflecting porosity layers at the sides.*

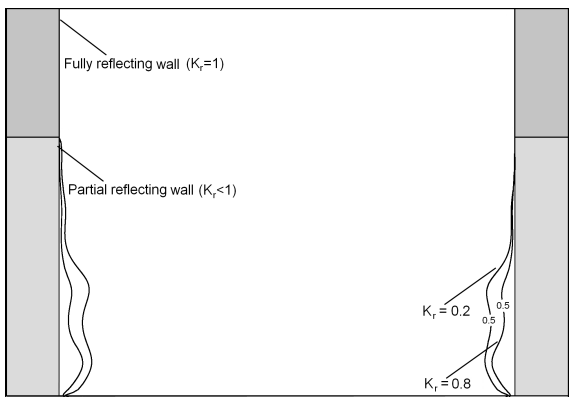

Figure 4.21 *Wave disturbance contours, $K_d = 0.5$, for $K_r = 0.2$ and $K_r = 0.8$.*

Further, timeseries of K_d are extracted from point $(x, y) = (10m, 40m)$ as illustrated in Figure 4.20. These are plotted in Figure 4.22, and the converged values of K_d as a function of K_r are plotted in Figure 4.23. Here it can be seen, that K_d is exponentially dependent on K_r.

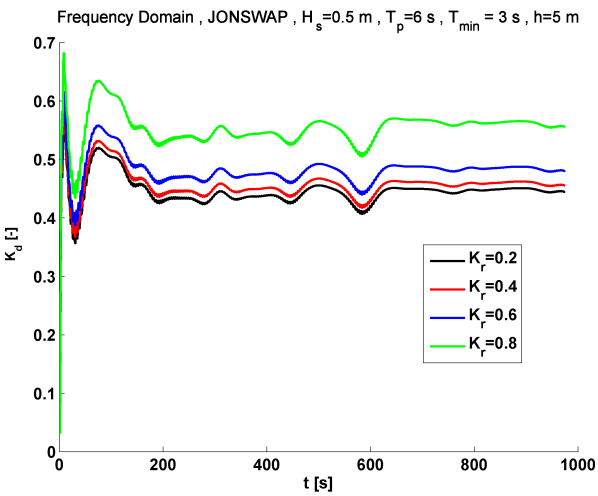

Figure 4.22 *Timeseries of K_d in case of varying K_r extracted from point $(x, y) = (10m, 40m)$.*

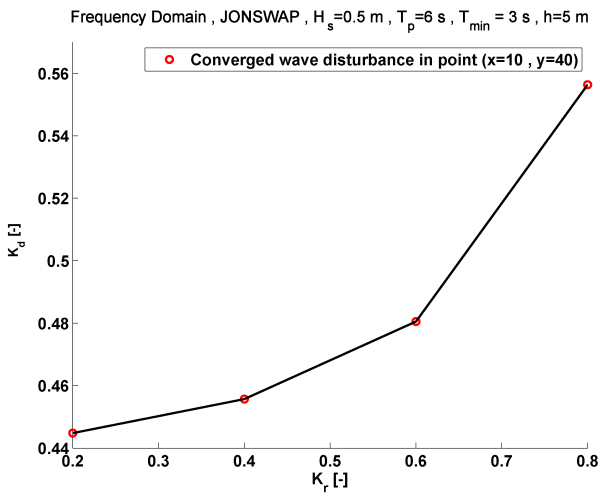

Figure 4.23 *Converged values of K_d, extracted from point $(x, y) = (10m, 40m)$, as a function of K_r.*

4.2.3 Verification of Wave Scattering around Fully and Partial Reflecting Obstacles

From the knowledge of sufficient spatial resolution, dx, a verification of the ability of MIKE21 BW to describe diffraction can be performed. Based on the solution of (Sommerfeld, 1896) for diffraction of light, (Penney and Price, 1952) has proposed an analytic solution for diffraction of water waves around a semi infinitely long impermeable breakwater. Further, they derived a solution for waves transmitting through a gap between two breakwaters by superposing the solution obtained for a single breakwater. (Kyung and Hanna, 2008) has extended the study of (Penney and Price, 1952) to waves scattered by a partial reflecting breakwater, where the wave-scattering is studied based on the linear potential wave theory. (Kyung and Hanna, 2008) performed the study to test the tranquillity of a harbor entrance by changing the reflection coefficient at the front face of the breakwater.

In this case, when modeling a farm of WD's in MIKE, it is highly relevant to test the ability of the program to describe diffraction both around a single WD, and through the gap of WD's lying side by side. The following listed test-cases will be analysed and compared to the analytic results obtained by (Kyung and Hanna, 2008).

- **Case 1:** Diffraction from fully- and partial reflecting breakwater (single WD).
- **Case 2:** Diffraction from fully- and partial reflecting gap between breakwaters (side lying WD's).

Case 1: Diffraction from Fully- and Partial Reflecting Breakwater

The plane view of the model setup, consisting of a detached breakwater, and the associated coordinate system is shown in Figure 4.24. The dimensions of the setup are presented by the dimensionless coordinates; x/L and y/L, and the origin of the system is located at the center of the tip of the breakwater. The spatial resolution of the model is chosen to $dx = 1$, resulting in $dx/L \approx 57$, which was found to be sufficient in Section 4.2.1. The analytical determination of water wave diffraction from (Kyung and Hanna, 2008) is based on the assumption of constant phase velocity, and hence a constant water depth of $h = 6\ m$ is used in the model. A regular wave is generated with an incident propagation-direction which is normal to the breakwater from the negative infinity in the y-direction. The wave height and period are chosen arbitrarily to $H = 0.5\ m$ and $T = 8\ s$. At boundaries, where the wave propagation is perpendicular, land is specified, to avoid "false" diffraction. At boundaries where the wave propagation is partly or fully normal, sponge layers are included to absorb wave energy and avoid "false" reflection. The breakwater in MIKE21 BW is implemented as a porous permeable structure which is most consistent with the nature of the WD where a part of the incident wave energy is transmitted through the structure, and hence the ability to model diffraction from a permeable structure is studied.

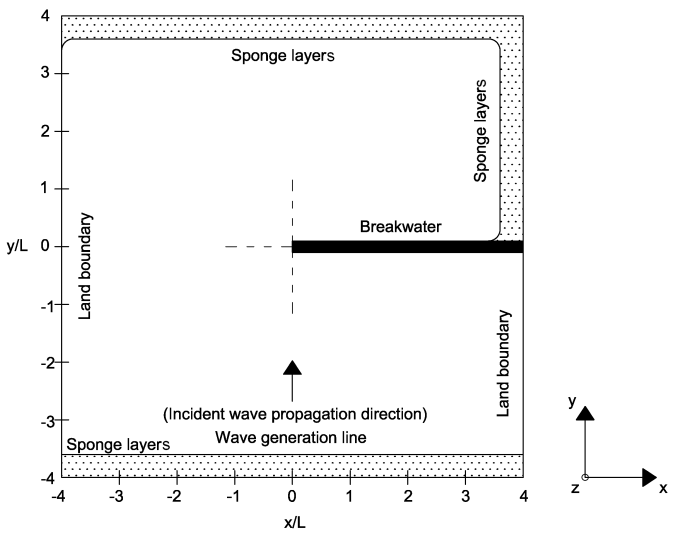

Figure 4.24 *Plane view of the model setup, consisting of a detached breakwater, and the associated coordinate system*

The analytic diffraction around a fully- and partial reflecting breakwater, determined from (Kyung and Hanna, 2008), is presented in Figure 4.27 and 4.28 in case of $K_r = 1$ and $K_r = 0.5$, respectively. It is seen, that the diffraction coefficient behind the breakwater is not affected by the reflection coefficient of the breakwater. The standing wave on the seaside of the breakwater, however, decreases as the reflection coefficient decreases. (Kyung and Hanna, 2008)

In Figure 4.25 and 4.26 the numerically determined diffraction from MIKE21 BW is shown in case of $K_r = 1$ and $K_r = 0.5$, respectively. The partial reflection is modelled by use of permeable porosity layers, and hence transmission through the breakwater appears. This is indicated in Figure 4.26 where a small part of disturbance appears behind the breakwater, which is not present in the analytical result in Figure 4.28. However, when taking the modelled boundaries in MIKE21 into account (porosity layers/sponge layers/land boundaries), approximately identical results are obtained if the modelled- and analytically obtained diffraction is compared.

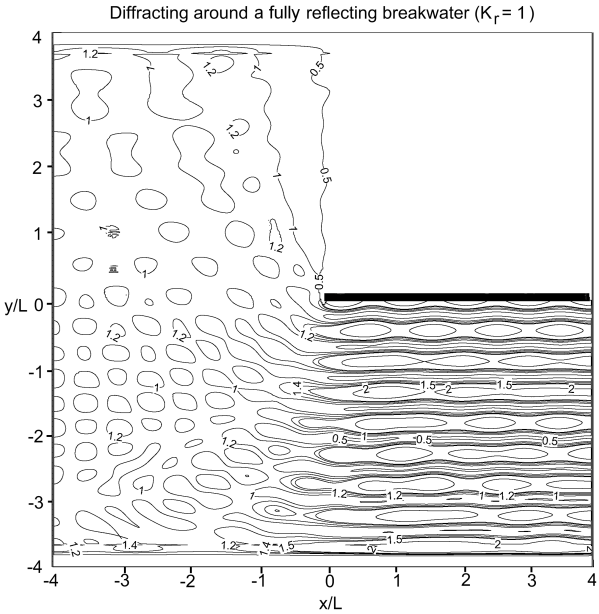

Figure 4.25 *Diffraction around a fully reflecting breakwater, $K_r = 1$, determined in MIKE21, and an overlying diffraction diagram.*

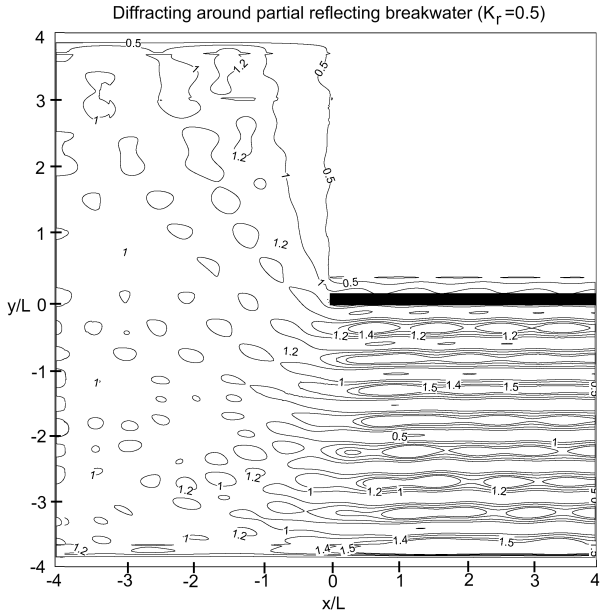

Figure 4.26 *Diffraction around a partial reflecting breakwater, $K_r = 0.5$, determined in MIKE21.*

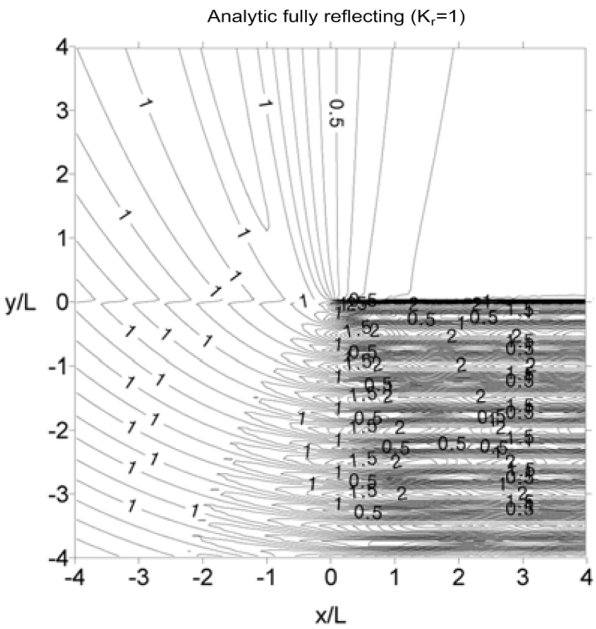

Figure 4.27 *Analytic diffraction around a fully reflecting breakwater, $K_r = 1$, determined from (Kyung and Hanna, 2008).*

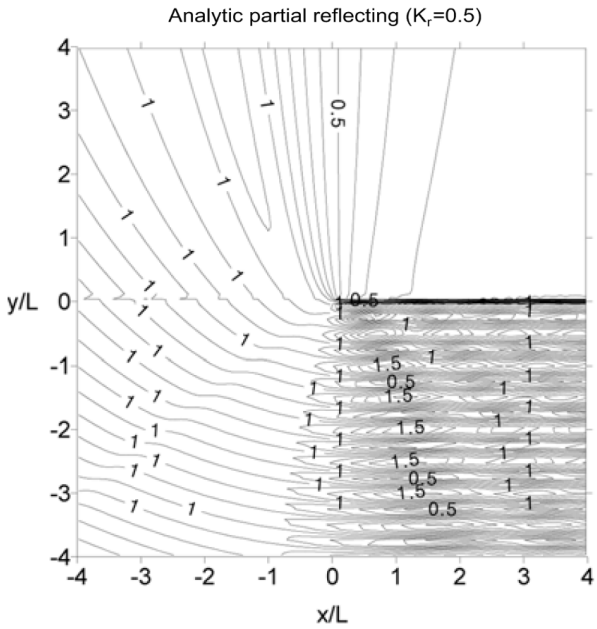

Figure 4.28 *Analytic diffraction around a partial reflecting breakwater, $K_r = 0.5$, determined from (Kyung and Hanna, 2008).*

In addition to the partial- and fully reflecting structures, a fully absorbing breakwater is implemented in Figure 4.29. This is done, since the diffraction around a breakwater with $K_r = 0$ becomes the solution of (Sommerfeld, 1896), and by overlying a so-called "diffraction diagram", obtained from the Sommerfeld solution, a comparison can be made. From Figure 4.29 it can be concluded that a good agreement is obtained.

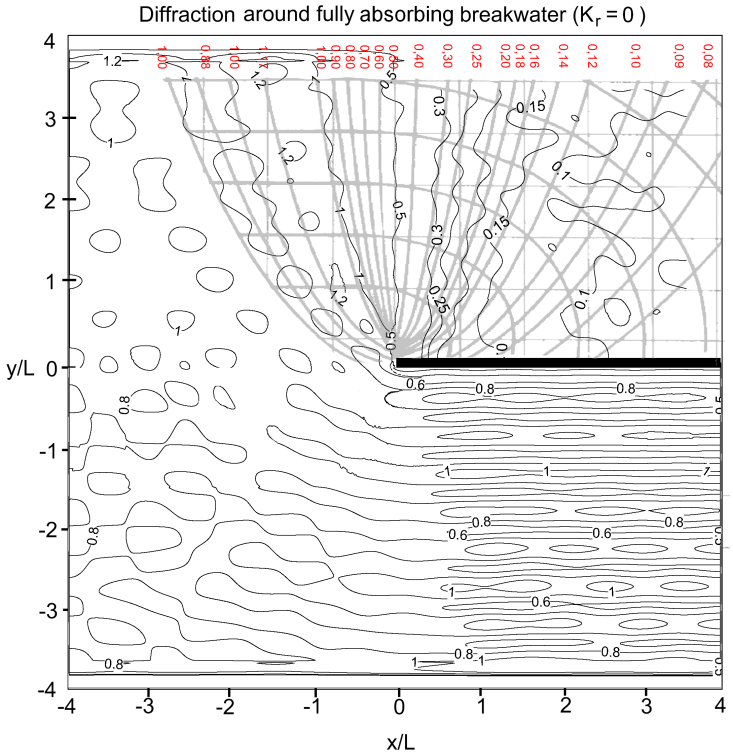

Figure 4.29 *Diffraction around a fully absorbing breakwater, $K_r = 0$, determined in MIKE21, and an overlying diffraction diagram proposed by (Sommerfeld, 1896).*

Case 2: Diffraction from Fully- and Partial Reflecting Gap Between Breakwaters.

The plane view of the model setup, consisting of two detached breakwaters with a gap of width $B = 2L$, and the associated coordinate system is shown in Figure 4.30. As in case 1. the dimensions of the setup are presented by the dimensionless coordinates; x/L and y/L with the origin of the system located at the center of the gap. An incident regular wave is generated perpendicular to the breakwater from the negative infinity in the y-direction. The wave height and period is chosen arbitrarily to $H = 0.5\ m$ and $T = 8\ s$, and a constant water depth of $h = 6\ m$ is used in the model.

Again, the breakwater in MIKE21 BW is implemented as a porous permeable structure to study the ability to model diffraction from a permeable structure (WD).

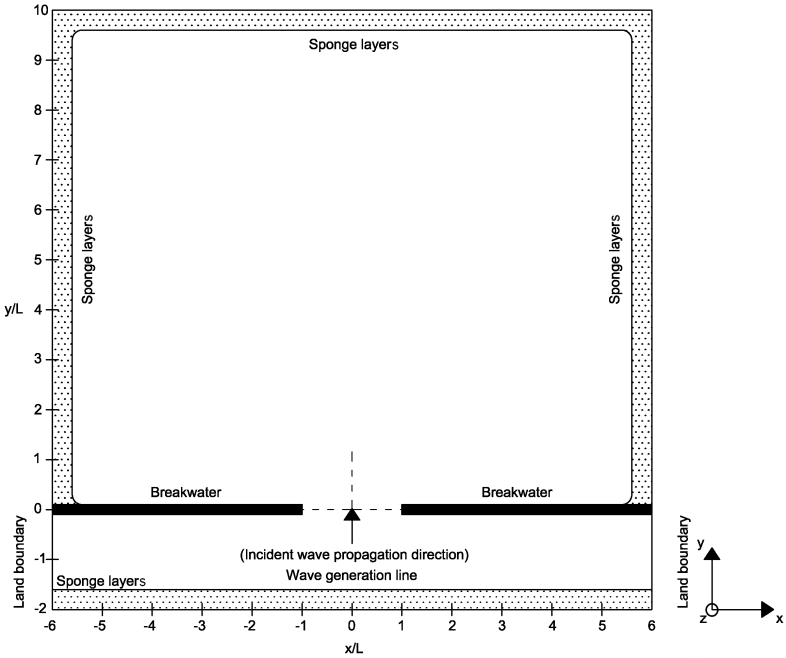

Figure 4.30 *Plane view of the model setup, consisting of two detached breakwaters with a gap of width $B = 2L$, and the associated coordinate system.*

The analytical diffraction through the gap of two fully- and partial reflecting breakwaters, determined from (Kyung and Hanna, 2008), is presented Figure 4.31 and 4.32 in case of $K_r = 1$ and $K_r = 0.5$, respectively. Again, from Figure 4.31 and 4.32 it is seen, that the diffraction coefficient behind the breakwaters is not affected by the reflection coefficient. In the seaward side of the gap, however, in addition to the decrease of standing wave height in front of the breakwaters ($x/L < -1$ and $x/L > 1$), the agitation in front of the gap ($-1 \leq x/L \leq 1$) also reduces, as the reflection coefficient decreases. (Kyung and Hanna, 2008)

In Figure 4.33 and 4.34 the numerically determined diffraction from MIKE21 BW is shown in case of $K_r = 1$ and $K_r = 0.5$, respectively. Again, a difference appears between the modelled partial reflecting breakwaters, compared to Figure 4.32, since the structures are implemented in MIKE21 BW by use of permeable porous layers, which introduces an additional transmission, unlike the analytic solution. However, when comparing the wave disturbance (diffraction) through the gap, approximate identical results are found in the analytical and modelled cases.

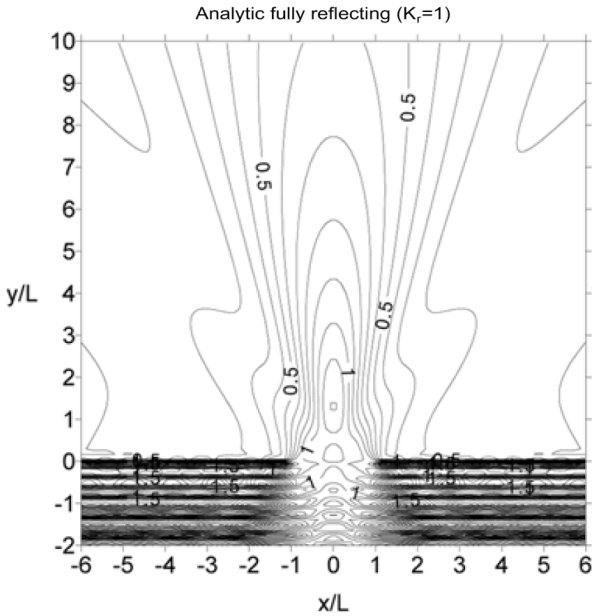

Figure 4.31 *Analytic diffraction through the gap of two fully reflecting breakwaters, $K_r = 1$, determined from (Kyung and Hanna, 2008).*

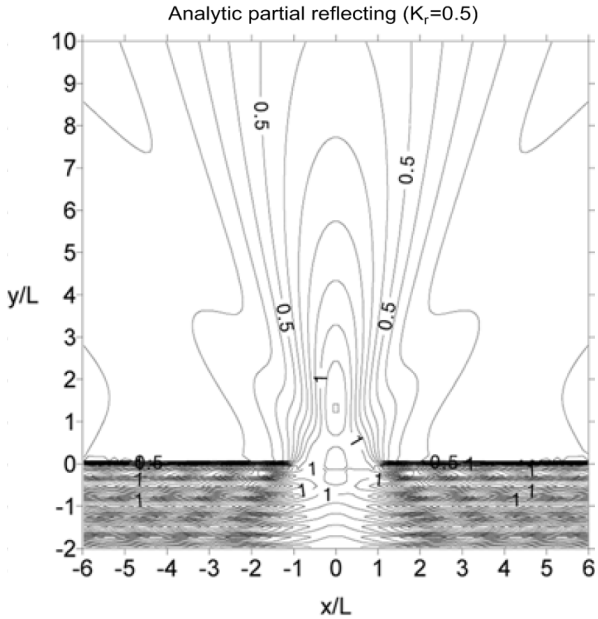

Figure 4.32 *Analytic diffraction through the gap of two partial reflecting breakwaters, $K_r = 0.5$, determined from (Kyung and Hanna, 2008).*

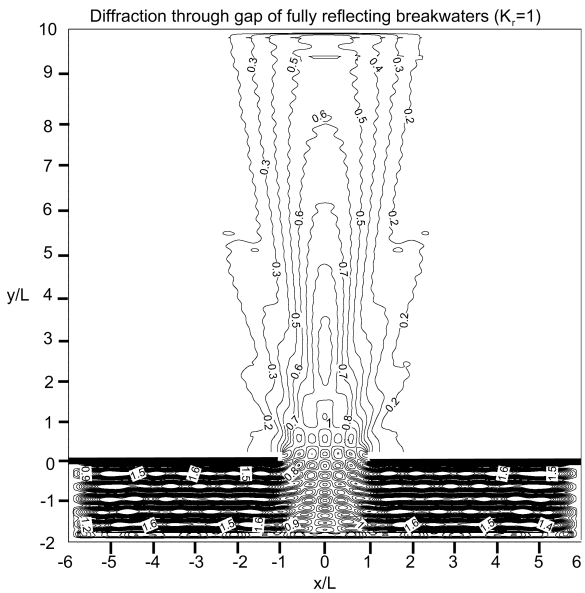

Figure 4.33 *Diffraction through the gap of two fully reflecting breakwaters, $K_r = 1$, determined in MIKE21 BW.*

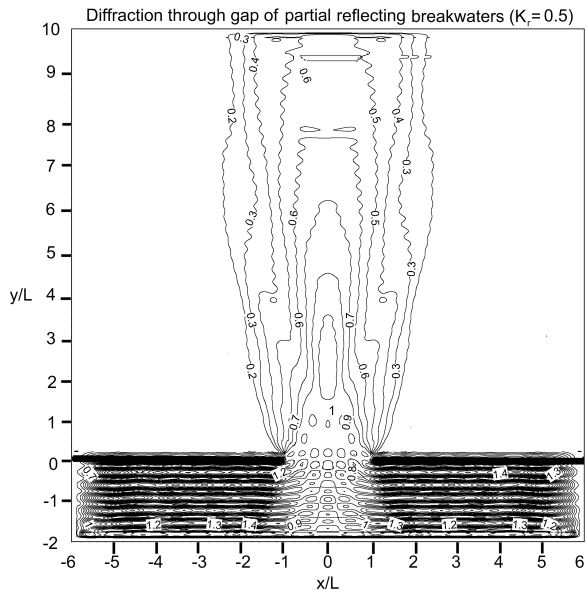

Figure 4.34 *Diffraction through the gap of two partial reflecting breakwaters, $K_r = 0.5$, determined in MIKE21 BW.*

From the comparisons in the two cases it is concluded, that MIKE21 BW provides an accurate description of diffraction.

4.3 Refraction in MIKE21 BW

The refraction phenomena is important when modeling wave propagation in a bay such as the case study site. To study whether MIKE21 BW is able to include the refraction-phenomena a simple example with a rip channel on a beach is created. The considered bathymetry is shown in Figure 4.35 which consists of a plane sloping beach of 1:30 with a rip channel excavated along the center line. The maximum water depth is 10 m at the offshore boundary. A regular wave with $H = 2\ m$ and $T = 8\ s$ is applied to the model.

In Figure 4.36 the wave disturbance in the model domain is illustrated. Here it is seen, that the incident wave height in the rip channel is reduced due refraction, where the wave energy is redistributed. The wave hight in the surrounding area is slightly increased due to shoaling. An extensive study on the present considered rip-channel is performed in (Madsen, 1997) where it is concluded that MIKE21 BW provides good results for both the refraction and shoaling phenomena.

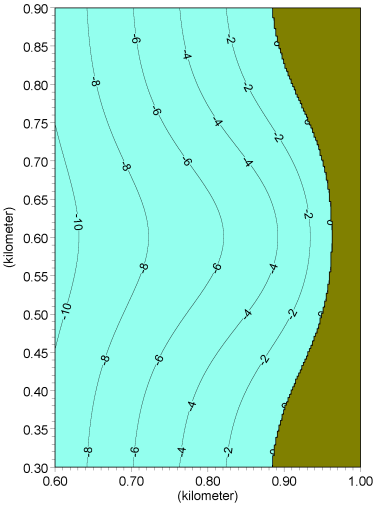

Figure 4.35 *Bathymetry of considered rip-channel. Contours are in m.*

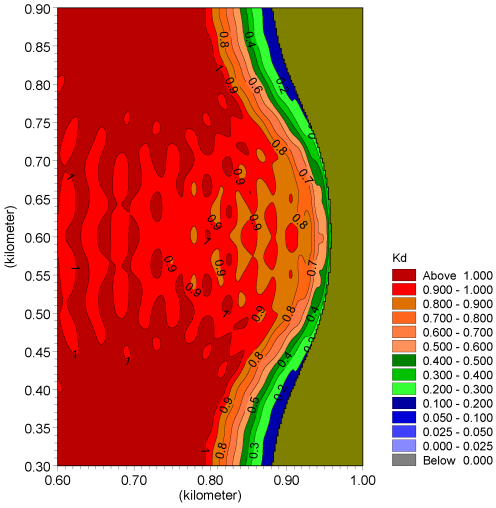

Figure 4.36 *Wave disturbance in rip-channel due to shoaling and refraction.*

4.4 Possibilities and Considerations when Implementing and Tuning a WD in MIKE21 BW

Since the WD is a floating structure, as mentioned in Section 3.1.2, the incident waves passing a WD are partly overtopping into the reservoir and thereby absorbed, and partly reflected or transmitted under the WD. Further, a part of the incident wave energy is diffracted around the structure. Due to the floating nature of the WD, an implementation of WD into the depth integrated MIKE21 BW by use of porosity layers, where K_r, K_t, and consequently P_a/P_i are coupled, is expected to require some tuning (decoupling) to be able to model the actual transmission and reflection. The following subsections sheds light on the possibilities and considerations which arises when implementing a WD in MIKE21 BW. An iterative decoupling method using porosity layers is described in the following. The method is inspired by an approach initially used in (Beels, 2009b) for decoupling sponge layer properties in the program MILDWAVE.

4.4.1 Decoupling of K_r and K_t in MIKE21 BW

As an example, the method is applied and illustrated for use when implementing the body of the WD in MIKE21 BW. The approach is, instead of specifying constant values for the porosity, S, to vary S through the structure, $S(x)$. The test set-up is illustrated in Figure 4.13 with $x = 34\ m$, where a JONSWAP spectrum is generated with $\gamma = 3.3$, $H_s = 0.1\ m$, $T_p = 10\ s$, and $T_{min} = 6\ s$. Three different porosity functions are considered; $S_1(x)$, $S_2(x)$, and $S_3(x)$, illustrated in Figure 4.37. $S_1(x)$ is constant, $S_2(x)$ is increasing from $S = 0.6$ to $S = 0.8$ through the structure, and $S_3(x)$ is decreasing from $S = 0.8$ to $S = 0.6$. Note that the mean value of S is 0.7 in all three cases.

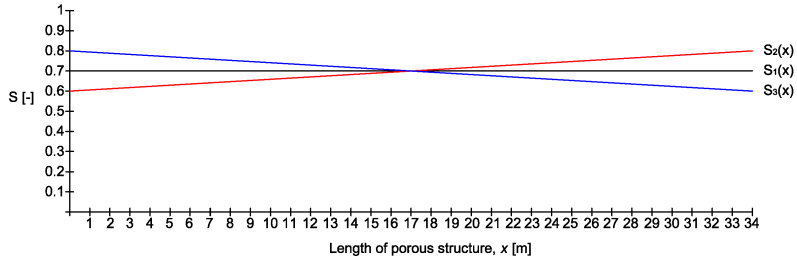

Figure 4.37 *Three different considered porosity functions; $S_1(x)$, $S_2(x)$, and $S_3(x)$.*

In Figure 4.38 the reflected and transmitted spectrum is illustrated, together with K_r, K_t, and p_a/p_i, for the three linear porosity functions. The reflected spectrum is extracted using gate 1, 2, and 3 and the transmitted spectrum is extracted from gate 4 in Figure 4.13. From Figure 4.38 it can be seen, that K_r and K_t differs in the three cases, and that the change in K_r and K_t is not proportional, especially in the high frequency-end of the spectrum. This illustrates the possibility for tuning the structure to fit a given amount of e.g. absorption.

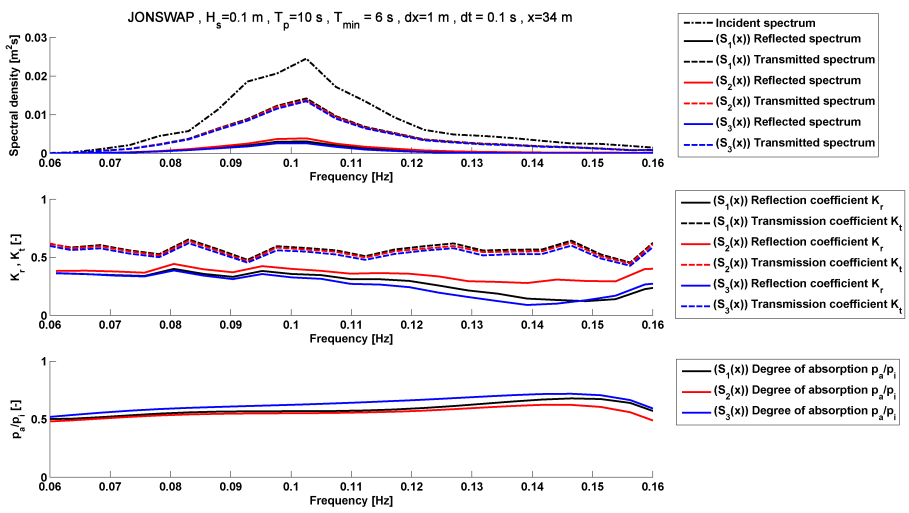

Figure 4.38 *The reflected and transmitted spectrum, together with K_r,K_t, and p_a/p_i, for the three linear porosity functions $S_i(x)$.*

A further decoupling can be obtained when applying absorbing sponge layers in combination with porosity layers. Again, as an example, the method is applied and illustrated for use when implementing the body of the WD in MIKE21 BW, using the test set-up in Figure 4.13. Two sponge layers (2 m width) with value μ are positioned in front of an obstacle with a constant porosity of $S = 0.7$ ($S_1(x)$). In Figure 4.39 the reflection, transmission, and consequently absorption, is illustrated for varying values of μ. Note that with $\mu = 1$ no absorption from the sponge layers is obtained. From Figure 4.39 it can be seen, that higher values of μ does not necessarily result in a higher degree of absorption, since higher gradients causes an increasing reflection, and a slightly reduced transmission.

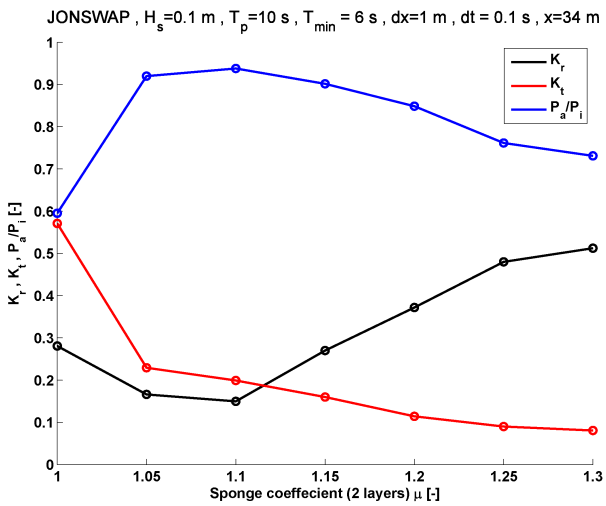

Figure 4.39 *Reflection, transmission, and consequently absorption for sponge layers with varying values of μ positioned in front of an obstacle with a constant porosity of $S = 0.7$ ($S_1(x)$).*

It should be noted, that $S(x)$ does not necessarily need to be varying linearly through a section. The same decoupling behavior is expected when specifying different sections with different constant values of S through e.g. the body of the WD.

4.4.2 Inclusion of Floating Structure in Depth Integrated Model and Awareness of Radiation from Waves Caused by Heaving Motions of the Floating WD

Incident waves causes the floating WD to move, which affect the reflection and transmission characteristics of the structure, and generates "secondary waves" in front of- and behind the WD. The movements of the WD are highly dependent on, among others, the length of the incident wave and the damping of the mooring system. In the following, the method for decoupling K_r and K_t in Section 4.4.1 is used to imitate an experimentally obtained behavior of a floating structure in the depth integrated MIKE21 BW.

The influence of the incident wave characteristics and certain geometric characteristics, such as the width and the draught of a structure, on its efficiency in means of reflection and transmission, is examined for different configurations of a floating breakwater in a large-scale facility in the CIEM flume of the Catalonia University of Technology (Kountandos et al., 2005). The test set-up implemented in MIKE21 BW imitates the same configuration as in the CIEM flume, is illustrated in Figure 4.40 where a fully reflecting floating breakwater, with a weight of 2240 kg, a draught of 0.4 m, and a length $L = 2$ m, is placed in a 10 m long flume with depth $h = 2$ m. Note that the length of the flume in MIKE21 BW differs from the actual setup, which, however, does not affect the results.

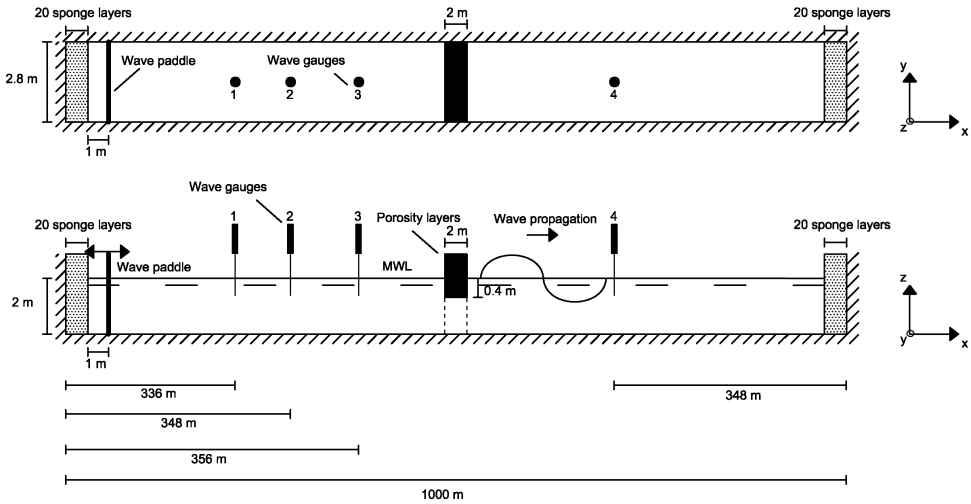

Figure 4.40 *Test set-up implemented in MIKE, with the same configuration as in the CIEM flume.*

To study the influence from different waves on a fixed floating structure and a heaving floating structure, K_r and K_t are determined as a function of the non-dimensionalized ratio between the width of the structure and the wave length, B/L, illustrated in Figure 4.41 and 4.42, respectively. A regular wave with height $H = 0.2\ m$ is used.

From Figure 4.41 and Figure 4.42 it is seen, that the heaving motion has an influence on both K_r and K_t, but especially K_r is affected. A somehow critical state in the variation of K_r is obtained, where a minimum reflection is reached at $B/L \approx 0.15$ after which K_r increases again. This is due to the fact, that the floating structure moves in/out of phase with the wave in case of shorter/longer wave lengths, controlled by the eigenfrequency of the system.

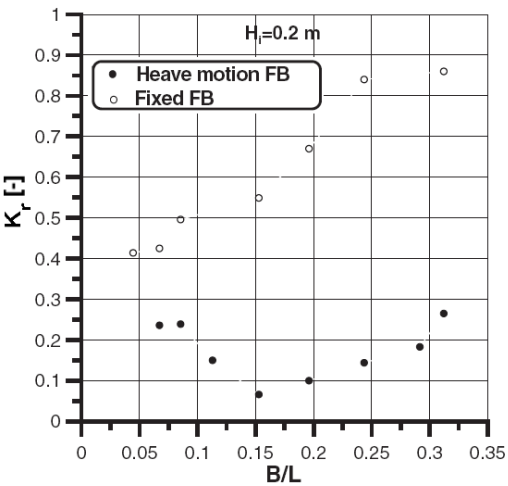

Figure 4.41 *K_r as a function of the non-dimensionalized ratio between the width of the structure and the wave length, B/L. (Kountandos et al., 2005).*

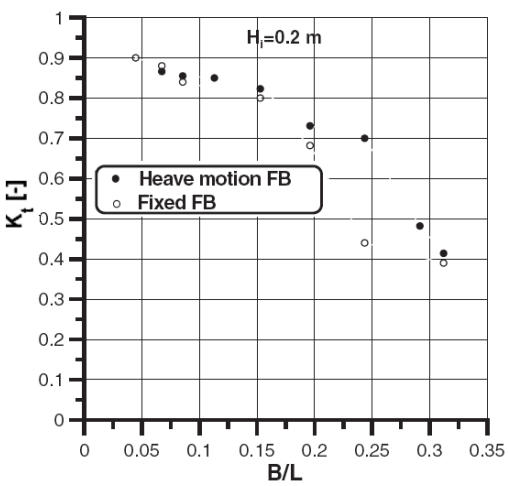

Figure 4.42 *K_t as a function of the non-dimensionalized ratio between the width of the structure and the wave length, B/L. (Kountandos et al., 2005).*

Using the approach in Section 4.4.1, a porous structure with $B = 2\ m$, is tuned to obtain the behavior of a heaving floating structure in MIKE21 BW, in means of K_r and K_t. As explained in Section 4.4.1, the method is highly iterative, with a high number of possibilities, and hence it is relatively time consuming to obtain an optimized tuning of the porosity layers and sponge layers. To study the possibility for modeling a floating structure, it is chosen to only use a linear variation of S in the porosity layers, and to use two sponge layers in front of the structure with a constant value of μ. This has resulted in two sponge layers with $\mu = 1.01$ which are placed in the front of the structure in MIKE21 BW to damp the reflection, followed by porosity layers which are varying linear from $S = 0.85$ to $S = 0.5$. A comparison of K_r and K_t obtained from experiments in the CIEM flume and obtained from the modeling in MIKE21 BW is illustrated in Figure 4.43.

From Figure 4.43 it is seen, that the modelled K_r and K_t are following the approximate same behavior as the real obtained transmission/reflection characteristics of a floating structure. Especially K_t shows good agreement. K_r, however, is slightly parallel displaced, and does not reach a critical state due to the inability of MIKE21 BW to model the actual floating behavior.

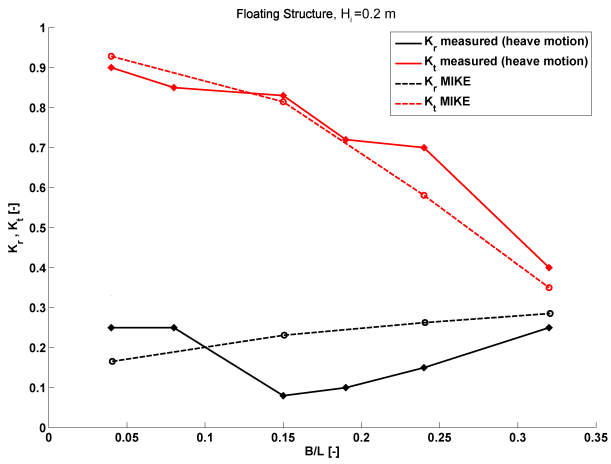

Figure 4.43 *Comparison of K_r and K_t obtained from experiments in the CIEM flume and obtained from the modeling in MIKE using two sponge layers in front of the structure with $\mu = 1.01$ and using varying porosity layers in the porous structure, $S = 0.85 - 0.5$.*

To implement radiation from waves, caused by heaving motions of the WD, an extra wave generation line can be placed in front of- and behind the structure. This, however, requires a rather complex description of the wave- and body motion introducing "secondary" wave generation, and will not be considered in the present thesis. On the other hand, the radiation is indirectly accounted for by tuning the porosity layers to fit the surrounding wave climate obtained from tests in the laboratory in a following chapter.

4.4.3 Considerations when Implementing Oblique Porous Structures in MIKE 21 BW

When implementing e.g. the oblique wave reflectors in MIKE21 BW one should be aware, that the discretization in the direction of the incident wave, and hence the theoretical specified K_r and K_t from a given width of the porosity layers, is influenced from the incident wave propagation angle. Oblique orientation is the non-alignment with a grid line in the model domain.

The issue of oblique partial reflecting structures is addressed in (Brorsen, 2000), where an oblique sponge layer is considered. Here the numerical wave propagation model MildSim is compared to experimental results obtained from (Brorsen, 1998). In Figure 4.44 the variation of the wave reflection from a porous breakwater with a vertical front, obtained from (Brorsen, 1998), is illustrated. From the considered incident wave angles it can be seen, that an increasing incident angle results in a decreasing reflection.

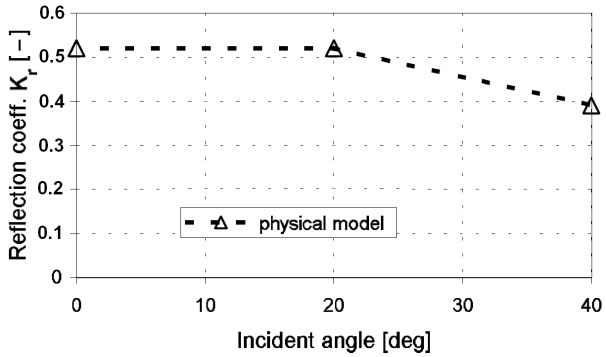

Figure 4.44 *Variation of the wave reflection from a porous breakwater with a vertical front, obtained from (Brorsen, 1998).*

Since the implemented WD in MIKE21 BW will be tuned to fit laboratory measurements in a later chapter, the reflection from the oblique orientated porosity layers is taken into account during the tuning. However, in case of 3D waves where changing wave directions occur, the reflection and transmission properties will be changing, which may also be the case when the reflectors are flexing and thereby changing their oblique orientation.

4.5 Summary of Findings in present Chapter

Findings from the present chapter will be used when constructing models in MIKE21 BW in following chapters. General key findings are listed in the following.

- To obtain approximately full absorption and reflection from sponge- and porosity layers, a spatial discretization of $L/dx > 20$ to $L/dx > 40$ is needed.
- Porosity layers provide varying reflection- and transmission characteristics through a wave energy spectrum, which is expected to be usable when implementing the WD in MIKE21 BW. The reflection and transmission from porosity layers are coupled, and to obtain a decoupling of K_r and K_t, varying porosity factors through a structure can be used. It is seen, that when using the decoupling method, MIKE21 BW can be calibrated to imitate the reflective and transmissive behavior of a floating breakwater.
- When simulating wave disturbance in MIKE21 BW a spatial discretization of $L_p/dx > 50$ is needed. From comparisons against analytical results it is concluded, that MIKE21 BW can be expected simulate phenomenons such as diffraction and refraction accurately.
- Cautions should be taken when modeling 3D waves since the reflection and transmission from oblique waves will be changing.

Part II

Analysis of Experimental Data and Calibration of Numerical Model

The present chapter deals with laboratory tests for obtaining measurements in the area close a single WD. Tests are performed on a model in scale 1:51.8 of a full-scale 260×150, $24kW/m$ WD. Preliminary numerical simulations are performed, in order to determine appropriate gauge positions for the test setup in the laboratory basin, followed by a description of the tests used for analyzing the wave disturbance in case of different mooring conditions and different sea states. Finally, the results from the different tests are analysed to determine how the different WD-setups and sea states affects the transmission and reflection characteristics of the WD. Conclusions from the present chapter contains observations of the sensitivity of wave disturbance from the WD against stiffness of the mooring-system, wave height, and draft. The findings will further be used in a later calibration of the numerical model for use in the case study of Santander.

4.6 Basis for Tests

Physical tests are performed in a 12.6 m wide and 9.25 m long wave basin at Aalborg University, as shown in Figure 4.45. A piston type paddle system composed of 25 actuators with a stroke length of 1.2 m is used for wave generation in front of the WD. The software AwaSys, developed by the same laboratory, is used for controlling the paddle system to generate waves. No active absorption on the wave paddles is used, but passive absorption is placed at the rear end of the basin, consisting of a 1:5 sloping gravel beach with $D_{50} = 1.5\ cm$. The sides of the basin are fully reflective until $6.05m$ from the back wall, where stone filled gabions ($1.21 \times 1.21\ m$, $0.70\ m$ deep), with $D_{50} = 5\ cm$, are used to absorb the waves. A mild slope of 1:37.5 is present in front of the wave generator. Surface elevations are measured using wave gauges at given positions in the basin.

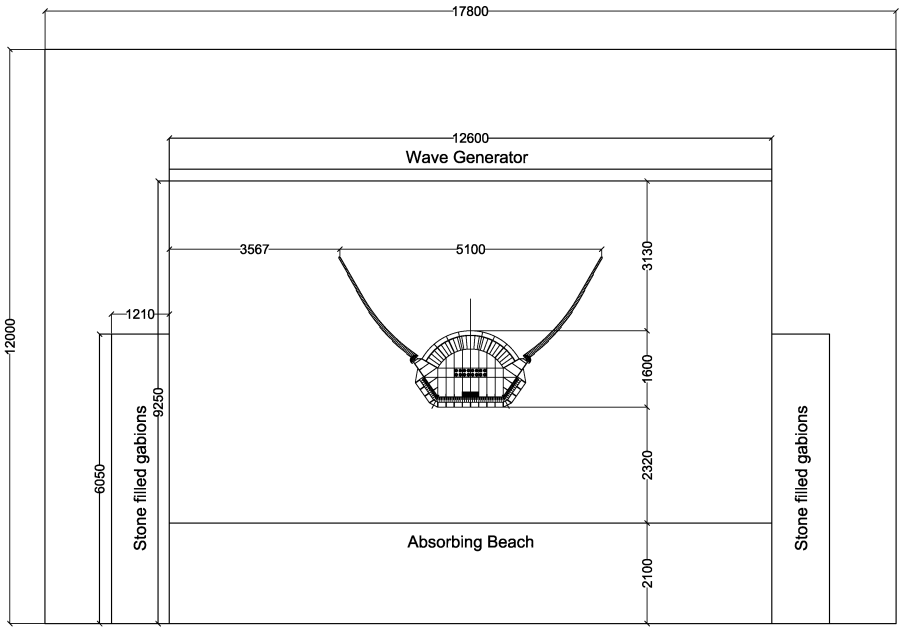

Figure 4.45 *Wave basin used for scaled model tests. Dimensions are in* mm.

As seen in Figure 4.45, the basin is relatively small compared to the scaled WD-model, and hence small distances to both the wave generator and the beach are present. This can result in waves being reflected from the basin boundaries having an effect on the results measured by the wave gauges close to the WD. These effects are investigated in Appendix B based on a number of preliminary tests in the empty basin. Here it is concluded, that the reflection from the gravel beach is not expected to have a major influence on the measurements in the basin. Further it is seen, that wave diffraction from the partial reflecting stone filled gabions only have a negligible effect on the wave heights measured near the WD.

It should be noted, that if the incident wave is reflected into areas with small transmitted wave heights, the reflected wave may have an increasing influence on the measurements.

4.6.1 Preliminary Study of Gauge Positions for Tests on WD

In order to determine the appropriate locations where the wave gauges will provide useful results, a preliminary un-calibrated numerical model is created in MIKE 21 BW, as shown in Figure 4.46. The model is based on the exact bathymetry of the basin with the same (un-calibrated) boundary conditions as in the laboratory. The WD is implemented with identical overall dimensions as in the laboratory, however, with slightly thicker reflectors than the real WD scale model, due to the spatial grid discretization, and with un-calibrated porosity layers. Hence the model does not provide the exact distribution of wave disturbances corresponding to the real experiments, but is expected to provide a rough estimate. This model will be calibrated in a later chapter.

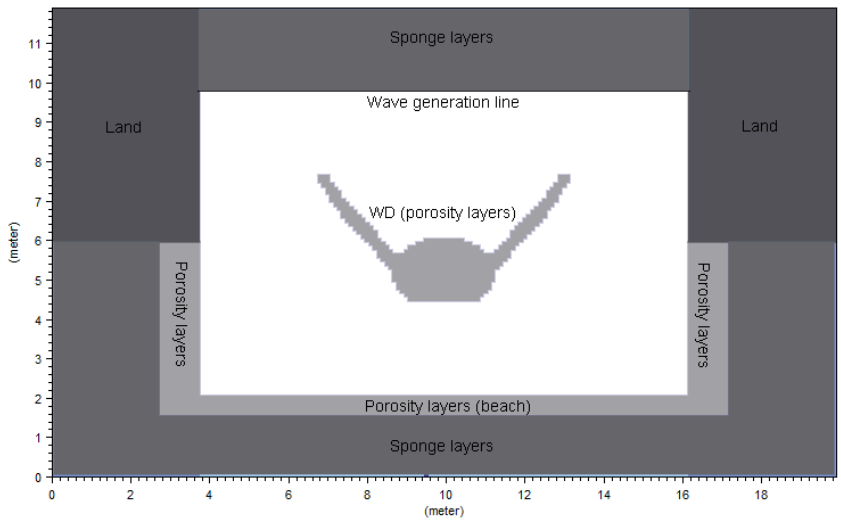

Figure 4.46 *Initial model, used for determining locations of wave gauges.*

A JONSWAP spectrum is specified corresponding to $H_s = 5\ m$ and $T_p = 10\ s$ with peak enhancement factor $\gamma = 3.3$, and a water depth corresponding to $h = 20\ m$. The distribution of the wave disturbance obtained from the preliminary model is illustrated in Figure 4.47.

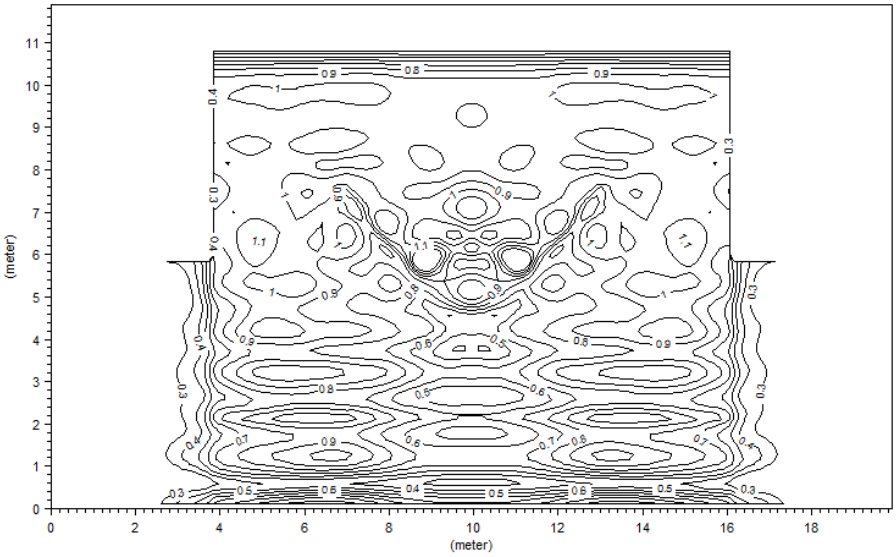

Figure 4.47 *The distribution of the wave disturbance obtained from the preliminary model.*

From Figure 4.47 it is observed, that the wave height increases between the reflectors and decreases behind the WD, especially directly behind the main body. This is expected, as the reflectors focus the waves in order to increase overtopping and dissipate energy, as described in Section 3.1.2. It is seen, that K_d in small areas close to the reflector tip reaches values above 1, which is due to diffraction from the WD. Further, since the wave disturbance slightly decreases behind the reflector towards the WD-body, it is useful to place gauges in front- of and behind- both the reflectors and body, and along the reflectors, to determine the variation of K_d.

Test Setups for Measuring Wave Disturbance from WD

Based on the observations from Figure 4.47, the appropriate gauge positions for measuring wave disturbance from the WD are found and illustrated in Figure 4.48. The setup in Figure 4.48 is named (*"Test Setup 1"*) in the following. A further illustration of *"Test Setup 1"* is given in Figure 4.49. The effect of the reflectors, as well as the reflection from the WD, will be calibrated using data from wave gauges A, B, C, E and F in Figure 4.48. In order to obtain measurements describing the change in wave height directly behind the WD, the wave gauges L-P in Figure 4.48 are placed a small distance behind the WD. The output from these gauges is expected to give an idea of the transmission through the WD and the wave radiation due to heaving movements of the structure.

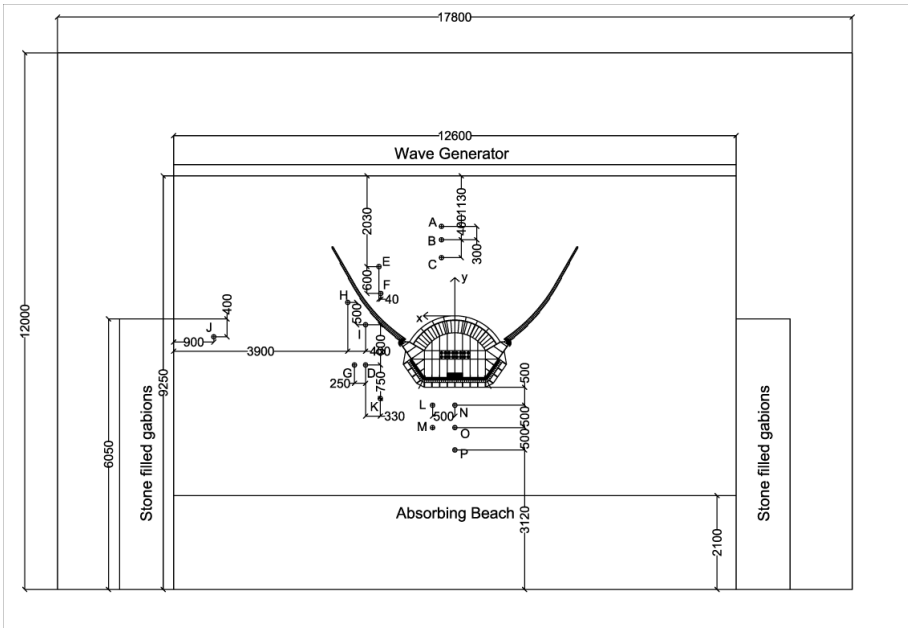

Figure 4.48 *Setup of wave gauges for "Test Setup 1". Dimensions are given in* mm.

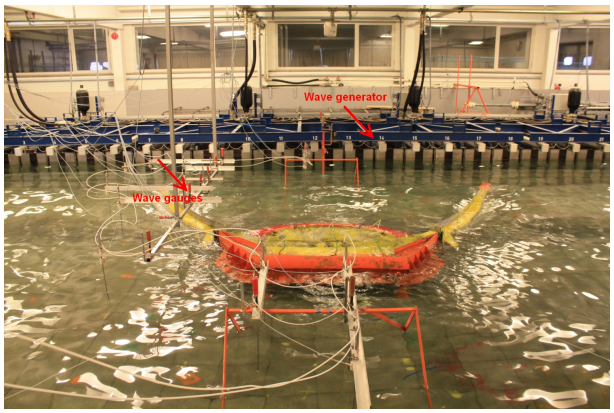

Figure 4.49 *Picture taken from the gravel beach behind the WD, illustrating "Test Setup 1" for use when determining wave disturbance from the WD.*

In addition to the measurements obtained from *"Test Setup 1"* the wave disturbance is determined in a line of 15 wave gauges behind the WD, using the setup shown in Figure 4.50 (*"Test setup 2"*). The results from this setup will give an indication of the variation in wave heights across the basin.

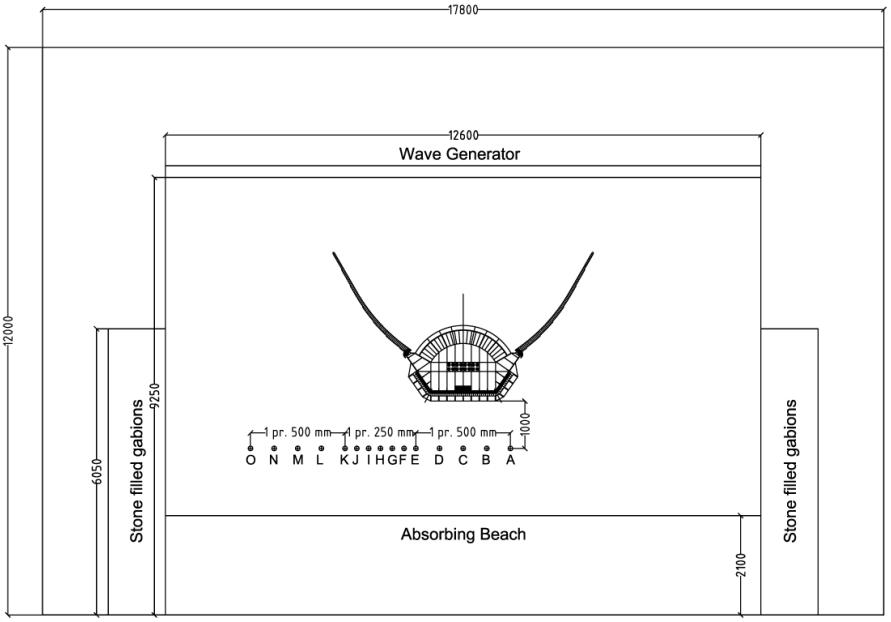

Figure 4.50 *Setup of wave gauges for "Test Setup 2". Dimensions are given in* mm.

4.7 Tests on Scaled WD-Model

As mentioned in Section 3.1.2, the draft of the full scale WD automatically adjusts to maximize the wave energy captured from overtopping for a given significant wave height. However, the buoyancy of the WD-model in the laboratory tests is set to a mean position, with draft of $d_r = 212\ mm$ measured from the bottom tip of the double curved front, as shown in Figure 4.51 corresponding to a prototype draft of $11.2\ m$ and a freeboard of $R_c = 4.5\ m$. A simulation performed by (Tedd, 2007) showed, that the optimal relative crest freeboard for energy production is around $R_c/H_s = 1.0$ which in this case is $R_c/H_s = 0.9$ with $H_s = 5\ m$.

Different relative crest freeboard ratios are considered for use in the sensitivity analysis, by performing tests with different H_s and constant crest freeboard R_c.

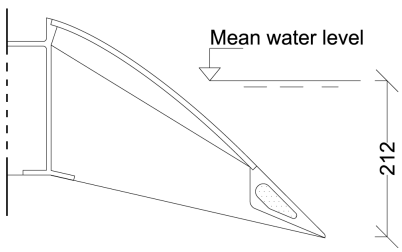

Figure 4.51 *Draft used for the scaled model. Measure is in* mm.

4.7.1 Scaling of Model

When performing tests in the laboratory, for use in a direct comparison with full scale conditions, geometric-, kinematic-, and dynamical-similarities are needed when comparing e.g velocities, forces, and geometrical dimensions. These similarities are determined from the Froude's scaling law (Hughes, 1993) with a geometrical length scale of $\lambda_L = 51.8$ compared to the full scale 260×150, $24kW/m$ WD. The time scale λ_t is found based on the length scale using (4.5).

$$\lambda_t = \lambda_L^{\frac{1}{2}} = 7.20 \tag{4.5}$$

Since the model is floating, the force scale λ_F is needed in order to correctly represent the mooring system used to keep the real WD in place. The force scale is found using (4.6).

$$\lambda_F = \frac{\gamma_p}{\gamma_m}\lambda_L^3 = \lambda_\rho \cdot \lambda_L^3 = 1.41 \cdot 10^5 \tag{4.6}$$

Where
$\frac{\gamma_p}{\gamma_m} = \lambda_\rho\ [-]$
γ_p is the water density for the full scale WD, $\gamma_p = 1020\ kg/m^3$
γ_m is the water density for the model, $\gamma_m = 1000\ kg/m^3$

The stiffness scale λ_S, used in the springs representing forces from the mooring system, is given by (4.7).

$$\lambda_S = \lambda_\rho \cdot \lambda_L^2 = 2.73 \cdot 10^3 \tag{4.7}$$

Scaling of Mooring System

Since the WD is a floating structure, it is not only important to model the structure correctly, but also the mooring lines used to keep it in place. The full scale WD is moored using anchors in front and behind the structure, as shown in Figure 4.52.

Figure 4.52 *Mooring system for full size WD (Tedd, 2007).*

In the laboratory mooring lines are fastened above the wave generator and at the wall behind the absorbing beach, using the arrangement shown in Figure 4.53, presented by (AAU, 1999). The stiffness of the mooring lines is modelled using springs at the ends of the lines which are scaled using (4.7).

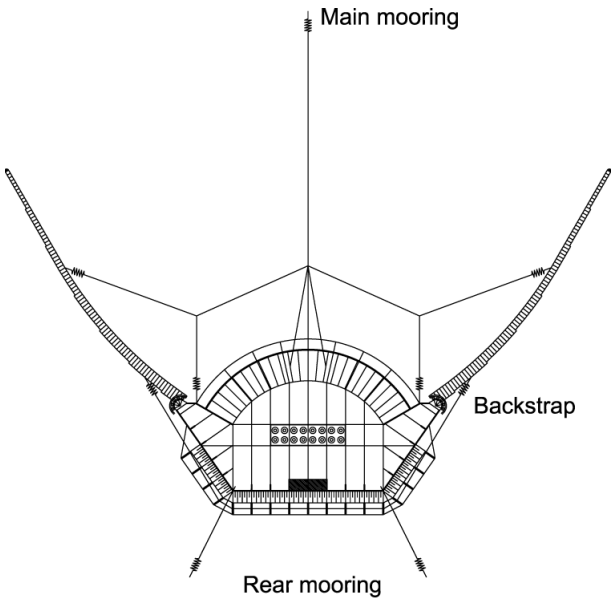

Figure 4.53 *Mooring arrangement for scaled model.*

The backstrap, as indicated in Figure 4.53, keeps the reflectors from closing in front of the WD, while the system between the reflectors keeps the reflectors from opening too wide. By applying initial stress to these strings the possible movement of the reflectors can be controlled. Greater initial stress in main mooring results in less movement in the direction of the waves, while greater initial stress in the rear mooring will prevent the WD from rotating.

At the Nissum Bredning model an elasticity of 70 kN/m is used for the central mooring line, while an elasticity of 25 kN/m is used for cables connecting the reflector arms to the central cable (Hald and Frigaard, 2001). The Nissum Bredning model is made with a stiffness scale of $\lambda_S = 4.5^2$ to the full size WD (Hald and Frigaard, 2001). Using this stiffness scale and the one found in Section 4.7.1, the elasticities in Table 4.2 are found.

Mooring line	**Stiffness** [N/m]
Main	517.9
Connecting	185.0

Table 4.2 *Elasticities of mooring lines used in model tests.*

4.7.2 Different Test Setups of WD

Since the movements of the wave reflectors and the WD body are expected to have an influence on the wave reflection and transmission characteristics, as mentioned in Section 4.4.2, experiments are carried out with different states of prestress in the springs, and different types of ”supports” for testing the sensitivity against heaving motions and lateral movements. These are described in the following.

Free/Fixed WD-Body

In the *”free WD-body”*-state, the floating structure is moored using a prestress on the main- and rear-mooring lines of 10.6 N (found by scaling the mooring forces given in (Hald and Frigaard, 2001)), allowing small lateral movements of the structure. Further, vertical movements of the structure are possible. In the *”fixed WD-body”*-state, the WD is fixed in place using vertically adjustable supports which are bolted to the floor of the basin. This setup is introduced to investigate the heaving effects from

the WD on the transmissive characteristics. Front supports are placed closely behind the reflector joints, while rear supports are placed at the back end of the WD, as shown in Figure 4.54. The supports are adjusted, so the WD has the same still water draft as when floating. Since the supports are placed under the WD, they will have some influence on the transmission under the WD. However due to their small size relative to the WD model, this effect is expected to be negligible.

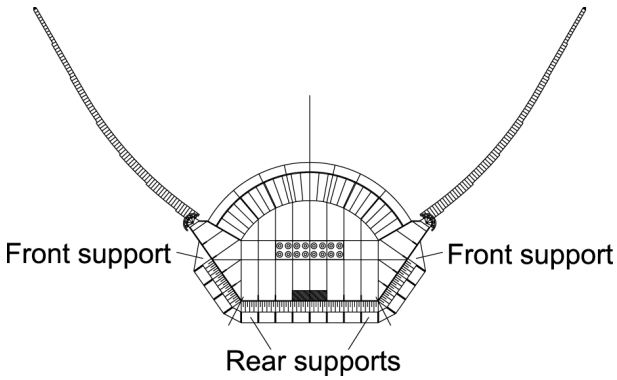

Figure 4.54 *Positions of supports keeping the WD fixed in place.*

Keeping the WD fixed in place is not practically possible for the real WD, since the unit will not be able to turn and face waves from different directions, as with the mooring system. The tests are, however, very useful for analyzing the effects of movement of the WD body and reflectors.

Flexible/Fixed Reflectors

In the *"flexible reflectors"*-state, a scaled prestress of 7.1 N (found by scaling the mooring forces given in (Hald and Frigaard, 2001)) is applied to the line system between the reflectors and the backstrap. In the *"fixed reflectors"*-state, the movement in the reflectors is minimized as much as possible (small relative to the movements from *"flexible"* reflectors) by applying a tight strings between the reflectors and along the backstrap. The reason for testing the *"fixed"*-state against the *"flexible"*-state of the reflectors, is to analyse how the stiffness of a fullscale WD affects its ability to reduce wave heights behind the structure.

4.8 Sea States and Test Schedule

The waves, used during the different tests, are based on 12 irregular reference sea states, specified as JONSWAP-spectrums with $\gamma = 3.3$, for determining how the wave climate affects the wave transmission through the WD. In addition, a number of regular waves are introduced, mainly for use in the calibration of the numerical model.

4.8.1 Irregular Reference Test Sea States

As mentioned in Section 1.4, a typical winter storm is evaluated. The specified significant wave height and peak periods which are considered in the present case, presented in Table 4.3, are based on observations from (Medellín, 2007) where it is seen, that typical winter storm produces $H_s = 5\ m$ and peak periods between $\approx T_p = 10\ s$ - $T_p = 16\ s$. Additionally a smaller wave height of $H_s = 2\ m$ is evaluated, for analyzing the effect of different relative floating levels.

$h\ [m]$	**20**						**25**					
$H_s\ [m]$	5	5	5	2	2	2	5	5	5	2	2	2
$T_p\ [s]$	16	12	10	16	12	10	16	12	10	16	12	10

Table 4.3 *Reference sea states used in experiments.*

The sea states in Table 4.3 correspond to the full scale conditions, and are scaled to be applicable in the laboratory experiments. This is done using the scaling factors found in Section 4.7.1, resulting in the JONSWAP spectrums given in Table 4.4. Since one of the objectives of the tests is to reproduce results in a numerical model, based on the Boussinesq equations, a frequency cutoff and rescaling of the spectrum is introduced in order to meet the h/L requirements, as described in Section 2.2.1. The cutoff periods T_{min} are further given in Table 4.4.

$h\ [m]$	**0.39**						**0.48**					
$H_s\ [m]$	0.10	0.10	0.10	0.04	0.04	0.04	0.10	0.10	0.10	0.04	0.04	0.04
$T_p\ [s]$	2.22	1.67	1.39	2.22	1.67	1.39	2.22	1.67	1.39	2.22	1.67	1.39
$T_{min}\ [s]$	1.11	0.83	0.83	1.11	0.83	0.83	1.11	0.83	0.83	1.11	0.83	0.83

Table 4.4 *Sea states scaled to fit the model.*

4.8.2 Test Schedule

The different sea states are applied to the different setups described in Section 4.7.2 and a number of tests using regular and irregular waves are performed. The regular waves are primarily used to obtain a faster calibration of the WD in the numerical model due to the reduced amount of waves needed to obtain a converged wave disturbance. Tests with regular waves are mainly specified with a waveheight and wave period corresponding to H_s and T_p in the JONSWAP spectrums, given in Table 4.4.

The majority of the tests performed in the laboratory are long crested waves, with a few additional tests with short crested waves. However, during the first 3D tests it was observed, that great movements of the WD was present, which resulted in collisions with the gauges positioned at close distances to both the body and the reflectors. Further, since the test basin is relatively small compared to the WD scale model, great reflections from the basin-sides arise from the short crested waves, affecting the measurements close to the WD. The wave conditions and setup for each test are given in Table 4.5 and 4.6.

From the results of the preliminary test used for calibration of the basin it is observed, that the waves, given as input for the wave generator, did not correspond to what was actually generated. Hence the tests, 69 to 90 are added to the test schedule, using the setup in the empty basin shown in Figure B.1 in Appendix B, to determine exactly which waves were generated at the different sea states. The wave paddle generation signals from the laboratory wave generator in test 69 - 90, are reused in test 3 - 68 with the different test setups of the WD to perform more exact comparisons of the setups. *"Test setup 3"* and *"test setup 4"*, which are referred to in Table 4.5 and 4.6, are shown in Appendix B.

Test Overview, JONSWAP spectrum									
Test no.	**Test Setup**	**WD (body/refl.)**	$h\ [m]$	$H\ [m]$	$T\ [s]$	$T_{min}\ [s]$	$L_{min}\ [m]$	**Signal**	**Wave**
1	3	Incident wave mea.	0.39	0.10	1.39	0.83	1.06	-	2D irr.
2	3	Incident wave mea.	0.39	0.10	1.67	0.83	1.06	-	2D irr.
3	4	Stone filled gabion	0.39	0.10	1.39	0.83	1.06	-	2D irr.
4	4	Stone filled gabion	0.39	0.10	1.67	0.83	1.06	-	2D irr.
5	1	*"Free / flexible"*	0.39	0.10	1.39	0.83	1.06	1	2D irr.
6	1	*"Free / flexible"*	0.39	0.10	1.67	0.83	1.06	2	2D irr.
7	1	*"Free / flexible"*	0.39	0.10	2.22	1.11	1.71	69	2D irr.
8	1	*"Free / flexible"*	0.39	0.04	1.39	0.83	1.06	70	2D irr.
9	1	*"Free / flexible"*	0.39	0.04	1.67	0.83	1.06	71	2D irr.
10	1	*"Free / flexible"*	0.39	0.04	2.22	1.11	1.71	72	2D irr.
11	1	*"Free / flexible"*	0.48	0.10	1.39	0.83	1.07	73	2D irr.
12	1	*"Free / flexible"*	0.48	0.10	1.67	0.83	1.07	74	2D irr.
13	1	*"Free / flexible"*	0.48	0.10	2.22	1.11	1.79	75	2D irr.
14	1	*"Free / flexible"*	0.48	0.04	1.39	0.83	1.07	76	2D irr.
15	1	*"Free / flexible"*	0.48	0.04	1.67	0.83	1.07	77	2D irr.
16	1	*"Free / flexible"*	0.48	0.04	2.22	1.11	1.79	78	2D irr.
17	1	*"Free / fixed"*	0.39	0.10	1.39	0.83	1.06	1	2D irr.
18	1	*"Free / fixed"*	0.39	0.10	1.67	0.83	1.06	2	2D irr.
19	1	*"Free / fixed"*	0.48	0.10	1.39	0.83	1.07	73	2D irr.
20	1	*"Free / fixed"*	0.48	0.10	1.67	0.83	1.07	74	2D irr.
21	1	*"Fixed / fixed"*	0.39	0.10	1.39	0.83	1.06	1	2D irr.
22	1	*"Fixed / fixed"*	0.39	0.10	1.67	0.83	1.06	2	2D irr.
23	1	*"Fixed / fixed"*	0.48	0.10	1.39	0.83	1.07	73	2D irr.
24	1	*"Fixed / fixed"*	0.48	0.10	1.67	0.83	1.07	74	2D irr.
25	1	*"Fixed / flexible"*	0.39	0.10	1.39	0.83	1.06	1	2D irr.
26	1	*"Fixed / flexible"*	0.39	0.10	1.67	0.83	1.06	2	2D irr.
27	1	*"Fixed / flexible"*	0.48	0.10	1.39	0.83	1.07	73	2D irr.
28	1	*"Fixed / flexible"*	0.48	0.10	1.67	0.83	1.07	74	2D irr.
28b	1	*"Fixed / flexible"*	0.48	0.10	1.67	0.83	1.07	74	2D irr.
31	1	*"Free / flexible"*	0.39	0.04	1.67	-	2.96	81	Regular
32	1	*"Free / flexible"*	0.39	0.04	1.39	-	2.35	80	Regular
34	1	*"Free / flexible"*	0.48	0.10	1.39	-	3.02	83	Regular
35	1	*"Free / flexible"*	0.48	0.04	1.67	-	3.20	87	Regular
36	1	*"Free / flexible"*	0.48	0.04	1.39	-	3.02	86	Regular
37	1	*"Free / fixed"*	0.39	0.04	1.67	-	2.96	81	Regular
38	1	*"Free / fixed"*	0.39	0.04	1.39	-	2.35	80	Regular
39	1	*"Fixed / fixed"*	0.48	0.04	1.67	-	3.20	87	Regular
40	1	*"Fixed / fixed"*	0.48	0.04	1.39	-	3.02	86	Regular
41	1	*"Fixed / fixed"*	0.39	0.04	1.67	-	2.35	81	Regular
42	1	*"Fixed / fixed"*	0.39	0.04	1.39	-	2.96	80	Regular
43	2	*"Fixed / fixed"*	0.39	0.10	1.39	0.83	1.06	1	2D irr.
44	2	*"Fixed / fixed"*	0.39	0.10	1.67	0.83	1.06	2	2D irr.
45	2	*"Fixed / fixed"*	0.48	0.10	1.39	0.83	1.07	73	2D irr.

Table 4.5 *Wave conditions and setup for each test performed in the laboratory basin. $H_s = H$ and $T_p = T$ in case of irregular waves. The specified number in the column "Signal" refers to the reused signal from the different wave tests (test 1,2 and 69 -90).*

It turned out, that significant errors was present in the results from test 29, 30 and 33, and hence these are removed from test schedule in Table 4.5. The removed tests was performed with regular waves, mainly for use in the calibration of the numerical model, but are found to be dispensable.

Test Overview, JONSWAP spectrum									
Test no.	**Test Setup**	**WD (body/refl.)**	h $[m]$	H $[m]$	T $[s]$	T_{min} $[s]$	L_{min} $[m]$	**Signal**	**Wave**
46	2	*"Fixed / fixed"*	0.48	0.10	1.67	0.83	1.07	74	2D irr.
47	2	*"Free / flexible"*	0.39	0.10	1.39	0.83	1.06	1	2D irr.
48	2	*"Free / flexible"*	0.39	0.10	1.67	0.83	1.06	2	2D irr.
49	2	*"Free / flexible"*	0.48	0.10	1.39	0.83	1.07	73	2D irr.
50	2	*"Free / flexible"*	0.48	0.10	1.67	0.83	1.07	74	2D irr.
51	2	*"Fixed / fixed"*	0.39	0.04	1.39	-	2.35	80	Regular
52	2	*"Fixed / fixed"*	0.39	0.04	1.67	-	2.96	81	Regular
53	2	*"Fixed / fixed"*	0.48	0.10	1.39	-	3.02	83	Regular
54	2	*"Fixed / fixed"*	0.48	0.10	1.67	-	3.20	84	Regular
55	2	*"Free / flexible"*	0.39	0.04	1.39	-	2.35	80	Regular
56	2	*"Free / flexible"*	0.39	0.04	1.67	-	2.96	81	Regular
57	2	*"Free / flexible"*	0.48	0.10	1.39	-	3.02	83	Regular
58	2	*"Free / flexible"*	0.48	0.10	1.67	-	3.20	84	Regular
59	2	*"Free / flexible"*	0.48	0.10	1.39	0.83	1.07	??	3D irr.
60	2	*"Fixed / fixed"*	0.48	0.10	1.39	0.83	1.07	??	3D irr.
61	2	*"Free / flexible"*	0.48	0.04	1.39	-	3.02	86	Regular
62	2	*"Free / flexible"*	0.48	0.04	1.67	-	3.20	87	Regular
63	2	*"Free / flexible"*	0.48	0.10	2.22	-	4.50	85	Regular
64	2	*"Free / flexible"*	0.48	0.04	2.22	-	4.50	88	Regular
65	2	*"Free / flexible"*	0.39	0.10	2.22	-	4.11	79	Regular
66	2	*"Free / flexible"*	0.39	0.04	2.22	-	4.11	82	Regular
67	2	*"Free / flexible"*	0.39	0.04	0.83	-	1.06	89	Regular
68	2	*"Free / flexible"*	0.39	0.10	0.83	-	1.06	90	Regular
69	3	Incident wave mea.	0.39	0.10	2.22	1.11	1.71	-	2D irr.
70	3	Incident wave mea.	0.39	0.04	1.39	0.83	1.06	-	2D irr.
71	3	Incident wave mea.	0.39	0.04	1.67	0.83	1.06	-	2D irr.
72	3	Incident wave mea.	0.39	0.04	2.22	1.11	1.71	-	2D irr.
73	3	Incident wave mea.	0.48	0.10	1.39	0.83	1.07	-	2D irr.
74	3	Incident wave mea.	0.48	0.10	1.67	0.83	1.07	-	2D irr.
75	3	Incident wave mea.	0.48	0.10	2.22	1.11	1.79	-	2D irr.
76	3	Incident wave mea.	0.48	0.04	1.39	0.83	1.07	-	2D irr.
77	3	Incident wave mea.	0.48	0.04	1.67	0.83	1.07	-	2D irr.
78	3	Incident wave mea.	0.48	0.04	2.22	1.11	1.79	-	2D irr.
79	3	Incident wave mea.	0.39	0.10	2.22	-	4.11	-	Regular
80	3	Incident wave mea.	0.39	0.04	1.39	-	2.35	-	Regular
81	3	Incident wave mea.	0.39	0.04	1.67	-	2.96	-	Regular
82	3	Incident wave mea.	0.39	0.04	2.22	-	4.11	-	Regular
83	3	Incident wave mea.	0.48	0.10	1.39	-	3.02	-	Regular
84	3	Incident wave mea.	0.48	0.10	1.67	-	3.20	-	Regular
85	3	Incident wave mea.	0.48	0.10	2.22	-	4.50	-	Regular
86	3	Incident wave mea.	0.48	0.04	1.39	-	3.02	-	Regular
87	3	Incident wave mea.	0.48	0.04	1.67	-	3.20	-	Regular
88	3	Incident wave mea.	0.48	0.04	2.22	-	4.50	-	Regular
89	3	Incident wave mea.	0.39	0.04	0.83	-	1.06	-	Regular
90	3	Incident wave mea.	0.39	0.10	0.83	-	1.06	-	Regular

Table 4.6 *Wave conditions and setup for each test performed in the laboratory basin. $H_s = H$ and $T_p = T$ in case of irregular waves. The specified number in the column "Signal" refers to the reused signal from the different wave tests (test 1,2 and 69 -90).*

4.8.3 Determination of Generated Incident Waves in Reused Wave Generation Signals

A reflection analysis, based on (Mansard and Funke, 1980), is carried out for the tests 1,2 and 69-90. From these reflection analyses, an incident wave spectrum is found for each of the tests which are then compared to the incident JONSWAP spectrum specified for wave generation in the specific case. The results are shown in Table 4.7, where it is seen, that the generated measured wave height $H_{i,meas.}$ does not correspond completely to the specified $H_{i,spec.}$. The actual generated wave heights in Table 4.7, $H_{i,meas.}$, will, in combination with $H_{meas.}$ measured from gauges at given locations around the WD, be used to determine the actual wave disturbance in the basin $K_d = H_{meas.}/H_{i,meas.}$, and further for use in the calibration of the WD in the numerical model.

Comparison of specified and measured waves				
Test no.	$H_{i,spec.}$ $[m]$	$H_{i,meas.}$ $[m]$	**Diff.,** H $[\%]$	**Wave**
1	0.10	0.08	-18.63	2D irr.
2	0.10	0.09	12.42	2D irr.
69	0.10	0.09	-9.30	2D irr.
70	0.04	0.04	2.18	2D irr.
71	0.04	0.05	19.18	2D irr.
72	0.04	0.05	15.08	2D irr.
73	0.10	0.08	-18.00	2D irr.
74	0.10	0.09	-14.00	2D irr.
75	0.10	0.09	-12.86	2D irr.
76	0.04	0.04	0.48	2D irr.
77	0.04	0.05	15.03	2D irr.
78	0.04	0.04	8.00	2D irr.
79	0.10	0.09	-6.38	Regular
80	0.04	0.05	13.83	Regular
81	0.04	0.05	28.88	Regular
82	0.04	0.04	2.50	Regular
83	0.10	0.09	-8.00	Regular
84	0.10	0.10	3.60	Regular
85	0.10	0.09	-6.40	Regular
86	0.04	0.05	24.10	Regular
87	0.04	0.05	27.50	Regular
88	0.04	0.05	12.50	Regular
89	0.04	0.04	0.00	Regular
90	0.10	0.09	-9.00	Regular

Table 4.7 *Generated Wave Spectrums.* $H_s = H$ *in case of irregular waves.*

4.9 Evaluation- and Analysis of Measured Data Concerning Wave Disturbance from WD

In the following, the results from the tests presented in Table 4.5 and Table 4.6 will be evaluated and primarily compared on the disturbance coefficient K_d.

4.9.1 Regression Analysis of Reused Wave Generator Signal

Before performing comparisons between the different WD-setups, it is studied, whether a reused wave generator signal of the incident waves, can produce identical results from the gauges in the basin. To this, the measured time series from test 28 and 28b are compared, where identical WD setups, gauge positions, and incident wave generation signals are present. The measurements from the different gauges are compared by calculating the regression coefficient, R^2, between the two tests, where possible time delays between the time series are accounted for. The results can be seen in Figure 4.55.

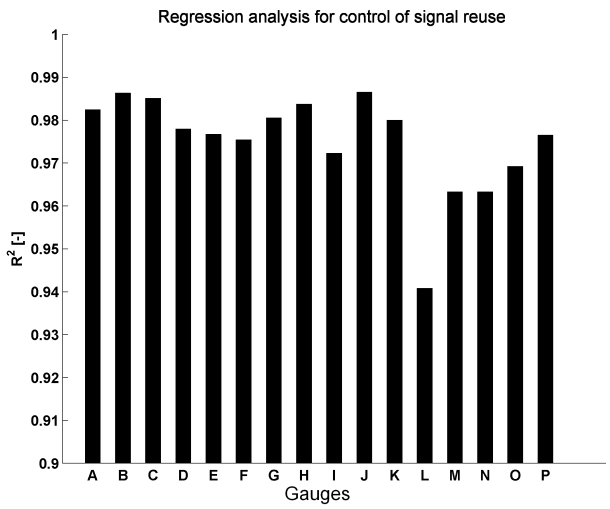

Figure 4.55 *Calculated regression coefficients, when comparing test 28 and test 28b using "test setup 1".*

From the results in Figure 4.55 it is concluded, that the influence of the different setups, using the same wave signals, can be determined by performing a direct comparison of the measurements from the different gauges.

4.9.2 Influence on K_d from Relative Crest Freeboard and Peak Period Wave Length

As mentioned before, and as seen in Section 3.1.2, the absorption of the WD is highly influenced by the draft d_r and thereby the ratio between the crest freeboard R_c and significant wave height H_s, due to wave overtopping on the WD-body. Smaller R_c/H_s results in an increased overtopping rate and hence increased wave energy dissipation. However, it is not yet exactly known how the transmission and reflection characteristics are affected by the absorption due to wave energy dissipation from overtopping, cf. Section 3.1.2. To test this behavior, K_d is determined in case of two different significant wave heights; $H_s = 0.1\ m$ (5 m in real scale) and $H_s = 0.04\ m$ (2 m in real scale), but with equal R_c (4.5 m in real scale). This results in two different crest free board ratios of $R_c/H_s = 0.9$ and $R_c/H_s = 2.25$ and two different wave steepness, H/L. It should be noted, that a ratio of 2.25 is unrealistic when considering the power production (Kofoed, 2002), but is still used as an extreme case to analyse the effect on the wave disturbance.

In Figure 4.56 the variation of K_d as a function of L_p (wave length corresponding to T_p in the irregular wave spectrum) in case of the two different crest freeboard ratios are plotted, using test; 5-7, 11-13 for $H_s = 0.1\ m$, and 8-10, 14-16 for $H_s = 0.04\ m$ - both with the setup of *"free"* WD-body and *"flexible"* reflector joints. In addition, the variation of K_d in front of- and behind the WD-body and -reflectors is illustrated in Figure 4.57.

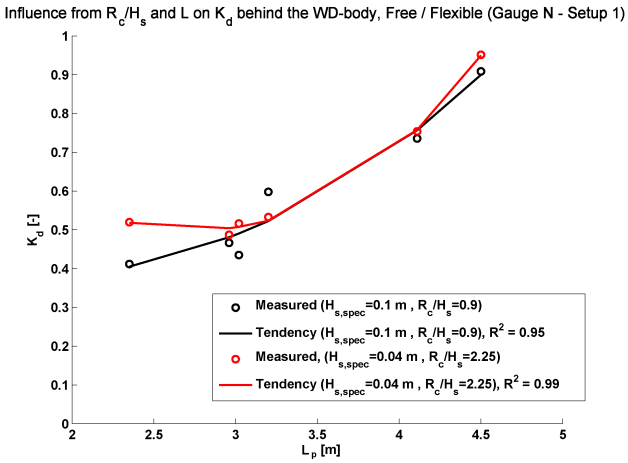

Figure 4.56 *Variation of K_d as a function of L_p in case of the two different wave heights and floating levels, using test; 5-7, 11-13 for $H_s = 0.1$ m, and 8-10, 14-16 for $H_s = 0.04$ m - both with the setup of "free" WD-body and "flexible" reflector.*

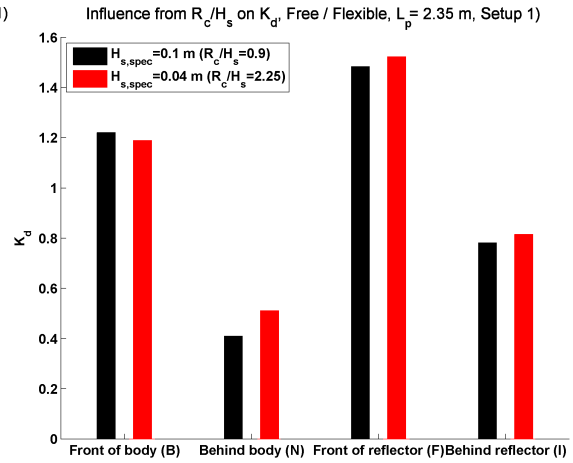

Figure 4.57 *Variation of K_d in front of- and behind the WD-body and -reflectors, using test 5 ($H_s = 0.1$, $L_p = 2.35$ m), and test 8 ($H_s = 0.04$, $L_p = 2.35$ m), with the same setup as in Figure 4.56.*

It is seen that, as expected, K_d increases with increasing L_p or decreasing wave steepness for both considered relative crest freeboard rates. Further it is observed from the tendency, that a smaller R_c/H_s results in a slightly smaller K_d or a more reduced H_s behind the WD. The same tendency was concluded in the analytical study of the transmission characteristics of the WD in Section 3.1.2.

From Figure 4.57 it is seen, that the same tendency as behind the WD-body is found behind the reflector (slightly smaller K_d for smaller R_c/H_s). As expected, the opposite tendency is found in front of the WD-body. This was also seen in the analytical study of the reflectors, where an increased amount of reflected wave power was obtained in case of an increased d_r or smaller R_c/H_s. The measured K_d in front of the reflector, however, in case of the two considered crest freeboard rates, does not correspond to the tendency in front of the body, which may be due to effects of the oblique nature of the reflector, and reflection from other parts of the WD.

Important observations are, that smaller R_c/H_s and smaller L_p (smaller H/L) results in a smaller K_d or a more reduced H_s behind the WD. A relative decrease of 64% of R_c/H_s results in a relative decrease of 20% of K_d behind the WD body, and even less behind the reflector. In comparison, a relative decrease in L_p of 46% results in an decrease of K_d of 56% behind the WD-body when $R_c/H_s = 0.9$, meaning that the wave disturbance is much more affected by the wave length than the crest freeboard rate in the present case.

4.9.3 Influence on K_d from Different WD-Setups

Based on the conclusions made in the study of (Kountandos et al., 2005) described in Section 4.4.2, it is expected, that the transmission characteristics of the WD are highly affected by its floating behavior. Therefore, to determine how sensitive the wave disturbance around the WD is to the stiffness of its supports, reflectors and body, comparisons are performed between the different test setups described in Section 4.7.2.

Wave Disturbance in Front of the WD in Case of Different WD-Setups

In Figure 4.58 and 4.59 the variation of K_d in case of different WD-setups and H_s/L_p, is plotted in front of the WD-body and -reflectors, respectively. All tests are performed with a specified significant wave height of $H_s = 0.1\ m$, which however, is regulated according to Table 4.7. At both locations in front of the WD it is observed, that K_d tends to decrease with increasing L_p or decreasing H_s/L_p corresponding to previous observations. Further, as expected, K_d is bigger in front of- and between the reflectors (at gauge F) than some distance away from the WD-body front (gauge B), due to the channeling of wave energy with the purpose to increase wave overtopping.

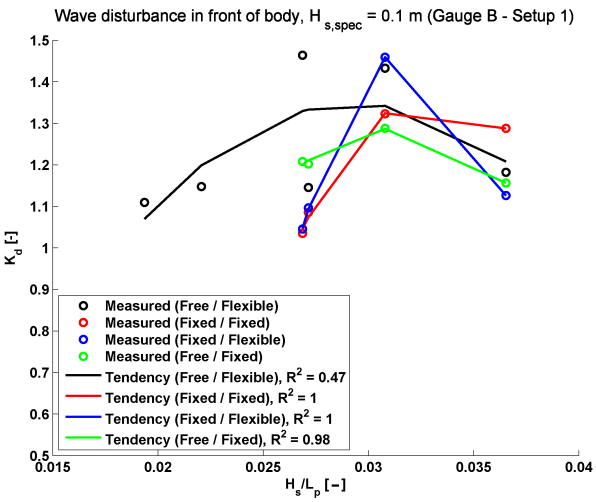

Figure 4.58 *Variation of K_d in front of the WD-body.*

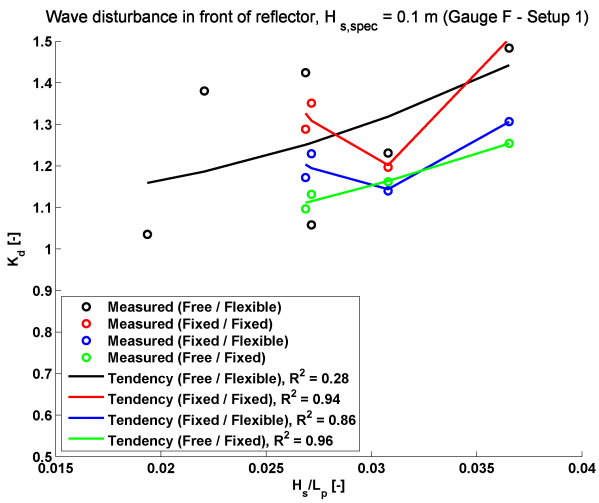

Figure 4.59 *Variation of K_d in front of the WD-reflectors.*

It is observed, that the *"free/flexible"*-setup seems to provide the biggest wave disturbance coefficient K_d in front of both the WD-body and -reflectors, compared to when either- or both the body and reflectors are fixed, and hence the biggest measured H_s, compared to the incident, is obtained from this setup. This is, however, with the exception for the smallest considered wave length, where the *"fixed/fixed"* setup provides the biggest K_d.

The combined setups; *"fixed/flexible"* and *"free/fixed"*, does not show any significant changes in the tendencies compared to the extremes; *"free/flexible"* and *"fixed/fixed"*.

Wave Disturbance Behind the WD in Case of Different WD-Setups

In Figure 4.60 and 4.61 the variation of K_d in case of different WD-setups and H_s/L_p, is plotted behind the WD-body and -reflectors, respectively. It should be noted, that different axis are present in the figures. Again, all tests are performed with a specified significant wave height of $H_s = 0.1\ m$.

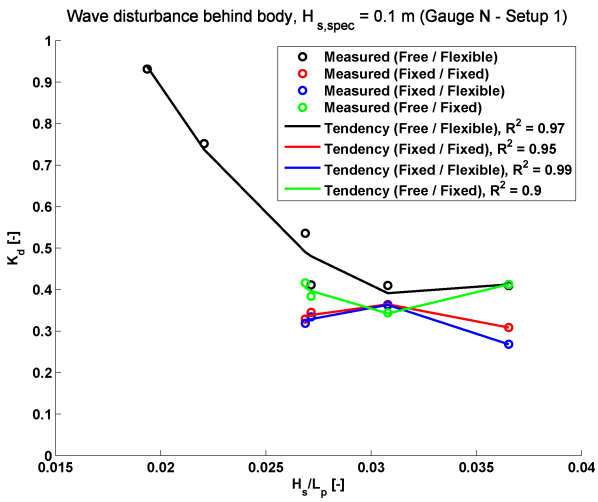

Figure 4.60 *Variation of K_d behind the WD-body.*

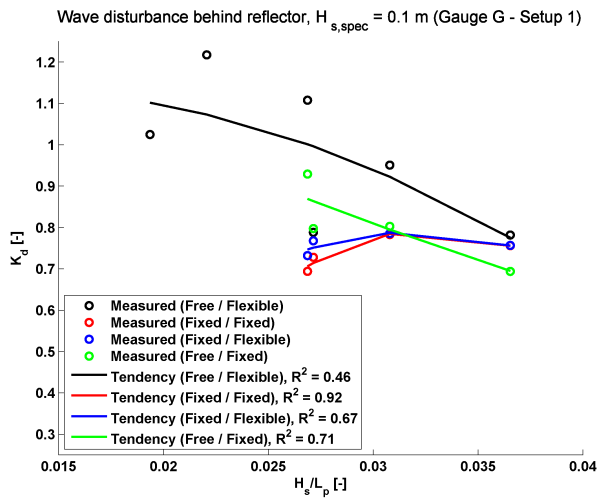

Figure 4.61 *Variation of K_d behind the reflectors.*

The tendency for all setups is, that K_d seems to increase with decreasing H_s/L_p in front of both the body and reflectors. As with the wave disturbance in front of the WD, the *"free/flexible"* setup provides the biggest wave disturbance behind both the WD-body and WD-reflectors. The remaining setups; *"fixed/flexible"*, *"free/fixed"*, and *"fixed/fixed"*, does not show any significant changes compared to the extreme; *"free/flexible"*. However, the tendency is, that the setups with *"fixed"* WD-body provides the smallest K_d both behind the body and reflectors. In Figure 4.61 it is seen, that K_d reaches values above 1, meaning that the measured wave height $H_{s,meas}$ is bigger than the specified incident wave height $H_{s,spec}$. The reason for this may be due to diffraction, which can result in increased wave heights at some locations, see Figure 4.29, and wave radiation generated behind the WD due to heaving effects from the floating structure.

In addition to the wave disturbance behind the WD-body and WD-reflector in Figure 4.60 and Figure 4.61, the varying K_d is plotted using *"test setup 2"* in Figure 4.62 and Figure 4.63 in case of different WD-setups and wave lengths (wave steepness), respectively. The plots are depicting measurements from gauge C to gauge L spanning from the center of the WD-body to the tip of the WD-reflector.

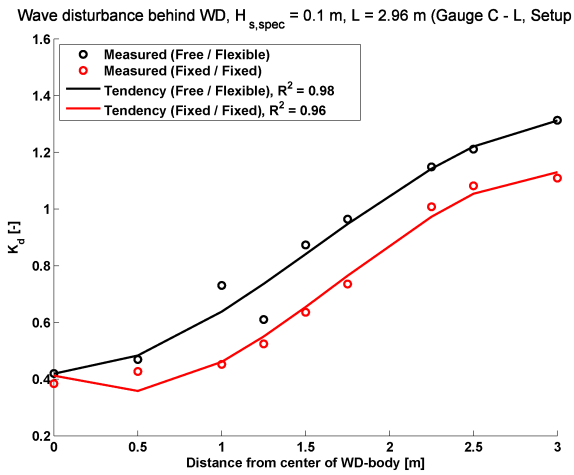

Figure 4.62 *Variation of K_d behind the WD using "test setup 2" in case of different WD-setups.*

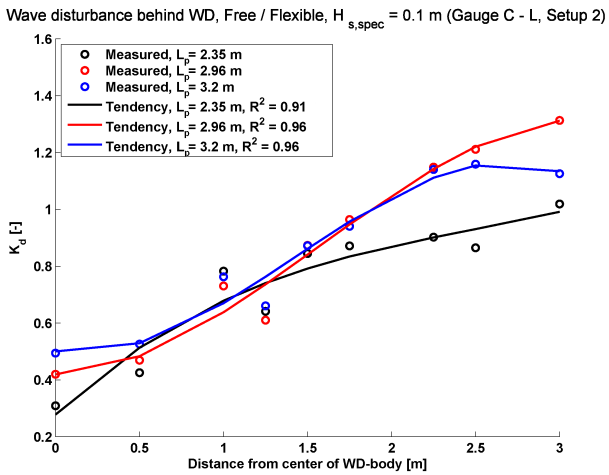

Figure 4.63 *Variation of K_d behind the WD using "test setup 2" in case of different wave lengths or H_s/L_p.*

From Figure 4.62 it is seen, that almost a parallel offset of the two curves from the *"free/flexible"*-setup and *"fixed/fixed"*-setup is present, where a mean relative percentage increase in K_d from the *"fixed/fixed"*-setup to the *"free/flexible"*-setup of $\approx 23\%$ is obtained. K_d increases towards the tip of the reflector, and again, as in Figure 4.61, K_d reaches values above 1 towards the reflector tip. From Figure 4.63 it is seen, that L_p has a significant influence on the wave disturbance behind the structure, and along the reflector.

4.9.4 Wave Energy Spectrum and Peak Period in front of- and Behind the WD in Case of Different Setups and Wave Lengths

The transmitted and reflected waves behind- and in front of- the WD in case of the *"free/flexible"*-setup and *"fixed/fixed"*-setup are further studied by analyzing the wave energy spectrums in Figure 4.64, which shows the results of tests with $T_p = 1.67\ s$ corresponding to the wave length $L_p = 2.96\ m$ with $h = 0.39\ m$. Here it is observed, that the spectral density in front of the WD approximately shows the same tendency for both setups, only with a difference in magnitude. Additionally, the spectral density behind the WD shows similar tendencies at the frequencies between 0.4 Hz to 0.7 Hz. However, at the frequencies from 1.1 Hz to 1.6 Hz, a higher spectral density is observed for the *"free/flexible"*-setup than for the *"fixed/fixed"*-setup. The reason for this may be due to wave radiation generated from the WD, which, due to vertically heaving- or lateral-movements, generates waves at the specific frequencies.

In Figure 4.65 the spectral density is plotted as a function of the wave period T, in case of the *"free/flexible"*-setup and the two specified incident peak period wave lengths; $L_{p,spec} = 2.96\ m$ and $L_{p,spec} = 3.20\ m$ but with the same specified incident peak period, $T_p = 1.67\ s$ and wave height $H_s = 0.1\ m$. The two different wave lengths are obtained by changing the water depth from $h = 0.39\ m$ to $h = 0.48\ m$. Here it is seen, that the peak period is almost unchanged in front of the WD. However, behind the WD-body it

is observed, that the peak period increases from $T_p = 1.65\ s$ to $T_p = 1.97\ s$ in case of the two considered incident peak period wave lengths. Hence, a relative percentage increase in T_p behind the WD of $\approx 20\%$ is obtained when L_p increases $\approx 9\%$, and therefore not only H_s is affected by the transmission through the structure in case of different wave lengths, but also T_p.

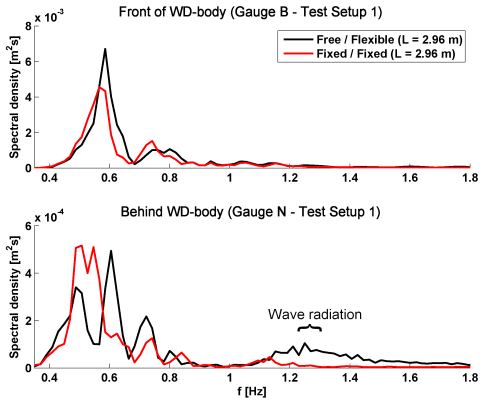

Figure 4.64 *Transmitted and reflected wave energy spectra's behind and in front of the WD in case of the "free/flexible"-setup and "fixed/fixed"-setup.*

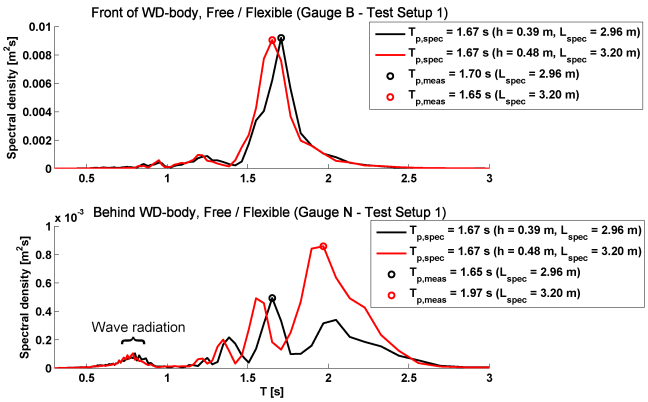

Figure 4.65 *Spectral density as a function of the wave period T, in case of the "free/flexible"-setup at the two specified incident peak period wave lengths; $L_{p,spec} = 2.96\ m$ and $L_{p,spec} = 3.20\ m$.*

4.9.5 Variation of K_d through a Wave Energy Spectrum

As mentioned before, tests with both regular and irregular waves are performed, where the regular waves are mainly used to perform fast calibrations on the WD in the numerical model. It is, however, interesting to analyse how the different frequencies in a wave energy spectrum affects K_d. In Figure 4.66 K_d is determined behind the WD with a specified incident wave height of $H_{s,spec} = 0.04\ m$ using *"test setup 2"* and *"fixed/fixed"*-setup for the WD, in case of regular and irregular waves. Here it can be seen, that an almost parallel offset of the two curves, presenting K_d for the regular and irregular waves, is obtained, where K_d is higher in case of irregular waves. The difference in K_d becomes slightly smaller when considering the *"free/flexible"*-setup with $H_{s,spec} = 0.1\ m$, as seen in Figure 4.67. However, the tendency still is, that irregular waves provides the highest values of K_d (averagely $\approx 12\%$ higher than for regular waves), meaning that more wave energy is transmitted through the structure.

The reason for the differences between the regular and irregular waves is due to the dependence of K_d on T or L, from which follows, that K_d varies through the spectrum. This is illustrated in Figure 4.68, where K_d (determined in case of $H_{s,spec} = 0.04\ m$ and $L_p = 2.96\ m$ from regular waves with different T) increases towards small frequencies or high wave periods, which corresponds to the observations made from the dependence on peak periods and frequencies in the irregular wave spectrums.

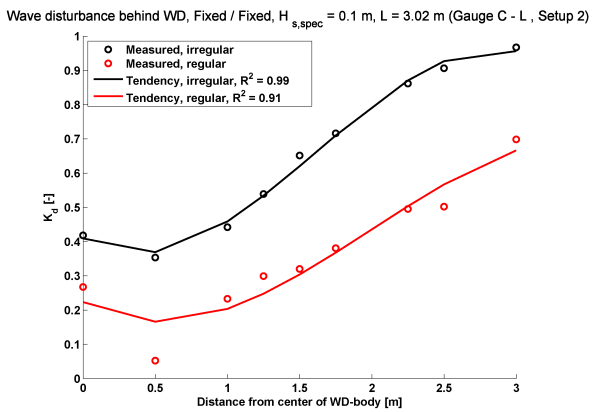

Figure 4.66 *K_d behind the WD with a specified incident wave height of $H_{s,spec} = 0.04$ m using* "test setup 2" *and "fixed/fixed"-setup for the WD, in case of regular and irregular waves.*

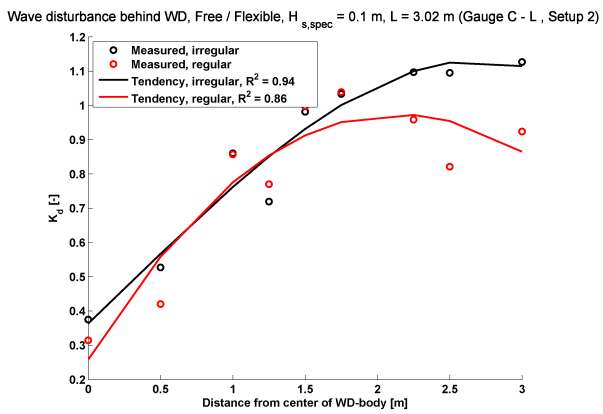

Figure 4.67 *K_d behind the WD with a specified incident wave height of $H_{s,spec} = 0.04\,m$ using* "test setup 2" *and "free/flexible"-setup for the WD, in case of regular and irregular waves.*

It should be noted, that if T for the regular waves is specified as T_e for the irregular waves (T_e corresponds to the weighted average of the wave energy in a energy spectra and can be shown to be $T_e = 0.9 \cdot T_p$ for a JONSWAP spectrum), instead of $T = T_p$ corresponding to the irregular waves, more equal results would have been observed. This is further illustrated when comparing the results in Figure 4.66 and Figure 4.68.

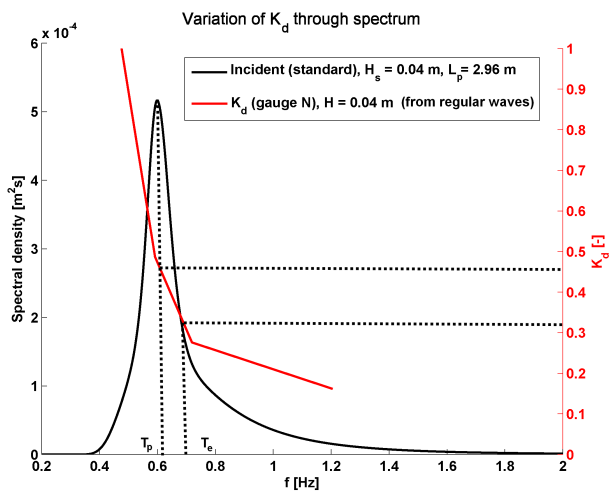

Figure 4.68 *Variation of K_d through a wave energy spectrum in case of "free/flexible-setup, with $H_{s,spec} = 0.04$ m and $L = 2.96$ m.*

An important observation is, that the different waves in the wave energy spectrum, with different wave periods, are not transmitted equally through the WD. A greater amount of wave energy at small frequencies (high wave periods), is transmitted through the WD, than at higher frequencies (small wave periods). This is the reason why an increased T_p is obtained behind the WD, compared to the incident spectrum, as seen in Figure 4.65.

4.9.6 Comparison of the Influence on K_d from Long Crested and Short Crested Waves

A spectrum of wave energy can have an angular distribution, as well as a distribution over a range of frequencies. This angular distribution of wave energy is termed ”directional spreading” and spectral representations which include both the frequency distribution and the angular spreading of wave energy are known as ”directional spectra”, given in (4.8).
(CERC, 1985)

$$S(f,\theta) = S(f) \cdot D(\theta) \tag{4.8}$$

where
$S(f,\theta)$ is the directional spectral density function $[-]$
$S(f)$ is the one-dimensional energy spectral density function $[-]$
$D(\theta)$ is the angular spreading function $[-]$
(CERC, 1985)

The formulation of $D(\theta)$ requires that the total energy in the directional spectrum, $S(f,\theta)$, must be the same as the total energy in the corresponding one-dimensional spectrum, $S(f)$. A spreading function is proposed by (Higgins, 1963) where the change in directional spread is given as a function of the spreading parameter s which is used for this case. $D(\theta)$ is given in (4.9).

$$D(\theta) = \left(\frac{2^{(2s-1)}}{\pi}\right)\left(\frac{\Gamma^2\left(s+1\right)}{\Gamma\left(2s+1\right)}\right)\cos^{2s}\left(\frac{\theta-\theta_0}{2}\right) \tag{4.9}$$

where
Γ is the Gamma function $[-]$
θ_0 is the mean wave direction $[^\circ]$
s is the spreading parameter $[-]$
(Higgins, 1963)

Tests on the WD with Short Crested Waves in the Laboratory Basin

For use in the laboratory test, to determine the influence from directional spreading on K_d, a spreading parameter of $s = 100$ is used, corresponding to a directional gaussian standard deviation of $\sigma_\theta \approx 8$ deg. It should be noted, that $\sigma_\theta \approx 8$ deg is relatively small compared to what can be expected at the site, but, as mentioned before, further spreading results in a greater amount of reflection from the basin boundaries, affecting the measurements around the WD. In Figure 4.69 the angular spreading function $D(f,\theta)$, used in (4.8), is illustrated as a function of the angular deviation from the mean direction $\theta - \theta_0$, with $s = 100$.

The corresponding variation of the measured K_d along the WD in case of short crested waves compared to K_d measured from directional waves with $H_{s,spec} = 0.1$ m and $L_p = 3.02$ m is illustrated in Figure 4.70. It is seen, that generally a smaller K_d is obtained in case of short crested waves, which, with the considered wave height and wave length, is averagely $\approx 15\%$ smaller than K_d measured from long crested waves. This observation of smaller K_d (less wave disturbance) in case of directional spreading does not directly correspond with the study in (Beels, 2009a), as mentioned in Section 2, where it is concluded, that the wake effect behind a single WD is decreasing with increasing directional spreading. However, the reason may be, that more wave disturbance in a close distance from the WD is obtained with short crested waves, which then decreases at a faster rate further behind the WD, resulting in a decreased wake area compared to the case with directional waves.

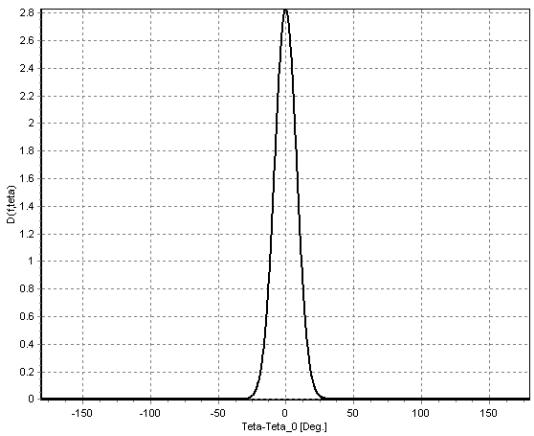

Figure 4.69 *The angular spreading function $D(f, \theta)$, used in (4.8), as a function of the angular deviation from the mean direction $\theta - \theta_0$, with $s = 100$.*

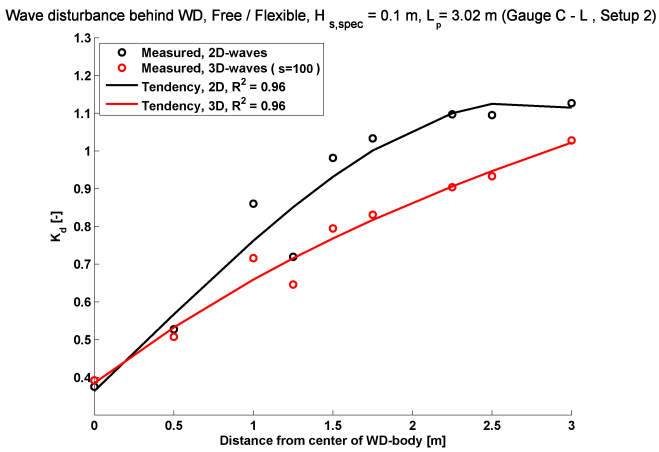

Figure 4.70 *Variation of the measured K_d along the WD in case of short crested waves compared to K_d measured from long crested waves with $H_{s,spec} = 0.1\ m$ and $L_p = 3.02\ m$.*

A further factor which may affect the results is, that the incident wave height in case of short crested waves is unknown, since no reflection analysis is performed on this sea state. The incident wave height from the 3D wave is expected to be smaller than the specified, since no corner reflection is included in the laboratory tests, and hence less total energy is present in the directional spectrum, $S(f, \theta)$, than the total energy in the corresponding one-dimensional spectrum. This affects the results in the way, that smaller K_d will be obtained from waves with directional spreading.

The WD will not be calibrated against short crested waves in the numerical model, since too many uncertainties are present in the measurements. However, it is expected, that a WD which is calibrated against long crested waves will achieve the approximate correct transmission and reflection characteristics in case of short crested waves.

4.10 Summary of Findings in present Chapter

General key findings from the present chapter are listed in the following:

- A decreasing crest freeboard rate results in decreasing transmission from the WD, and a decreasing wave length, or increasing wave steepness, results in a decreasing transmission. From this follows, that the peak period in the transmitted wave from the WD is increased. The wave length has a bigger influence on the wave disturbance than the crest freeboard rate.

- The moored WD, using the mooring-stiffness as specified from the Nissum Bredning prototype (*"free/flexible"*-setup), provides the smallest wave height reduction in the wake, compared to when the WD is *"fixed"*. Hence it is concluded that the transmission characteristics are relatively sensitive to vertical and lateral movements of the structure. The difference in transmission characteristics between the *"fixed"* and *"flexible"* reflector-setup is small and almost negligible.

- A small amount of wave radiation is generated behind the WD when using the *"free/flexible"*-setup at small frequencies due to vertical and lateral movements.

Chapter 5

Implementation of Test Results in Numerical Wave Propagation Model

In the present chapter, the results obtained from the experiments, described in Chapter **??**, will be used to calibrate a numerical model of the test setup from the laboratory, where the calibration is based on the wave disturbance obtained from experimental results. The calibrated WD will be used in a later chapter to study the possibilities for obtaining wave height reduction in Santander, from a farm of WD's.

Since the WD model used in the laboratory is scaled, a direct transfer to the full scale conditions in Santander is not possible, and thus the numerical model of the test setups is scaled to the real conditions. Scaling, as well as the calibration of the boundary conditions in the wave basin, is described in Appendix B.3.

5.1 Calibration of WD

Once it is ensured, that the boundaries representing the laboratory basin produce the correct results, the WD is added to the model in order to calibrate its properties against the test data. In Chapter **??** it was concluded, that the stiffness of the reflectors has no influence on the transmission characteristics of the WD. From this follows, that the *"fixed/fixed"*- and *"free/free"*-setup are referred to as *"fixed"*- and *"free"*-setup through out the rest of the project.

Regular waves, are used to perform a fast and rough calibration of the WD. It was seen in Section 4.9, that the wave length has a large influence on the amount of energy transmitted through the WD, and hence it needs to be ensured, that the model can describe these properties correctly. To do this, both the *"fixed"*- and *"free"* WD-setups are calibrated against the irregular wave with shortest considered peak wave length, $L_p = 2.35m$, and validated against the considered irregular wave with the largest peak wave length $L_p = 3.20m$, when using an unchanged relative floating level in the two tests. Only long crested waves, approaching the WD directly from the front, are applied.

The calibration will be done in three parts: A regression analysis on polynomials describing the average distribution of K_d behind the WD, a comparison of the transmitted wave energy, and a direct comparison of K_d at the different gauges.

5.1.1 Numerical model of WD

The WD is modelled using porosity layers with varying values through the geometry, as shown in Figure 5.1. The geometry formed by the porosity layers does not correspond completely with the geometry of the actual WD. Most notably is a significant increase in the thickness of the reflectors. The cause of this increase is the method used to decouple reflection and transmission, where multiple porosity layers are given varying porosity values, further described in Section 4.4.1. Since the size of the porosity layers correspond to the grid spacing, using multiple layers will introduce an inaccuracy in these areas. With the calibrated distribution of porosity layers, the reflectors have a thickness of $5.2 - 15.5m$ as opposed to the real thickness of $1.8 - 3.4m$. However, since the area of interest is not under, or close to the WD, the geometrical inaccuracy is acceptable. More accurate results close to the WD can be achieved by using a smaller grid spacing, but this will add substantial computational requirements to the simulation.

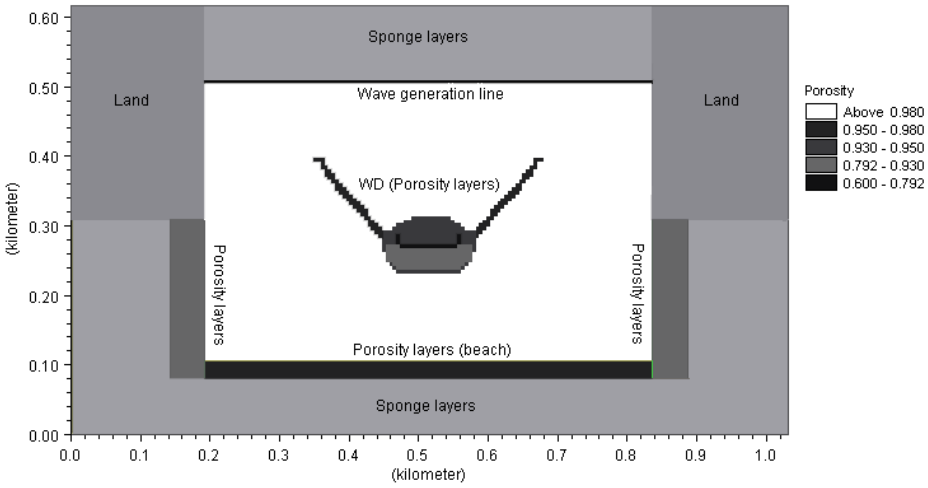

Figure 5.1 *Porosity layers used to model the WD in the scaled laboratory basin.*

5.1.2 Calibration of *"fixed"* WD

The distribution of the wave disturbance behind the WD gives an indication of not only the wave height reduction behind the WD, but also how the waves diffract around it. This distribution is found based on tests with *"test setup 2"*, where the wave gauges are placed along a line behind the WD. As written, the porosity layers are calibrated against an irregular wave spectrum with $H_s = 0.086\ m$, $L_p = 2.35m$ ($H_s/L_p = 0.043$) in Figure 5.2 and validated against a spectrum with $L_p = 3.20m$ ($H_s/L_p = 0.031$) in Figure 5.3. A regression analysis is performed on the fitted polynomials, and it is found that $R^2 = 0.99$ for the test with $L_p = 2.35m$ and $R^2 = 0.98$ for the test with $L_p = 3.20m$. The largest deviation is seen at the center of the WD where the numerical model has a tendency to overestimate the wave height reduction from the WD, resulting in slightly lower values of K_d.

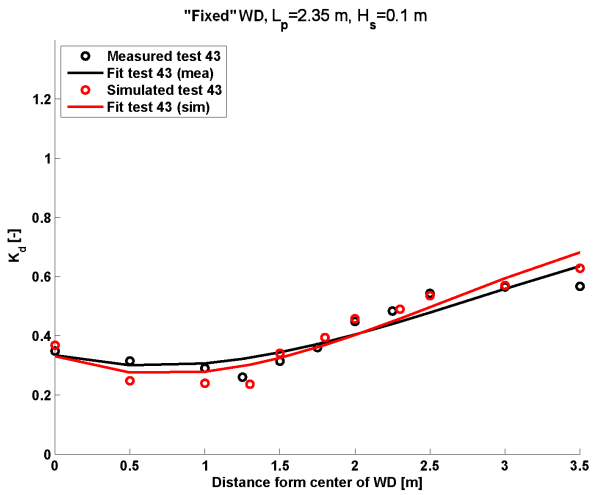

Figure 5.2 *Measured and simulated distribution of K_d with $L_p = 2.35m$ - used for calibration.*

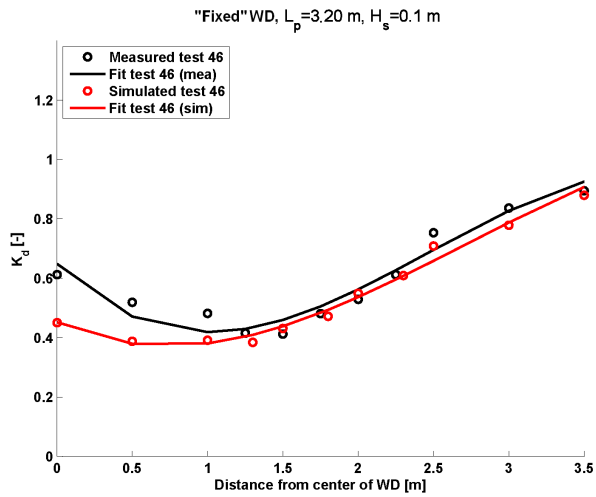

Figure 5.3 *Measured and simulated distribution of K_d with $L_p = 3.20m$ - used for validation.*

The relative difference in transmitted wave energy is calculated based on the area under the fitted polynomials in Figure 5.2 and 5.3. Table 5.1 show the results, where the WD part "Body" corresponds to the first $1.3\ m$ in Figure 5.2 and 5.3 and "Reflectors" corresponds to the remaining part. It is seen, that the model overestimates the dampening effect of the WD in both cases, most notably in the body area with long waves. A reason for the large relative difference behind the body is that *"fixed"* setup introduces a large reduction of the wave height behind the body, meaning small influences from the boundaries will have a larger impact on K_d. The difference is accepted, but kept noted, as the *"fixed"* model is mainly used as a reference to the *"free"* setup.

$L_p\ [m]$	$H_s\ [m]$	WD part	Relative difference in wave energy [%]
2.35	0.1	Body	-12.11
2.35	0.1	Reflectors	5.97
Total			-6.14
3.20	0.1	Body	-38.76
3.20	0.1	Reflectors	-4.33
Total			-43.09

Table 5.1 *Relative difference in transmitted wave energy between measured and simulated values.*

In addition to the distribution of K_d behind the WD it is also of interest to ensure that the waves are modelled correctly in the area around it. This is done by comparing the wave disturbance obtained at the gauge positions in *"test setup 1"*. Figure 5.4 and 5.5 show the measured and simulated results.

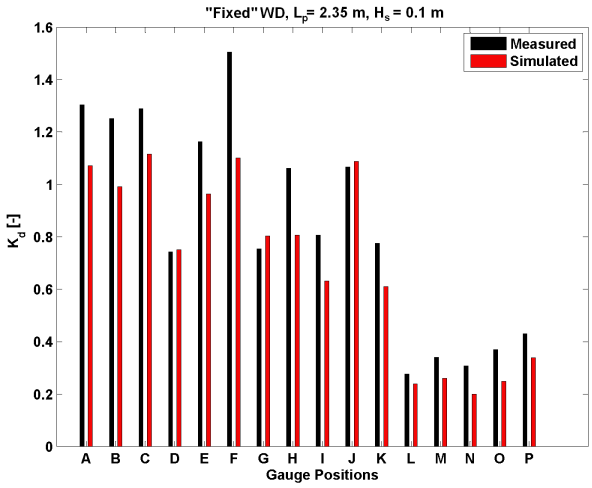

Figure 5.4 *Comparison of wave disturbance with $L_p = 2.35m$ - validation against measurements from "test setup 1".*

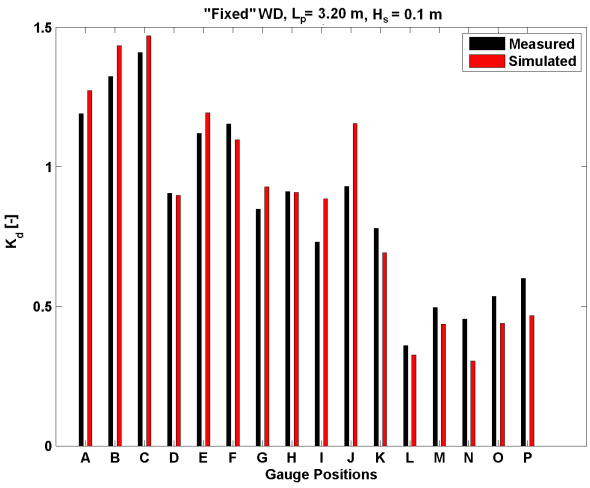

Figure 5.5 *Comparison of wave disturbance with $L_p = 3.20m$ - validation against measurements from "test setup 1".*

In both cases it is seen, that the largest deviation is found at gauge F, which is placed in front of the WD and close to the reflector. In addition, the gauges A, B, C and E show a certain deviation. All these gauges are placed in front of the WD and it is seen that K_d, in all cases, is larger for the measured data than for the simulated. This suggest that the reflection from the WD is underestimated in the model. However, the remaining gauges, placed behind the WD have very little deviation, suggesting that the transmission trough the WD is modelled correctly. The cause of the deviations in front of the WD can be due to an inaccurate decoupling of the reflection, absorbtion and transmission or influence from the fact that the WD is placed very close to the wave generator, which can cause disturbance. It was seen in Section 4.2, that only the transmission through a structure has influence on the diffraction around it, and thus the inaccurate distribution of absorbed and reflected energy is accepted.

5.1.3 Calibration of *"Free"* WD

The same analysis as in the previous section is performed for the *"free"* WD-setup. As with the *"fixed"* WD, two tests, with different wave lengths are used where calibration is performed on the wave spectrum with the shortest L_p (biggest wave steepness), and validation is performed on the spectrum with the longest L_p (smallest wave steepness). The results are shown in Figure 5.6 and 5.7.

As in the previous section, a regression analysis is performed on the polynomials fitted to the measured and simulated data, where a regression coefficient of $R^2 = 0.90$ is obtained in both the calibration and validation of the model. While these values suggest that the models provide good estimates of the real results, it should be noted that the measured values are more scattered compared to what was obtained from the model, especially for the short waves. This was not observed for the tests with the *"fixed"* WD, shown in Figure 5.2 and 5.3, suggesting that the scattering is caused by the horizontal movement of the WD, which cannot be recreated in the present model. When short waves hit the WD, they will apply a

larger horizontal force than long waves with the same wave height. This force will then move the WD, causing a disturbance behind it, which results in deviation from the shape of the tendency seen for the *"fixed"* WD and numerical model. While the effects of the horizontal movements of the WD cannot be modelled accurately, the model is still accepted as it follows the same tendency as the measured data.

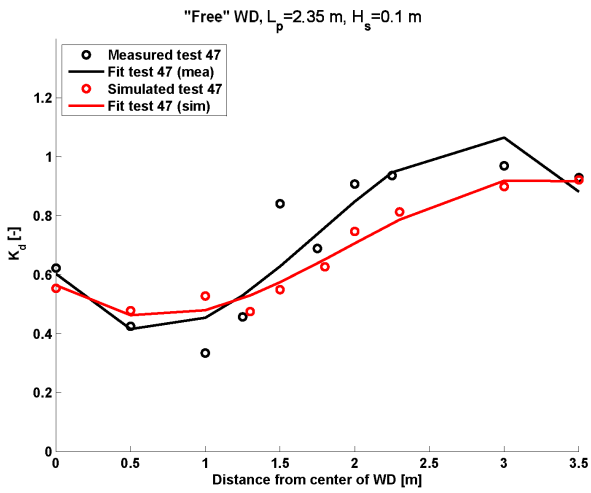

Figure 5.6 *Measured and simulated distribution of K_d with $L_p = 2.35m$ - used for calibration.*

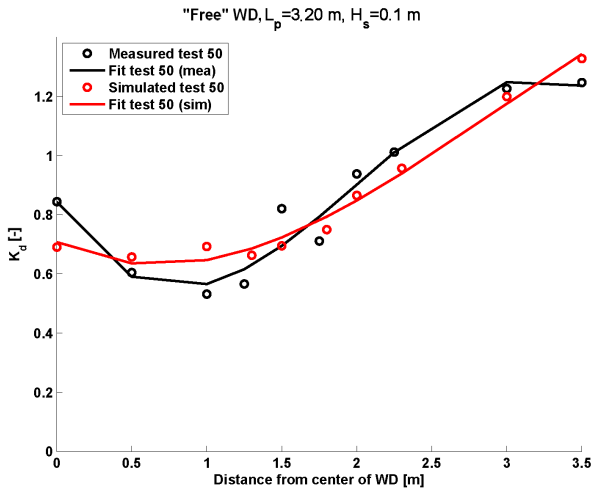

Figure 5.7 *Measured and simulated distribution of K_d with $L_p = 3.20m$ - used for validation.*

Table 5.2 show the relative difference in wave energy, based on the areas under the fitted polynomials. It is seen that the total transmitted energy is slightly underestimated. However in both cases the energy transmitted through the body, where the majority of dampening takes place, is. Due to the relatively small difference in wave energy and good correlation between the fitted polynomials, the calibrated model is found to be acceptable for determining the effects of the *"free"* WD.

L_p $[m]$	H_s $[m]$	WD part	Relative difference in wave energy [%]
2.35	0.1	Body	6.73
2.35	0.1	Reflectors	−18.29
Total			−11.56
3.20	0.1	Body	−0.15
3.20	0.1	Reflectors	−1.40
Total			−1.55

Table 5.2 *Relative difference in transmitted wave energy between measured and simulated values.*

The comparison of the wave disturbance at the gauge positions in *"setup 1"* is once again performed with two wave lengths, and the results are shown in Figure 5.8 and 5.9. As with *"fixed"* WD, the largest deviation is seen at the gauge F which is placed close to the reflectors and thus subject to disturbance. Since the gauges behind the WD provide good results, and the main interest lies in the transmissive properties of the WD, the model is accepted, regardless of the inaccuracies concerning the reflection.

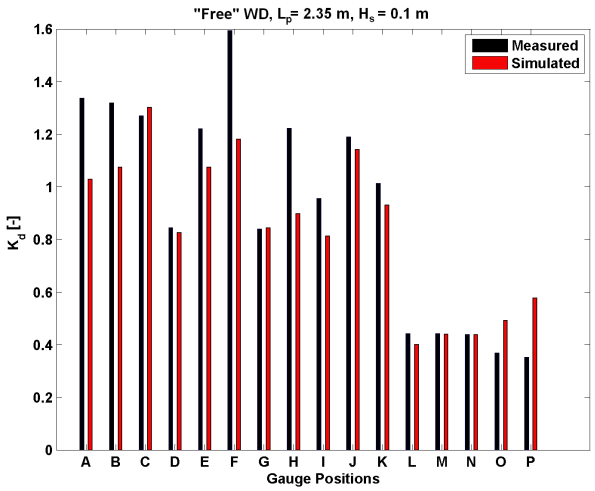

Figure 5.8 *Comparison of wave disturbance with $L_p = 2.35m$ - validation against measurements from "test setup 1".*

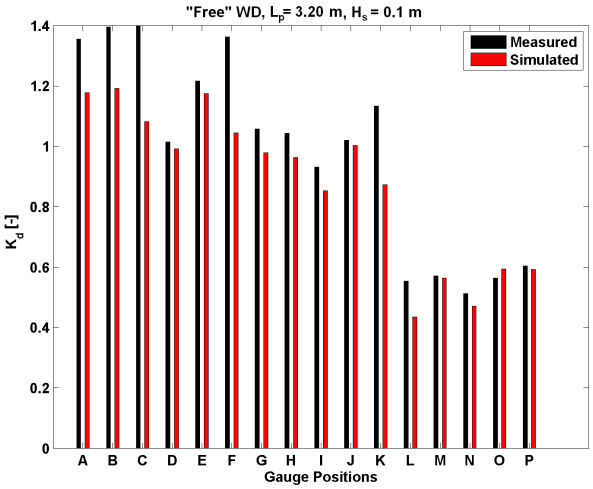

Figure 5.9 *Comparison of wave disturbance with $L_p = 3.20m$ - validation against measurements from "test setup 1".*

5.1.4 Influence from Varying Wave Periods - Wave Steepness

It was seen, in Section 4.9, that the wave disturbance behind the WD varies throughout the wave spectrum. In order to verify that the calibrated model has the same behavior, a similar analysis is performed. Regular waves, with different wave periods, are applied to the model, using a water depth $h = 20.2\ m$ (up-scaled from $h = 0.39\ m$). The result is shown in Figure 5.10, where it can be seen, that K_d is higher at lower frequencies, meaning less transmission of energy at higher wave periods, as was the case in Section 4.9. The tendency is apparent for both the *"fixed"* and *"free"* WD.

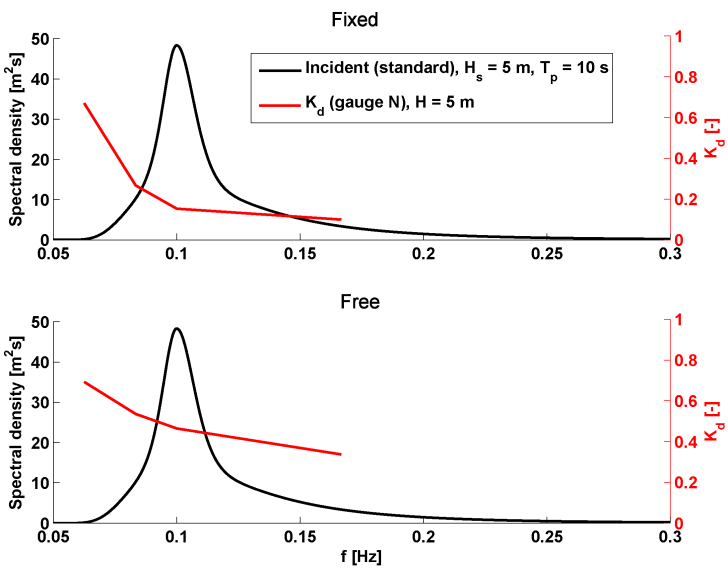

Figure 5.10 *Variation of K_d through a wave energy spectrum, for numerical models of both free and fixed WD.*

5.2 Summary of Findings in present Chapter

General key findings from the present chapter are listed in the following:

- The calibrated model using the *"fixed"* setup shows a regression coefficient of $R^2 = 0.99$ when validating against measured data, and the calibrated model using the *"free"* setup shows a regression coefficient of $R^2 = 0.9$ from the validation. The relative difference in transmitted wave energy show that the model overestimates the dampening effect of the WD, most notably when using the *"fixed"* setup. These deviations are accepted, but kept noted when the model is applied. Hence it is concluded, that the simulated wave disturbance behind the WD correspond sufficiently well with the measured, and the wave disturbance can be expected, to be found with satisfactory accuracy, when using the calibrated WD in a case study.

Part III

Case Study

Chapter 6

Modeling and Investigation of Wake Behind WD's in Santander Bay

In the present chapter, a numerical model of Santander bay is constructed, in order to determine the effects of an offshore WD-farm on the wave climate inside the bay. First a description of the "Santander model"-setup is given, including a description of the bathymetry, model boundaries, and sufficient time- and spatial discretization. The calibrated *"fixed"* and *"free"* WD's are considered, and a preliminary study is performed to obtain the appropriate offshore distance of the farm at which a satisfactory wave height reduction is obtained in the bay, and a reasonable electricity production can be expected. After this, the wake from different WD-farm layouts is evaluated using the same wave conditions as in Chapter **??**, consisting of both long- and short crested waves with different wave periods. Moreover an evaluation of the available wave power in front of the each individual WD in a farm is investigated, together with a study of the influence on wave direction, wave period, and directional spreading, in the wake of an offshore WD-farm. The chapter ends up with a proposal for an appropriate WD-farm layout for use in wave height reduction in Santander bay. The influence on the shoreline from the chosen WD-farm will be further evaluated in a later chapter where the cross shore sediment transport at Santander spit is evaluated.

6.1 Setup of Numerical Model of Santander Bay

The bathymetry and the setup of the Santander model is described in the following, including an analysis of the influence from calibration factors such as bottom friction and grid spacing. The influence from bottom friction in the Santander bay model will be studied, since no calibration or validation is performed, and hence it is important to determine whether this may influence the results.

6.1.1 Bathymetry of Santander Bay and Area of Interest

The bathymetry is implemented in MIKE21 BW by using bilinear interpolation between contour lines copied from Figure 6.1. The considered part of the beach, for use in the analysis of the wave height reduction in a later section, is illustrated in Figure 6.1, marked with a red box. The simulation in MIKE21 BW is, however, run on a bigger bathymetry to avoid diffraction from absorbing boundaries in the area of interest, cf. Section 4.2. This is further described in Appendix C.

The minimum water depth in Figure 6.1 is $0\ m$ at the beach, which causes the waves to break as they approach land. Wave breaking introduces a need for smaller grid spacing and time steps, and hence a need for substantially higher CPU time in the numerical model, cf. (DHI, 2008d). Therefore, since wave

breaking at the shoreline is not of particular interest when simulating the wave disturbance from WD's, the minimum water depth at the beach is modified to avoid wave breaking. Wave breaking is caused either by the water level being too low compared to the wave height, or the waves becoming too steep. The depth limit is given in (6.1), while the steepness limit is given in (6.2).

$$H \geq 0.8h \tag{6.1}$$

$$\frac{H}{L} = 0.142 \cdot \tanh\left(\frac{2\pi \cdot h}{L}\right) \tag{6.2}$$

(Miche, 1944) H_{max} and T_p are used in (6.2) to find a minimum water depth in the domain. Here a minimum depth of $h_{min} = 10\ m$ is estimated, and hence shallower water depths than h_{min} are replaced by -10 m in the bathymetry. In Figure 6.2 the modified water depths in the area of interest is illustrated.

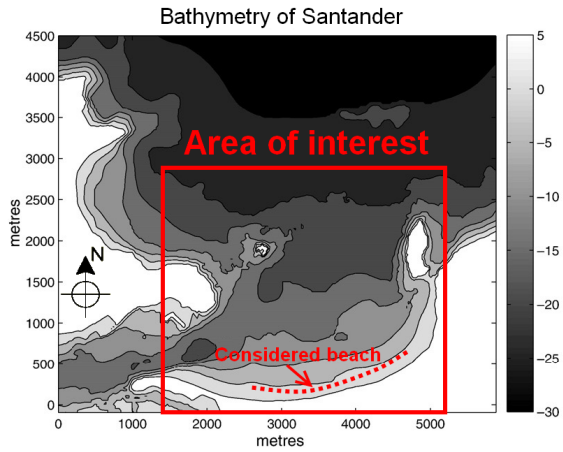

Figure 6.1 *Bathymetry of El Puntal spit (orientated to the north), and illustration of area and beach of interest. (Medellín, 2007).*

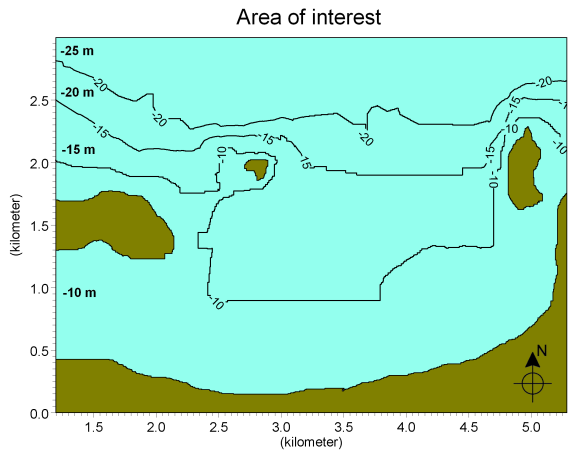

Figure 6.2 *The area of interest with the modified minimum water depth (set to $h = -10$ m).*

All comparisons in following sections will be performed in areas outside the modified bathymetry where wave breaking normally would have occurred. Hence the modified bathymetry is not expected to influence conclusions made from the models.

6.1.2 Modeling of Boundaries and Wave Generation Direction

The coastline of Santander consist of a mixture of sand beaches and cliff sides with different reflective properties. These are modelled using porosity layers. In all cases, the porosity layers are given a thickness of approximately 30 m, but with different porosity values S depending on the type land boundary. The beach areas are given a porosity value $S = 0.96$ corresponding to $K_r \approx 0.1$ with $T_p = 10\ s$, while the areas with cliffs are given a values of $S = 0.6$ corresponding to $K_r \approx 0.78$. It should be noted, that an increase in K_r arise with increasing L, cf. Section 4.1.3. In addition to the reflective boundaries, sponge layers are defined at open boundaries as described in Section 4.1.1 where 50 layers are used, which is seen from Section 4.1.1 to only provide a negligible amount of reflection back into the model domain. The boundaries in the numerical model of Santander bay are illustrated in Figure 6.3 and summarized in Table 6.1. It should be noted, that in order to avoid diffraction from open absorbing boundaries it has been necessary to extend the west and east side-boundaries. This is further explained in Appendix C.

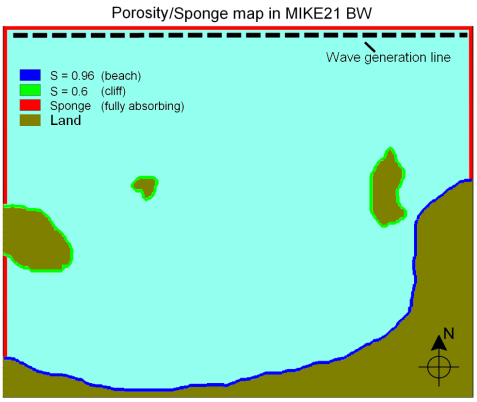

Figure 6.3 *Porosity- and sponge layers for use in the numerical model of Santander bay.*

Boundary type	S	K_r (with $T_p = 10\ s$)
Beach	0.96	0.1
Cliff	0.6	0.78
Open	Sponge	≈ 0

Table 6.1 *Specification of boundaries in model of Santander.*

In Section 1.3 it was seen that the most common wave direction is north west (NW) some distance from the coast of Santander. It is however observed, that the waves refract along the coast, and turn towards a more northerly direction when approaching the entrance to Santander bay. Due to this, and to minimize the size of the computational domain, further explained in Appendix C, the majority of the study on wave height reduction behind WD's in Santander, from different farm-layouts, is performed using waves approaching from north (N). A few additional tests with waves from the NW-direction will, however, be performed and compared to the case with waves from N.

6.1.3 Convergence of K_d as Function of Grid- and Time Discretization and Number of Incident Waves

The importance of having a sufficiently fine grid spacing was investigated in Section 4.1, where it was seen, that the ratio between the wave length and grid spacing should be $L/dx > 50$ to obtain good absorption and reflection characteristics.

With the smallest wave period $T_{min} = 6\ s$, and a water depth $h = 10\ m$, the minimum wave length is $L_{min} = 48.4\ m$ corresponding to a grid spacing of $0.968\ m$. Given the size of the model area, this grid spacing will result in substantial computational requirements and thus large CPU-time requirements for each simulation. In order to lessen this problem, an analysis of the influence of the grid spacing on the wave disturbance in the Santander model is carried out. This is done in Appendix C by performing a convergence analysis on the wave disturbance at given positions in the model domain. Additionally, the needed number of generated incident waves for obtaining converged values of K_d, is studied in Appendix C.

It is found, that a minimum number of 1200 incident waves (corresponding to T_p) are needed for obtaining a converged K_d in the whole model domain. Additionally it is seen, that an element size of $dx = dy = 5.18\ m$ is sufficient. Concerning the time discretization, a time step of $dt = 0.15\ s$ is chosen for the model, corresponding to a Courant number of 0.45. The model discretization and required number of incident waves for use in the Santander model is summarized in Table 6.2.

Discretization of Santander model	
$dx = dy$	$5.18\ m$
dt	$0.15\ s$
Required number of incident waves (corresponding to T_p)	1200

Table 6.2 *Model discretization and required number of incident waves for use in the Santander model.*

6.1.4 Influence from Un-calibrated Model Variables

As mentioned previously, the simulation of the wave propagation in Santander will be performed on an un-calibrated model, hence calibration factors such as incident waves/currents, bed-resistance, and bathymetry are not adjusted to obtain the actual wave conditions in the considered area.

However, the influence from the un-calibrated bed-resistance is studied. This is done in Appendix C, where the extreme cases, with no bottom friction and a specified equivalent roughness height of $k_s = 0.3$ m are compared, with and without an inserted WD in the domain. Here it is seen, that the biggest relative percentage difference between the presence and non-presence of bed roughness in the model is $\approx 4\ \%$ and $\approx 6\ \%$. Hence it is expected, that the un-calibrated bed roughness will only have a little influence on the conclusions made from the simulations.

Influence from eddy viscosity, briefly described in Appendix A, is neglected, since these are only expected to influence the wave disturbance in the breaker-zone which is not considered. Since simulations of the wake behind a WD will not be compared with existing measurements from the area, but only with results from a numerical model with no WD's included, possible introduced errors in the un-calibrated model are expected to be negligible.

6.2 Positioning and Layout of Considered WD-farms in Santander Bay

A brief preliminary study of a single WD with the *"free"*- and *"fixed"* WD-setup is performed in a wave basin with constant depth, in Appendix C. A part of the results from the study are summarized in Figure 6.4 and 6.5. It is concluded, that that an increasing wave length and increasing directional spreading results in an increasing K_d or deceasing wave height reduction behind the WD, as expected cf. Chapter **??**. Further it is seen in Appendix C, that the wake shortens with increasing directional spreading due to a faster redistribution behind the WD. A wider wake is observed when short-crested waves are generated due to changing diffraction contours. From Figure 6.5 it is seen, that a small increase in wave height is obtained at the edges of the wake in case of long crested waves, due to diffraction. This tendency, however, disappears when directional spreading is introduced.

To obtain a profitable energy production, and to preserve ship traffic going in and out of Santander bay, the WD's should be placed in a sufficient distance from the entrance of the bay, but still at an appropriate distance from the shore to provide a sufficient wave height reduction. From Figure 6.4 it is seen, that the WD's should not be placed more than 2000 m from the beach to still provide a reasonable wave height reduction. The same tendency is observed in case of short crested waves. Further it is seen, that the difference in K_d from the *"free"* and *"fixed"* setup damps out in a greater distance behind the WD. The same tendency is seen in (Smith and Venugopal, 2007) and is expected to be caused by redistribution of

wave energy which is expected to be faster in case of bigger gradients of wave height differences.

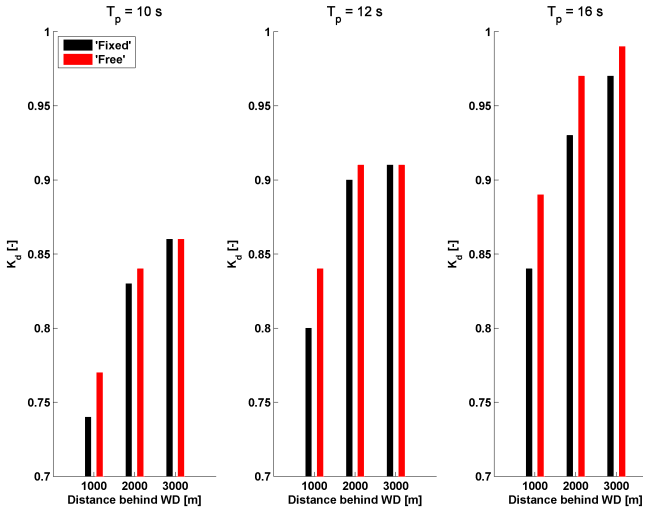

Figure 6.4 *Wave disturbance in a longitudinal section behind the WD in case of long crested waves.*

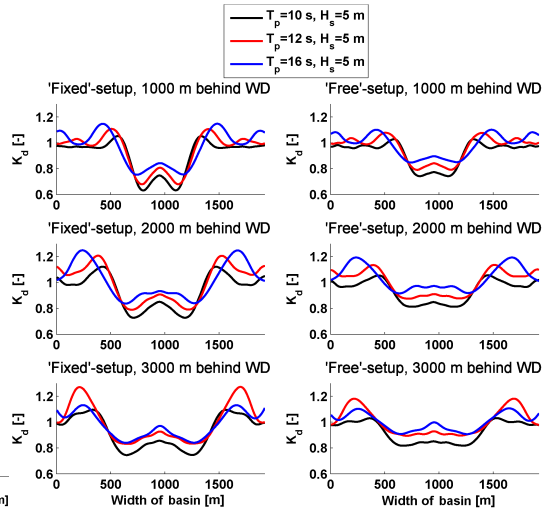

Figure 6.5 *K_d in lateral sections behind the WD, in case of long-crested head on waves.*

6.2.1 Distance Between Individual WD's in Farm

When the WD's are placed in a farm, an individual lateral distance of 260 m is chosen to prevent collision in the case where one WD is fixed in its far position due to a fault, and its neighbouring WD turn to the other far position. Here the rotation of the WD is assumed to be restricted to a rotation of $\pm 60°$ by its mooring system, (Beels, 2009b), illustrated in Figure 6.6 (a). In the case where the WD's are placed in a staggered pattern with two rows, a longitudinal distance of 340 m between the reflector tip's is chosen to avoid collision, illustrated in Figure 6.6 (b).

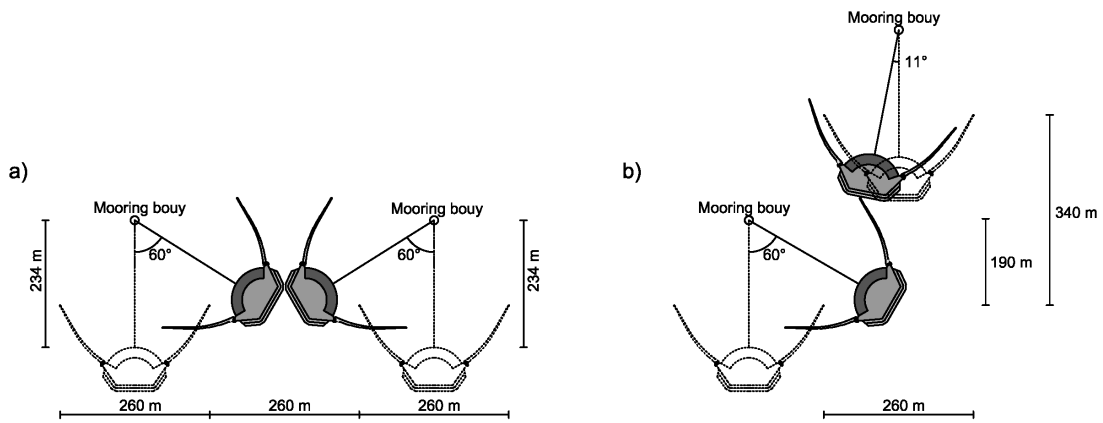

Figure 6.6 *Lateral distance, a), and longitudinal distance, b), between individual WD's, inspired by (Beels, 2009b).*

6.2.2 Considered Farm Layouts

Due to the relatively small water depth between the eastern island and Magdalena beach, cf. Figure 6.1, waves are expected to break here, and hence no WD's will be positioned in this area. Instead, the WD farms will be positioned between the eastern and western islands at the entrance to Santander bay. To investigate how different farm layouts affects the wave height reduction, one-, two, three, and five WD's are placed in a line or in a staggered pattern. The different farm layouts are illustrated in Figure 6.7.

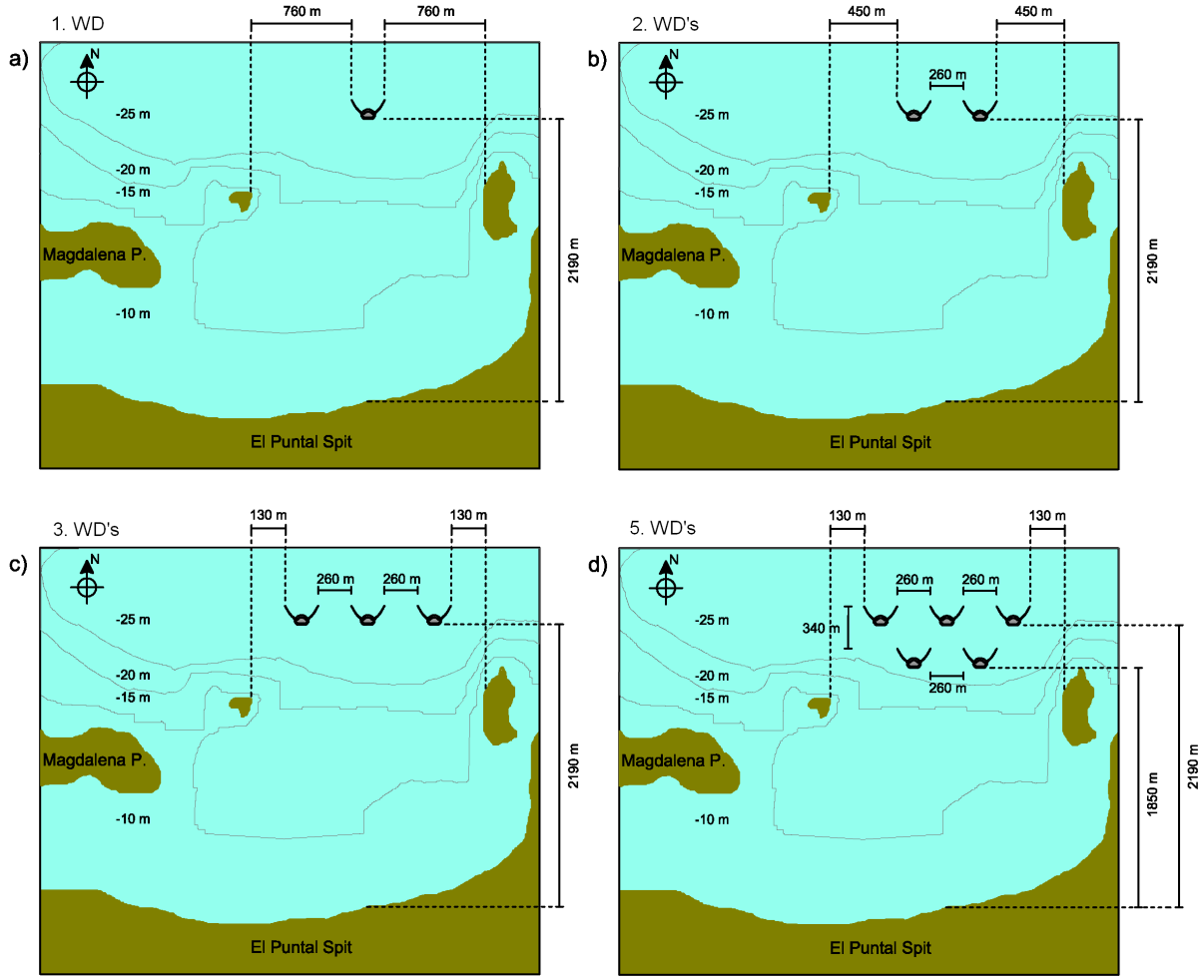

Figure 6.7 *a) one WD, b) two WD's on a line, c) three WD's on a line, d) five staggered WD's.*

The majority of the study, and comparison of different farm layouts, concerning wave height reduction of waves approaching the shore in Santander bay, will be based on WD's with the *"free"* setup, which is also the most realistic. Additional simulations will, however, be performed to study the sensitivity of the mooring stiffness.

6.3 Investigation of Wave Height Reduction Behind Different WD-farm Layouts in Santander Bay

As mentioned in Section 1.4.3, a winter-storm with $H_s = 5\ m$ is considered. The wave periods used to calibrate implemented WD's in Chapter 5 are further considered in the numerical model of Santander.

The effects from the different WD-farm layouts are compared along an output line positioned between the islands, illustrated in Figure 6.8, in the majority of the analyses. The output line is located just outside the wave breaking zone, since this is not included in the model. Further, information from the wave height reduction outside the breaking zone can be used in a later investigation of the shoreline evolution, where waves will be propagated to the beach. Hence it should be noted, that the presented wave height reductions in the following are not the actual wave height reductions at the beach.

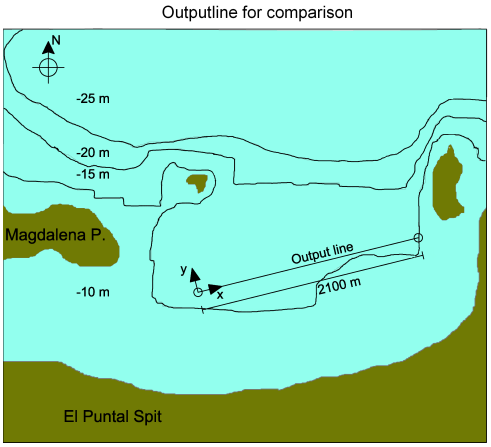

Figure 6.8 *Illustration of output line used for comparison of the wave height reduction from the different WD-farm layouts.*

6.3.1 Evaluation of Wave Propagation in Santander Bay During "Normal Conditions"

In Figure 6.9 and 6.10 the wave disturbance contours in the bay are illustrated in case of long- and short crested waves, respectively.

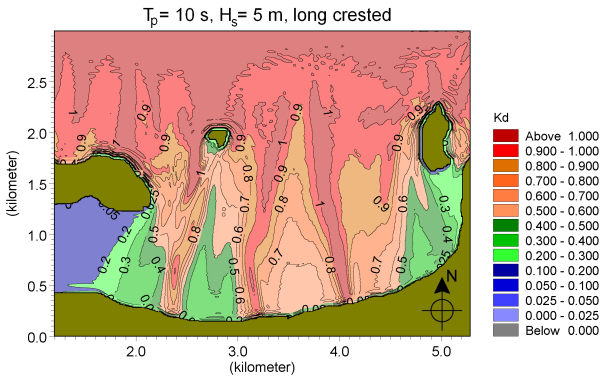

Figure 6.9 *Wave disturbance contours in case of long crested waves approaching from north.*

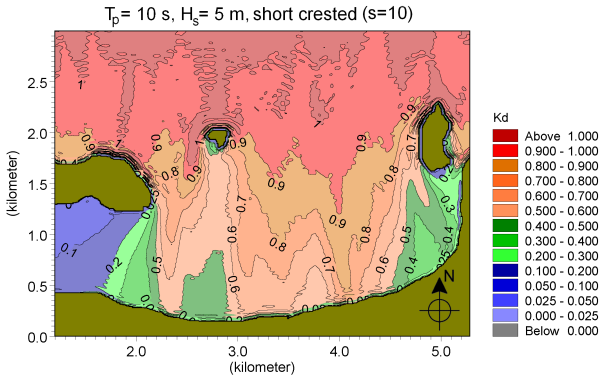

Figure 6.10 *Wave disturbance contours in case of short crested waves approaching from North.*

Due to refraction from the bottom contours, wave heights are reduced when approaching the coast, as the case in Section 4.36. However, especially in case of long crested waves, "spikes" appears in the bay, where bigger wave heights are obtained than in the surrounding areas. These arise from a combination of diffraction and reflection from the eastern and western islands and beaches. When short crested waves

are applied to the model, the diffraction lines change position, and the spikes fade out. The spikes are further seen to disappear when removing the islands and beaches from the bathymetry, but leaving the correct contours in the bay. This is, however, not illustrated here.

6.3.2 Comparison of Wake from Different WD-Farm Layouts

Long crested waves from north are considered. The wake effect from the different WD-farms are illustrated in Figure 6.11 to 6.14 in case of one-, two-, three, and five- WD's, respectively.

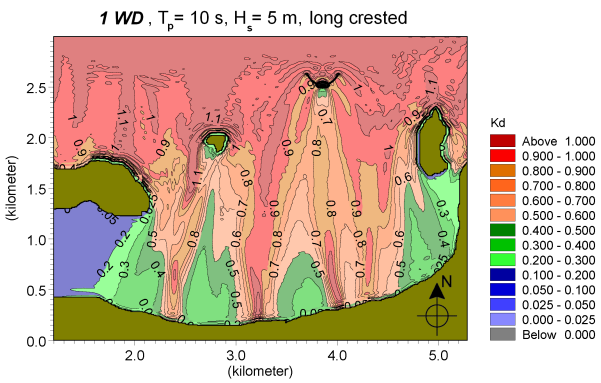

Figure 6.11 *Wake effect from one WD, using "free" WD setup. Incident waves are propagating from north.*

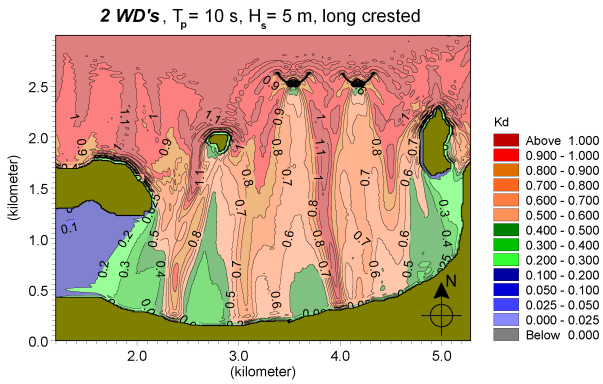

Figure 6.12 *Wake effect from two WD's, using "free" WD setup. Incident waves are propagating from north.*

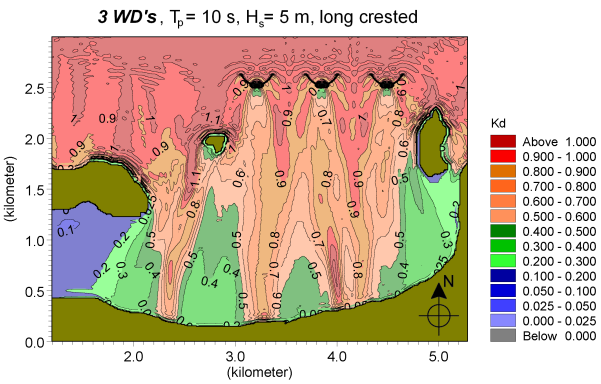

Figure 6.13 *Wake effect from three WD's, using "free" WD setup. Incident waves are propagating from north.*

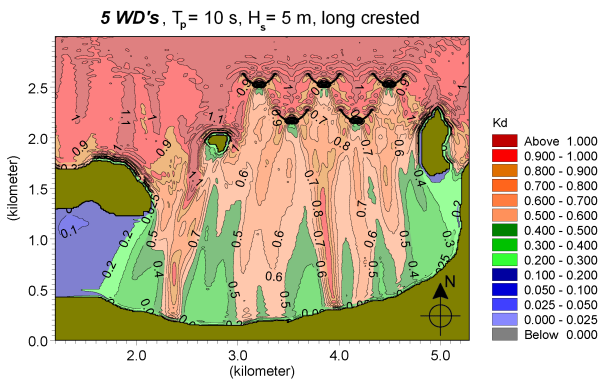

Figure 6.14 *Wake effect from five WD's, using "free" WD setup. Incident waves are propagating from north.*

As a comparable measure of the wake from the different WD-farm layouts, the ratio between the significant wave heights in case of WD's placed offshore, $H_{s,WD}$, and the significant wave height obtained during "normal conditions", $H_{s,normal}$, given the same incidents wave conditions, is plotted in Figure 6.15. This is done along the output line in Figure 6.8. The mean relative percentage difference between $H_{s,WD}$ and $H_{s,normal}$ is further plotted in Figure 6.15. It is seen, that a higher number of WD's in the farm provides a bigger wave height reduction compared to normal conditions, as could be expected.

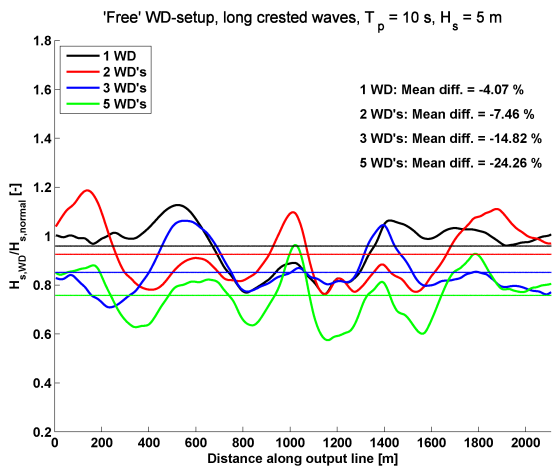

Figure 6.15 *Influence from different farm-layouts. Incident waves are propagating from north.*

Choice of Appropriate WD Farm Layout for Present Study

The choice of appropriate layout for use in Santander is a compromise between optimum wave height reduction and optimum electricity production. Due to limited available CPU-capacity and time (each run in the "Santander model" have a duration of $\approx$ 30 hours using a 2.8 GHz, 12 GB ram computer), mainly one WD-farm layout will be considered in this project. A high degree of wave height reduction is wanted, hence the farm layout with five WD's in a staggered grid is chosen. As written in Chapter 2, it is concluded from the study of (Beels, 2009b), that five WD's in a staggered grid, with an individual lateral distance of $2 \times D$ (where D is the width of the WD), provides an electricity production which is five times higher than from one WD. It is further concluded, that a small decrease in the electricity production is obtained in the second row of the farm if an individual distance of $1 \times D$ between the WD's is considered. These conclusions are, however, based on long crested waves only. The available wave power in front of each WD in the considered farm will be evaluated in a later section.

In Figure 6.16 the influence from different wave periods when considering the 5 WD's in a staggered grid, is illustrated. Again, long crested waves are considered, and it can be seen, that a bigger wave height reduction is obtained in case of smaller wave periods, which is the same tendency as seen in Chapter **??**.

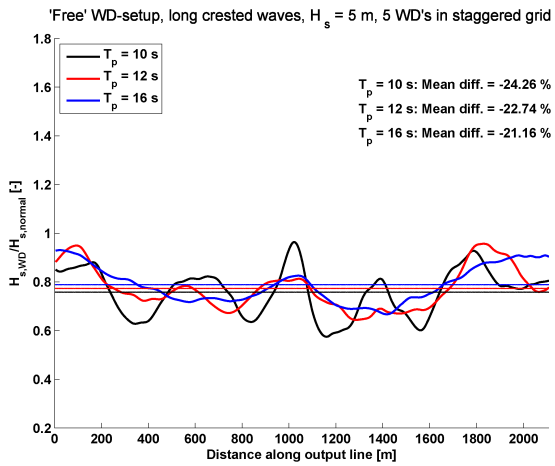

Figure 6.16 *Influence from different wave periods using a farm layout with 5 WD's in a staggered grid. Incident waves are propagating from north.*

From Figure 6.16 it is seen, that the wave height at some positions along the output line is higher - and in some positions much smaller - than during normal conditions. The reason for the relatively big differences in these areas, is due to diffraction from the islands and WD's, cf. Figure 6.9 and Figure C.12, respectively. A part of the increased wave heights due to diffraction from the islands is reduced by the WD's, but new diffraction is introduced from the WD's. This tendency is expected to damp out with increasing directional spreading, cf. Appendix C.

6.3.3 Comparison of Wake from WD's in Long- and Short Crested Waves

The wake from the WD-farm in case of short crested waves, with $s = 100$ and $s = 10$, from north is illustrated in Figure 6.17 and Figure 6.18, respectively. Compared to Figure 6.14, where long crested waves are considered, it is seen, that the small area with relatively big wave heights in the middle of the WD-farm, due to diffraction from side-lying WD's, slightly damps out in case of short crested waves. The same tendency with fading diffraction in the wake of a WD when considering short crested waves was obtained in the preliminary study in the basin, cf. Appendix C.

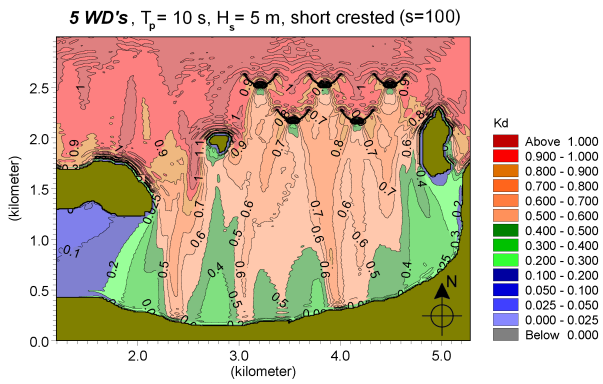

Figure 6.17 *Area plot of wake behind 5 staggered WD's in case of short crested waves with $s = 100$, using "free" WD setup. Incident waves are propagating from north.*

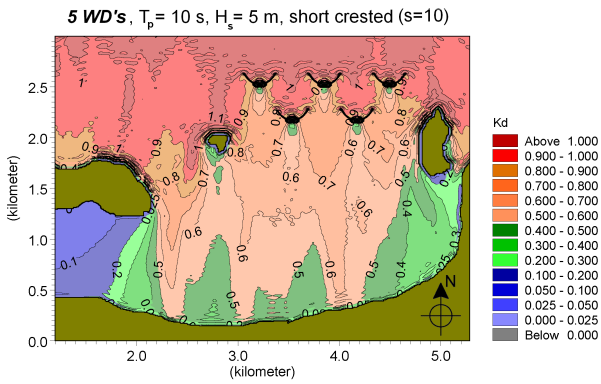

Figure 6.18 *Area plot of wake behind 5 staggered WD's in case of short crested waves with $s = 10$, using "free" WD setup. Incident waves are propagating from north.*

Additionally, the wake effect, compared to normal conditions, along the output line is plotted in Figure 6.19 and 6.20, respectively. It is seen, that a small area with higher wave disturbance is present near the middle of output line, but fades out with increasing directional spreading, as expected.

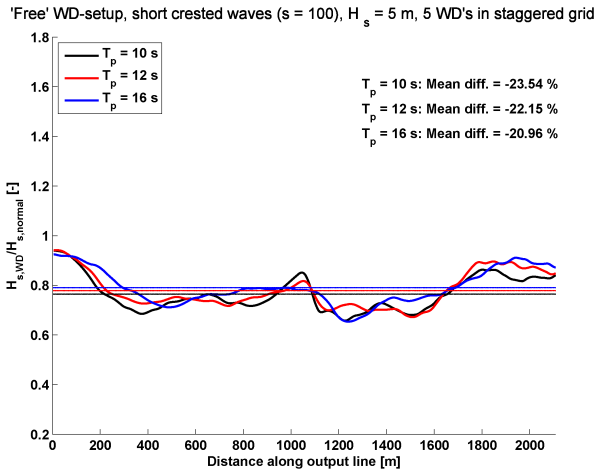

Figure 6.19 *Wake behind 5 staggered WD's in case of short crested waves with $s = 100$, along output line. Incident waves are propagating from north.*

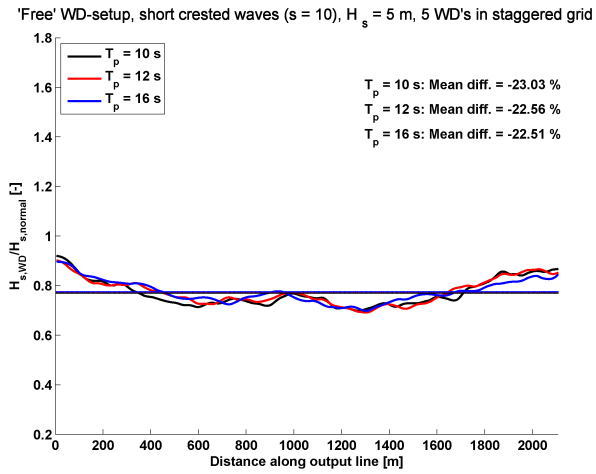

Figure 6.20 *Wake behind 5 staggered WD's in case of short crested waves with $s = 10$, along output line. Incident waves are propagating from north.*

In Figure 6.21 a comparison of the wave height reduction, in case of long and short crested waves is illustrated, where it is seen, that the approximate same average reduction along the output line is obtained for all considered wave periods.

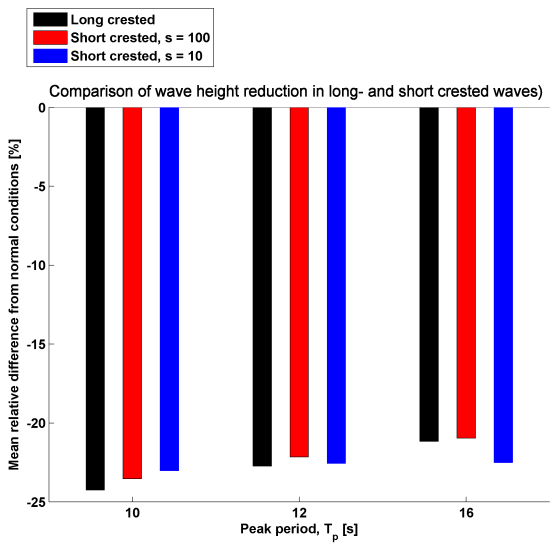

Figure 6.21 *Comparison of wave height reduction in case of long- and short crested waves. Incident waves are propagating from north.*

Investigation of Available Wave Power in Second Row of WD's in Staggered Grid

The available wave power between the reflector tips for the individual WD's in the staggered 5 WD-farm is compared for different wave conditions. Using H_s and $T_e = 0.9 \cdot T_p$ from each grid element, the average wave power, P_{mean}, along a line between the reflector tips is determined from (3.1) in case of long- and short crested waves with different wave periods, respectively.

In Figure 6.22 the relative difference between the average available wave power in front of WD's in the first- and second row of the farm is plotted. It is seen, that a wave power reduction of up to 17 % is obtained in the WD's in the second row, corresponding to a reduction in P of up to $0.23 \cdot 10^5\ W/m$. However, the farm layout is still concluded to be reasonable due to it's relatively good wave height reduction properties. It should be noted, that if gaps between the WD's in the farm are left "open", a part of the beach will be left unprotected, hence two rows are needed to obtain a wave height reduction along the whole beach.

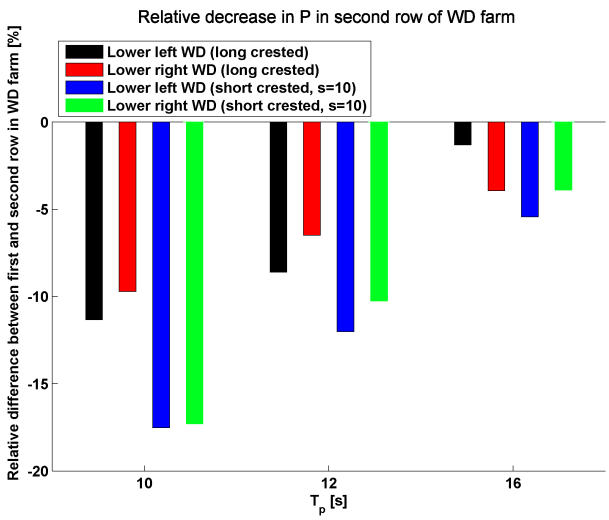

Figure 6.22 *Relative difference between the average available wave power in front of WD's in the first row of the farm and the WD's in the second row of the farm.*

It should be noted, that the available wave power in front of the WD's is not the actual electricity production, since a part of the wave power will be transmitted or reflected, cf. Chapter **??**. Further, when using (3.1) for determining wave power, deep water waves are assumed, which is not the actual case, cf. Appendix C. Additionally, the waves approaching the WD's in the second row of the farm may have slightly changed direction and e.g steepness, affecting the overtopping. However, since only a comparison between the individual WDs is performed, the inaccuracies can be neglected. The wave propagation directions will be further analysed in a later section.

6.3.4 Evaluation of Alternative WD-farm Layouts

To study whether it is possible to reduce the wave heights in the bay even further, a sixth WD is inserted in the farm, see Figure 6.23, with the corresponding wave height reduction along the output line in Figure 6.24. When comparing with the results in Figure 6.16 and Figure 6.20 it is seen, that the farm with 6 WD's only provides a wave height reduction which is up to $\approx 5\%$ higher than with 5 WD's in the farm when $T_p = 10\ s$ and even less with $T = 16\ s$.

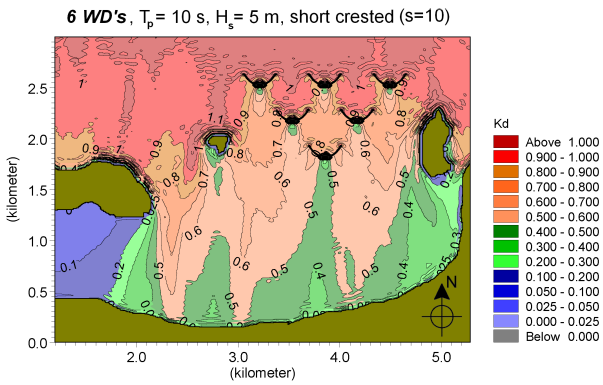

Figure 6.23 *Area plot of wake behind 6 staggered WD's in case of short crested waves with $s = 10$, using "free" WD setup. Incident waves are propagating from north.*

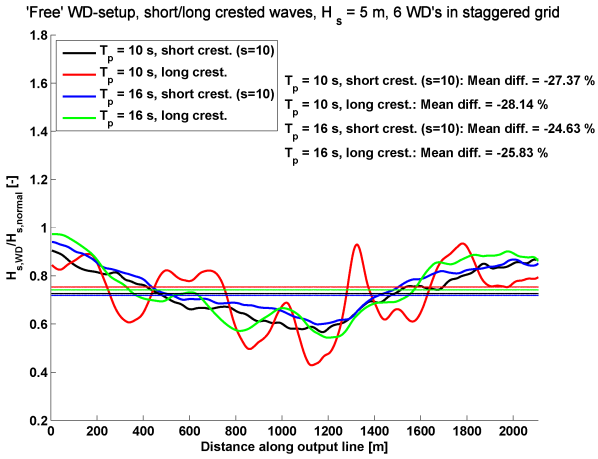

Figure 6.24 *Wake behind 6 staggered WD's in case of short- and long-crested waves, along output line. Incident waves are propagating from north.*

In Figure 6.25 the relative difference between the average available wave power in front of WD's in the first row of the farm and the WD's in the second and third row of the farm is plotted in case of long- and short crested waves, respectively. It can be seen, that the wave power in front of the lowest (sixth) WD is significantly reduced compared to the remaining WD's. Hence, due to the only small decrease in wave height behind the farm, and due to the decreased available wave power in front of the extra WD, this WD-farm layout is concluded to be unprofitable.

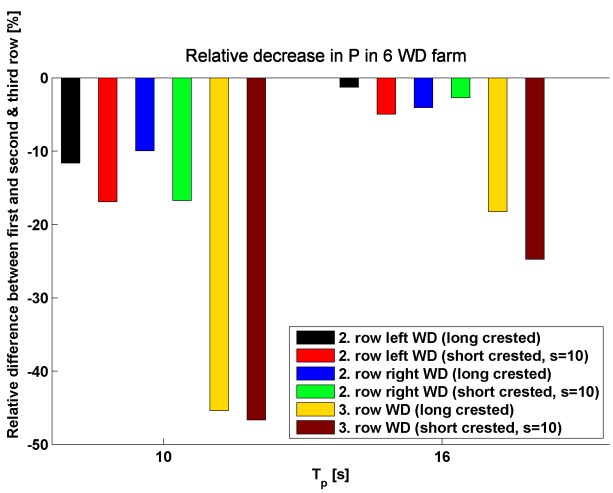

Figure 6.25 *Relative difference between the average available wave power in front of WD's in the first row of the farm and the WD's in the second and third row of the farm.*

6.3.5 Comparison of Influence on Wake from *"Fixed"* and *"Free"* WD-setups

An illustration of the wake from *"free"* and *"fixed"* WD-setup is given in Figure 6.26 and Figure 6.27, in case of short crested waves with $s = 10$, for comparison. It is seen, that the *"fixed"* WD-setup provides a bigger wave height reduction than the *"free"* WD-setup in the lee of the farm, as expected.

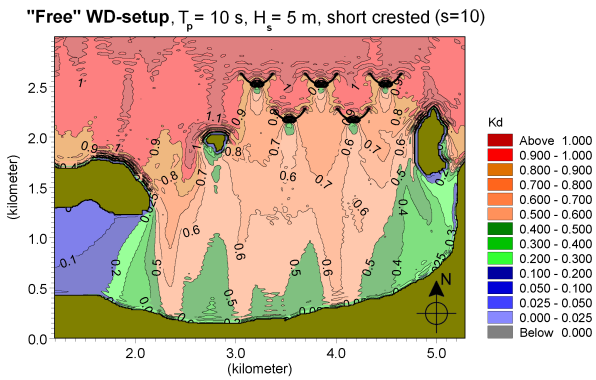

Figure 6.26 *Area plot of wake behind 5 staggered WD's in case of short crested waves with $s = 10$, using* "free" *WD setup. Incident waves are propagating from north.*

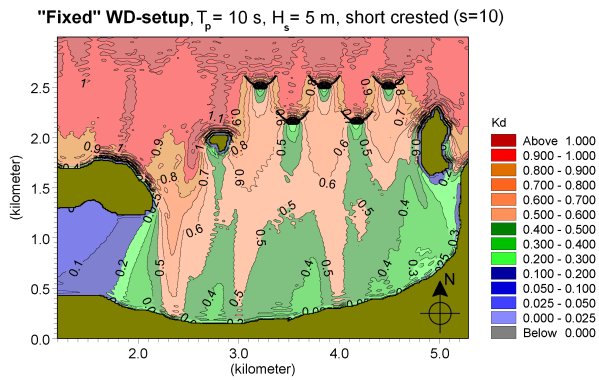

Figure 6.27 *Area plot of wake behind 5 staggered WD's in case of short crested waves with $s = 10$, using* "fixed" *WD setup. Incident waves are propagating from north.*

The wave height reduction along the output line from a farm of 5 WD's using the *"fixed"* WD-setup, compared to normal conditions in the bay, is illustrated in Figure 6.28 and Figure 6.27 where short-crested waves with $s = 100$ and $s = 10$ are applied to the model, respectively.

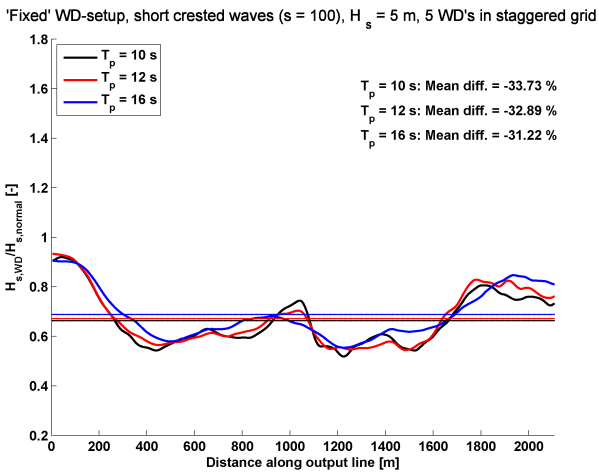

Figure 6.28 *Wake behind 5 staggered WD's, using* "fixed" *WD-setup, in case of short crested waves with $s = 100$, along output line. Incident waves are propagating from north.*

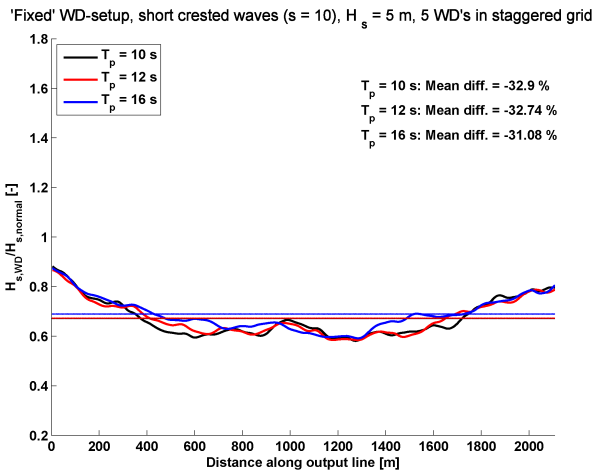

Figure 6.29 *Wake behind 5 staggered WD's, using* "fixed" *WD-setup, in case of short crested waves with $s = 10$, along output line. Incident waves are propagating from north.*

A further comparison is given in Figure 6.30 and Figure 6.31 where it is seen, the *"fixed"* WD-setup provides ≈ 50% more wave height reduction compared to normal conditions, than the *"free"* WD-setup. It should be noted that, as written before, the *"fixed"* setup is unrealistic, but gives an idea of the influence from lateral- and vertical heaving movements of the WD on the wave height reduction properties. The wave height reduction from the *"fixed"* WD's can be considered as the maximum possible in the considered wave conditions.

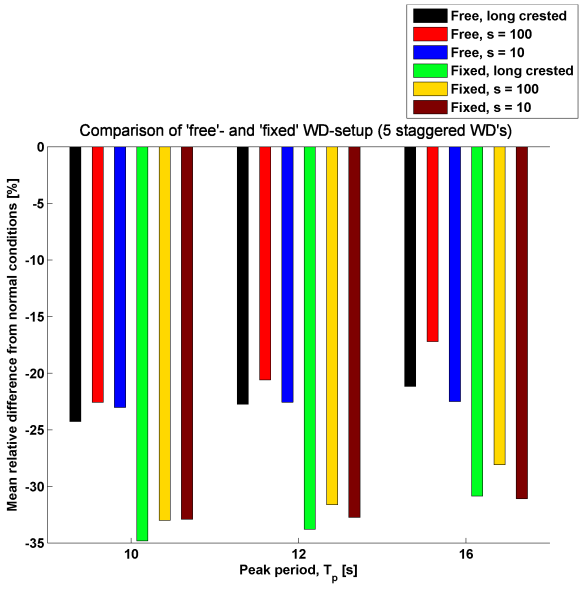

Figure 6.30 *Comparison of mean relative wave height reduction in case of different WD-setups and wave conditions. Incident waves are propagating from north.*

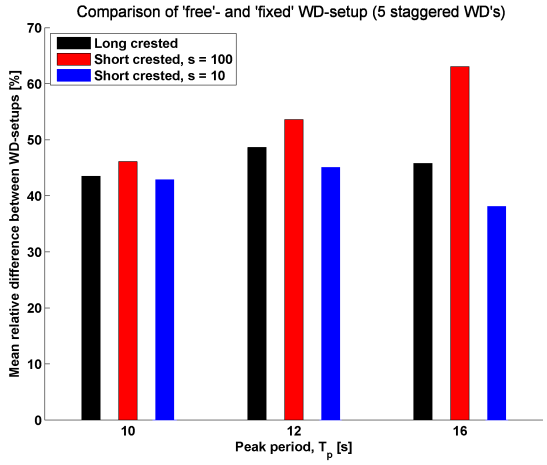

Figure 6.31 *Difference between* "fixed" *and* "free" *WD-setup compared to normal conditions. Incident waves are propagating from north.*

6.3.6 Comparison of Wake from WD's in Different Incident Wave Directions

To study how, or whether, the incident wave direction affects the wave height reduction in the bay, waves with an incident direction corresponding to NW, cf. Appendix C, is applied to the model. It is assumed, that the WD's turn to face the incident wave direction (facing NW) with the exact same individual distances as in Figure 6.7 and 6.6, and with the approximate same location between the islands as in Figure 6.7 (d), illustrated in Figure 6.32. In Figure 6.33 the wave disturbance in the wake of the WD-farm is illustrated in case of a short crested wave with $T_p = 10\ s$ and $s = 10$.

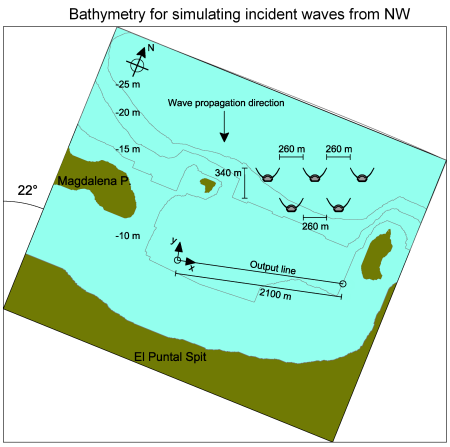

Figure 6.32 *Model used for analyzing wave propagation from NW with 5 WD's in a staggered grid.*

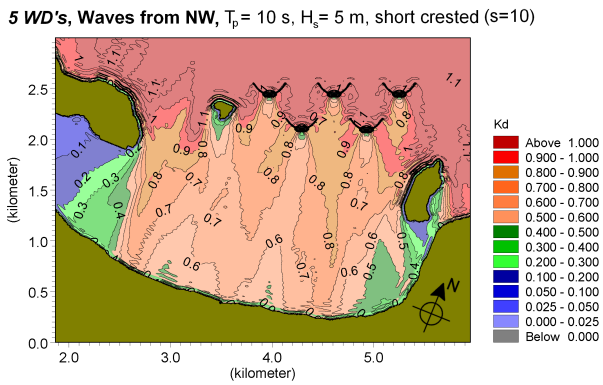

Figure 6.33 *Wave disturbance in Santander bay in case of incident waves propagating from north west.*

The wave disturbance is extracted along the output line in Figure 6.32 with the approximate same location as in the case with waves propagating from N, illustrated in Figure 6.34. Additionally, a comparison between the wave height reduction compared to normal conditions in case of waves from N and NW is illustrated in Figure 6.35. It can be seen, that the approximately same wave height reduction is obtained from the two wave directions.

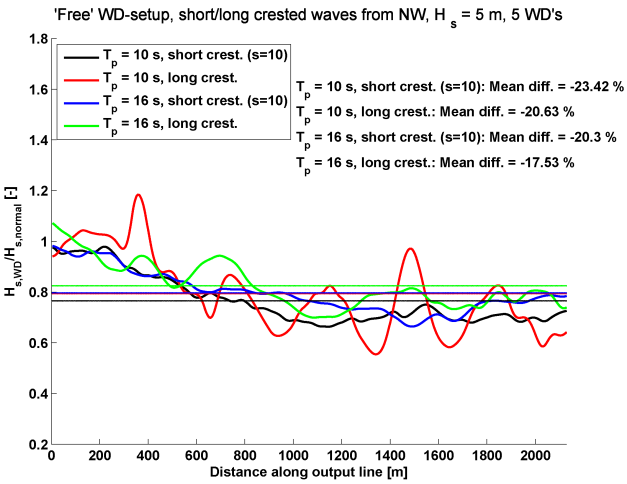

Figure 6.34 *Wave disturbance along output line in case of incident waves propagating from north west.*

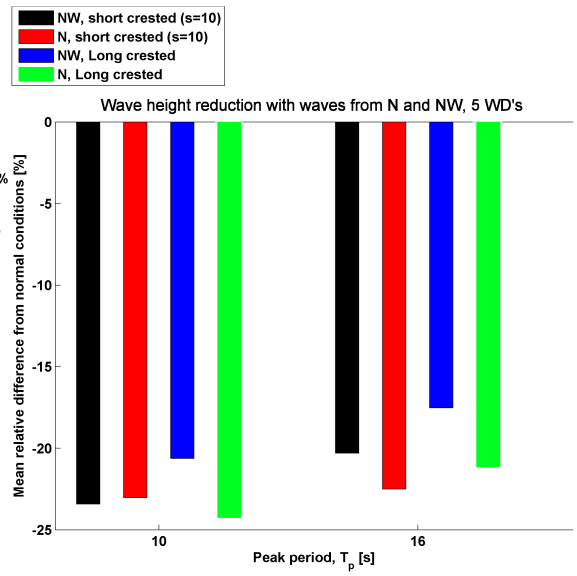

Figure 6.35 *Wave disturbance compared to normal conditions in case of incident waves propagating from north and north west.*

6.4 Investigation of Wave Period and -Direction in Wake of WD-farm in Santander Bay

Besides wave height reduction in the wake of the considered WD-farm, it is interesting to analyze possible influences on parameters such as wave period, propagation direction, and directional spreading behind the WD's. These parameters may, in combination with reduced wave heights, affect the shoreline evolution at Santander Spit.

6.4.1 Investigation of Wave Period in Wake of a WD-Farm

From Chapter **??** it was concluded, that the wave period is slightly increased in a small distance behind the WD, due to a bigger absorption from the WD's in case of short wave periods. To study whether the same tendency is present in Santander the mean wave period, T_m is extracted from three columns along the WD-farm and at different positions behind the WD's, illustrated in Figure 6.36. The extracted values of T_m at the different positions are given in Figure 6.37. The reason for considering T_m instead of T_p is due to less sensitivity to "spikes" in the frequency spectrum.

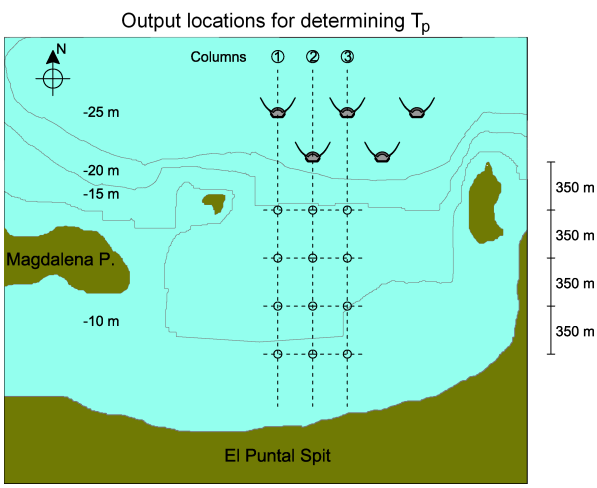

Figure 6.36 *Specification of positions for extracting T_m.*

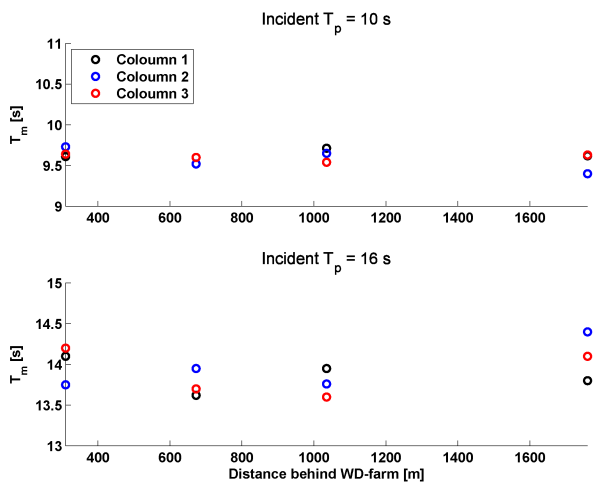

Figure 6.37 *Determined T_m at different positions behind the WD-farm in case of different incident wave periods. Incident waves are propagating from north.*

From Figure 6.37 no tendency in changing wave period behind the WD-farm is found. A further illustration of the influence on the wave period or -length is illustrated in Figure 6.38, where the wave energy spectrum from "normal conditions" is compared to a spectrum at the same point in the wake of a WD-farm. The energy spectrums are smoothed to avoid spikes which will influence the peak period. Here it is seen, that the approximate same energy is found for the different frequencies in the spectrum, only with an evenly distributed increase. Hence it is concluded, that the influence from the WD's on the transmitted wave periods and -lengths is insignificant.

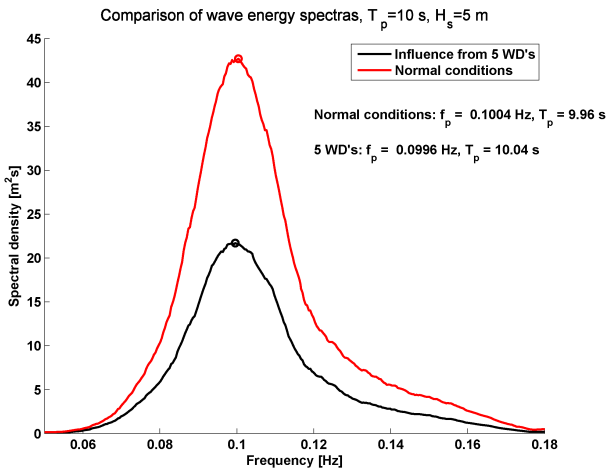

Figure 6.38 *Influence on the wave energy spectrum when installing 5 WD's offshore. The spectrum is extracted 700 m behind the WD farm along column 3. Incident waves are propagating from north. A bandpass filter of 0.1 Hz is used in the figure.*

6.4.2 Investigation of Wave Propagation Direction in Wake of WD-farm

When studying the cross shore sediment transport at Santander Spit in a later chapter, an important factor is the incident wave propagation direction. Hence it is studied whether the offshore WD-farm may influence the wave direction in the bay due to e.g. diffraction, and whether the incident wave propagation direction at the entrance of the bay, may influence the wave directions at the shore.

In Figure 6.39 and 6.40 the mean wave propagation direction in the bay is illustrated in case of incident short crested waves from N and NW, respectively. It is seen, that the waves changes direction in the area close to the farm, but corrects in a further distance behind the WD's to the incident propagation direction. The incident waves from NW slightly refracts into the N-direction when approaching the spit.

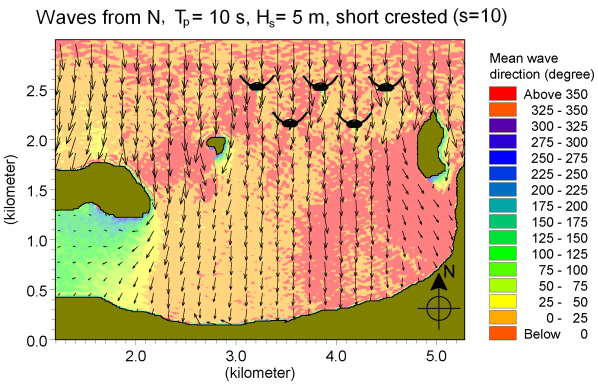

Figure 6.39 *Mean wave propagation direction in the bay. Incident waves are propagating from N. Vectors depicts the magnitude of the wave heights, and the mean wave directions.*

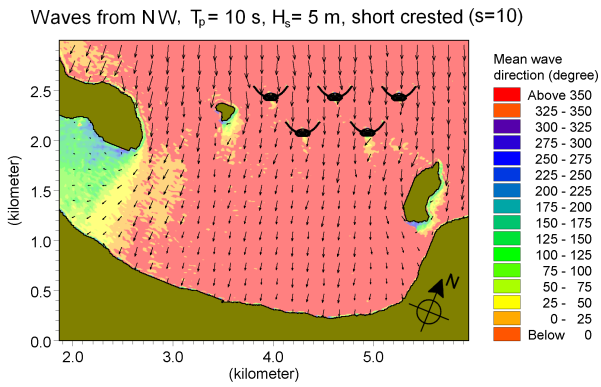

Figure 6.40 *Mean wave propagation direction in the bay. Incident waves are propagating from NW. Vectors depicts the magnitude of the wave heights, and the mean wave directions.*

Wave Propagation Directions in the Area Close to the WD Farm

As mentioned in Chapter 3, the obliqueness of the waves approaching the WD, affects the wave overtopping, and hence the electricity production. So far, in the simulations using the 5 WD's in a staggered grid it is assumed, that the WD's in the first row of the farm do not affect the wave directions for the waves approaching the second row of WD's, and hence all WD's are facing the same direction.

Therefore, it will be studied whether the WD's in the first row of the WD-farm may influence the propagation direction of the waves approaching the second row in the farm, due to e.g. diffraction. The wave propagation direction in the area close to the WD-farm is given in Figure 6.41. From this it is seen, that the propagation direction is only affected in a small distance behind the first row of WD's in the farm, but turns back into the N-direction when approaching the second row. Hence the mean wave direction is the same for all WD's, which can then be expected to face the same mean incident wave direction.

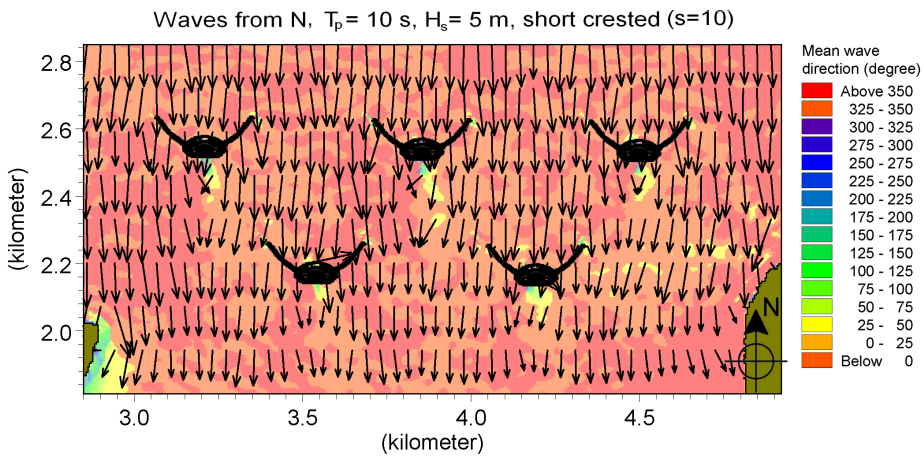

Figure 6.41 *Wave propagation direction in the area close to the WD-farm. Incident waves are propagating from N. Vectors depicts the magnitude of the wave heights, and the mean wave directions.*

6.4.3 Investigation of Influence on Directional Spreading in Wake of WD-farm

An increasing directional spreading is known to produce a deceased sediment transport on a beach, cf. (Fredsøe and Deigaard, 1992). Hence it is interesting to study whether the directional spreading of the waves inside the bay is influenced by the presence of the WD-farm. In Figure 6.42 and 6.43 the mean directional spreading is illustrated with- and without WD's, respectively. It is seen, that an increased directional spreading is present in the area close to the WD-farm, which is mainly due to reflection and diffraction from the individual WD's.

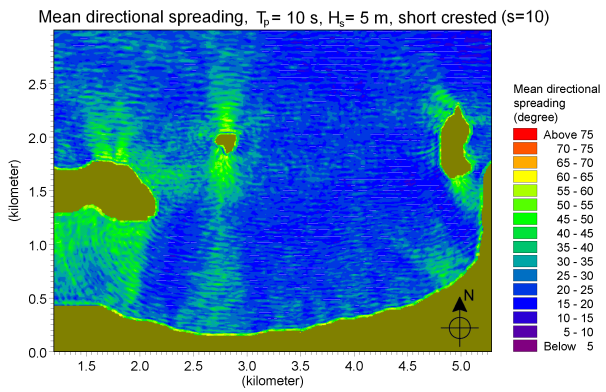

Figure 6.42 *Mean directional spreading during "normal conditions". Incident waves are propagating from N.*

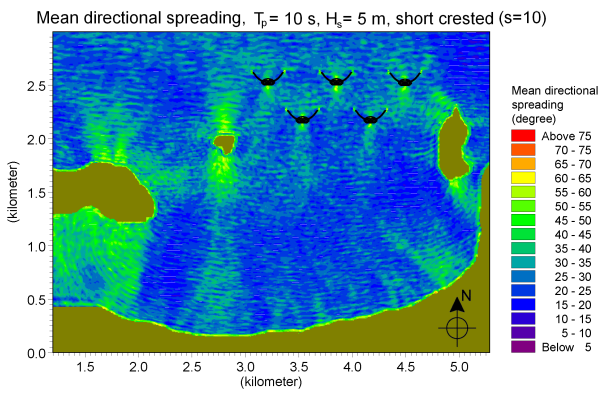

Figure 6.43 *Mean directional spreading in case of five WD's positioned offshore. Incident waves are propagating from N.*

Additionally, the mean directional spreading, compared to normal conditions, is evaluated in a further distance behind the WD's along the output line in Figure 6.8. The result is illustrated in Figure 6.44, where it is seen, that a small average increase is obtained when installing the WD's offshore, which is slightly increasing with increasing T_p.

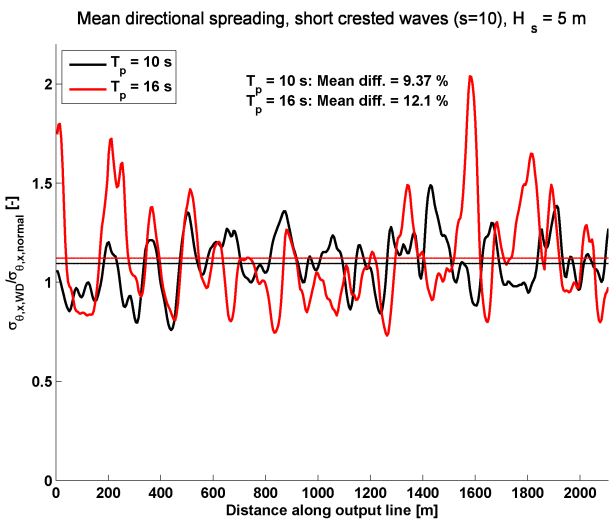

Figure 6.44 *Mean directional spreading, compared to normal conditions, along output line. Incident waves are propagating from N.*

6.5 Investigation of Reduced Wave Heights in Harbour Entrance

As mentioned earlier, only the spit is considered when analyzing the influence from an offshore WD-farm. However, since the waves turn towards a westerly direction when propagating around the Magdalena Peninsula, cf. Figure 6.39 and 6.40, a small additional study on the expected wave height reduction at the Santander harbour entrance is performed, to determine whether calmer conditions can be expected at the more populated areas of Santander bay. The wave heights during normal- and "protected" conditions are extracted along the output line in Figure 6.45.

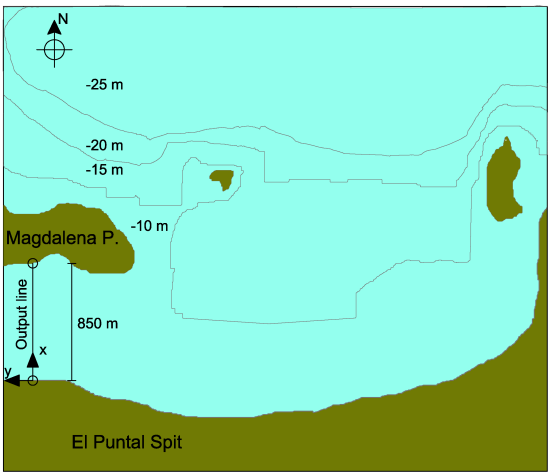

Figure 6.45 *Output line for comparing wave heights at the harbor entrance.*

It should be mentioned, that simulations are still run on a modified bathymetry where a minimum water depth of $h = -10\ m$ is used to avoid wave breaking. Since the output line is located inside the modified area, this may slightly affect the modelled wave heights in the harbour. Further, the area between the western island and Magdalena P. is modified, which may introduce slightly bigger wave heights approaching the harbor entrance. However, since only a comparison is performed, and not a determination of the actual wave heights at the entrance, the introduced model-errors are expected to be negligible.

The relative difference between the wave heights during the two conditions are illustrated in Figure 6.46 and 6.47 in case of long- and short crested waves, respectively. It is seen, that the WD's introduce a rather small but measurable wave height reduction at the entrance.

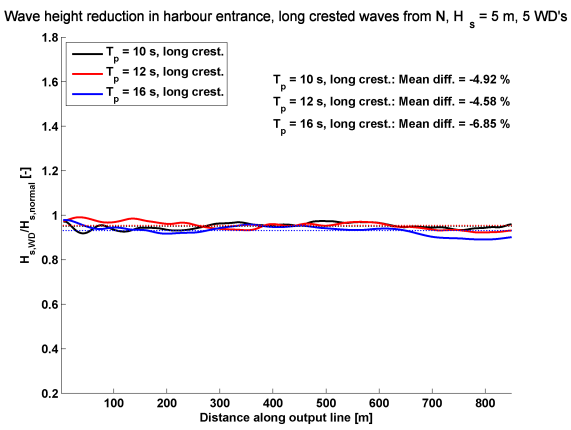

Figure 6.46 *Relative difference in wave heights at harbour entrance, in case of long crested waves from N.*

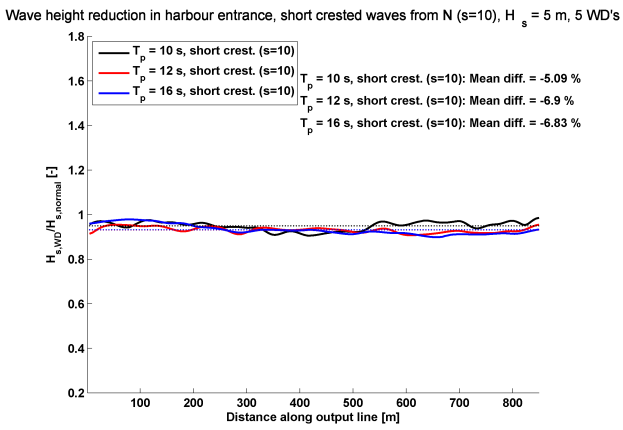

Figure 6.47 *Relative difference in wave heights at harbour entrance, in case of short crested waves from N.*

6.6 Investigation of Influence on Reduced Wave Heights in Surf Zone from an Offshore WD-farm

So far all analyses of the influence from an offshore WD-farm are performed outside the breaker zone. To determine the influence of a reduced wave height closer to the shore, a simulation is performed using the 1DH Boussinesq Wave Module in MIKE21 BW, which is capable of determining undertow in the breaker zone and performing fast simulations of breaking nonlinear waves.

The cross shore bathymetry used in the model is extracted from the center of the spit between the two islands. H_s and H_{max} from "normal" conditions using an incident short crested wave spectrum with $s = 10$, $H_s = 5\ m$, and $T_p = 10\ s$, are compared to the reduced wave heights from the presence of a 5 WD-farm in a staggered grid, illustrated in Figure 6.48. In addition, the wave undertows from the two conditions are illustrated in Figure 6.49. The wave direction is perpendicular to the shore in the model, cf. Section 6.4.2 and a bed roughness of $k_s = 0.05\ m$ is used. It should be noted, that even during normal conditions the wave height is reduced (in this case from $H_s = 5\ m$ to $H_s = 3.6\ m$) when entering the bay.

From Figure 6.48 and 6.49 it is seen, that the offshore WD's are significantly reducing the wave heights in the breaker zone as well as offshore. The reduced breaking wave heights results in a decreased undertow which is expected to reduce the beach erosion during a storm. This will, however, be further analysed in a later chapter.

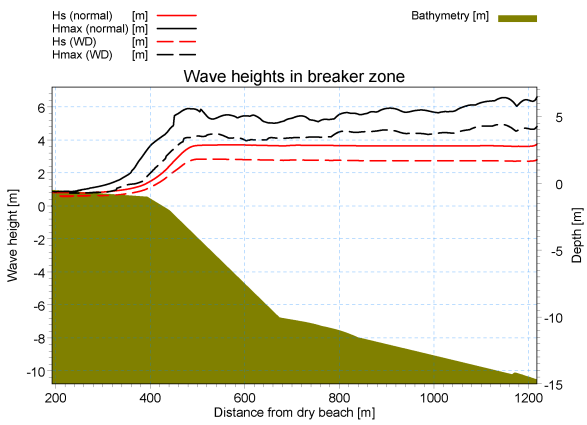

Figure 6.48 *H_s and H_{max} in case of the presence and non-presence of an offshore WD-farm.*

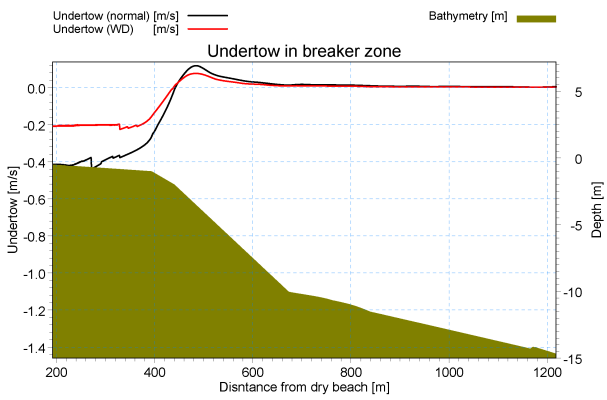

Figure 6.49 *Wave undertow in case of the presence and non-presence of an offshore WD-farm.*

6.7 Summary of Findings in present Chapter

General key findings from the present chapter are presented in the following. Through out the analysis of the wave height reduction in Santander, the percentage mean difference between normal conditions and the wave heights in the wake of an offshore WD-farm have been used for comparisons. In Table 6.3 the actual wave mean wave height reductions, in meters, are presented for the case with 5 WD's in a staggered grid.

Mean wave height reduction from 5 WD's in staggered grid									
	Long crested			Short crested ($s = 100$)			Long crested ($s = 10$)		
T_p $[s]$	10	12	16	10	12	16	10	12	16
"Free" (realistic) $[m]$	1.03	1.01	0.95	0.99	0.94	0.9	0.98	0.92	0.86
"Fixed" (conservative) $[m]$	1.41	1.34	1.25	1.48	1.41	1.29	1.36	1.34	1.22

Table 6.3 *Wave height reduction in Santander bay.*

- From the considered layouts it is concluded, that the five WD's positioned in a staggered grid provides the biggest wave height reduction in Santander bay, while still having a sufficient amount of wave power available between the reflector tips of each individual WD.
- The *"free"* and *"fixed"* WD-setups are compared, and it is seen, that the *"fixed"* WD-setup provides a significantly greater wave height reduction than the *"free"* setup in Santander bay.
- The approximate same average wave height reduction along the output line is obtained for both long and short crested waves. Different incident wave propagation directions are analysed, and it is concluded, that the wave propagation directions, independent of the incident directions, approximately becomes perpendicular to the spit.
- A reduced wave height in Santander bay will provide a reduced undertow in the surf zone, which is expected to decrease the rate of beach erosion.

Chapter 7

Sediment Transport at Santander

In the present chapter an analysis of the expected influence from a farm of WD's on the cross-shore sediment transport at Santander spit will be performed. A numerical sediment transport model is included in the analysis, and general assumptions are described, together with a description of the model setup. The analysis is based on determining the effects of placing a farm of 5 WD's of the coast in Santander, by using the results of reduced wave heights obtained from the simulations presented in Chapter 6. To this, a storm event is considered with same wave climate as in the previous chapters, but with increasing water levels due to expected climate changes. Conclusions will be based on the appliance of a WD-farm for coastal protection in means of effect on sediment transport.

Normally two types of sediment transports are present at a beach; the cross-shore transport, and the long-shore transport. Long-shore sediment transport is mostly due to the wave-induced long-shore currents, whereas cross-shore transport is a result of the water motions due to wave undertow, where the profile of a sandy beach changes continuously and may be modified considerably during a single storm.
(Fredsøe and Deigaard, 1992)

Only the cross-shore transport is considered in the present chapter since it is expected, that long-shore transport in general will only have a small influence on the coastline evolution in Santander compared to cross-shore transport.

7.1 Expected Influence on Cross Shore Sediment Transport from WD-farm in Santander

In Chapter 6 it was seen, that a WD farm will reduce the wave heights in Santander with up to $\approx 23\%$. Regarding cross-shore sediment transport, this change in wave height will influence the cross shore erosion at the spit. This can be seen in (7.1), based on several wave tank experiments (Larson, 1990), which can be used as an estimation of whether erosion or accretion can be expected. From (7.1) it is seen, that bigger wave heights and smaller wave periods increase the erosion, where sand is moved seaward and form a bar further offshore. In case of smaller wave heights, and longer wave periods, the sand will move shoreward, where the accretion will cause the beach to widen. Hence the presence of the offshore WD-farm in Santander is expected to decrease the erosion rate at Santander spit. The same was concluded in Chapter 6 where it was seen, that a reduced wave height in the surf zone provides a reduced undertow and hence a reduced off-shore transport.

$$\frac{H_o}{L_o} < M \cdot \left(\frac{H_o}{\omega \cdot T_0}\right)^3 \Rightarrow Erosion \Downarrow \qquad \text{(Larson, 1990)} \qquad (7.1)$$

$$w < \frac{T_0}{\sqrt[3]{M \cdot 1.56 \cdot H_0^2 \cdot T_0^{-1}}} \Rightarrow \underline{Erosion}$$

$$w > \frac{T_0}{\sqrt[3]{M \cdot 1.56 \cdot H_0^2 \cdot T_0^{-1}}} \Rightarrow \underline{Accretion}$$

where
H_o is the deep-water wave height $[m]$
L_o is the deep-water wave length ($L_0 = 1.56 \cdot T_0^2$) $[m]$
$M = 0.00070$ is an empirically determined coefficient from wave tank experiments $[-]$
w is the sand fall speed $[m/s]$
T_0 is the deep water wave period $[s]$

When using e.g. $H_s = 5\ m$ and $T_p = 10$, 12, and 16 s in (7.1), and using the wave height reduction from Chapter 6, it is seen in Figure 7.1 that erosion can be expected in all cases, both with- and without the presence of a WD-farm. While this is the case, the wave height reduction, caused by the WD-farm, is still expected to reduce the erosion during a storm event.

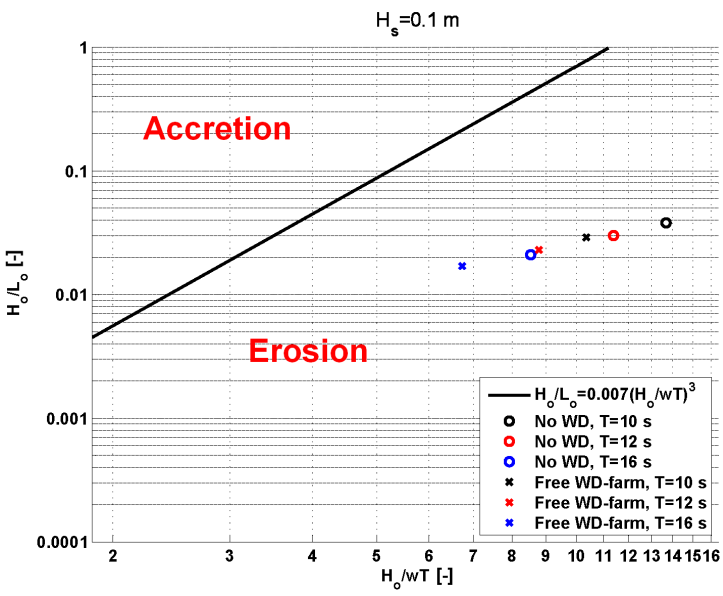

Figure 7.1 *Transport directions with and without the WD.*

In addition to decreasing the erosion during storm events, the WD-farm is expected to increase the accretion during calmer periods, where sand is deposited at the beach. For this reason, it is interesting to simulate a long period of time, e.g. a year, where seasonal variations are taken into account. However, such an analysis requires a great amount of data, and the available sediment-models are not suited for long term analyses, hence only a short period storm is considered.

7.2 Setup of Cross Shore Sediment Transport Model

Due to the complexity of the nonlinear wave and sediment dynamics and their interactions, different approaches can be taken to simplify the modeling. In this project, a short-term model based on the equilibrium-profile approach is used to predict the behavior of the beach in Santander during a storm.

7.2.1 SBEACH

The SBEACH module of the program CEDAS will be utilized. SBEACH calculates the cross-shore transport rate based on wave energy dissipation per unit water volume, through a finite difference scheme, and has been calibrated based on experiments in a wave tank and field data. For use in a specific case it should be noted that the program needs to calibrated. This calibration is, however, not performed in the present case, due to insufficient data. The introduced errors are expected to be neglible since only a comparison between the conditions with- and without the presence of a WD-farm is wanted.

Model Input

A storm is given as input from time-series of significant wave heights, peak periods and propagation directions, as well as mean water level. These input define the incoming wave climate at each time-step in the model.

The bathymetry, corresponding to a winter profile, is given as an initial profile along with the effective grain size and maximum slope before avalanching. In addition, the sediment transport parameters, transport rate coefficient, coefficient for slope dependent term, transport rate decay coefficient multiplier and water temperature are defined. The influence from these parameters in the model is further described in Appendix D. The effective grain size is set to $0.3\ mm$ and maximum slope before avalanching to $30°$, while the sediment transport parameters are kept at their default values, given in Appendix D.

7.2.2 General Assumptions in Model

In SBEACH an equilibrium profile is assumed, meaning the situation is two-dimensional with no longshore transport. If the beach profile differs from this equilibrium form, the dissipation rate across the surf zone (dependent upon wave conditions and profile shape) differ from the constant value. Therefore, it is assumed that the amount of transported sediment depends on the difference between the actual energy dissipation rate and that for an equilibrium profile.

It should be noted, that in nature the assumption of zero long shore transport will, in many cases, not be valid. Small deviations from a uniform coastal profile may generate horizontal circulation currents and even a completely uniform situation may be unstable, ending up with a series of horizontal circulation currents. In addition, the model assumes that contour lines are straight and parallel, and energy dissipation due to bottom friction is neglected. Since shoaling and refraction do not occur instantaneously, wave height calculations are done based on a smoothed profile, rather than the exact topography. By doing this, errors from small ripples on the bottom are avoided.

7.3 Modeling- and Investigation of Effects on Cross Shore Profile at Santander Spit from Offshore WD-farm

Simulations are performed using the profile in Figure 7.2, corresponding to the bathymetry during winter time. The offshore part of the profile (until a depth of $10m$) is extracted from the bathymetry used in MIKE21 BW, while the shoreward part is based on the cross-shore profile in Figure 1.6. The profile is created along the line shown in Figure 7.3.

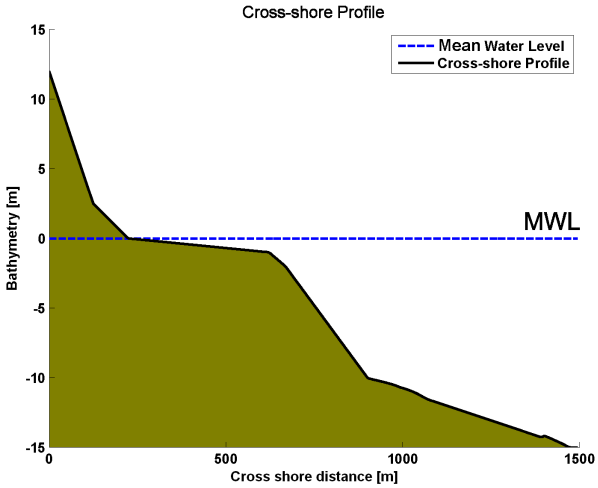

Figure 7.2 *Initial cross-shore profile.*

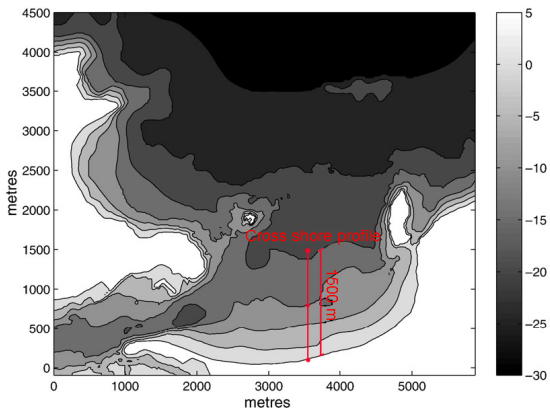

Figure 7.3 *Position of the cross shore profile.*

Simulations are run using 72 hr storms with the same significant wave height and peak period in each timestep. While this storm configuration is not realistic, it is considered as an extreme case which will give a rough indication of the influence from offshore WD's. Based on the findings in Chapter 6, the wave direction is set normal to the beach. The effect of the WD farm is included by reducing the incoming wave heights based on the mean differences found in Chapter 6, where the case with a farm of 5 *"free"* WD's in a staggered grid is considered. When using other wave heights than $H_s = 5\ m$, to which the WD is calibrated against, an unchanged relative wave height reduction is assumed (only dependent on L_p), which is expected to be realistic when changing the relative floating level of the WD's, cf. Chapter **??**. No directional spreading is included in the model.

7.3.1 Offshore- and Nearshore Effects

When considering the effects on the beach, the main area of interest is stretching approximately 300 m from the dry beach. Erosion in this area will result in a loss of dry beach, and ultimately danger to e.g buildings near the beach. However, the actual erosion on the dry beach is greatly affected by the location of possible offshore bars, causing waves to break (in the cross shore area 300 m - 800 m) before propagating toward the dry beach. Hence the beach erosion is analysed in two areas of the cross shore profile, illustrated in Figure 7.4. The effects of a storm are compared based on the relative difference in total eroded volume compared to "normal conditions" where no WD's are placed offshore.

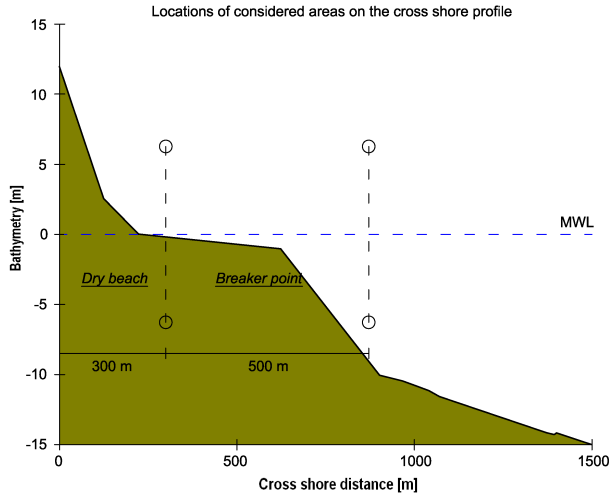

Figure 7.4 *Areas considered when determining cross-shore sediment transport.*

Investigation of Erosion on Dry Beach

Figure 7.5 and 7.6 show the relative difference in displaced volume, with and without the WD farm, at different wave periods and wave heights. In most of the cases it is observed that the displaced volume is slightly larger when the WD farm is in place. This is a result of the lower wave height, caused by the WD farm which is decreasing the wave steepness and thereby moving the breakpoint closer to the shore. Since the difference in wave height (and thereby steepness) is defined as fraction of the initial wave height, the increased volume becomes more apparent at larger wave heights.

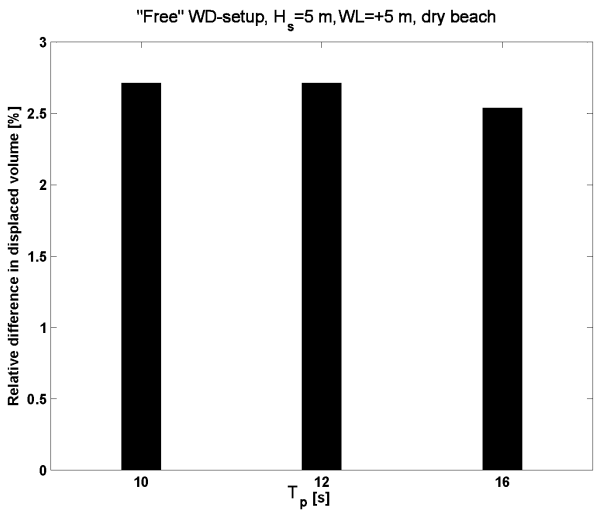

Figure 7.5 *Nearshore relative difference in displaced volume at different peak wave periods.*

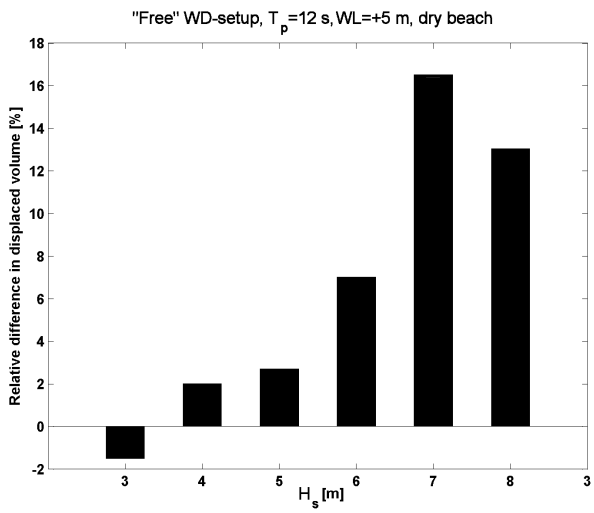

Figure 7.6 *Nearshore relative difference in displaced volume at different significant wave heights.*

Storm surges and climate changes can cause the mean water level to rise above the normal spring tide of 5 m, cf. Chapter 1, and for this reason, the effect of a WD-farm is analysed for different levels. Figure 7.7 shows the relative differences in displaced volume at different mean water levels, using $H_s = 5\ m$ and $T_p = 12\ s$. As with varying wave heights, the displaced volume is slightly larger with the WD farm for WL = $+5\ m$ to $+7\ m$ above the mean, indicating that the waves are breaking closer to the shore. The relative difference is seen to lessen as the water level is increased, indicating that breakpoint moves towards the shore, for both damped and undamped waves. When the mean water level is set to $+8\ m$, the waves break directly on the dry beach and the reduced wave height from the WD farm nets a significant reduction in displaced volume. The tendency of increased erosion at smaller wave steepness is illustrated in Figure 7.8 based on the data obtained with different wave heights and periods.

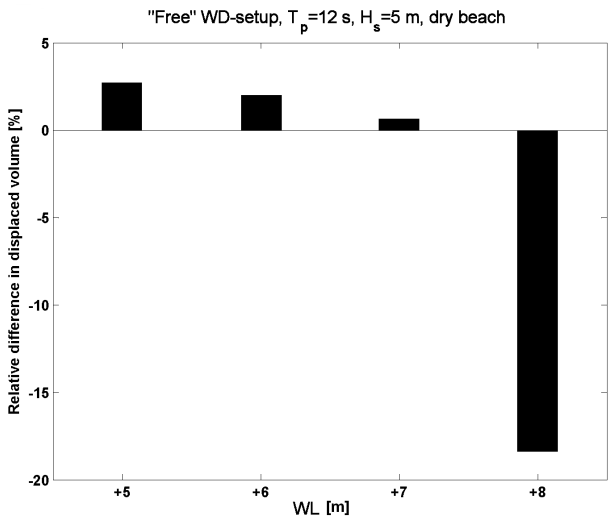

Figure 7.7 *Relative difference in displaced volume at different surface levels.*

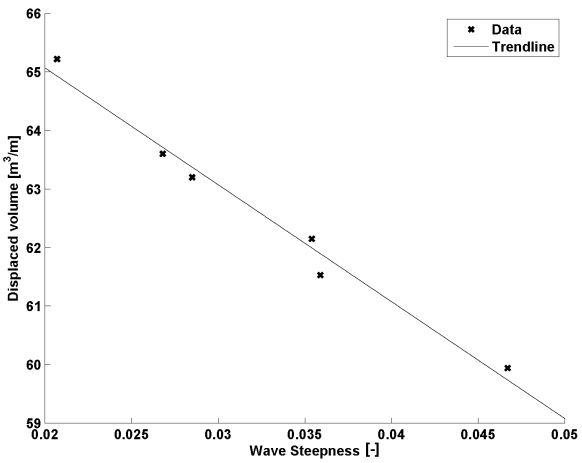

Figure 7.8 *Displaced volume at different wave steepness.*

7.3.2 Investigation of Erosion at Breaker Point

Figure 7.9 shows the displaced volume along the entire cross shore profile for a storm with $H_s = 5$ m, $T_p = 12\ s$, and surface level 5 m above mean, while Figure 7.10 show the change in profile shape. The bar created at the wave breaking point is seen to be smaller and positioned slightly closer to the shore when the WD-farm is in place, as a result of the reduced wave heights. This corresponds with the observations in the previous analysis for the dry beach. The difference in displaced volume at the seaward bar, with and without the WD farm, is found to be 68% less with the WD farm in place. This difference is greater, and opposite, to what what was found at the shore, except when the surface level is high enough for the breaking point to be positioned in a small distance from the beach.

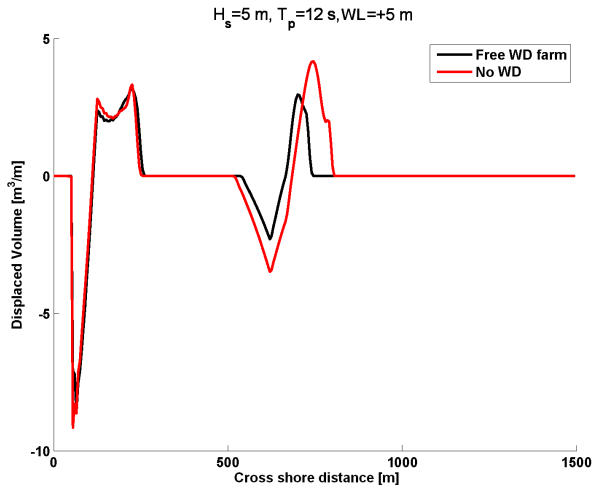

Figure 7.9 *Displaced volume along profile.*

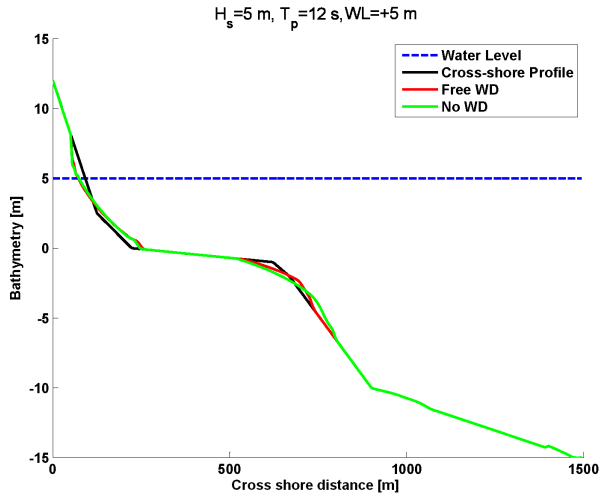

Figure 7.10 *Change in profile shape.*

It is seen, that simulations performed with different wave heights and periods provide similar results, suggesting that the WD farm lessens the erosion at the wave breaking point, while moving it slightly closer to the shore. Figure 7.11 and 7.12 show the offshore relative displaced volumes, where it can be seen the WD-farm protects the shore more effectively with higher waves and lower wave periods. This corresponds well with the observations in Chapter **??**, where it was seen that increased wave steepness led to a larger influence from the WD.

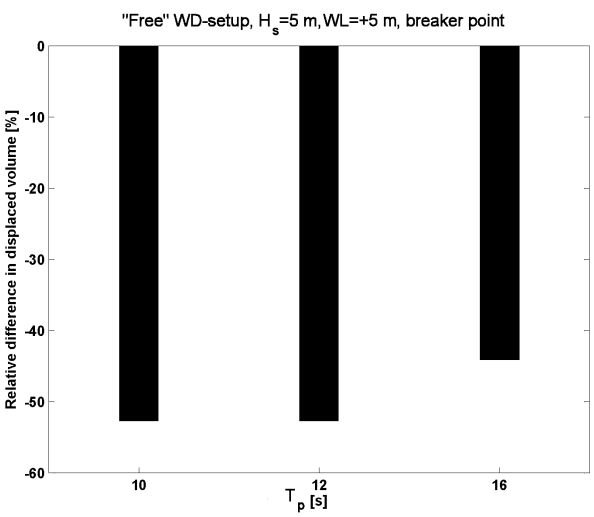

Figure 7.11 *Offshore relative displaced volume at different wave periods.*

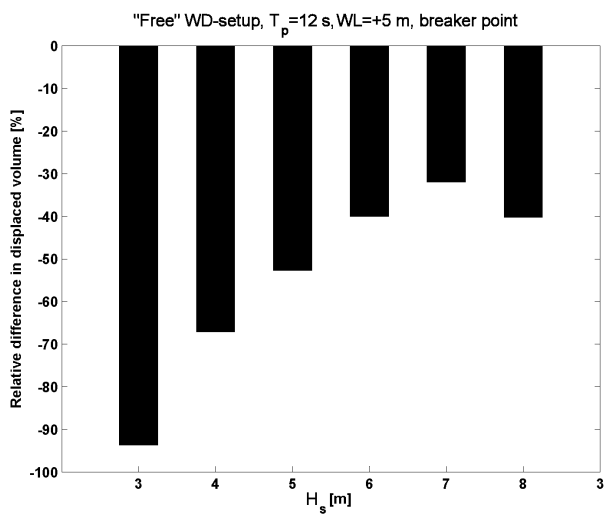

Figure 7.12 *Offshore relative displaced volume at different wave heights.*

Figure 7.13 and 7.14 show the profile development after 3 and 5 storms with $H_s = 5\ m$, $T_p = 12\ s$ and $MWL = +5\ m$. Here a clear indication of the effect from an offshore WD-farm can be seen, where the profile remains noticeably higher and flatter, when the farm is in place. Preventing erosion of the relatively flat area at $200 - 800m$ is important, because it serves not only as a barrier for the waves, but also as an attractive beach area, at low tides.

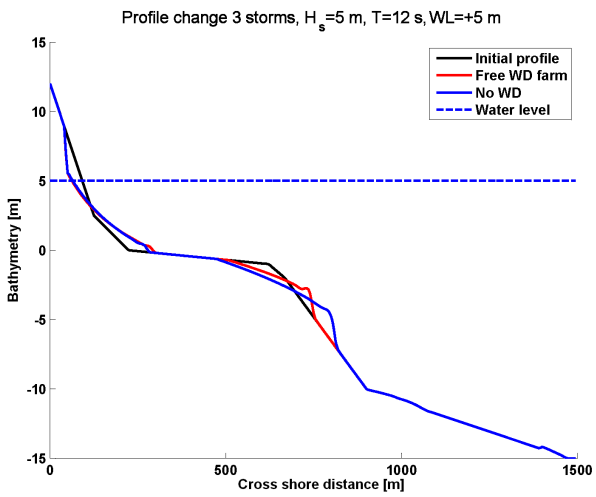

Figure 7.13 *Profile change after 3 storms.*

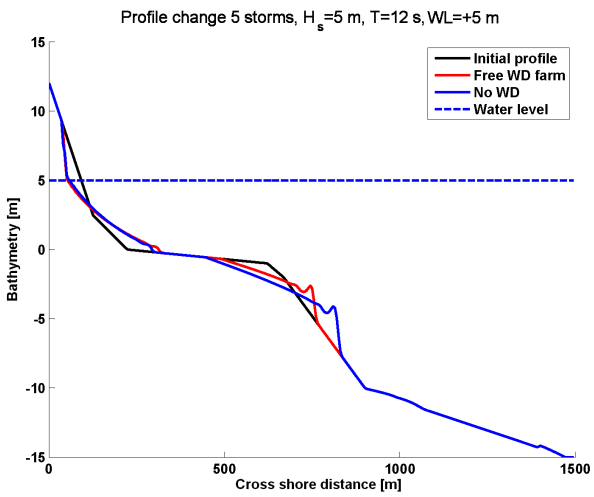

Figure 7.14 *Profile change after 5 storms.*

It can be concluded, that the WD helps prevent erosion at the shore when the surface level is high enough for the waves to break on the dry beach, while slightly increasing the erosion when the waves break further offshore. However, erosion in the shallow area, positioned between $200 - 800m$, during storms can ultimately lead to a steeper profile where the waves break further shoreward, which can lead to a larger erosion closer to the shore, especially if the sea level rises. The WD farm will slow down this process, and help protect the shoreline during extreme events.

7.3.3 Difference Between *"Fixed"* and *"Free"* WD

In previous tests, the effects of the WD farm was based on the results from a farm of *"free"* WD-setup. As mentioned earlier, while a *"fixed"* WD-setup is not practically feasible, it can be used as a reference for determining the effects of the heaving motions of the WD. Figure 7.15 and 7.16 illustrates the distribution of the volume displacement and the change in the profile at the breaking point, with *"free"* and *"fixed"* WD farms, using $H_s = 5\ m$, $T_p = 12\ s$ and surface level $+5\ m$. As the *"fixed"* WD farm reduces the wave height more than the *"free"*, the wave breaking point move further shoreward and the displaced volume becomes smaller at the breaking point. The displaced volume in the breaker zone is nearly the same for the two setups, as well as without any WD farm, with only a slight increase due to the waves breaking closer to the shore. The conclusion is, that preventing lateral and horizontal movements of the individual WD's in a farm will improve their ability to protect the coast.

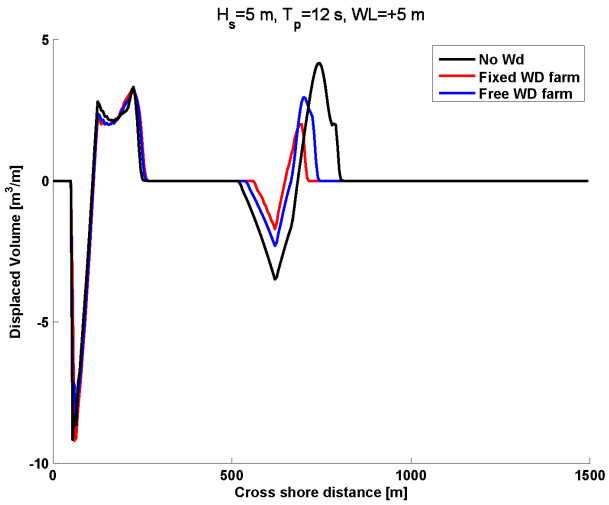

Figure 7.15 *Distribution of displaced volume with fixed and free WD.*

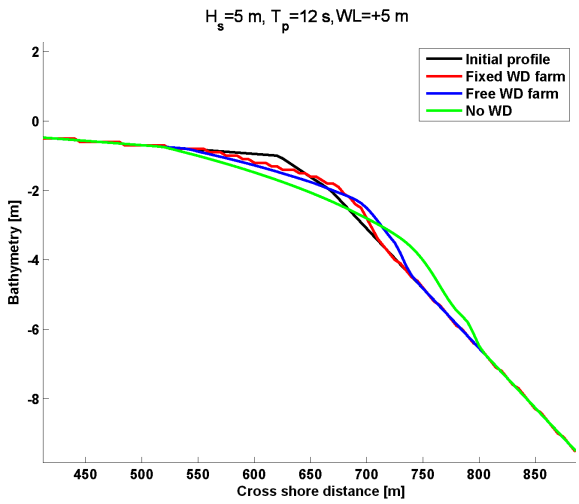

Figure 7.16 *Change in cross-shore profile at the wave breaking point.*

7.4 Summary of Findings in present Chapter

General key findings from the present chapter are listed in the following:

- Reduced wave heights in the surf zone slightly moves the breaking point closer to the shore. While this will not affect the dry beach directly at low mean water levels, it will prevent the bottom from evolving towards a steep profile which can lead to waves breaking more directly on the dry beach. Hence WD's are expected to help protecting the shoreline at Santander spit.

Part IV

Conclusions and Discussion

Chapter 8

Conclusions in Project and Discussion of Results

In the present chapter a sum up of conclusions and findings in the project will be given. Additionally, a discussion of the assumptions and shortcomings will be performed, together with a discussion of the results. Finally a proposal for further study on the subject will be presented.

8.1 Summary and Conclusions from the Different Parts in the Project

A summary of conclusions in the different parts of the project will be summarized in the following.

8.1.1 Conclusions from Part 2. ”Preliminary Study”

From the summary of the present state of knowledge it is seen, that all considered studies are based on transmitting porous structures which are tuned to obtain a given amount of absorption as specified by the developer. However, no actual measurements of the wave height reduction behind any types of WEC's are performed in the considered studies, and non of the studies have evaluated the influence from e.g. heaving movements of the floating structures on the transmission characteristics.

Different available phase averaging- and phase resolving models are described and evaluated for choosing the most applicable. Since MIKE21 BW introduces the possibility for including porous structures, with varying transmission/reflection-characteristics through a spectrum of waves, this model is concluded to be the most applicable for implementation of a WD. The use of MIKE21 BW, however, requires some cautions due to the introduced error in case of deep-water waves. It has been necessary to truncate, and thereby re-scale JONSWAP spectrums where the smallest wave lengths do not fulfill the requirements for a maximum depth to deep-water wave length ratio of $h/L_0 \leq 0.5$.

The reflection on- and transmission under- the wave reflectors of the WD is studied analytically, together with an analytical study of the reflection on-, transmission under- and absorption by- the main body. It is concluded, that more wave energy is transmitted under the reflectors with high wave periods/length and small drafts. The same study is performed on the body of the WD, where the absorption of wave power, due to overtopping, is plotted as a function of T and H. From this it is concluded, that due to decreasing absorption with increasing values of T, it is expected that, as for the reflectors, an increasing transmission under the body appears with increasing wave period and thereby wave length. Further it is seen, that an increasing wave height results in an increasing absorption of wave power.

Wave transformation processes such as wave reflection, transmission, diffraction, and energy absorption are found to be important when modeling a WD in MIKE21 BW. A validation of diffraction and

refraction is studied, and it is seen that MIKE21 BW provides results which are in agreement with analytical results. Additionally, the sufficient discretization, to correctly model the different transformation processes, is evaluated.

It is found, that cautions shall be taken when implementing a WD in the depth integrated MIKE21 BW, such as the need for decoupling K_r and K_t, changing K_r and K_t due to oblique orientation of porosity layers, and wave radiation from the heaving floating WD. Here it is concluded, that it is possible to achieve a decoupling of K_r and K_t by introducing e.g. a varying porosity factor S through a section, and by applying sponge layers in front of the structure. The decoupling-method is applied when imitating the behavior of a floating structure in a large scale flume, where a relatively good agreement is found for especially K_t which is the most important factor when simulating the wake effect of a WD. Finally, it is concluded, that an oblique orientation of porosity layers results in a slightly decreasing reflection which may cause problems when simulating 3D-waves with a spectra of changing incident wave propagation angles.

8.1.2 Conclusions from "Sensitivity Analysis of Measurements and Calibration of Numerical Model"

Laboratory tests are performed to determine the sensitivity of wave disturbance from the WD against stiffness of mooring system and WD-reflectors. The influence on wave disturbance from the WD with different relative crest freeboard and wave lengths is analysed. Here it is concluded, that a smaller ratio of R_c/H_s, and a bigger wave steepness H_s/L_p, results in a more reduced wave height behind the WD. However, a 64% relative decrease of R_c/H_s results in a 20% relative decrease of K_d behind the WD body, and even less behind the reflectors. In comparison, a 46% relative decrease of L_p results in a 56% decrease of K_d, behind the WD-body, when $R_c/H_s = 0.9$, meaning the wave disturbance is more affected by the wave length than the crest freeboard ratio.

The *"free/flexible"*-setup provides the biggest wave disturbance coefficient K_d in front of- and behind both the WD-body and -reflectors, compared to when either- or both the body and reflectors are *"fixed"*. When considering K_d behind the WD in case of $L_p = 2.96\ m$, a mean relative increase of $\approx 23\%$ is obtained when comparing the *"fixed/fixed"*-setup and the *"free/flexible"*-setup. Further it is observed, that K_d increases towards the tip of the reflector, where, at some WD-setups and L_p, K_d reaches values above 1. This is due to diffraction and wave radiation from the floating structure.

When considering the wave energy spectrum behind the WD-body, wave radiation is observed from the *"free/flexible"*-setup at high frequencies or small periods. From a study of the variation of K_d through the wave energy spectrum it is seen, that the different waves in a wave energy spectrum, are not transmitted equally through the WD. A greater amount of wave energy is transmitted through the WD at small frequencies (high wave periods), than at higher frequencies (small wave periods). From this follows, that the peak period of the transmitted spectrum is increased 20% compared to the incoming wave spectrum.

Results from the physical experiments are implemented in MIKE21 BW. Based on the validation of K_d, and the transmitted wave energy, it is found, that the calibrated numerical model provide reasonable estimates of the wave climate behind the WD, especially for the *"free"* setup at longer wave periods. For the *"fixed"* setup the model is seen to overestimate the absorbed wave energy in case of relatively long waves at the WD body. The difference is likely to, in part, be caused by a higher sensitivity to influences from boundaries, due to a smaller wave height. This is accepted, but kept noted, as the *"fixed"* model is mainly used as a reference for the *"free"* model. The model is not able to directly depict the movement of the WD when using the *"free"* WD-setup, especially at short wave periods. This inaccuracy is, however, accepted, as the numerical model still provide good estimates of the general tendencies behind the WD,

including varying transmission depending on the wave period to which the model is validated. When comparing the calibrated models it is found, that there is a clear difference between the transmissive properties of the *"fixed"* and *"free"* WD-setups.

8.1.3 Conclusions from "Case Study"

A preliminary study of a single WD with the *"free"*- and *"fixed"* WD-setup is performed in a wave flume with constant depth. Here it is concluded, that an increasing wave length and increasing directional spreading results in an increasing K_d, or deceasing wave height reduction, behind the WD. It is further concluded, that the wake shortens with increasing directional spreading due to a faster redistribution behind the WD, and that diffraction becomes more scattered, when directional spreading is introduced.

Different WD-farm layouts are considered, and from the considered layouts is concluded, that the layout with five WD's positioned in a staggered grid provides the biggest wave height reduction in Santander bay, while still having a sufficient amount of wave power available at each WD. Hence this farm layout is considered in the majority of the analyses. Since an appropriate wave height reduction with a reasonable power production is wanted, the available wave power, P, between the reflector tips for the individual WD's in the staggered 5 WD-farm is determined and compared for different wave conditions. It is concluded, that a small decrease in P appears in the second row of the farm in the smallest considered wave periods. If a sixth WD is inserted in a third row, only a slightly bigger wave height reduction is obtained, but the available wave power in front of the extra WD is reduced significantly.

The *"free"* and *"fixed"* WD-setups are compared, and it is seen, that the *"fixed"* WD-setup provides a significantly greater wave height reduction than the *"free"* setup. Thus, it is concluded, that implementing a WD in a numerical wave propagation model without accounting for movements of the structure, provides an overestimation of the wave height reduction. A realistic wave height reduction of up to 23% (with $T_p = 10\ s$) is obtained from 5 staggered WD's positioned offshore using the *"free"* WD-setup, and a conservative wave height reduction of up to 33% is found from 5 staggered WD's using the *"fixed"* WD-setup. The wave height reduction is slightly decreasing in case of $T_p = 16\ s$, to 22% and 31% for the *"free"* and *"fixed"* WD-setup, respectively.

When considering long crested waves, small areas appears behind the WD-farm where the wave heights are bigger than during normal conditions, due to diffraction. These areas are seen to fade out with increasing directional spreading. However, it is further seen, that the approximate same average wave height reduction along the output line is obtained for both long and short crested waves. Different incident wave propagation directions are analysed, and it is concluded, that the wave propagation directions, independent of the incident directions, approximately becomes perpendicular to the spit. It is further concluded, that the wave direction in the second row of the WD-farm is not affected by the first row, hence all WD's are facing the same direction. The peak wave period in the wake of the WD's is unchanged, and a slightly increased directional spreading in the wake is observed behind the farm.

It is concluded, that the reduction in wave height, caused by a WD-farm, will reduce the undertow and thereby beach erosion, caused by wave breaking. Further it is seen, that reduced wave heights in the surf zone will move the breaking point slightly closer to the shore. While this will not affect the dry beach directly at low water levels, it will prevent the bottom from evolving towards a steep profile which can lead to waves breaking more directly on the beach. If the water level is high enough for the waves to propagate and break directly on the dry beach e.g. during a storm surge, the WD farm will reduce the dry beach erosion significantly. Hence it is concluded, that an offshore WD-farm in Santander will have a protecting effect on the spit during extreme conditions.

Since the reduction in wave height is greater, and more power is produced when the WD is kept fixed, it is desirable to minimize movements of the WD, while still retaining the ability to face the wave direction and adjust to water levels.

8.2 Discussion of Assumptions and Shortcomings

Main assumptions are listed in the introduction, Chapter 1. The consequence of using these, and the related shortcomings, will be discussed in the following.

- **Only individual storms are considered:** No data study from Santander is performed, and only individual storms are considered. Hence long period effects from an offshore WD-farm are not evaluated.

  There is no doubt, that a long period simulation with varying wave propagation directions together with varying water level, will provide a more precise idea on the impact of offshore positioned WD's. As an example, the wave height distribution inside the bay during e.g. a year could be compared for the cases with- and without the presence of an offshore WD-farm. Additionally, it is interesting to study long period effects on the coastline evolution which, however, requires a long period simulation of the wave propagation.

  Performing long period simulations in a changing wave climate requires an extensive amount of physical tests for calibration of the numerical model, since the model needs to be calibrated and validated to obtain reasonable results in a great range of wave periods and wave heights. Additionally, the implementation of a WD-farm, which is capable of facing different incident wave directions, cannot be performed using the present MIKE21 BW-model. Hence longer simulation-periods needs to be split up into shorter periods.

  Conclusions based on observations from a single storm, however, gives an indication of the wave height reduction and shoreline protection during extreme situations, which is highly relevant due to expected future climate changes which are expected to introduce increasing storminess at, among others, European coasts.

- **No calibration of the Santander-model is performed:** No detailed information or measurements containing wave heights etc. from the study site are available, and hence no actual calibration and validation of the normal wave conditions in Santander is performed.

  Conclusions, concerning wave height reduction from an offshore WD-farm in the present thesis, are based on relative comparisons between normal conditions and the presence of a WD-farm. Hence it is expected, that the obtained effects from the positioning of an offshore WD-farm are relatively accurate.

- **Wave loads on the WD during extreme conditions are not evaluated:** It is assumed, that the considered WD's can withstand extreme loads and hence function normally during a storm. No actual tests or simulations are performed to support this assumption, but if WD's are to function as wave barriers it is a prerequisite that they can withstand extreme loads. Additional study concerning the robustness of the WD may be needed, where a solution could be to shorten the reflectors to reduce bending moments at the reflector connections.

- **Energy production considerations when placing the WD-farm are neglected:** The actual energy production is not directly taken into consideration in the placements of the WD-farm. However, it is not expected that an optimum wave height reduction at the shore, in combination with

an optimum placement for energy production purposes, can be obtained. Hence a compromise based on e.g. a cost benefit analyses must be performed. This thesis, however, sheds light on the possibilities for using e.g. a farm of five WD's in a staggered grid for wave height reduction, where all WD's have an approximately identical wave power potential between the reflector tips.

8.3 Discussion of Findings

A numerical wave propagation model is seen to be a powerful tool when investigating the possibilities for obtaining wave height reduction from a farm of WEC's. When tuning the numerical model to provide realistic estimates of the wave disturbance behind the considered structure, scaled physical tests from a laboratory basin are needed. These can further be used to evaluate the behavior of the considered WEC in different wave climates. In this thesis it is seen, that heaving motions of the floating structure have a great influence on especially the transmissive characteristics, and when assuming a bottom fixed structure, errors are introduced. Among others, this is done in the work of (Beels, 2009a), where the wave reflectors are assumed to be fixed, and where the transmission characteristics are based on the analytically determined energy flux integrated from the draft of the reflector up to the surface. This may provide an overestimation of the wave height reduction in the wake of the WD.

From the present work it is seen, that when planning the installation of an offshore WEC-farm, several factors should be taken into consideration. Among these is the distance of the farm from the shore, which affects the wave height reduction at the shoreline, and the electricity production of the farm. When the farm is positioned at deep water, more wave power is available. In addition, the wave climate at the site has a rather big influence on the wave height reduction, where especially the wave steepness affects the wave transmission. The stiffness of the mooring system, against horizontal- and vertical- movements, should further be taken into consideration.

An objective of this thesis has been to determine the effectiveness of WD's as a mean of wave height reduction and shore protection, and from the findings it is seen, that a great potential is present. When considering expected climate changes in the future, introducing increasing storminess and rising sea levels, an even bigger influence is obtained from the WD's. Ocean wave energy is in its infancy today but can lead to clean, affordable and renewable electrical power in the future. To take the step and go to large scale application requires strong political support and large financial investments. Cost savings using the concept of WECs functioning as multi-functional breakwaters may help introducing wave energy converters as a green alternative to other types of coastal protection.

8.4 Recommendation- and Proposal for Further Study

Parts of the work presented in this thesis are worth further investigating, and to this, an overview of suggestions for future research is given below.

- In this work the calibration is performed on a single scaled WD-model which is then superposed to the different positions in the farm. It could be interesting to study the total wake effect of e.g. 5 WD's in a staggered grid, to determine whether the identical total reduced wave height can be obtained as when calibrating against a single WD. The reflection between the individual WD's in the farm, which is not modelled very correctly in this thesis, may slightly affect the transmission characteristics and power production. Additionally, calibration against directional spreading should be performed.

- WD's will operate in both wind and waves, and it is interesting to determine how regeneration of the wake from wind may affect the wave height reduction in the wake of the farm. It is expected, that wake effects behind a farm are largest when no wind is present. Additionally, it may be interesting to include current fields in the simulations to study the impact from these on the wake or the impact of the wake on wave-driven currents and near shore sediment transport.
- Concerning the case study of the effects in Santander, it could be interesting to perform a calibration of the model, and to perform long-term simulations of the impact on the cross shore sediment transport at the spit to obtain the effects on the variations in beach bathymetry from an offshore WD-farm during e.g. a year. Additionally, it is interesting to determine the effects on the bed-transport in the wake area behind the WD's due to changed wave-driven currents. Further, it is interesting to study the use of eg. WD's for wave height reduction at the exposed Magdalena beach.
- Concerning the design of the WD, it is interesting to determine whether the structure can be expected to withstand extreme loads during a storm, or whether a modification in e.g. the reflector-lengths should be performed.
- As economy plays a large role in the feasibility of using the WD for coastal protection, a cost benefit analysis for a nearshore WD-farm is of interest.

Bibliography

AAU: 1999, *Evaluation of hydraulic responce of the Wave Dragon*

AAU: 2010, *WaveLab 3.34*

Andersen, T. L. and Frigaard, P.: 2008, *Lecture Notes for the Course in Water Wave Mechanics*

ATV: 2003, *Effekter af klimaændringer, tilpasninger i Danmark*

Beels, C. et al., .: 2009a, *Application of the time-dependent mild-slope equations for the simulation of wake effects in the lee of a farm of Wave Dragon wave energy converters*

Beels, C.: 2009b, *Optimization of the Lay-out of a Farm of Wave Energy Converters in the North Sea. Analysis of Wave Power Resources, Wake Effects, Production and Cost.*, PhD thesis, Department of Civil Engineering, Ghent University.

Boud, R.: 2003, *"Status and Research and Development Priorities, Wave and Marine Accessed Energy,"*

Brorsen, M.: 2000, *Reflection of Short-Crested Waves from Thin Sponge Layers in Numerical Models*

Brorsen, M.: 2008, *Linear Wave Models*, Aalborg University

Brorsen, M., P. H.: 1998, *On the Reflection of Short-Crested Waves in Numerical Models.*

CERC: 1985, *Directional Wave Spectra using Cosine-Squared and Cosine 2s Spreading Functions*

Delft: 2009, *SWAN user manual*

DHI: 2008a, *MIKE 21 EMS - Elliptic Mild-Slope Wave Module - User guide*

DHI: 2008b, *MIKE 21 PMS - Parabolic Mild-Slope Wave Module - User guide*

DHI: 2008c, *MIKE21 Boussinesq waves module - scientific documentation*

DHI: 2008d, *MIKE21 Boussinesq waves module - User guide*

Embley-Energy: 2010, *SPEERBOY*, http://www.sperboy.com/

Ferziger, J. H. and Perie, M.: 2002, *Computational Methods for Fuid Dynamics*, Springer

Fredsøe, J. and Deigaard, R.: 1992, *Mechanics of Coastal Sediment Transport*, World Scientific

GIOC: 2001, *Modelo de Propagación de Oleaje Espectral (Oluca-SP 2.0).*

Goda, Y. and Suzuki, Y.: 1976, *Estimation of Incident and Reflected Waves in Random Wave Experiments*

Hald, T. and Frigaard, P.: 2001, *Forces and Overtopping on 2. Generation Wave Dragon for Nissum Bredning*, Aalborg Universitet

Hasselmann et al., .: 1973, *Measurements of Wind and Wave growth and swell decay during the joint north sea wave project JONSWAP*

Higgins, L.: 1963, *Observations of the Directional Spectrum of Sea Waves Using the Motions of a Floating Buoy*

Hughes, S. A.: 1993, *Physical models and laboratory techniques in coastal engineering*, World Scientific Publishing Co. Pte. Ltd.

Ilic S., et al., .: 2007, *Multidirectional wave transformation around detached breakwaters*

IPPC: 2000, *IPCC Special Report on Emissions Scenarios*

Kofoed, J. P.: 2002, *Ph.D. thesis*, Hydraulics &Coastal Engineering Laboratory, Department of Civil Engineering, Aalborg University

Kountandos et al., .: 2005, *Floating breakwaters under regular and irregular wave forcing, reflection and transmission characteristics*

Kyung, D. and Hanna, K.: 2008, *Water Wave Scattering by Partially Reflecting Breakwaters*

Larsen, J. and Dancy, H.: 1983, *Open Boundaries in Short Wave Simulations -a New Approach*

Larson, M.: 1989, *SBEACH: Numerical Model for Simulating Storm-Induced Beach Change Report 1: Emperical Foundation and Model Development*

Larson, M.: 1990, *SBEACH: Numerical Model for Simulating Storm-Induced Beach Change Report 2: Numerical Formulation and Model Tests*, Report

Losada, M. A. et al., .: 1991, *Historical Evolution and Morphological Analysis of "El Puntal" Spit, Santander (Spain)*

Madsen, P.A. et al., .: 1997, *Surf zone dynamics simulated by a Boussinesq type model*

Madsen, P.: 1983, *Wave Reflection From a Vertical Permeable Wave Absorber*

Madsen, P. A. and Sørensen, O. R.: 1991, *A new form of the Boussinesq equations with improved linear dispersion characteristics. Part 1*

Madsen, P. A. and Sørensen, O. R.: 1992, *A new form of the Boussinesq equations with improved linear dispersion characteristics. Part 2*

Mansard and Funke: 1980, *The Measurement of Incident and Reflected Spectra Using a Least Squares Method*

Mattioli, F. and Turrini, S.: 1988, *Linear Absorbing Boundary Conditions for Surface Water Wave Propagation*

Medellín, et al., .: 2007, *Coastline sand waves on a low-energy beach at "El Puntal" spit, Spain*

Mendes, L., e. a. .: 2010, *The impact of wave energy farms in the shoreline wave climate: Portuguese pilot zone case study using Pelamis energy wave devices*

Miche, R.: 1944, *Mouvement ondulatoires de la mer en profondeur constante ou decroissante, Annales des Ponts et Chaussees.*

Muetze, A.: 2005, *Ocean Wave Energy Conversion*

Pelamis: 2010, http://www.pelamiswave.com

Penney, W. and Price: 1952, *The diffraction theory of sea waves and the shelter afforded by breakwaters.*

SEEWEC: 2010, *Sustainable Economically Efficient Wave Energy Converter*, http://www.seewec.org

Smith and Venugopal: 2007, *Wave climate investigation for an array of wave power devices*

Smith et al., .: 2007, in *Proceedings of the 7th European Wave and Tidal Energy Conference*

Sommerfeld, A.: 1896, *Mathematische theorie der diffraction.*

Tedd, J. et al., .: 2005, *The Wave Energy Challenge - The Wave Dragon Case*

Tedd, J.: 2007, *Testing, Analysis and Control of Wave Dragon, Wave Energy Converter*, PhD Thesis defended in public at Aalborg University

THESEUS: 2009, *Innovative technologies for safer European coasts in a changing climate*

Vidal, C., e. a. .: 2007, *Impact of Santoña WEC installation on the littoral processes*

Vining, J. G. and Muetze, A.: 2007, *Governmental Regulation of Ocean Wave Energy Converter Installations*

Wave-Dragon: 2010, *Wave Dragon, Wave Dragon ApS*, http://www.wavedragon.net

Wavemill Energy Corp., h.: 2005, *Electric Power from Ocean Waves*

WAVEPLAM: 2009, *A Cautiously Optimistic Review of the Technical Status of Wave Energy Technology*

WWF: 2006, *Stormy Europe - the power sector and extreme weather*

www.ABB.com: 2006, *A wave of renewable energy*

Part V

Appendix (on enclosed CD)

Appendix A

Overview of Numerical Model Types and Description of MIKE21 BW

This appendix describes the different types of numerical models, considered for modeling a WD farm, as well as an evaluation of their strengths and shortcomings.

In addition, the general recommendations concerning model-discretization and model tuning from the MIKE21 BW developer, DHI, will shortly be described. These will, in combination with the findings in Section 4.1, give an idea of the difference between ”optimal” and ”compromised” model-discretization for obtaining usable results.

A.1 Available Numerical Wave Propagation Models

Different available phase averaging- and phase resolving models are described in the following, for use when deciding which model is the most appropriate when modeling a WD farm in a later chapter.

A.1.1 Phase Averaged Models

The phase averaged models describes the evolution of the wave energy spectrum where e.g steady wave heights and depth averaged velocities can be determined from a given wave input (wave action equation is fulfilled). A brief description of available spectral models will be given in the following.

SWAN

SWAN is a nearshore spectral wave model, which predicts average properties of the wave field in the form of significant wave height, H_s and peak period, T_p. It is a so-called shallow water model, which is able to simulate processes that occurs in shallow water - both in form of wave propagation (refraction, diffraction, shoaling) and generation/dissipation (dissipation due to wave breaking, dissipation due to whitecapping, dissipation due to bottom friction, and dissipation/generation due to wave-wave interaction) (Delft, 2009). The performance of the diffraction feature in SWAN, is examined in (Ilic S., 2007) where the ability to predict the multidirectional wave transformation around shore-parallel emerged breakwaters is examined using laboratory and field data. Excellent agreement between the model predictions and measurements was found for broad frequency and directional spectra. The performance of the model, however, worsened with decreasing frequency and directional spread. A further limitation in SWAN is, that it does not account for frequency dependent transmission and reflection, and further, according to (Delft, 2009), it is recommended to use a spatial resolution from $dx = dy = 50\ m$ - $dx = dy = 1000\ m$, which significantly limits the dimensions of obstacles included in the model, such as a WD. Further, the distances between WD’s in a farm are limited by the grid resolution.

A.1.2 Phase Resolving Models

Phase resolving model are able to calculate the sea surface as a function of time (conservation of mass and momentum equations are fulfilled). Time series of e.g wave-heights and -currents can be determined. A brief description of available time domain models will be given in the following.

MIKE21 EMS (Elliptic Mild-Slope Equation)

MIKE21 EMS is based on an efficient numerical solution of the mild-slope wave equation, which governs the motion of time harmonic water waves of infinitesimal height (linear waves) on a gently sloping bathymetry with arbitrary water depth. The model accounts for refraction-diffraction, including; wave breaking, friction and back-scattering. Further, frequency dependent partial reflection and transmission through piers and breakwaters are included. The main application-area of MIKE21 EMS is the calculation of wave fields in smaller coastal areas, where diffraction and wave breaking are important, and where the forcing wave conditions can be represented by a monochromatic and unidirectional wave. The greatest restriction is that non-linear effects such as e.g. amplitude dispersion and wave-wave interaction are not included, and further that irregular wave trains can not be specified in the model.
(DHI, 2008a)

MIKE21 PMS (Parabolic Approximation of Epileptic Mild-Slope Equation)

MIKE 21 PMS is a linear refraction-diffraction model based on a parabolic approximation to the elliptic mild slope equation. The model takes into account the effects of refraction and shoaling due to varying depth, diffraction along the perpendicular to the predominant wave direction, and energy dissipation due to bottom friction and wave breaking. Unlike MIKE21 EMS, irregular wave trains can be specified in the program. A major restriction is, that MIKE 21 PMS does not include diffraction accurately (diffraction along the x-direction is neglected), and that reflection into the incoming wave field is not included in the model. Thus, it should not be used in studies where diffraction is the most important phenomenon of interest.
(DHI, 2008b)

MildSim (Elliptic Mild-Slope Equation)

The possibility for specifying irregular wave trains in MildSim is included in the model and further corrections are introduced for allowing bottom slopes up to 1:1. MildSim accounts for dissipation due to wave breaking and bottom friction. Non-linear effects such as e.g. amplitude dispersion and wave-wave interaction are not included in the model.
(Brorsen, 2008)

MIKE21 BW (Boussinesq Equation)

This model is capable of reproducing combined effects of all important wave phenomena such as diffraction, refraction, shoaling, wave breaking, non-linear wave-wave interaction, and bottom dissipation. Further, it can handle partial reflection and wave transmission from partial reflecting porous structures, directional wave spreading, and internal wave generation. The Boussinesq equations includes nonlinearity as well as frequency dispersion. Basically, the frequency dispersion is introduced in the momentum equations by taking into account the effect of vertical accelerations on the pressure distribution. An extensive verification of the model is performed both against experimental- and analytical data, involving e.g the ability to describe non-linear wave-wave interactions, wave breaking, shoaling, refraction, etc. The equations in MIKE 21 BW have been modified to include porosity, and the effects of non-Darcy flow through a porous media. In this way, it is possible for MIKE 21 BW to simulate frequency dependent partial reflection, -absorption and -transmission of wave energy from porous structures such as a WD. The classical Boussinesq equations are limited to a maximum depth to deep-water wave length

ratio of $h/L_0 \leq 0.22$, but so-called enhanced Boussinesq equations are introduced for extending the maximum depth to deep-water wave length ratio to $h/L_0 \leq 0.5$, making the model appropriate for describing the propagation of directional wave trains from relatively deep water to shallow water. However, $h/L_0 \leq 0.5$ is still a big constraints in the Boussinesq model, together with a need of an increased computational CPU-time, compared to e.g the mild-slope models.

A.2 General Discretization- and Model Setup Recommendations from Model Developer

According to (DHI, 2008d), the grid spacing typically used in practical applications is in the range $dx = 2 - 10\ m$ when no wave breaking is included in the model. If wave breaking and moving shoreline is applied to the model, the normally used range is $dx = 1 - 2\ m$. It is important to select the grid spacing to provide adequate resolution for the main characteristics of the specific wave under consideration. When modeling short waves, the main requirement is, that the grid size is sufficiently small to adequately resolve all the individual waves in the simulation. Additionally, when wave breaking and wave run-up is included, the minimum water depth is theoretically zero, and a very small spatial resolution is required to resolve the wave field. It is recommended to define a grid spacing, so the minimum wave length is resolved by at least 7 grid points, and that the most energetic waves are resolved by 20 - 40 points.
(DHI, 2008d)

Concerning the choice of time steps it is recommended, that a minimum of 35 time steps should be used to resolve the smallest wave period in the spectrum. Further it is required, that the grid spacing in combination with the time step fulfills the Courant number criterion, which should be less than 1 in case of classical Boussinesq equations or less than 0.5 in case of enhanced equations. The Courant number criterion is given in (A.1).

$$Cr = c\frac{dt}{dx} < 1\ ,\ 0.5 \tag{A.1}$$

where
c is the wave celerity $[m/s]$

A.2.1 Calibration Parameters in MIKE121 BW

The purpose of the calibration is to tune the model so differences between results obtained from e.g measurements and from simulation become negligible. Several factors in the model can be adjusted for this purpose, depending on the complexibillity of the model. Some of the calibration factors are listed in the following:

- *Wave conditions and currents* - can be adjusted to achieve the wanted wave conditions
- *Reynolds stresses* - can be adjusted to achieve the wanted wave conditions
- *Porosity* - can be changed to achieve wanted reflection from boundaries or obstacles included in the model.
- *Bed resistance* - can be changed to obtain wanted amount of wave dissipation in the model, or numerical damping can be applied
- *Bathymetry* - can be changed at some locations to achieve the wanted wave conditions

Reynolds stresses arise from a decomposition of the prognostic variables into a mean quantity and a turbulent fluctuation. This leads to additional stress terms in the governing equations to account for the non-resolved processes both in time and space. If the eddy viscosity concept is adopted, these effects are expressed through the eddy viscosity and the gradient of the mean quantity. Thus the effective shear stresses in the momentum equations contain the laminar stresses and the Reynolds stresses (turbulence).

In the breaking zone, the viscous shear is to some extent take into account by the additional convective terms due to the surface roller. Outside the breaking zone, the eddy viscosity is usually very small. Hence no eddy viscosity is included in following simulations.
(DHI, 2008d)

A.3 Description of Governing Equations in MIKE21 BW

MIKE21 BW is based on the two dimensional Boussinesq equations with depth-integrated velocity-components, P and Q, given in (A.2), with enhanced linear dispersion characteristics in a depth integrated flux-formulation presented in (Madsen and Sørensen, 1992). The classical Boussinesq approximation eliminates the vertical coordinate, x_3, in the flow equations, and waves are thereby only described in the horizontal plane, x_1 and x_2. The approximation is performed by use of a Taylor expansion of the velocity potential, φ, at a given depth. Hereafter, the continuity equation for an incompressible fluid and the condition of irrotational fluid are used to replace partial derivatives in relation to x_3 in the taylor expansion with respect to x_1 and x_2.
(Madsen and Sørensen, 1992)

$$
\begin{aligned}
&\frac{\partial \eta}{\partial t} + \frac{\partial P}{\partial x_1} + \frac{\partial Q}{\partial x_2} = 0 \\
&\frac{\partial P}{\partial t} + \frac{\partial \left(\frac{P^2}{d}\right)}{x_1} + \frac{\partial \left(\frac{PQ}{d}\right)}{x_2} + gd\frac{\partial \eta}{\partial x_1} + \psi_1 = 0 \\
&\frac{\partial Q}{\partial t} + \frac{\partial \left(\frac{Q^2}{d}\right)}{x_2} + \frac{\partial \left(\frac{PQ}{d}\right)}{x_1} + gd\frac{\partial \eta}{\partial x_2} + \psi_2 = 0
\end{aligned}
\tag{A.2}
$$

where
P is the flux density in the x_1-direction $[m^3/m/s]$
Q is the flux density in the x_2-direction, $[m^3/m/s]$
t is the time $[s]$
d is the still water depth $[m]$
η is the water surface level above datum $[m]$
g is the gravitational acceleration $[m/s^2 2]$
ψ_1 and ψ_2 are the Boussinesq terms given in (A.3) and (A.4) $[-]$
(DHI, 2008c)

The terms ψ_1 and ψ_2 are dispersive Boussinesq type terms derived under the mild-slope assumption and enhanced to provide improved frequency dispersion characteristics by adopting a Pade expansion scheme in the truncation of the velocity terms instead of using Taylor expansion. These equations were first derived by (Madsen and Sørensen, 1991) and given in (A.3) and (A.4).

$$\begin{aligned}\psi_1 = &-\left(B+\tfrac{1}{3}\right)h^2\left(\tfrac{\partial^3 P}{\partial^2 x_1 \partial t}+\tfrac{\partial^3 Q}{\partial x_1 \partial x_2 \partial t}\right)-Bgh^3\left(\tfrac{\partial^3 \eta}{\partial x_1^3}+\tfrac{\partial^3 \eta}{\partial x_1 \partial x_2^2}\right)\\ &-h\tfrac{\partial h}{\partial x_1}\left(\tfrac{1}{3}\tfrac{\partial^2 P}{\partial x_1 \partial t}+\tfrac{1}{6}\tfrac{\partial^2 Q}{\partial x_2 \partial t}+2Bgh\tfrac{\partial^2 \eta}{\partial x_1^2}+Bgh\tfrac{\partial^2 \eta}{\partial x_2^2}\right)\\ &-h\tfrac{\partial h}{\partial x_2}\left(\tfrac{1}{6}\tfrac{\partial^2 Q}{\partial x_1 \partial t}+Bgh\tfrac{\partial^2 \eta}{\partial x_1 \partial x_2}\right)\end{aligned} \tag{A.3}$$

$$\begin{aligned}\psi_2 = &-\left(B+\tfrac{1}{3}\right)h^2\left(\tfrac{\partial^3 Q}{\partial^2 x_2 \partial t}+\tfrac{\partial^3 P}{\partial x_1 \partial x_2 \partial t}\right)-Bgh^3\left(\tfrac{\partial^3 \eta}{\partial x_2^3}+\tfrac{\partial^3 \eta}{\partial x_1^2 \partial x_2}\right)\\ &-h\tfrac{\partial h}{\partial x_2}\left(\tfrac{1}{3}\tfrac{\partial^2 Q}{\partial x_2 \partial t}+\tfrac{1}{6}\tfrac{\partial^2 P}{\partial x_1 \partial t}+2Bgh\tfrac{\partial^2 \eta}{\partial x_2^2}+Bgh\tfrac{\partial^2 \eta}{\partial x_1^2}\right)\\ &-h\tfrac{\partial h}{\partial x_1}\left(\tfrac{1}{6}\tfrac{\partial^2 P}{\partial x_2 \partial t}+Bgh\tfrac{\partial^2 \eta}{\partial x_1 \partial x_2}\right)\end{aligned} \tag{A.4}$$

where
B is the Boussinesq dispersion factor, $B = 1/15\ [-]$
(Madsen and Sørensen, 1991)

In MIKE21 BW an additional factor n is included to describe flow through a porous media based on based on resistance coefficients for laminar and turbulent flows. Further a part is included to account for dissipation due to wave breaking, based on the concept of surface rollers, which is adapted from the breaking characteristics of a spilling breaker. The surface roller concept assumes that the effect of wave breaking can be modelled by imposing a volume of water (a roller) on the wave front (from the moment of breaking) traveling with the wave celerity c. This is further described in (Madsen, 1997).

Numerical Scheme and Spatial/Time Discretization

The differential equations used in the 2D-module of the MIKE21 BW can be discretisized using different schemes with variables defined on a space-staggered rectangular grid. As default, the equations are solved by implicit finite difference techniques where the convective terms are discretisized using central differences and the normal ADI algorithm with 'side-feeding' for numerical integration. The 'side-feeding' technique is introduced to center the cross-momentum derivatives (the so-called cross-terms) without numerical dissipation. Alternative schemes, however, can be used, such as; "central differencing with simple upwinding at steep gradients and near land", "Quadratic upwinding with simple upwinding at steep gradients and near land", and "Simple upwinding differencing". The alternative schemes are recommended to be used in models where numerical instabilities cause a blow up in the model, since the introduced damping in the schemes may avoid these. The simple upwinding scheme is the most dissipative scheme, and one should be aware, that smaller wave amplitudes are obtained when using this. When resolving the Boussinesq cross-terms the standard representation results in these terms to be back centering half a time-step, which will result in an artificial dissipation of waves traveling with an angle to the grid. As a result a linear extrapolation scheme has been used to avoid this effect. However this method of time-centering the cross-terms will sometimes result in model instability, which is accounted for in the model by incorporating a time-extrapolation factor, which can attain values between 0 and 1. A value of 1 represents a correct time centering and 0 represents a backward centering of the Boussinesq cross-terms.
(DHI, 2008c)

Appendix B

Calibration of Wave Bassin

This appendix describes the experiments performed to determine the effects of the boundaries in the wave basin used for the experiments described in Section 4.9.

B.1 Tests for use in Calibration of Laboratory Basin

Preliminary tests are conducted in order to investigate reflection characteristics of the boundaries in the wave basin for use in the numerical model. Moreover, they are used to determine whether wave disturbance from the basin boundaries can be expected to affect the measurements of the wave disturbance from the WD. As explained in Section 4.6, the wave basin is relatively small compared to the size of the WD-model, and hence an exact calibration of the basin is of great importance to obtain useable wave disturbance coefficients in the area close to the WD.

Test Setup for use in Calibration of Gravel beach

The first test in the empty basin (named *"test Setup 3"*) uses the test setup in Figure B.1, and is primarily performed in order to determine reflection from the gravel beach. Reflection from the beach is found from gauge A, B and C which are placed with distances to the beach as recommended by (Mansard and Funke, 1980). It should be mentioned, that a relative short distance from the gauges to the wave generator is present, which may slightly affect the measurements. Additionally, gauge D to H are placed along the gabions in order to determine diffraction due to the presence of these.

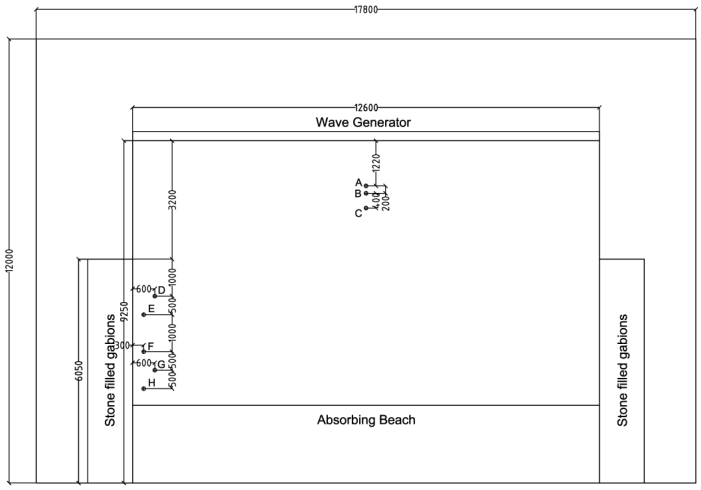

Figure B.1 *Setup of wave gauges for "test Setup 3". Dimensions given in* mm.

Test Setup for use in Calibration of Partial Reflecting Basin Sides

After the tests with the empty basin, one of the gabions is placed in the basin as shown in Figure B.2 (*"test Setup 4"*), to determine the reflection. This is done since, as found in Section 4.2.2, the diffraction, along the sides of the basin, is dependent on their reflective properties, and hence a specification of these properties, in combination with a calibration against the reduced wave heights found using *"test Setup 3"*, can be used to include the empty basin wave disturbance in MIKE21 BW.

Since the reflection analysis is based on a flume, with the reflective surface spanning the entire width, diffraction around the gabion is likely to affect the results of the test and hence fully reflective walls are placed on either side of the gabion. These walls essentially create a flume, preventing interference from diffraction.

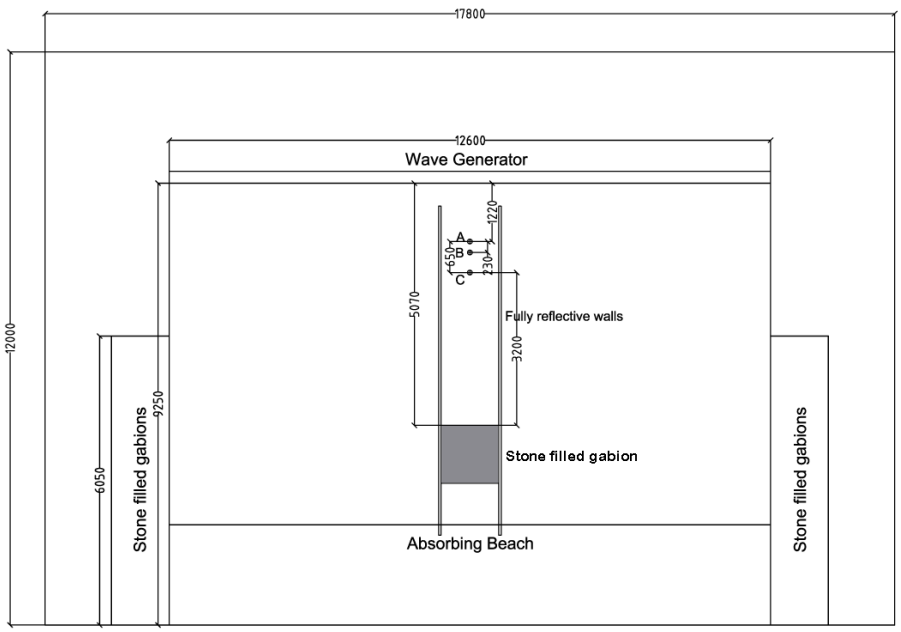

Figure B.2 *Setup of wave gauges for "test Setup 4". Dimensions given in* mm.

A further illustration of *"test Setup 4"* is given in Figure B.3.

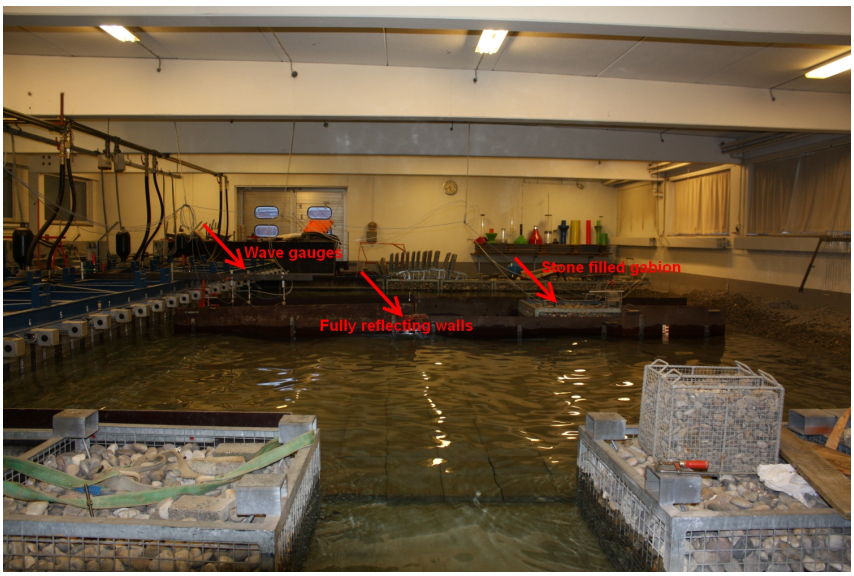

Figure B.3 *Picture taken from the side of the laboratory basin, illustrating "Test Setup 4" for use when determining the reflection from the stone filled gabion.*

B.2 Evaluation of Results Concerning Wave Disturbance and Reflection in Empty Wave Basin

As written earlier, a number of tests in the empty basin are conducted in order to perform calibration of the boundaries for use in the numerical model. Further, the tests are used to get an idea of the wave dis-

turbance in the basin without the WD, which will be kept in mind when analyzing the wave disturbances from the WD. The results from these tests are presented and evaluated in the following.

B.2.1 Analysis of Reflection from Gravel Beach and Stone Filled Gabions

Based on the same reflection analysis as described in Section 4.8.3, reflection coefficients, K_r, are determined from irregular waves with different specified incident peak period, wave lengths $L_{p,spec}$ and different specified incident significant wave heights $H_{s,spec}$ using *"test setup 3"*. Since the reflection characteristics varies through the spectrum (as seen in Section 4.1.3), mean values of the reflection coefficient $K_{r,mean}$ are plotted as a function of $L_{p,spec}$ in case of $H_{s,spec} = 0.04\ m$ and $H_{s,spec} = 0.1\ m$, presented in Figure B.4. Here it can be seen, that generally an increasing reflection coefficient is obtained with increasing wave length and decreasing wave steepness, H/L, and with an approximate average reflection coefficient of $K_{r,mean} \approx 0.2$ for the considered waves. For identical wave lengths the low steepness wave give more reflection due to less dissipation by breaking as also predicted by the porosity layers in MIKE21 BW. A reflection coefficient of $K_r \approx 0.2$ corresponds to a reflected amount of wave energy of $\approx 4\%$, and hence the reflection from the gravel beach is not expected to have a major influence on the measurements in the basin. It should be noted that if the incident wave is reflected into areas with small transmitted wave heights, the reflected wave will have an increasing influence on the measurements

In addition to the reflection from the gravel beach, a reflection analysis on the stone filled gabions is performed, to determine the wave reflection from the sides of the basin. This is done using *"test setup 4"*, where only two irregular waves, with different wave lengths and equal wave heights, are considered. $K_{r,mean}$ is presented in Figure B.5 where it is seen, that a slightly increasing reflection is obtained with increasing wave length.

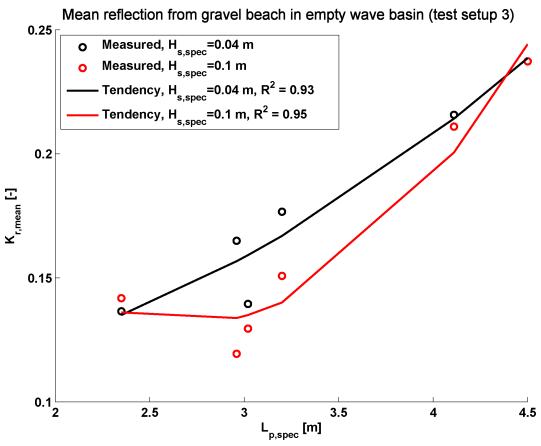

Figure B.4 *Mean values of the reflection coefficient $K_{r,mean}$ from the gravel beach as a function of the peak period wave length $L_{p,spec}$ in case of different specified incident significant wave heights $H_{s,spec}$.*

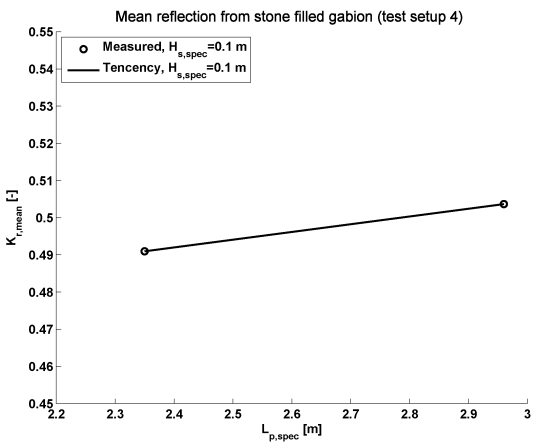

Figure B.5 *Mean values of the reflection coefficient $K_{r,mean}$ from the stone filled gabions as a function of the peak period wave length $L_{p,spec}$ in case of a specified incident significant wave height of $H_{s,spec} = 0.1\ m$.*

K_r from the considered waves will be specified as a starting point in MIKE21 BW in a later chapter, and then further calibrated against wave disturbances. To this, an analysis of the influence from the side-boundaries in the basin will be performed in the following section.

B.2.2 Wave Disturbance from Stone Filled Gabions

To analyse the wave disturbance from the boundary-sides, K_d from gauge E and gauge G in *"test setup 3"* is considered and presented in Figure B.6 and Figure B.7, respectively. As seen in Figure B.1, Gauge E is placed 1.5 m from the beginning of the gabions in the direction of the wave propagation, and a distance of 0.3 m perpendicular to the boundary sides. Gauge G is placed 3 m from the beginning of the gabions in the direction of the wave propagation, and 0.6 m in the perpendicular direction from the sides.

From Figure B.6 and Figure B.7 it can be seen, that a more reduced wave height is observed further away from the wave generator, along the gabion (gauge G compared to gauge E), corresponding to the study in Section 4.2.2, and that the wave height increases (K_d increases) with increasing L. Further, the diffracted wave height increases with increasing distance from the gabions (gauge G compared to gauge E), which is also expected from the study in Section 4.2.2.

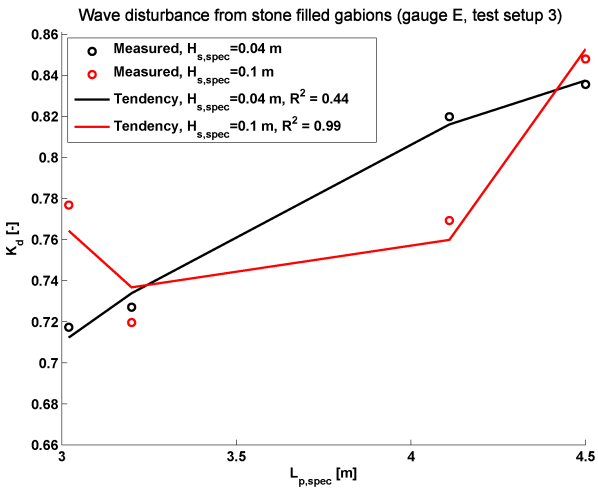

Figure B.6 *Wave disturbance from the stone filled gabions, measured at gauge E in* "test setup 3".

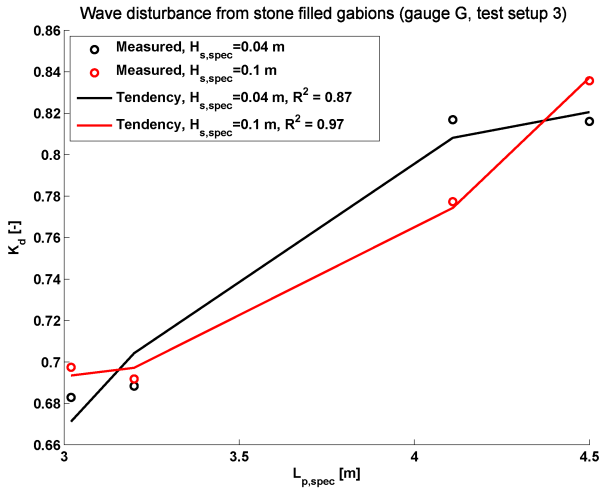

Figure B.7 *Wave disturbance from the stone filled gabions, measured at gauge G in* "test setup 3".

To determine whether the wave disturbance from the side-boundaries affects the measurements in the area close to the WD, gauge O in *"test setup 2"*, placed ≈ 3.5 m from the gabions and 1.7 m from the tip of the WD-reflector, is considered. K_d from gauge O as a function of L is presented in Figure B.8. Here it can be seen, that K_r is above 1 at all considered waves due to diffraction, which is seen, from the Sommerfeld Diagram in Figure 4.29, to increase the wave heights with a factor of up to 1.17. Further, as seen in Figure 4.29, the diffraction is affected by the wave length, and hence K_d decreases with increasing L. However, since no wave disturbance coefficients below 1 are obtained, it is expected that wave diffraction from the partial reflecting stone filled gabions only have a negligible effect on the wave heights measured near the WD.

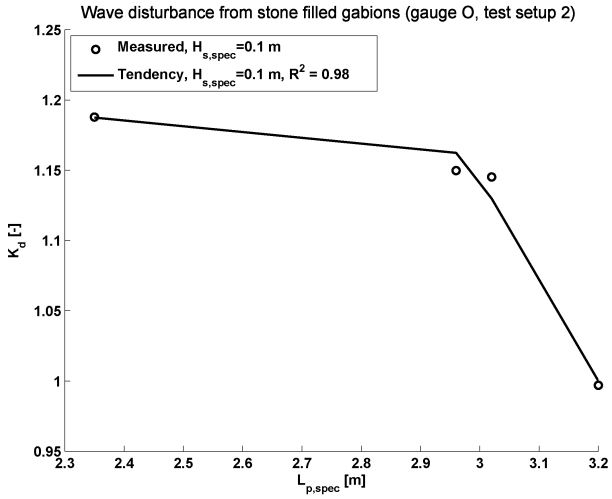

Figure B.8 *K_d from gauge O in* "test setup 2" *as a function of L.*

B.3 Calibration of Numerical Model

Before the model with the WD can be calibrated, it must be ensured that the effects from the boundaries in the wave basin are modelled correctly. This is done by comparing results from the tests on the empty basin, with a numerical model, describing only the boundaries of the basin. Once this model has been calibrated, the WD will be added.

The numerical model is a rescaled version of the one described in Section 4.6, except that the WD is replaced by open water. The water depth is also changed depending on which test is used. The calibration factors are: The incoming waves, porosity of the gabions and porosity of the beach.

B.3.1 Rescaling of model

Since the goal of the calibration is to use the resulting model in the bathymetry of Santander bay, the numerical model is scaled to fit this scenario, based on the values found in Section 4.7.1. After this is done, the wave basin has the dimensions shown in Figure B.9.

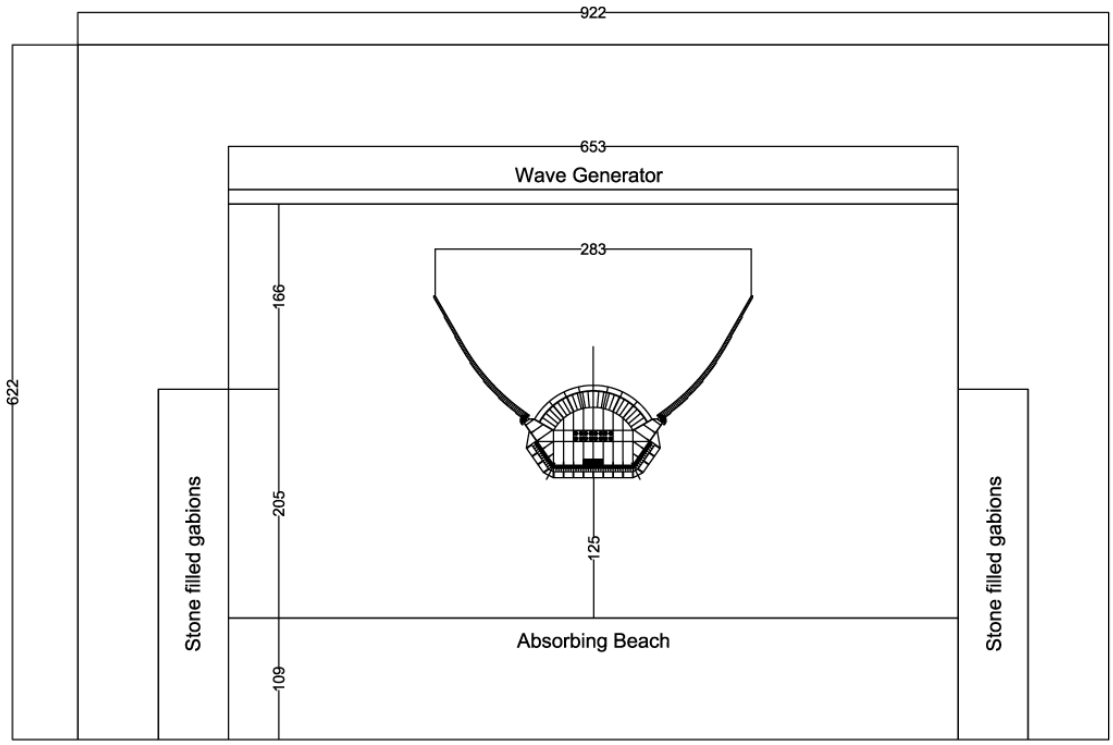

Figure B.9 *Wave bassin rescaled to full size WD. Dimensions given in* m.

In addition to the dimensions of the basin, the waves are also scaled. In order to be to compare the results obtained from the model and experiments respectively, the waves applied in the model are rescaled based on the generated incident waves found in Section 4.8.2, rather than the ones given in Table 4.3. The resulting sea states are given in Table B.1. Since the signals, used to generate the waves, are reused in the laboratory, these waves can be expected to be identical to the ones generated when the WD is placed in the bassin.

Test no	$H_{s,bassin}$	$H_{s,scaled}$	h_{bassin}	h_{scaled}
1	0.08	4.14	0.39	20.20
2	0.09	4.66	0.39	20.20
69	0.09	4.66	0.39	20.20
70	0.04	2.07	0.39	20.20
71	0.05	2.59	0.39	20.20
72	0.05	2.59	0.39	20.20
73	0.08	4.14	0.48	24.86
74	0.09	4.66	0.48	24.86
75	0.09	4.66	0.48	24.86
76	0.04	2.07	0.48	24.86
77	0.05	2.59	0.48	24.86
78	0.04	2.07	0.48	24.86
79	0.09	4.66	0.39	20.20
80	0.05	2.59	0.39	20.20
81	0.05	2.59	0.39	20.20
82	0.04	2.07	0.39	20.20
83	0.09	4.66	0.48	24.86
84	0.10	5.18	0.48	24.86
85	0.09	4.66	0.48	24.86
86	0.05	2.59	0.48	24.86
87	0.05	2.59	0.48	24.86
88	0.05	2.59	0.48	24.86
89	0.04	2.07	0.39	20.20
90	0.09	4.66	0.39	20.20

Table B.1 *Sea states used in scaled numerical model.*

Since the wave period is increased it is also necessary to increase the simulation period in order to obtain usable results. The tests where run for a duration of $50\ min$, which is scaled to $6\ hrs$ in the numerical model. The grid spacing is set to $dx = 5.18\ m$ and the time step to $dt = 0.15\ s$ corresponding to a courant number $C_r = 0.45$.

B.3.2 Reflection Analysis

In order to calibrate the numerical model, based on the test data, the scaled waves, applied to the model, must correspond to the incident waves observed in the model. This is ensured, not only by defining the desired wave spectrums as input, but also by performing a reflection analysis on the results obtained from the model. Since the reflection from the beach should not have an influence on the incoming wave spectrum, this can be done before the porosity layers are calibrated. Once the correct waves are obtained, the porosity layers, used to model the beach, will be calibrated in order to obtain the correct reflection from the beach. The mean reflection coefficient $K_{r,mean}$ obtained from each of the tests, as well as the wave length corresponding to the unscaled peak period, is given in Table B.2. These values of $K_{r,mean}$ can be applied to the numerical model as well, as $K_{r,mean}$ will remain the same when depth, wave height, wave length and wave period are all scaled correctly. Table B.2 does not include the regular wave from test 79-90, as these are used to find quick estimates for the model of the WD, rather than detailed calibration.

Test no.	$K_{r,mean}$ $[-]$	L $[m]$
1	0.14	2.26
2	0.12	3.11
69	0.22	3.92
70	0.13	2.26
71	0.17	3.02
72	0.20	3.92
73	0.13	2.59
74	0.14	3.30
75	0.24	4.75
76	0.13	2.49
77	0.17	3.30
78	0.23	5.01

Table B.2 *Reflection coefficients from tests on the empty bassin.*

The beach is modelled using using 25.9 m of porosity layers, backed by 77.7 m of sponge layers, meaning any wave energy transmitted through the porosity layers will be absorbed by the sponge layers. The initial porosity value applied to the beach is determined based on the results of test 1, using the method described in Section 4.1.3, resulting in a porosity factor $S = 0.98$. A test simulation, based on test 1, is run using this value and it is found that $K_{r,mean} = 0.14$, corresponding to the value given in Table B.2.

As with the beach, a reflection analysis is also carried out, based on the results of the tests 3 and 4, where one of the gabions is placed in the bassin. Both of these tests show a reflection coefficient $K_{r,mean} = 0.54$ for the gabions. Based on this, a porosity factor $S = 0.81$ is found, using the MIKE21 toolbox. This value is not calibrated based on the $K_{r,mean}$, as was the case with the beach, since they are not hit directly by the waves in the model of interest. Instead S will be calibrated based on a comparison of the wave disturbances obtained from the tests and the model respectively.

B.3.3 Comparison of Wave Disturbance

After the reflection from the beach has been calibrated and the correct waves applied, the model is validated against the measurements obtained from the experiments. This is done by comparing the wave disturbances $K_d = H_s/H_{s,i}$ at the different gauge positions in *"test setup 3"*.

The incoming significant wave height $H_{s,i}$ is defined based on the findings in Table B.1, while H_s is determined from a time series analysis in the experiments and extracted as phase averaged data from the model. The results from test 1 are shown in Figure B.10.

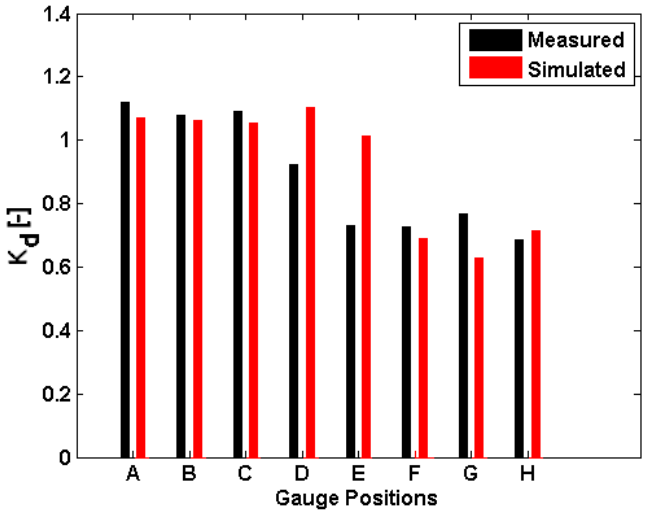

Figure B.10 *Comparison of measured and modelled wave disturbances for Test 1.*

It is seen that K_d is slightly above 1 for the gauges A-C, as a result of the reflection from the beach. For these gauges the results from the model show a slightly smaller H_r, which suggest the reflection from the beach is underestimated. However, this deviation is small enough to be accepted. As expected, H_r decreases below 1 for gauges D-H, depicting the reduction of wave heights as the waves pass the gabions.

Appendix C

Setup of Numerical Model of Santander Bay

This appendix gives a detailed description of the setup of the numerical model in MIKE21BW. The appendix is related to Chapter 6 in the main report.

C.1 Wave Generation and Investigation of Influence from Absorbing Boundaries

Waves are generated at the upper boundary in the domain from the north direction, illustrated in Figure C.1. To study whether "false" diffraction from absorbing sponge boundaries in the model affects the area of interest, diffraction and refraction is decoupled, by applying a constant depth of 25 m in the bathymetry. A long crested wave spectrum with $T_p = 10\ s$ and $H_s = 5\ m$ is applied to the model, and the wave disturbance in Figure C.1 is obtained.

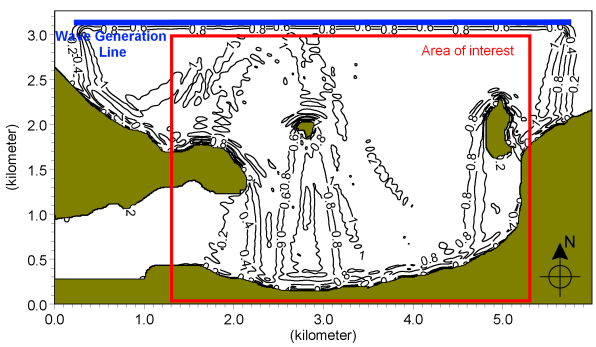

Figure C.1 *Illustration of wave generation line and area of interest.*

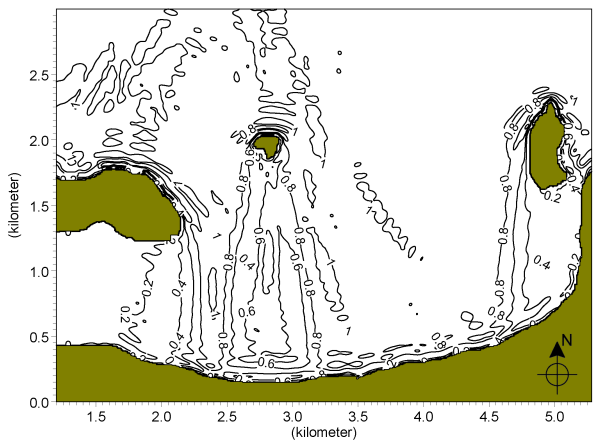

Figure C.2 *Area of interest, $h = 25\ m$ to study whether "false" diffraction appears in the model.*

From Figure C.1 it can be seen, that diffraction from the sponge layers in the sides is present, however, the diffraction do not enter the actual area of interest. The same analysis is performed on a wave with $T_p = 16\ s$, where no diffraction in the considered area is obtained either. Therefore, all analysis's will be run in this model-size, corresponding to the area in Figure C.2.

C.1.1 Additional Tests with Waves from NW

In the Chapter 1 it was seen, that the most common wave direction is NW. However, it is observed, that the waves are turning into a more northerly direction due to refraction, cf. Figure C.3. To include this oblique wave direction in the model, without turning the WD's, which is not possible due to the grid-

spacings, the bathymetry is turned, so the waves generated from a horizontal generation line propagates in the same direction as in Figure C.3, see Figure C.4. When turning the bathymetry, an extra amount of water points are included in the NW-corner of the model which requires substantial more CPU-time for the simulations. Hence the majority of the simulations are performed on models with waves from north.

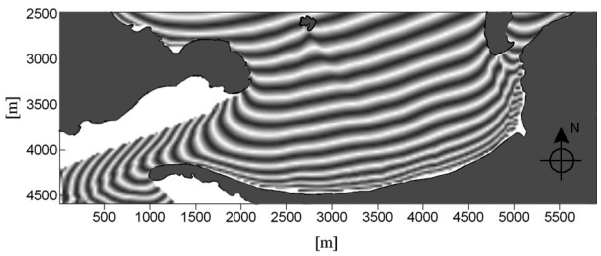

Figure C.3 *Wave propagation associated with typical storm wave conditions ($H_s = 5\ m$, $T_p = 16\ s$) from the NW-direction during high tide, performed by (GIOC, 2001). Figure is orientated to the north.*

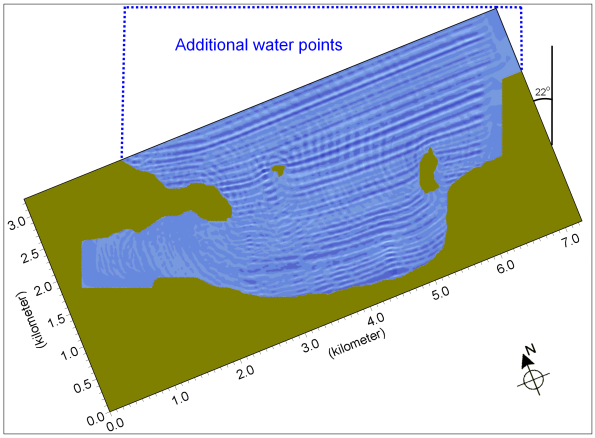

Figure C.4 *Turned bathymetry,* $22°$.

C.2 Convergence Analysis on Wave Disturbance

As written in Chapter 4, it is important to ensure that discretization-errors, decrease with the number of discrete elements in the expected way. Since most study on the model of Santander will be based on the wave disturbance from WD's, the convergence analysis will be performed on K_d.

However, before studying the influence from the element discretization, the sufficient number of generated incident waves for obtaining a converged value of K_d is studied. This is done in Figure C.5 where the variation of K_d as a function of model time (time in simulation), at different locations is plotted. The indicated locations in Figure C.5 have the reference to Figure 6.2. A wave with $H_s = 5\ m$ and $T_p = 10\ s$ is applied at the boundary, and it is seen, that approximately 1200 generated incident waves are sufficient for obtaining a converged value of K_d at all considered locations. In addition, by considering the wave disturbance contours in the whole model domain at different time steps, it is seen, that all locations in the model are converged at 1200 generated incident waves.

Using the 1200 incident waves, K_d is determined in case of varying element discretization in Figure C.6 at the different considered locations, together with the CPU-time needed for performing the simulation. Here it is seen, that only very small changes in K_d appears. The tendency is, however, that a bigger value K_d is obtained in case of smaller dx, which is expected to be due to a greater amount of numerical damping when the element sizes increases. The change is, however, on the third decimal, and hence an element size of $dx = dy = 5.18\ m$ will be used in the following.

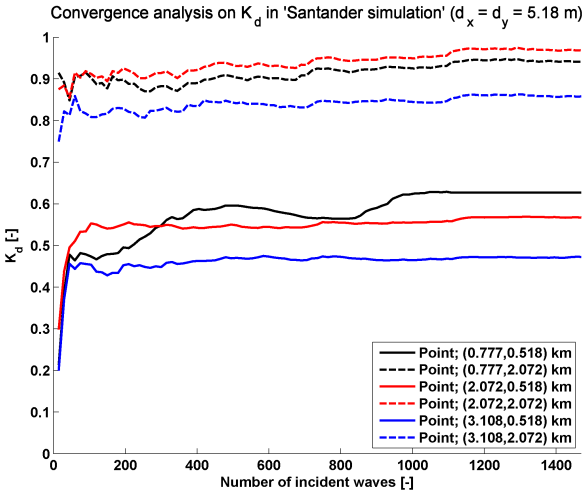

Figure C.5 *Sufficient number of generated incident waves for obtaining a converged value of K_d*

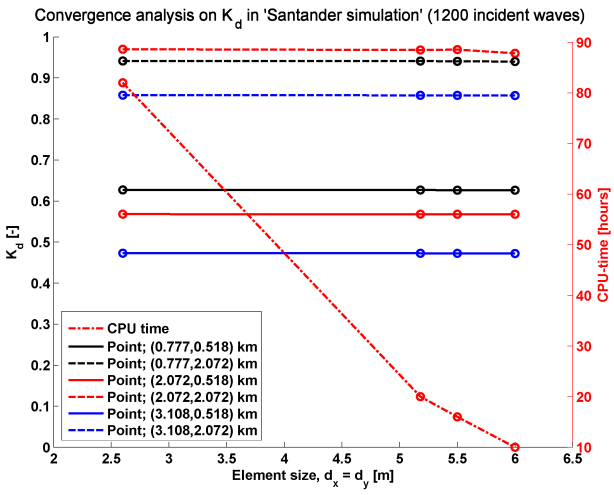

Figure C.6 *Variation of K_d and needed CPU-time, in case of different element sizes.*

An element size of $dx = 5.18\ m$ corresponds to a ratio of $L/dx_{min} = 9.4$ when $T_{min} = 6\ s$ and $h_{min} = 10\ m$, which, cf. Chapter A, is sufficient to resolve the smallest wave in the spectra. The ratio of $dx/L_{min} = 9.4$ does not correspond to the requirements found in Chapter 4 ($L_{min}/dx > 50$), which however, does not seem to have any influence on the results in the model of Santander.

Cf. Chapter A a minimum of 35 time steps should be used to resolve the smallest wave period in the spectrum. Further, a Courant number less than 0.5 is required in case of enhanced deep water Boussinesq terms, which are used in this case. From this follows, that a time step of $dt = 0.15\ s$ is used.

C.3 Sensitivity Analysis on Influence from Bottom Friction

To analyse how sensitive the model is to changes in the bed friction, the influence from varying values of the equivalent roughness height, k_s, are studied.

Whether the wave is influenced by the sea bed, depends on the ratio between the water depth and the wave length, h/L. When considering small amplitude waves ($h/L << 1$), it can be shown, that the wave penetrate into the ocean corresponding to $L/2$, and that particle paths are circular (unaffected from seabed) if $h/L > 1/2$. In case of $h/L < 1/2$, the wave "feels" the sea bed, and is affected by the bed friction. If $h/L < 1/20$, the wave is considered as "shallow water wave" and is greatly affected by dissipation due to bed friction. In Figure C.7 the particle path for the shallow- and deep water wave is illustrated.

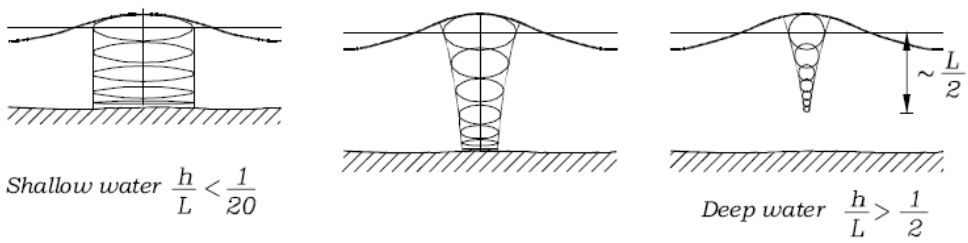

Figure C.7 *Particle path for shallow and deep water waves. (Andersen and Frigaard, 2008)*

When considering the smallest water depth in the domain, $h = 10\ m$, the ratios in Table C.1 in case of the considered incident peak periods are obtained. Here it can be seen, that the considered waves are somewhat in between shallow and deep water waves, where the wave with T_p is almost a shallow water wave.

	$h_{min} = 10\ m$		
$T_p\ [s]$	**10**	**12**	**16**
$L\ [m]$	92	113	154
$h/L\ [-]$	0.11	0.09	0.06

Table C.1 *h/L-ratios for the considered peak periods and minimum water depth.*

As mentioned in Section 1.1, the spit is made up of beaches and dunes of relatively fine sand with a mean grain size along the spit of 0.3 mm. Hence it is expected that the seabed will be relatively smooth in the area. However, to be sure on whether bottom friction may influence following conclusions, the extreme cases, with no bottom friction and a specified equivalent roughness height of $k_s = 0.3\ m$ are compared. This is done in the cases with- and without a WD positioned offshore and in case of different incident peak periods, where K_d is plotted in the line (2200,0) m - (2200,2900) m with the reference in Figure 6.2. In Figure C.8 no WD is included in the model, and in Figure C.9 a WD with the *"free/free"* setup is positioned 2300 m offshore.

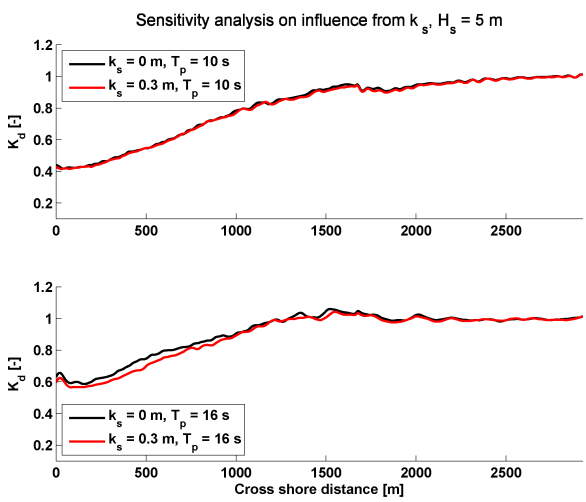

Figure C.8 *Investigation of influence from bed friction. No WD is included in the model.*

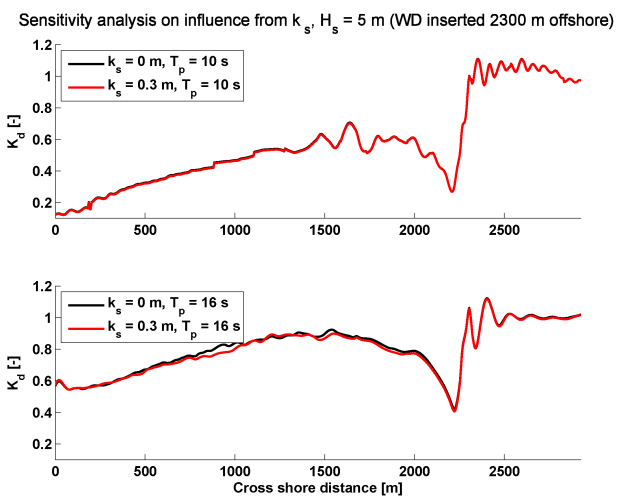

Figure C.9 *Investigation of influence from bed friction. 1 WD is included in the model.*

From Figure C.8 and Figure C.9 it is seen, that the biggest influence from k_s is obtained with $T_p = 16$ s near the shore, as expected from the ratios in Figure C.7. The biggest relative percentage difference in the cases with- and without a WD positioned offshore are ≈ 4 % and ≈ 6 %, respectively, with $T_p = 16$ s. Hence it is expected, that the unknown actual value of K_s will no influence on the conclusions made from the simulations.

C.4 Preliminary Study of Wake Behind WD

Before performing simulations on the wake behind WD's in Santander a brief preliminary study of a single WD with different setups is performed in a wave flume with constant depth. This is done in order to get an idea of the extension of the wake from the different setups and wave conditions for use when placing WD's in Santander bay. The calibrated WD's with the *"free"* setup and *"fixed"* setups are installed in a wave flume with constant depth, $h = 25$ m, see Figure C.10. To study the wake behind the WD, K_d is plotted in a longitudinal section, and three lateral sections at respectively 1000 m, 2000 m, and 3000 m behind the WD (all sections are illustrated in Figure C.10). To avoid wave disturbance due to diffraction from the absorbing boundaries, only wave disturbance in the "output area" in Figure C.10 is considered.

In Figure C.11 the wave disturbance in a longitudinal section is plotted for irregular long-crested head on waves with different periods. It can be seen, that immediately behind the WD a large decrease in the transmitted significant wave height is seen, while a gradual redistribution occurs in a further distance behind the WD due to diffraction. In a distance of 3000 m behind the WD the wave disturbance is $K_d \approx 0.8$ (when $T_p = 10$ s, $H_s = 5$ m) and $K_d \approx 0.95$ (when $T_p = 16$ s, $H_s = 5$ m), using the *"free"* setup. When comparing the *"fixed"* WD-setup to the *"free"* WD-setup, a relative decrease of $\approx 6\%$ is obtained 1000 m behind the WD which is reduced to a decrease of only $\approx 2\%$ 3000 m behind the WD for the considered peak periods.

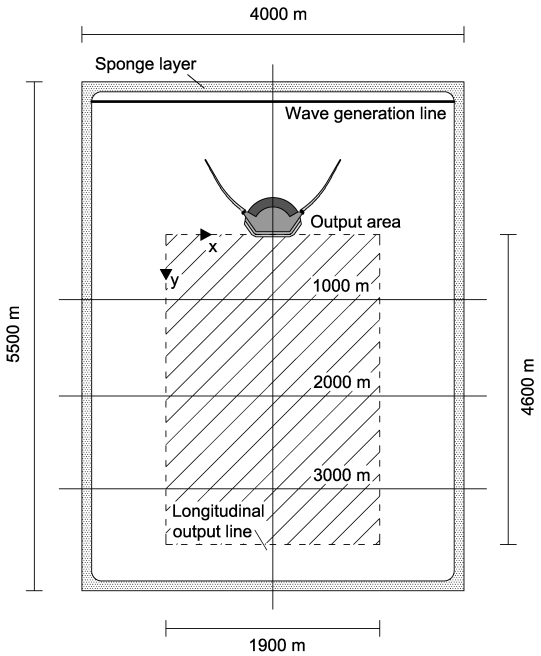

Figure C.10 *Wave flume with constant depth, $h = 25\ m$, for testing wake behind WD.*

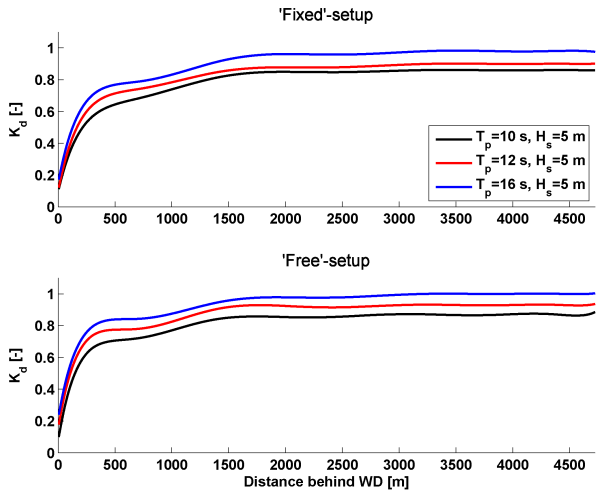

Figure C.11 *Wave disturbance in a longitudinal section is plotted for irregular long-crested head on waves with different periods*

The three lateral sections behind the WD are shown in Figure C.12 for the same wave conditions as considered in Figure C.11. Generally it is seen, that the wake effect is gradually filled up due to diffraction effects. An increasing width of the wake is obtained further away from the WD. The remaining wave height behind the WD increases with increasing directional spreading. This is illustrated in Figure C.13, where two short crested waves with $s = 10$ and $s = 100$ are compared to a long crested wave. The greatest effect is obtained in case of $s = 10$ where almost no wave height decrease is found at a distance of 3000 m behind the WD.

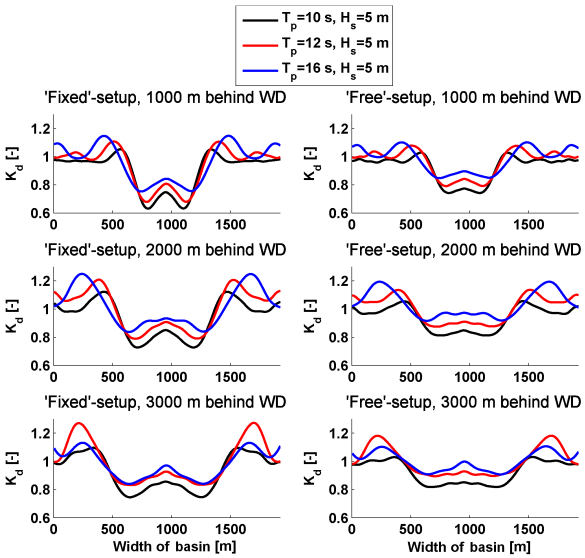

Figure C.12 *K_d in lateral sections behind the WD, in case of long-crested head on waves.*

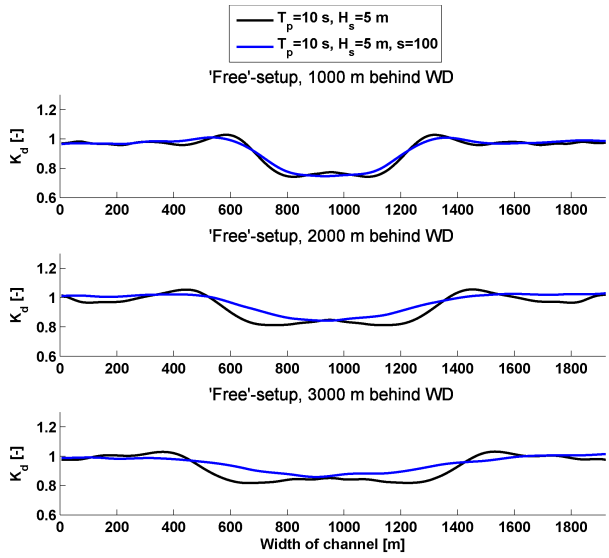

Figure C.13 *K_d in lateral sections behind the WD, in case of short-crested head on waves.*

Observations from the longitudinal and lateral sections are summarized in and Table C.2 and Table C.3 for the case with different peak periods and directional spreading. It can be concluded, that an increasing wave length and directional spreading results in an increasing K_d, or deceasing wave height reduction, behind the WD, as expected. Further, it is seen, that the wake shortens with increasing directional spreading due to a faster redistribution behind the WD. A wider wake is observed when short-crested waves are considered. Further, the small increase in wave height, due to diffraction, as seen at the edges of the wake in Figure C.12 disappears in a short-crested sea. It is expected, that this tendency will increase with increasing directional spreading.

$H_s = 5\ m$, $s = 0$	**Fixed WD-setup**			**Free WD-setup**		
$T_p =$	**10** s	**12** s	**16** s	**10** s	**12** s	**16** s
K_d, 1000 m behind WD	0.74	0.8	0.84	0.77	0.84	0.89
K_d, 2000 m behind WD	0.83	0.9	0.93	0.84	0.91	0.97
K_d, 3000 m behind WD	0.86	0.92	0.97	0.86	0.91	0.99

Table C.2 *Wave disturbance along longitudinal section behind WD in case of different peak periods.*

$H_s = 5\ m$, $T_p = 10\ s$	**Free WD-setup**	
$s =$	**0**	**100**
K_d, 1000 m behind WD	0.77	0.75
K_d, 2000 m behind WD	0.84	0.84
K_d, 3000 m behind WD	0.86	0.88

Table C.3 *Wave disturbance along longitudinal section behind WD in case of different values of directional spreading.*

Appendix D

SBEACH Theory

This appendix deals with a description of the SBEACH program, used for determining the cross-shore sediment transport at Santander, mainly based on (Larson, 1990).

D.1 General Description

SBEACH is an empirically based model, used for determining short term cross-shore effects of storm waves and water levels for sandy beaches. Net transport rates and directions are calculated based on wave input, and in turn used to determine the profile change.

D.2 Applied Theory

The model is based on the equilibrium beach profile approach, meaning it is assumed that the beach profile attains a constant shape after being exposed to the same wave climate for a sufficient amount of time.

An important part of describing the development of the beach, is to determine the direction in which the cross-shore transport takes place. In some cases the waves will move the sand seawards and deposit it in the form of a bar further from the shoreline, causing an erosion of the beach. This is often the case if the incoming waves have large wave heights and short wave periods. If the opposite is true, sand from seaward bars will be moved towards the shore, where the accretion will cause the beach to widen. SBEACH uses (D.1), which is represented in Figure D.1, to determine the direction of the transport. Values placed above the line in Figure D.1 (left side of (D.1) greater than the right) correspond to accretion, while values below (left side of (D.1) smaller than the right) correspond to erosion of the beach. The plotted data are experimental, further described in (Larson, 1990), and used for determining M in (D.1). It is seen, that both the wave steepness and wave height influence the erosion and accretion. In addition, the fall speed accounts for the settling characteristics of the sand particles. The fall speed is dependent on the water temperature, which must be defined in the model.

$$\begin{aligned} \frac{H_o}{L_o} &> M \cdot \left(\frac{H_o}{\omega \cdot T}\right)^3 \Rightarrow Accretion \\ \frac{H_o}{L_o} &< M \cdot \left(\frac{H_o}{\omega \cdot T}\right)^3 \Rightarrow Erosion \end{aligned} \tag{D.1}$$

where
H_o is the deepwater wave height $[m]$
L_o is the deepwater wave length $[m]$
$M = 0.00070$ is an empirically determined coefficient $[-]$
w is the sand fall speed $[m/s]$
T is the wave period $[s]$

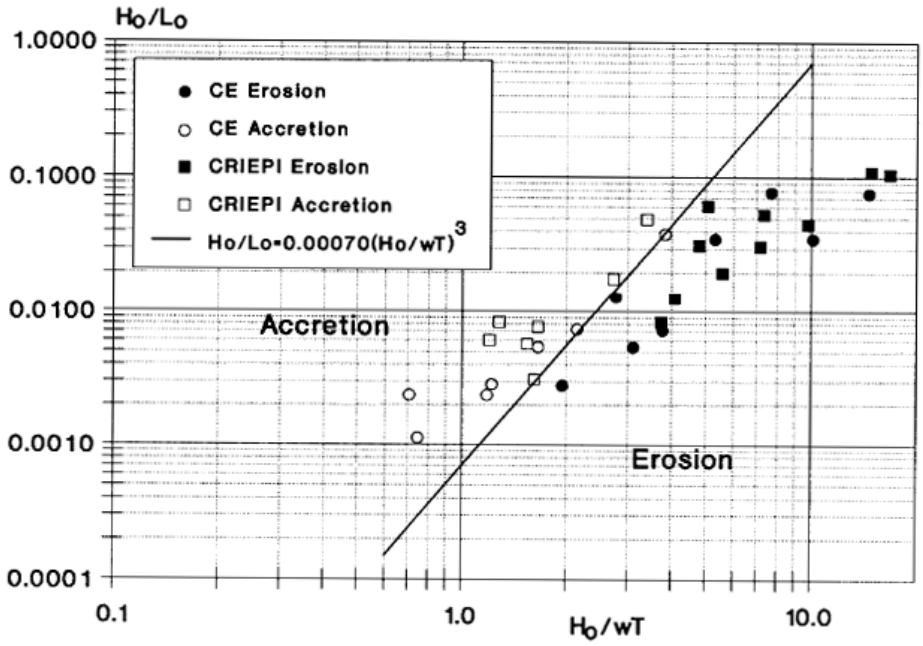

Figure D.1 *Criterion for predicting beach erosion and accretion based on monochromatic wave data (Larson, 1990, Figure 1).*

As the shape of the wave is not constant when propagating towards the beach, the net cross-shore sand transport is calculated differently at the different zones illustrated in Figure D.2, using the equations given in (D.2). The calculation is started by using the equation for Zone III at the plunge point and then applying results in the different zones.

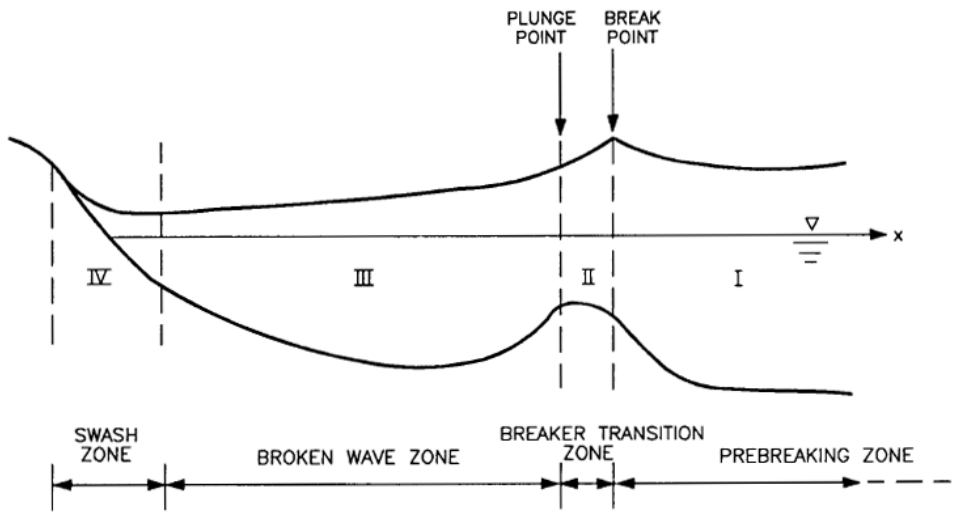

Figure D.2 *Principal zone for cross-shore transport(Larson, 1990, Figure 4)*

$$
\begin{array}{llcll}
Zone & I & : & q = q_b \cdot e^{\lambda_1 (x - x_b)} & x_b < x \\
Zone & II & : & q = q_b \cdot e^{-\lambda_2 (x - x_b)} & x_b < x \leq x_b \\
Zone & III & : & q = K \cdot \left(D - D_{eq} + \frac{\varepsilon}{K}\frac{dh}{dx}\right) & D > \left(D_{eq} - \frac{\varepsilon}{K}\frac{dh}{dx}\right) \\
 & & & 0 & D \leq \left(D_{eq} - \frac{\varepsilon}{K}\frac{dh}{dx}\right) \\
for & x_z \leq x \leq_p & & & \\
Zone & IV & : & q = q_z \left(\frac{x - x_r}{x_z - x_r}\right) & x_r < x < x_z
\end{array}
\tag{D.2}
$$

where
q is the net cross-shore transport rate $[m^3/(m \cdot s)]$
$\lambda_{1,2}$ is the spatial decay coefficients in Zones I and II $[1/m]$
K is the sand transport rate coefficient $[m^4/N]$
D is the wave energy dissipation per unit water volume $[N \cdot m/(m^3 \cdot s)]$
D_{eq} is the equilibrium wave energy dissipation per unit water volume $[N \cdot m/(m^3 \cdot s)]$
ϵ is the coefficient for slope-dependent term $[m^2/s]$
b, p, z and r denote values at the break point, plunge point, end of surf zone, and run-up limit, respectively

Expressions for the spatial decay coefficients have been determined empirically in (Larson, 1989), resulting in (D.3) and (D.4), where they are seen to be related to the median grain size D_{50} and the breaking wave height H_b.

$$\lambda_1 = 0.4 \cdot \left(\frac{D_{50}}{H_b}\right)^{0.47} \tag{D.3}$$

$$\lambda_2 = 0.2 \cdot \lambda_1 \tag{D.4}$$

The transport rate coefficient K mainly governs the response time of the profile, where larger values of K cause the profile to attain equilibrium more rapidly. K has only little influence on the size of the displaced volume. No relation between K and the wave or beach properties have been found. Instead K functions as a calibration parameter to find the right time scale for the profile change (Larson, 1989, p. 151). The default value is set to $K = 1.75e - 006m^4/N$ based on experimental results from a large wave tank. (Larson, 1989, p. 169). In SBEACH a transport rate decay coefficient multiplier is introduced, which describes the transport rate seaward of the breaker line and from the wave reformation point to the next breakpoint, in the case wave reformation occurs. The default value is 0.5.

The coefficient for slope-dependent term ϵ is introduced as the experiments have shown a dependence of q on the slope, and the inclusion have shown to induce increased numerical stability (Larson, 1989, p. 168). Higher values tend to produce flatter bars. The default value is set to $\epsilon = 0.002m^2/s$.

In order to determine the energy dissipation per unit water volume, it is necessary to describe the waves as they approach the beach. This is done using linear wave theory from the offshore boundary until the breaking point of the waves, after which a generalized wave decay model is applied. The wave breaking point is determined based on the breaking criterion given in (D.5), which is empirically determined in (Larson, 1989).

$$\gamma = 1.14 \cdot \xi^{0.21} \tag{D.5}$$

$$\xi = tan\beta \cdot \left(\frac{H_o}{L_o}\right)^{-0.5} \tag{D.6}$$

where
$\gamma = H_b/h_b$ is the wave breaking criterion $[-]$
ξ is the surf similarity parameter $[-]$
$tan\beta$ is beach slope seaward of the breakpoint evaluated over $L/3$
H_o/L_o is the deep water wave steepness $[-]$

The calculation of the wave height starts at the most seaward boundary and runs through the cells used to describe the model towards the shore. At each cell the wave height and angle with respect to bottom contours are determined based on the conservation of energy flux and Snell's law, which describes refraction based on the incoming wave angle and the velocity ratio.

For the generalized wave decay model the equation for conservation of energy flux has been derived as (D.7) in (Larson, 1990).

$$\frac{d}{dx}(F \cdot cos\theta) = \frac{\kappa}{d}(F - F_s) \tag{D.7}$$

where
F is the wave energy flux $[Nm/(m \cdot s)]$
θ is the wave angle with respect to the bottom contours
$\kappa = 0.15$ is an empirical wave decay coefficient
F_s is the stable wave energy flux $[Nm/(m \cdot s)]$
d is the water depth $[m]$

Energy dissipation in the surf zone is determined as the excess energy compared to a stable energy flux F_s. F_s can be determined based on (D.8), and corresponds to a stable wave height H_s, which is given as a function of the water depth in (D.9).

$$F_s = E_s \cdot C_g \tag{D.8}$$

$$H_s = \Gamma \cdot d \tag{D.9}$$

where
E_s is the stable energy density $[Nm/m^2]$
C_g is the group velocity $[m/s]$
$\Gamma = 0.4$ is an empirical stable wave height coefficient $[-]$
d is the water depth $[m]$

The empirical values κ and Γ are determined based on experiments in wave tanks, where the given values are found to be applicable for varying bottom slopes. This has further been validated based on field measurements and found to be in good agreement.

The energy dissipation pr. unit water volume D is calculated based on the energy dissipation in the surf zone using (D.10). κ is set to zero outside the surf zone, meaning no energy dissipation takes place, as bottom friction is neglected.

$$D = \frac{\kappa}{d^2}\left(F - F_s\right) \tag{D.10}$$

where
d is the total water depth $[m]$

D.2.1 Overview of Program Methodology

The SBEACH model consists of 3 calculation modules that are executed consequently at each time step a simulation:

- Module 1: Uses the specified offshore waves to determine the cross-shore wave heights. Linear wave theory is used for determining offshore until the breakpoint, after which a generalized form of the wave decay model is applied.
- Module 2: Uses the wave heights from Module 1 to determine the net cross-shore transport rate. Transport rates are calculated differently in different zones of the cross-shore profile, shown in Figure D.2, using (D.2).
- Module 3: Uses the transport rate from Module 2 to calculate the profile change, which is the applied in the next time step. The transport direction is determined based on (D.1)

Appendix E

List of Files

In the following, a list of the files on the appendix CD will be given, along with a short description of each model, and their location on the CD.

E.1 MIKE21 BW Models

The numerical models set up in MIKE21 BW consist of a number of files, describing different parameters. References are made to the MIKE Zero project files, which give an overview of the model. The models are run from the model setup type files in the project. Due to space restrictions on the CD, the wave input used in the model must be generated using the MIKE Zero toolbox files, before the model can be run.

E.1.1 Experimental Setup

Model of the experimental setup described in Chapter **??**, used for calibrating the numerical representation of the WD.
Location: \Experimental Setup\Wavedragon.mzp

E.1.2 Santander Model

Model used for determining the effect of a farm of 5 WD's at Santander bay, as described in Chapter 6.
Location: \Santander Model\Santander Bathymetry tests.mzp

E.1.3 WD Porosity maps

Porosity maps representing different WD setups at Santander. Best viewed loading the palette "porosity palette.pal" in the same folder.
Location:\Santander porosity WD

E.2 Test Data

The data obtained from different wave gauges during the experiments can be found in the folder: \Testdata. The data is organized in folders, named after the test numbers, containing data files extracted from WaveLab. In addition to the voltage, the data files give the calibration factor used at each wave gauge, along with sample frequency and sample duration.

E.3 Photographs

A number of photographs of different test setups is included in the folder: \Laboratory photos.